Application of Transition Metal Phosphine Complexes in the Modeling of Catalytic Processes: Reactivity with Hydrosilanes and Other Industrially Relevant Substrates

Ashley Zuzek

Submitted in partial fulfillment of the
requirements for the degree
of Doctor of Philosophy
in the Graduate School of Arts and Sciences

Columbia University
2014

ABSTRACT

Application of Transition Metal Phosphine Complexes in the Modeling of Catalytic Processes: Reactivity with Hydrosilanes and Other Industrially Relevant Substrates

Ashley Zuzek

The first two chapters of this thesis are devoted to exploring the reactivity of electron rich molybdenum and tungsten trimethylphosphine complexes with hydrosilanes. These complexes, $Mo(PMe_3)_6$ and $W(PMe_3)_4(\eta^2\text{-}CH_2PMe_2)H$, have been shown to be highly reactive species that undergo a number of bond cleavage reactions. In the presence of the hydrosilanes Ph_xSiH_{4-x} (x = 0 – 4), $Mo(PMe_3)_6$ and $W(PMe_3)_4(\eta^2\text{-}CH_2PMe_2)H$ effect Si-H and Si-C bond cleavage, along with Si-Si bond formation; however, the products derived from these reactions are drastically different for $Mo(PMe_3)_6$ and $W(PMe_3)_4(\eta^2\text{-}CH_2PMe_2)H$ and are highly dependent on the substitution of the silane.

$Mo(PMe_3)_6$ reacts with SiH_4, $PhSiH_3$, and Ph_2SiH_2 to afford novel silyl, hypervalent silyl, silane, and disilane complexes, as respectively illustrated by $Mo(PMe_3)_4H_2(SiH_3)_2$, $Mo(PMe_3)_4H(\kappa^2\text{-}\mathit{H}_2\text{-}H_2SiPh_2H)$, $Mo(PMe_3)_3H_4(\sigma\text{-}HSiHPh_2)$, and $Mo(PMe_3)_3H_2(\kappa^2\text{-}\mathit{H}_2\text{-}H_2Si_2Ph_4)$. $Mo(PMe_3)_4H(\kappa^2\text{-}\mathit{H}_2\text{-}H_2SiPh_2H)$ is the first example of a complex with a hypervalent [H_2SiPh_2H] ligand, and $Mo(PMe_3)_3H_2(\kappa^2\text{-}\mathit{H}_2\text{-}H_2Si_2Ph_4)$ represents the first structurally characterized disilane complex. In addition to being structurally unique, these complexes also possess interesting reactivity. For example, $Mo(PMe_3)_4(SiH_3)_2H_2$ undergoes isotope exchange with SiD_4, and NMR spectroscopic analysis of the SiH_xD_{4-x} isotopologues released indicates that the reaction occurs *via* a sigma bond metathesis pathway.

In contrast, $W(PMe_3)_4(\eta^2\text{-}CH_2PMe_2)H$ affords a range of products that includes metallacycle, disilyl, silane, and bridging silylene complexes. The disilyl compounds, $W(PMe_3)_4H_3(SiH_2SiHPh_2)$ and $W(PMe_3)_3H_4(SiH_2Ph)(SiH_2SiHPh_2)$, exhibit the ability of $W(PMe_3)_4(\eta^2\text{-}CH_2PMe_2)H$ to cause both redistribution and Si-Si bond formation. A mechanism involving silylene intermediates is proposed for the generation of these complexes, and this mechanism is supported computationally. Additional support for the presence of intermediates comes from the isolation of a unique complex with a bridging silylene ligand, "WSiW". The bridging silylene bonding motif is unprecedented.

The reactivity of the simplest hydrosilane, SiH_4, was also examined with $IrCl(CO)(PPh_3)_2$ (*i.e.* Vaska's compound). Previous reports on this reaction have assigned the product as *trans*-$IrH(SiH_3)(Cl)(CO)(PPh_3)_2$, in which the hydride and silyl ligands are mutually *trans*. It is noteworthy, therefore, that we have now obtained a crystal structure of the product of this reaction in which the hydride and silyl ligands are *cis*, namely *cis*-$IrH(SiH_3)(Cl)(CO)(PPh_3)_2$. Calculated energies of the isomeric species also suggest that the product of this reaction was originally misassigned. These results, and the analogous reactions with germane (GeH_4), are described in Chapter 4.

Chapter 4 also discusses some reactions of transition metal phosphine complexes, including $Ru(PMe_3)_4H_2$, $Mo(PMe_3)_6$, $W(PMe_3)_4(\eta^2\text{-}CH_2PMe_2)H$, and $Mo(PMe_3)_4(\eta^2\text{-}CH_2PMe_2)H$, with industrially relevant substrates. $Ru(PMe_3)_4H_2$ effects the water gas shift reaction of CO and H_2O to form CO_2 and H_2. Furthermore, $Ru(PMe_3)_4H_2$ reacts with CO_2, CS_2, and H_2S to respectively form formate, thiocarbonate, and hydrosulfido complexes. The reactivity of $Mo(PMe_3)_6$ and $W(PMe_3)_4(\eta^2\text{-}CH_2PMe_2)H$ towards molecules relevant to the hydrodeoxygenation industry, including dihydrofuran and benzofuran, was studied. The products of these reactions exhibit hydrogenation of

unsaturated bonds and C-O bond cleavage, both of which are essential to the hydrodeoxygenation process. $Mo(PMe_3)_4(\eta^2\text{-}CH_2PMe_2)H$ reacts with PhI to form an alkylidyne species, $[Mo(PMe_3)_4(\equiv CPMe_2Ph)I]I$, which was structurally characterized by X-ray diffraction. $W(PMe_3)_4(\eta^2\text{-}CH_2PMe_2)H$ forms a κ^2-adduct when treated with 2-seleno-2-methylbenzimidazole, namely $W(PMe_3)_4(sebenzim^{Me})H$.

Chapter 3 discusses the development of two new ruthenaboratrane complexes, $[\kappa^4\text{-}B(mim^{But})_3]Ru(CO)(PR_3)$ (R = Ph, Me). The structures of these complexes are described, and their d^6 metal configuration is supported by both Fenske-Hall and Natural Bond Orbital calculations. Some reactivity of these complexes was also explored. For example, $[\kappa^4\text{-}B(mim^{But})_3]Ru(CO)(PMe_3)$ appears to add MeI across the Ru-B bond.

Finally, as an extension of the work that we have done on tungsten trimethylphosphine complexes, the structure of $W(PMe_3)_3H_6$ in solution was investigated, and the results are presented in Chapter 5. T_1 measurements of the hydride ligands and deuterium isotope effect shifts both confirm that this complex exists as a classical hydride in solution, which is in accord with the classical hydride formulation in the solid state that was previously determined by X-ray diffraction.

TABLE OF CONTENTS

ACKNOWLEDGEMENTS

The past five years have been a true learning experience. A lot has happened since I first moved to New York, and it's hard to believe that it all went so quickly. There are many people who really impacted my experience in graduate school, both in and outside of lab, and I would like to acknowledge those people here.

It goes without saying that some of the people who've influenced me the most over the course of my graduate studies have been the people that I've worked with every day. To that end, I'd first like to thank Ged, who has been my advisor for the past five years. I have learned a lot in the Parkin lab – for example, I've learned that I will always be impressed by magic tricks, and I'll never figure out how they work. More importantly (maybe), however, is that I've learned a lot about chemistry, particularly with respect to understanding how to think about the description of molecules and the bonding within them. One of the fun parts of writing this thesis is that I've had to go back and revisit the research that I did in my first couple of years here, and in the process, I realized that everything makes a lot more sense now than it used to. That's because I've had the opportunity to learn a lot from you, and for that I'm truly grateful. It's also been a wonderful experience to really dig my heals into research projects that I'm passionate about – I now know more about metal-silyl chemistry than I ever thought I would, and I feel lucky because of that.

My labmates, former and present, have also had an immense impact on my experience in graduate school. Someone once described a typical research lab to me as a big, dysfunctional family – you can't choose your labmates, and sometimes they drive you crazy, but at the end of the day, you care about them a ton and wouldn't have it any other way. That just about sums up my feelings towards my lab, who have been a great crew to do research with over the past five years. So, in chronological order:

Thanks to "the twins," Aaron and Wes Sattler. Wes was my host here during visiting weekend, so it's arguable that his recruiting skills are the reason why I ended up at Columbia! Not only were you some of my first friends in New York, and my neighbors for a while, but you were also a big part of my experience in the Parkin lab. Aaron – thank you for being a tremendous resource on X-ray and for helping me out when I started working with Mo_6 and WP_5. Wes – thank you for also being a great resource on all things chemistry and for being a supportive labmate during your time here. I'm grateful to you both for all of your help!

Thanks to Ahmed Al Harbi, who is now back in Saudi Arabia. We miss you here! You are not only a great chemist, but you are also one of the nicest people I've ever met. Grad school can be tough sometimes, and you were never too busy to listen to me gripe, or cry, or get upset about anything. I will always appreciate your patience and your insight on life in general – you were definitely the wisest Parkin lab member! I wish you all the best and am sure that you will do great chemistry in your new lab.

Thanks to Yi Rong, who is consistently one of the friendliest, happiest, and most resourceful people I know. I don't think that there was a single problem in lab that you weren't willing to tackle, and I particularly appreciate your help with some of the computational work that I've done – I don't think I'd ever figure out how to submit NBO calcs if you hadn't told us all how. So thank you for being a great friend and labmate, and I hope you have a great time living in New York.

I'd also like to thank all of my current labmates – Joshua Palmer, Michelle Neary, Ava Krieder-Muller, Serge Ruccolo, Patrick Quinlivan, and Neena Chakrabarti. You are collectively an endless source of inspiring lunch conversations and a great help in and around lab. Michelle and Josh – thanks for being my desk-neighbors, for lack of a current deskmate, and for helpful conversations about chemistry. You've been good

friends here, and I enjoy both our serious and non-serious talks. To my fellow fifth years, Ava and Neena – it's been fun. Ava, I hope that both of us are better drivers the next time we meet! To Serge, our resident Frenchman – thanks for being such a fun and helpful labmate (*i.e.* helping me to stitch back together our argon box after its surgery)! And Patrick, our newest addition – I hope you have a great graduate school experience and that you are as happy in your fifth year as you were in your first :)

I'd also like to thank my committee members, Jack Norton and Jon Owen. To Jack – thank you so much for all of your help over the past five years. I learned a lot in your class, and I am grateful that I had the opportunity to work with you. I also can't thank you enough for all of your support during my job search – your help and advice was invaluable, and I really appreciate it. To Jon – thanks for always being a friend and for your support. Also, thank you to my external committee members, Daniela Buccella and John Magyar. I really appreciate that you are willing to take the time to do this. And thank you to you all for reading this thesis – I hope you find it interesting, and if not, it might make a good doorstop!

I'd also like to thank John Decatur and Michael Appel, who have been incredibly helpful resources. I think that John has set up about a dozen new silicon-related spectroscopic experiments for the work presented here, and I'm very grateful for that!

I would like to acknowledge the U.S. Department of Energy (Office of Basic Energy Sciences) for supporting research described in this thesis.

Equally important to my experience in graduate school have been the people in my life outside of lab. During our STAT orientation week, I remember Luis Avila asking all of us in my year whom among us was married. A handful of students raised their hands, and Luis said: You all are the lucky ones. Because when things aren't going well in lab

– and there will definitely be times when things aren't going well – you're the ones who will have someone to support you and help you through graduate school. Well, there was no husband here, but my friends and family have been incredibly supportive through these years. I'll never be able to thank them enough, but I'll try.

To my friends – I'd list you here, but you know who you are anyway, and I expect you'll never read this thesis! – thank you for all of the dinners, brunches, yoga dates, drinks, adventures, conversations (serious and ridiculous), and good times that we've had over the last five years. You have defined my New York experience, and when I think of my favorite memories of this city, most of them are with you. Thank you for that, and thank you for being so wonderful. I will miss you immensely, and I hope that you will come to visit me in California!

Most importantly, I'd like to thank my family. I love you more than I can put in words, and you mean everything to me. It goes without saying that I would not be where I am today without you. Being able to see you often over the past five years has been the best part of my graduate school experience. Tinči – thanks for being the best and for being my favorite sister. I'm so glad that we got to be in the same country (and time zone) for a while, so that we could talk all the time about literally anything and everything. Now, of course, I'm ruining that by moving to Cali… but three hours difference is not so bad, and you'll just have to come visit me all the time. Papa – thank you for your love and insight, and thanks for being the only other Zuzek who likes (or does a very good job pretending to like) chemistry. Our road-trip conversations and phone-chats are the greatest, and they always make me realize that in some ways, you know me better than I know myself! You're the best, and I love you so much. And to my Mama – I don't know what I would do without my mama. Thank you for being the best, most loving, supportive, caring, wonderful mom in the world. No matter what

happens during my day, I know that it will be better after speaking to you. I love you so much! Mama and Papa – this thesis is dedicated to you!

For Mama and Papa Z – Thank you for everything!

CHAPTER 1

Reactivity of SiH_4 and Ph_xSiH_{4-x} Towards $Mo(PMe_3)_6$: Silyl, Hypervalent Silyl, Silane, and Disilane Complexes

Table of Contents

Reproduced in part from Zuzek, A. A.; Parkin, G. *J. Am. Chem. Soc.* **2014**, *136*, 8177-8180.

1.1 Introduction

The interaction of Si-H bonds with transition metal complexes is of fundamental interest.[1] The dehydrogenative polymerization of silanes, the hydrosilation of olefins, and the redistribution of silanes are all catalyzed by transition metal complexes.[2] The products of these reactions have significant applications in industry and have received broad interest within academia. For example, organosilanes derived from hydrosilation reactions are used as coupling agents, which are essential for the production of polymers reinforced with inorganic materials such as glass fibers.[3] Polysilanes, which are frequently prepared by the dehydrogenative coupling of hydrosilanes, have been studied extensively for their unique electronic and optical properties.[4] In addition, silanes have been examined as models of organic compounds in an effort to learn more about C-H activation processes.[5,6] An in-depth knowledge of both the reactivity of transition metals with hydrosilanes and the coordination of silanes to metal complexes is, therefore, valuable in gaining a better understanding of metal-catalyzed silane chemistry. Here we explore the reactivity of electron-rich molybdenum compounds towards hydrosilanes with the goal of gaining a greater understanding of how silanes interact with these reactive molybdenum species.

1.2 $Mo(PMe_3)_6 + SiH_4$

1.2.1 Preparation of $Mo(PMe_3)_4H_2(SiH_3)_2$

The reactions of silane (SiH_4) with transition metal complexes have been explored relatively little compared to substituted silanes,[5,6b,7] presumably due to the extreme pyrophoricity of this reagent. The reactivity of some zerovalent molybdenum complexes with SiH_4 has, however, been examined previously.[5] Kubas *et al.* reported that molybdenum compounds of the type $Mo(CO)(R_2PC_2H_4PR_2)_2$ (R = Ph, Bu^i) react with SiH_4 to form the σ-complexes $Mo(\sigma\text{-}SiH_4)(CO)(R_2PC_2H_4PR_2)_2$ (R = Ph, Bu^i). The corresponding ethyl derivative, $Mo(CO)(Et_2PC_2H_4PEt_2)_2$, reacted similarly to form a σ-

complex; however, this σ-complex was observed to exist in equilibrium with the silyl hydride complex, $MoH(SiH_3)(CO)(R_2PC_2H_4PR_2)_2$.[5]

It is significant, therefore, that $Mo(PMe_3)_6$ cleaves the Si-H bond of SiH_4 to form the oxidative addition product $Mo(PMe_3)_4H_2(SiH_3)_2$ (Scheme 1) rather than a σ-complex. This reaction is facile at room temperature and proceeds cleanly in the presence of excess silane. This transformation represents the first example of the oxidative addition of two equivalents of SiH_4 to a molybdenum center. Confirmation that this compound is in fact a silyl hydride is provided by ^1H NMR spectroscopic analysis (Figure 1). For example, the signal attributable to the Mo-SiH_3 groups (δ 4.02) demonstrates coupling to silicon ($^1J_{Si-H}$ = 157 Hz) and phosphorus ($^3J_{P-H}$ = 8 Hz); the signal corresponding to the hydrides (δ -4.80), on the other hand, shows coupling to phosphorus ($^2J_{P-H}$ = 26 Hz), but no coupling to silicon is observed (J_{Si-H} < 15 Hz). $^2J_{Si-H}$ coupling constants for silyl-hydride compounds are generally < 20 Hz,[1a,8] whereas compounds with direct Si–H interactions often have larger J_{Si-H} coupling constants, as illustrated by $Mo(R_2PC_2H_4PR_2)_2(CO)(\sigma\text{-}SiH_4)$ (J_{Si-H} = 31 – 50 Hz);[5] therefore, the lack of observable J_{Si-H} coupling for the hydride signal supports the formulation of this compound as a silyl-hydride. The molecular structure of $Mo(PMe_3)_4H_2(SiH_3)_2$ is shown in Figure 2.

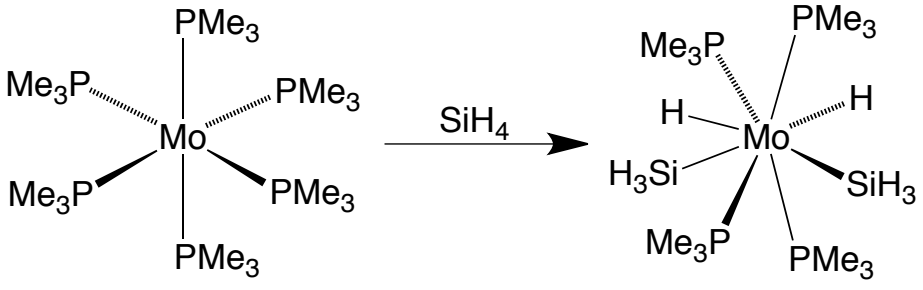

Scheme 1. Formation of $Mo(PMe_3)_4H_2(SiH_3)_2$

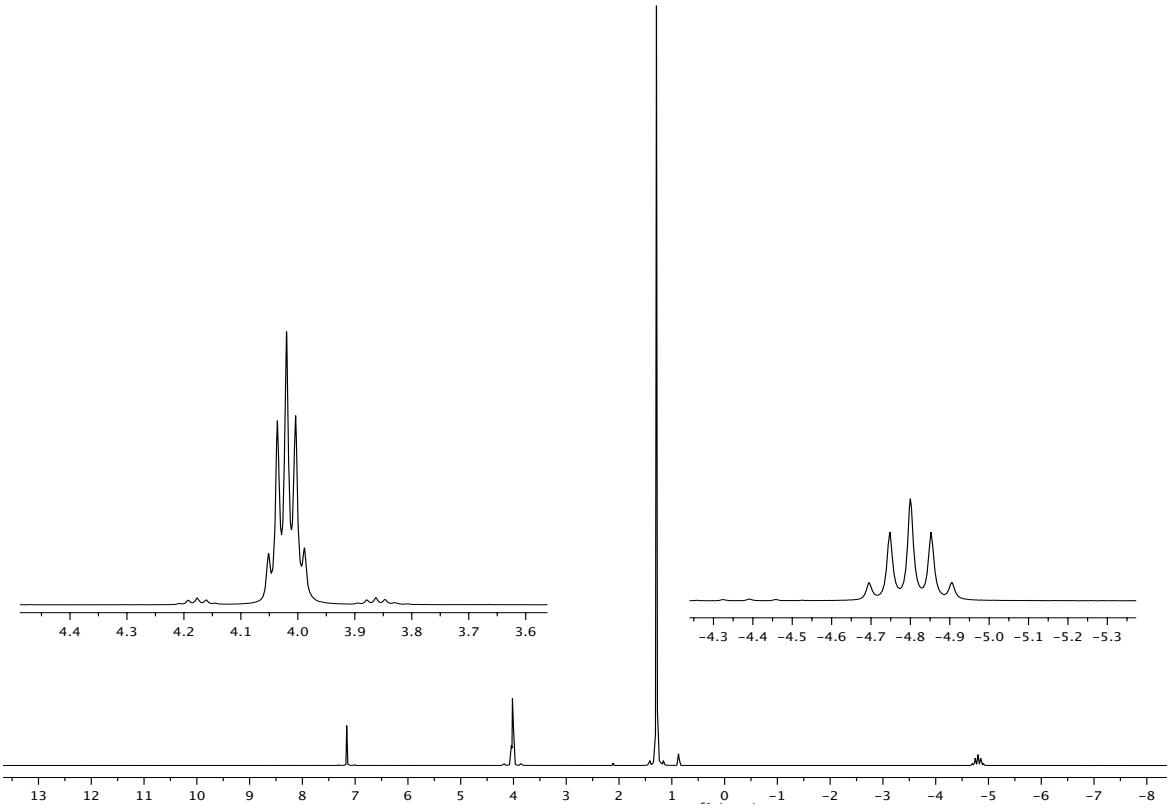

Figure 1. ^{1}H NMR Spectrum of $Mo(PMe_3)_4H_2(SiH_3)_2$

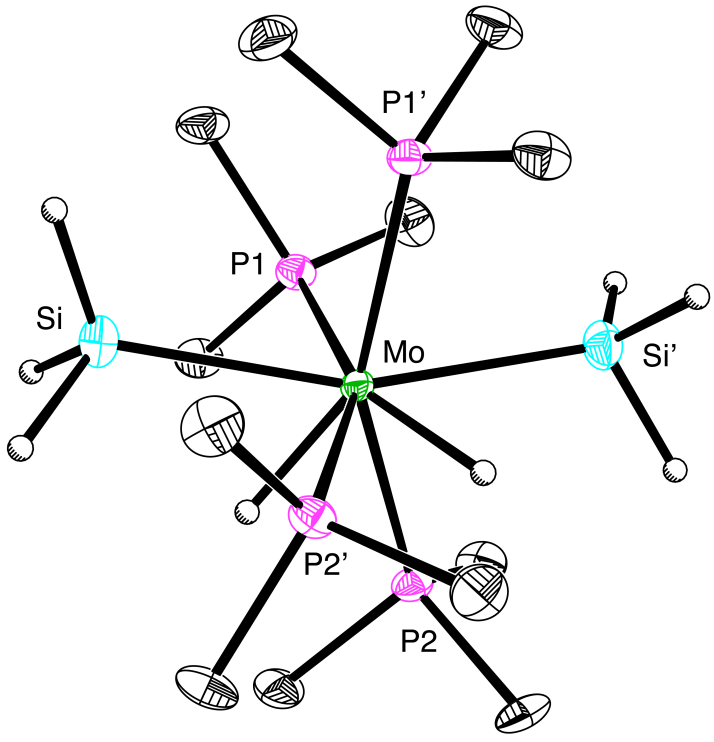

Figure 2. Molecular Structure of $Mo(PMe_3)_4H_2(SiH_3)_2$

1.2.2 Reactivity of $Mo(PMe_3)_4H_2(SiH_3)_2$ towards SiD_4

The reactivity of $Mo(PMe_3)_4H_2(SiH_3)_2$ towards SiD_4 was explored, both (*i*) to gain a sense of how this d^2 metal complex reacts with silanes and (*ii*) to provide a model system for the silyl exchange that occurs in the reaction of $Mo(PMe_3)_6$ with $PhSiH_3$ (see Section 1.3). Reaction did indeed occur between $Mo(PMe_3)_4H_2(SiH_3)_2$ and SiD_4, as evidenced by deuterium incorporation into both the silyl and hydride positions of $Mo(PMe_3)_4H_2(SiH_3)_2$. A number of possible mechanisms may be considered for the H/D exchange, which was monitored by ^1H and ^2H NMR spectroscopy. One straightforward mechanism could involve reductive elimination of SiH_4 followed by oxidative addition of SiD_4 (Scheme 2); the resulting complex, $Mo(PMe_3)_4HD(SiH_3)(SiD_3)$, would be characterized by deuterium incorporation into the silyl and hydride positions in a 3:1 ratio. In addition, SiH_4 would be expected to be the predominant isotopologue of silane observed by ^1H NMR spectroscopy. Similar mechanisms have been invoked for non-d^0 metal phosphine hydride compounds.[9]

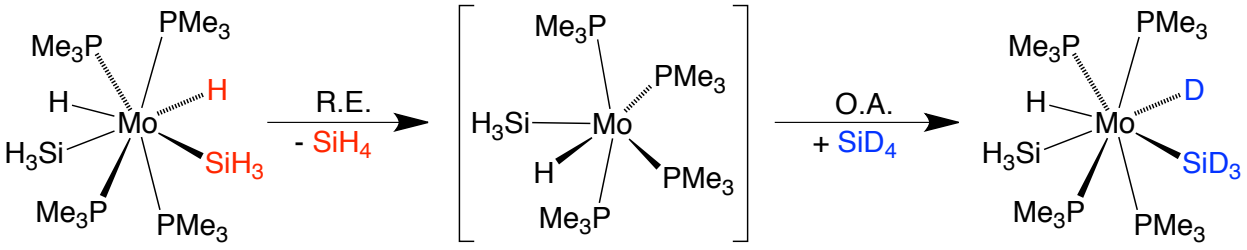

Scheme 2. Simple R.E. / O.A. mechanism for H/D exchange

A number of experimental observations, however, indicate that this mechanism does not operate. First, ^2H NMR spectroscopy shows that deuterium incorporation into the silyl and hydride moieties occurs in an approximately 6:1 ratio rather than a 3:1 ratio, which is inconsistent with $Mo(PMe_3)_4HD(SiH_3)(SiD_3)$ as the major initial product. Second, ^1H NMR spectroscopy indicates that $SiHD_3$ is the initially formed and major silane isotopologue, with SiH_2D_2 and SiH_3D being formed as the reaction progresses. SiH_4, on the other hand, is produced in only negligible quantities over the course of the

reaction. Third, the consecutive formation of Mo-SiH_2D and Mo-$SiHD_2$ groups is observed by ^1H NMR spectroscopy. The absence of SiH_4 (Figure 3) provides conclusive evidence that reductive elimination of the silyl and hydride ligands from $Mo(PMe_3)_4H_2(SiH_3)_2$ does not occur, and the other experimental observations confirm that oxidative addition of SiD_4 to $[Mo(PMe_3)_4H(SiH_3)]$ is not part of the operative mechanism.

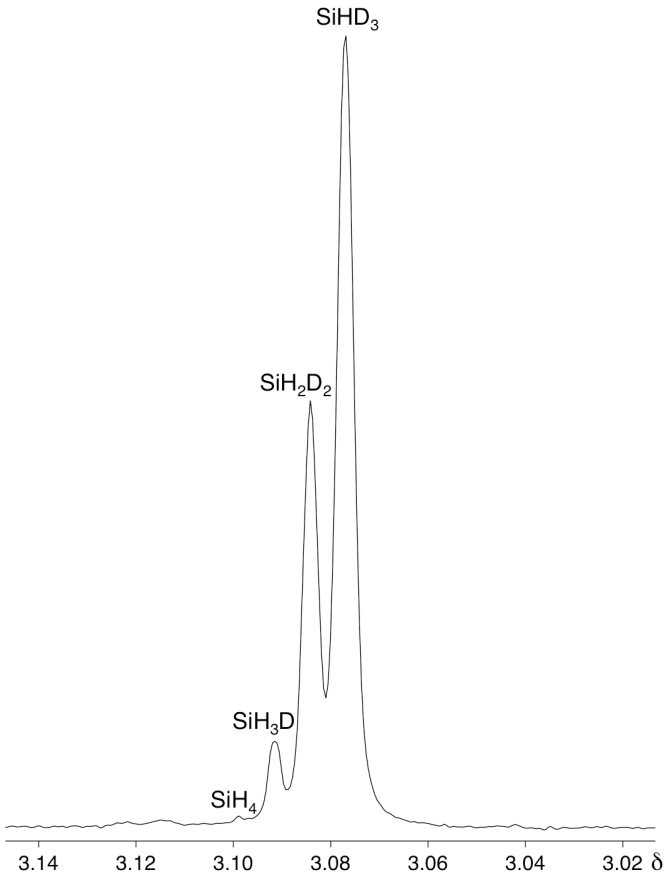

Figure 3. Distribution of silane isotopologues from $Mo(PMe_3)_4H_2(SiH_3)_2$ + SiD_4

Nevertheless, other mechanisms involving oxidative addition and reductive elimination can be considered for this system. For example, initial dissociation of PMe_3 followed by oxidative addition of SiD_4 could produce a complex with deuterium in the silyl and hydride positions, but the anticipated production of SiH_4 from this intermediate would be inconsistent with experimental results (Scheme 3). Initial reductive elimination of H_2

followed by oxidative addition of SiD_4 does result in deuterium incorporation at the metal center; however, the silane isotopologue that is observed by ^1H NMR spectroscopy is SiH_3D rather than $SiHD_3$ (Scheme 4).

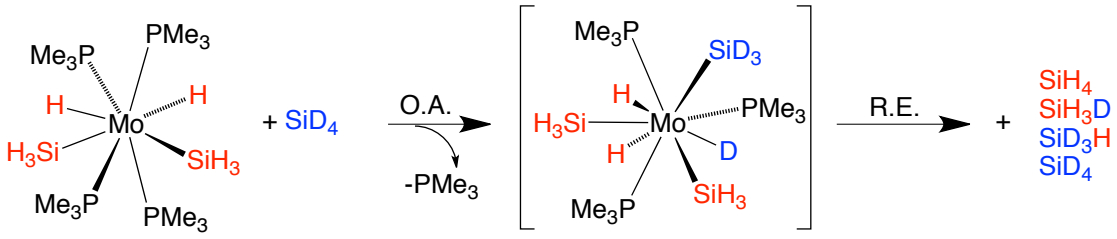

Scheme 3. R.E. / O.A. mechanism invoking a hexavalent intermediate

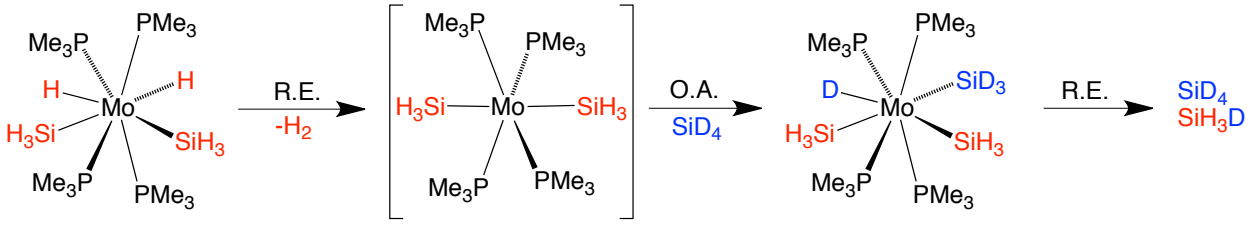

Scheme 4. R.E. / O.A. mechanism involving initial elimination of H_2

A mechanism involving a silylene intermediate may also be considered for this system (Scheme 5). For example, dissociation of PMe_3 followed by α-H elimination from the bis(silyl) complex would produce a species of the type $H_3[Mo](=SiH_2)(SiH_3)$, which could undergo 1,2-addition of SiD_4 to produce $H_3[Mo](SiD_3)(SiH_3)(SiH_2D)$. However, reductive elimination from this species would produce a mixture of silane isotopologues, including SiH_4, so this is also an unlikely mechanism.

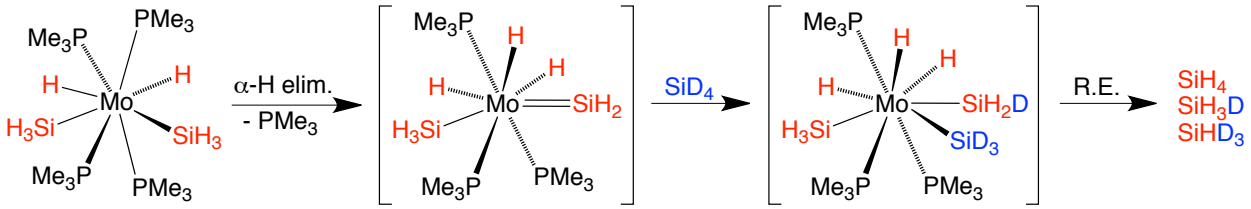

Scheme 5. Mechanism invoking silylene intermediate

On the other hand, sigma bond metathesis of SiD_4 with the Mo-H moiety explains both deuterium incorporation into the metal complex and the production of primarily $SiHD_3$. Subsequent incorporation of deuterium into the molybdenum-silyl groups may be achieved by $Mo(PMe_3)_4HD(SiH_3)_2$ accessing a fluxional silane adduct, $Mo(PMe_3)_4(SiH_3)(\sigma\text{-}SiH_3D)H$, in which H/D scrambling may occur (Scheme 6).[10,11] These observations also indicate that metathesis of SiD_4 with the molybdenum-silyl group, as opposed to the hydride, does not operate; if this were the mechanism, SiH_3D would be the major isotopologue produced. The reverse reaction, in which $Mo(PMe_3)_4D_2(SiD_3)_2$ is treated with SiH_4, produces primarily SiH_3D (Figure 4). This is consistent with a mechanism that involves sigma bond metathesis of SiH_4 with the Mo-D moiety.

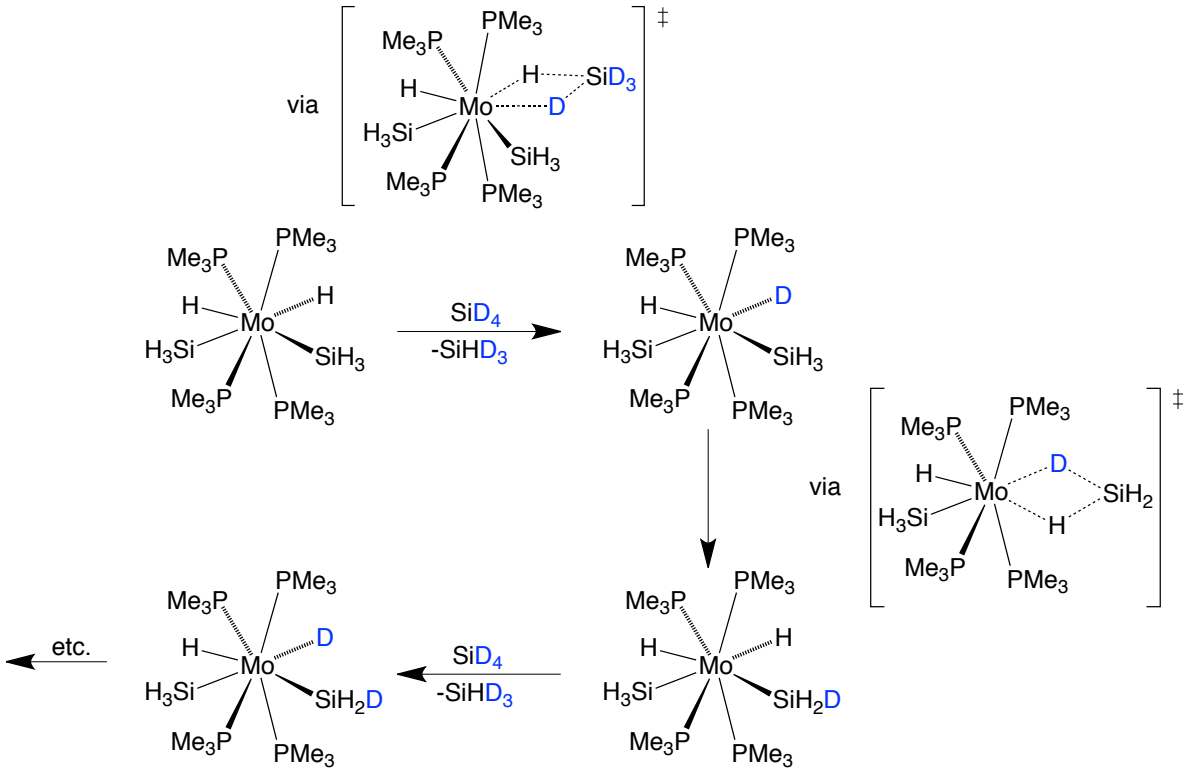

Scheme 6. Proposed mechanism invoking sigma bond metathesis

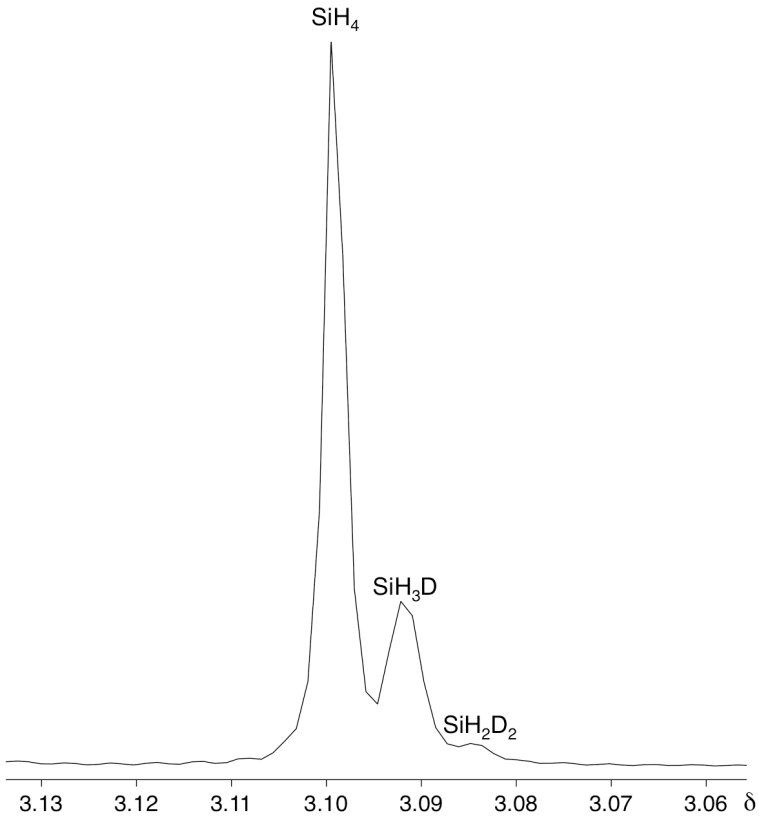

Figure 4. Distribution of silane isotopologues from $Mo(PMe_3)_4D_2(SiD_3)_2 + SiH_4$

1.2.3 Formation of $Mo(PMe_3)_4H_3(SiH_3)$

$Mo(PMe_3)_4H_2(SiH_3)_2$ also reacts with H_2 at room temperature to form the trihydride complex, $Mo(PMe_3)_4H_3(SiH_3)$ (Scheme 7). It is worth noting that this transformation occurs even in the absence of H_2, but the conversion is cleaner in its presence. It is also significant that this reaction proceeds to an equilibrium. An equilibrium constant of 1.0(1) was derived for this reaction from the concentrations of $Mo(PMe_3)_4(SiH_3)_2H_2$, H_2, $Mo(PMe_3)_4(SiH_3)H_3$, and SiH_4, as determined by integration of the ^1H NMR spectrum. Relative Mo-H and Mo-Si bond dissociation energies were calculated using this equilibrium constant and the values of D(H–H) = 104.2 kcal mol^{-1}, D(H–SiH_3) = 91.7 kcal mol^{-1},[12] $S^0(H_2)$ = 31.2 cal mol^{-1} K^{-1} and $S^0(SiH_4)$ = 48.9 cal mol^{-1} K^{-1}.[13] Using these values, the Mo-H bond is calculated to be approximately 7 kcal/mol stronger than the Mo-SiH_3 bond.[14]

The reaction of $Mo(PMe_3)_4H_2(SiH_3)_2$ with D_2 proceeds in an analogous fashion to produce the monosilyl trihydride complex; furthermore, monitoring this reaction by ^1H NMR spectroscopy provides additional evidence that $Mo(PMe_3)_4H_2(SiH_3)_2$ does not undergo reductive elimination of SiH_4. Specifically, a mixture of $SiHD_3$, SiH_2D_2, SiH_3D, and SiH_4 are produced over the course of the reaction, rather than primarily SiH_4.[15]

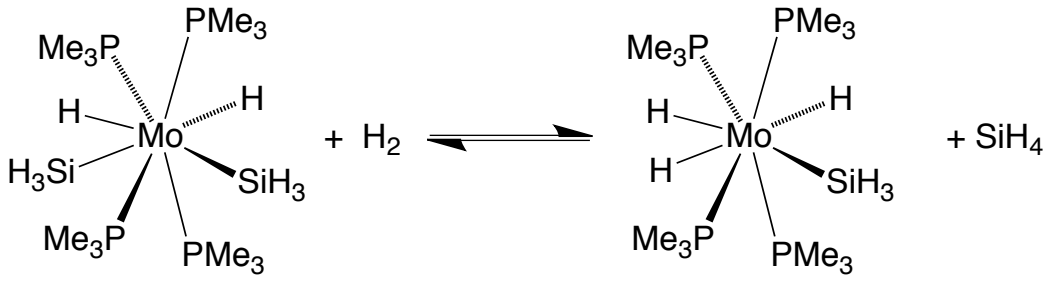

Scheme 7. Reaction of $Mo(PMe_3)_4H_2(SiH_3)_2$ with H_2

Both $Mo(PMe_3)_4H_2(SiH_3)_2$ and $Mo(PMe_3)_4H_3(SiH_3)$ are fluxional at room temperature, such that the four phosphorus nuclei of each compound appear equivalent by $^{31}P\{^1H\}$ NMR spectroscopy. Low temperature $^{31}P\{^1H\}$ NMR spectroscopy, however, reveals spectra that are consistent with the solid-state structures of these compounds. Specifically, both structures are based on a dodecahedral arrangement in which the PMe_3 ligands adopt a flattened tetrahedral array that interpenetrates the elongated tetrahedral array of the silyl and hydride ligands.[16] The solid state structure of $Mo(PMe_3)_4H_2(SiH_3)_2$, therefore, suggests an A_2X_2 set of PMe_3 ligands, and the structure of $Mo(PMe_3)_4H_3(SiH_3)$ (Figure 5) indicates an AMX_2 arrangement. Accordingly, two signals are seen in the $^{31}P\{^1H\}$ NMR spectrum at 210 K for $Mo(PMe_3)_4H_2(SiH_3)_2$, and three signals are observed at 250 K for $Mo(PMe_3)_4H_3(SiH_3)$.

Also of note is the fact that the ^1H NMR spectrum of $Mo(PMe_3)_4H_3(SiH_3)$ demonstrates coupling of the silyl ligand to the hydride ligands ($^3J_{H\text{-}H} = 2$), whereas no such coupling

is observed for $Mo(PMe_3)_4H_2(SiH_3)_2$. The coupling of the hydrides to the phosphine ligands is also significantly larger ($^2J_{P\text{-}H}$ = 34 Hz) in this complex than in the bis(silyl) species. The ^1H NMR spectrum of $Mo(PMe_3)_4H_3(SiH_3)$ is shown in Figure 6.

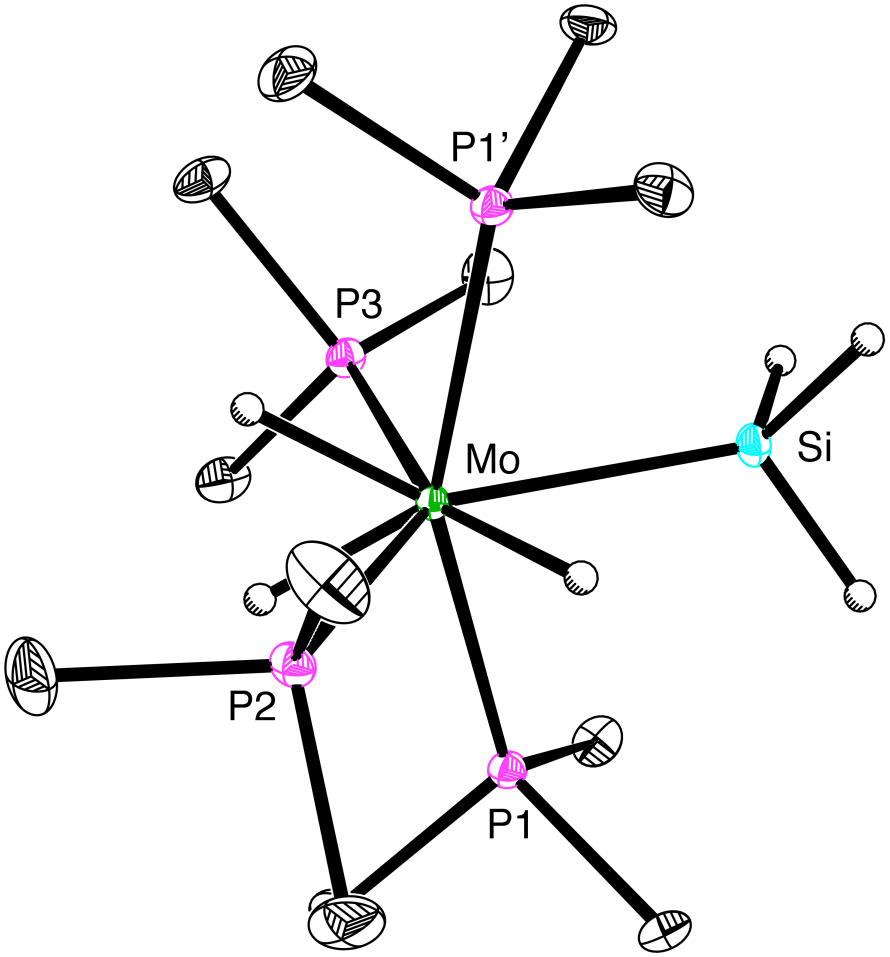

Figure 5. Molecular Structure of $Mo(PMe_3)_4H_3(SiH_3)$

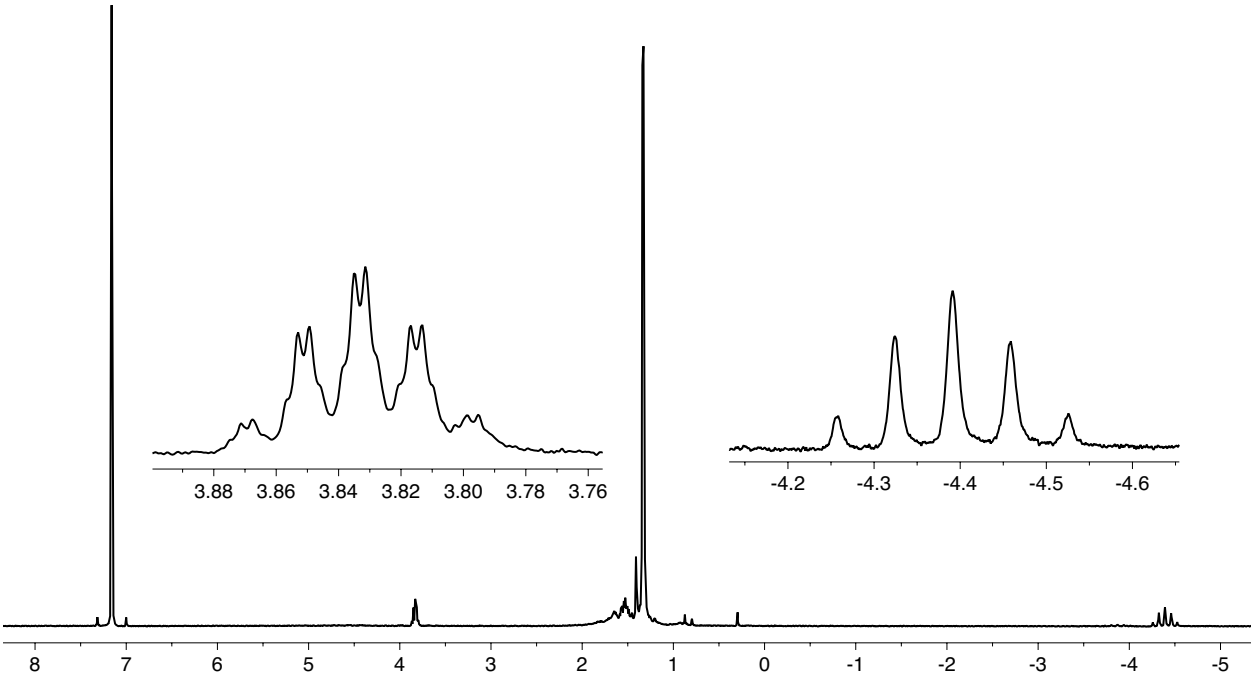

Figure 6. ^{1}H NMR Spectrum of $Mo(PMe_3)_4H_3(SiH_3)$

1.3 $Mo(PMe_3)_6$ + $PhSiH_3$

1.3.1 Generation of $Mo(SiH_3)$ Compounds from $PhSiH_3$

The addition of phenylsilane ($PhSiH_3$) to metal complexes is well precedented. The predominant reactivity of many systems is to produce $M(H)(SiH_2Ph)$ compounds *via* oxidative addition of the Si-H bond; in some instances, cleavage of the Si-H bond is not achieved, and σ-complexes of the type $M(\sigma\text{-}HSiH_2Ph)$ are obtained instead.[1] Oxidative addition products and σ-complexes are structurally related in terms of the location of their atoms, but the electron density is distributed differently. For example, the valence of the metal center is increased by two upon oxidative addition, and the Si-H bond is cleaved; in the case of σ-complex formation, the valence of the metal remains unchanged, and the Si-H bond remains intact. The reaction of $Mo(PMe_3)_6$ with $PhSiH_3$, however, provides a unique series of complexes rather than simple adducts of phenylsilane.

When $Mo(PMe_3)_6$ is treated with an excess of $PhSiH_3$ at room temperature (Scheme 8), $Mo(PMe_3)_4H_2(SiH_2Ph)_2$ is formed as the initial product and may be isolated if the reaction mixture is immediately cooled to -15 ˚C. This complex is presumably formed by the oxidative addition of two equivalents of $PhSiH_3$ across molybdenum and represents fairly conventional metal-silane chemistry. This complex exhibits limited stability, however, and in the presence of $PhSiH_3$, it converts to the *silyl* (SiH_3) complex, $Mo(PMe_3)_4H_2(SiH_2Ph)(SiH_3)$. $Mo(PMe_3)_4H_2(SiH_2Ph)(SiH_3)$ further reacts with $PhSiH_3$ to form $Mo(PMe_3)_4H_2(SiH_3)_2$, which may also be prepared directly *via* addition of silane (SiH_4) to $Mo(PMe_3)_6$ (see Section 1.2). Both diphenylsilane (Ph_2SiH_2) and silane are produced over the course of this reaction, demonstrating that $Mo(PMe_3)_6$ is capable of effecting the redistribution of $PhSiH_3$. In solution, $Mo(PMe_3)_4H_2(SiH_2Ph)_2$, $Mo(PMe_3)_4H_2(SiH_2Ph)(SiH_3)$, and $Mo(PMe_3)_4H_2(SiH_3)_2$ all form a single final product, $Mo(PMe_3)_4H_3(SiH_3)$, with varying degrees of decomposition. The molecular structures of $Mo(PMe_3)_4H_2(SiH_2Ph)_2$ and $Mo(PMe_3)_4H_2(SiH_2Ph)(SiH_3)$ are shown in Figures 7 and 8, respectively.

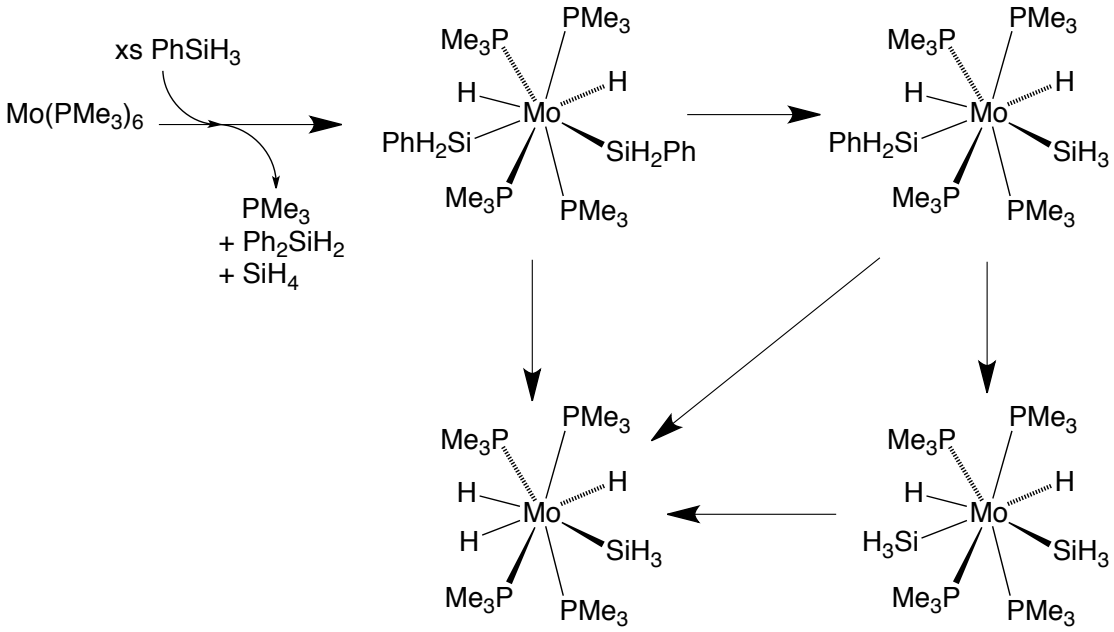

Scheme 8. Reaction of $Mo(PMe_3)_6$ with excess $PhSiH_3$

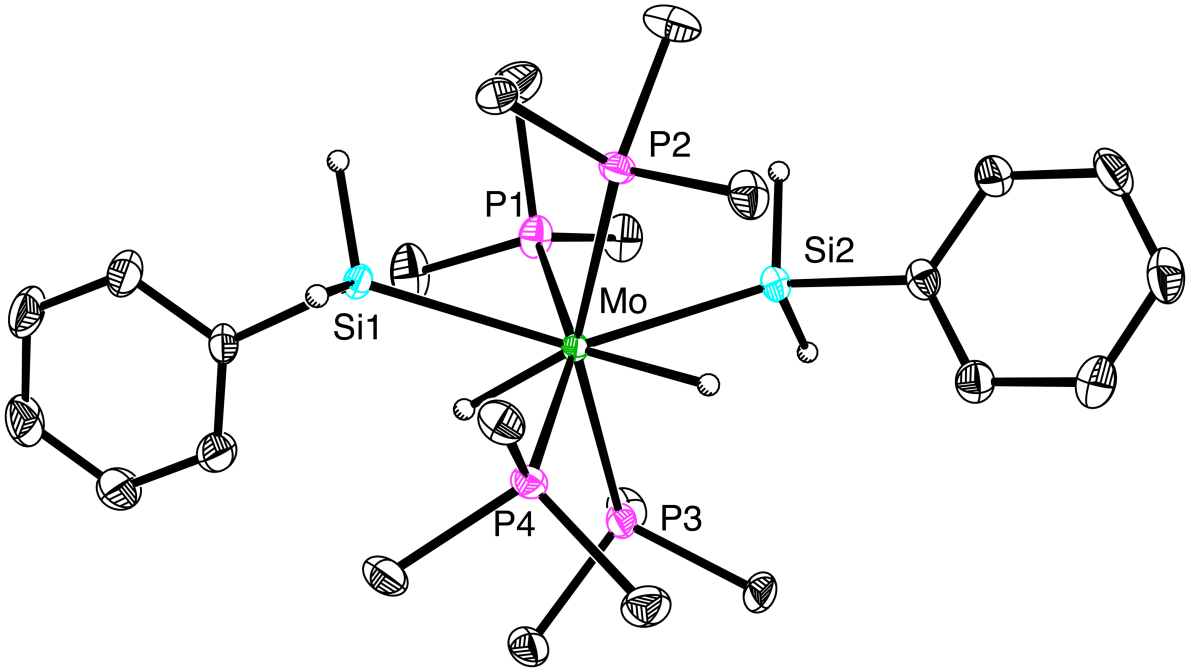

Figure 7. Molecular Structure of $Mo(PMe_3)_4H_2(SiH_2Ph)_2$

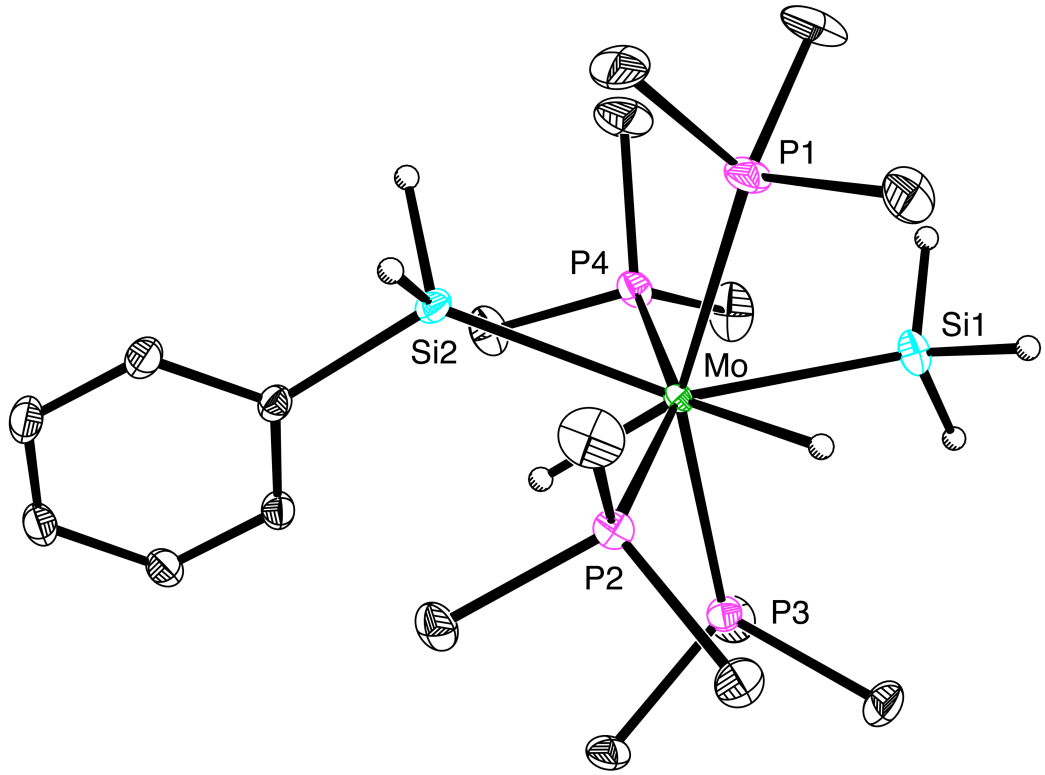

Figure 8. Molecular Structure of $Mo(PMe_3)_4H_2(SiH_2Ph)(SiH_3)$

This sequence of products is noteworthy for a couple of reasons. First, the isolation of M-SiH_3 compounds is rare; there are only six compounds of the type TM-SiH_3 (TM = transition metal) in the Cambridge Structural Database.[7d,f,17,18] The fact that a series of products featuring Mo-SiH_3 moieties is produced in favor of the initial $Mo(PMe_3)_4H_2(SiH_2Ph)_2$ compound is, therefore, of interest. Second, there is no precedent for the isolation of metal complexes with a terminal SiH_3 ligand derived from phenylsilane.[19] This is somewhat surprising given the well-established ability of transition metals to catalyze the redistribution of organosilanes.[20]

1.3.2 Mechanistic Considerations

While the mechanistic details of this reaction have not been explored in great detail, the H/D exchange experiments of $Mo(PMe_3)_4H_2(SiH_3)_2$ with SiD_4 suggest that these molybdenum bis(silyl) compounds may also be generated *via* a sigma bond metathesis pathway. For example, sigma bond metathesis would explain the generation of SiH_4, Ph_2SiH_2, and the Mo-SiH_3 moieties. Two versions of such a mechanism may be considered: (*i*) one in which $PhSiH_3$ undergoes metathesis directly with a Mo-SiH_2Ph ligand, or (*ii*) one in which a fluxional sigma complex enables metathesis of the free silane with the Mo-Ph group (Scheme 9). Computational work done by other groups, along with the mechanistic analysis of the $Mo(PMe_3)_4H_2(SiH_3)_2$ system, suggest that path (*ii*) may be the more energetically favored alternative.[21,22] Furthermore, the catalytic redistribution of $PhSiH_3$ into Ph_2SiH_2 and SiH_4 is well known; it is typically observed for d^0 transition metals[23] and lanthanides,[19a,b,24] for which σ-bond metathesis mechanisms are generally invoked.[25]

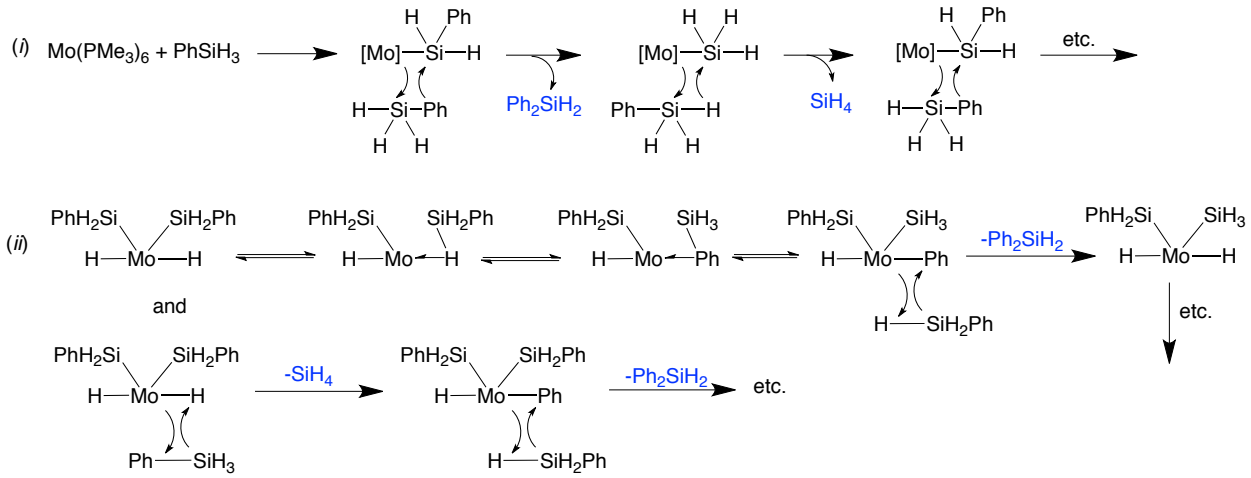

Scheme 9. Proposed Sigma Bond Metathesis Mechanism for Mo-SiH_3 Generation

It is worth noting that mechanisms involving oxidative addition and reductive elimination may also explain the observed products. For example, direct oxidative cleavage of the Si-C bond would form a Mo(Ph)(SiH_3) intermediate, which could undergo reductive elimination of Ph_2SiH_2 to produce the observed products (Scheme 10). It may be expected that elimination of PhH would also occur from this intermediate; however, no benzene was observed when the reaction was performed in deuterated cyclohexane. Furthermore, no toluene was produced when the reaction was performed in benzene with *para*-tolyl silane.

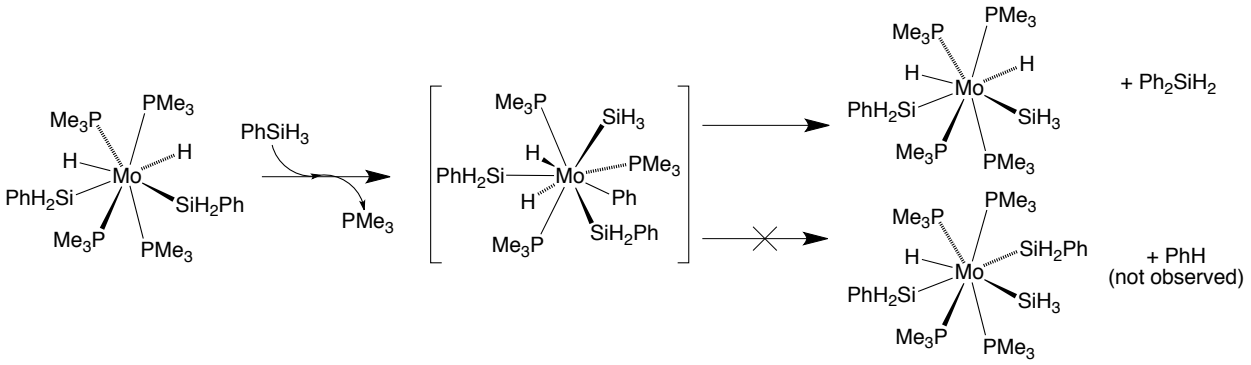

Scheme 10. An O.A. / R.E. mechanism to explain Mo-SiH_3 generation

While the formation of M-SiH_3 groups from $PhSiH_3$ is unusual, DFT calculations support this observed reactivity and confirm that it is energetically favorable. For

example, the energies of the geometry optimized structures of $Mo(PMe_3)_4H_2(SiH_2Ph)_2$, $Mo(PMe_3)_4H_2(SiH_2Ph)(SiH_3)$, $Mo(PMe_3)_4H_2(SiH_3)_2$, $PhSiH_3$, and Ph_2SiH_2 indicate that the generation of the Mo-SiH_3 compounds is thermodynamically downhill (Scheme 11).

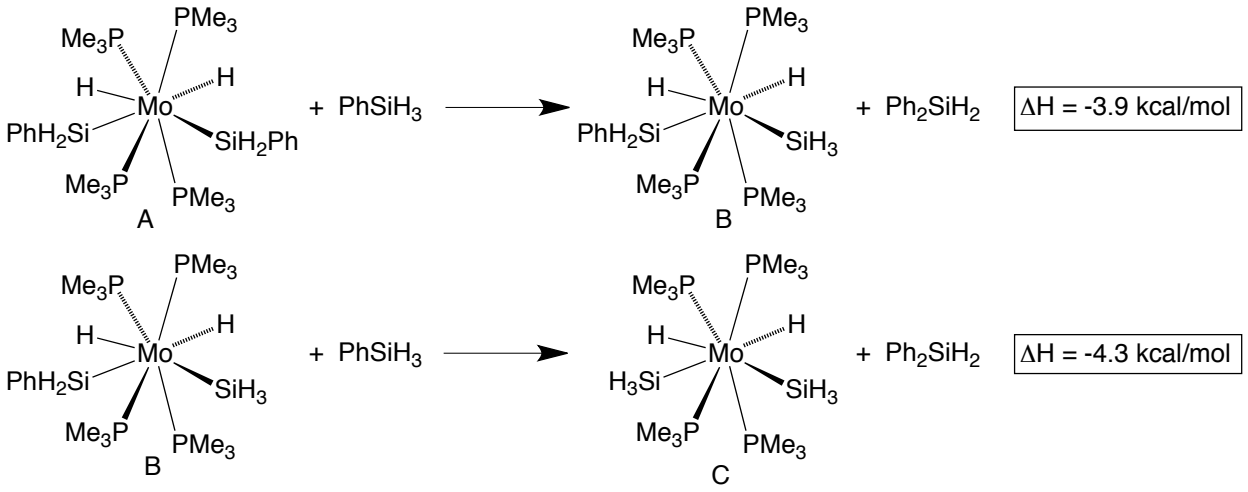

Scheme 11. Thermodynamics of Mo-SiH_3 Generation

1.4 $Mo(PMe_3)_6 + Ph_2SiH_2$

1.4.1 Formation of Hypervalent Silyl, Disilane, and Silane Complexes

The reactivity of $Mo(PMe_3)_6$ towards Ph_2SiH_2 is quite different from that towards SiH_4 and $PhSiH_3$. As described above, $Mo(PMe_3)_6$ oxidatively cleaves the Si-H bond of two equivalents of SiH_4 or $PhSiH_3$ to form bis(silyl) or bis(phenylsilyl) species, which can then undergo further reaction in the presence of free silane. Rather than simply cleave the Si-H bond of Ph_2SiH_2, $Mo(PMe_3)_6$ forms, *inter alia*, novel hypervalent silyl and disilane complexes. Specifically, the major products of this reaction are $Mo(PMe_3)_4H(\kappa^2\text{-}H_2\text{-}H_2SiPh_2H)$ and $Mo(PMe_3)_3H_2(\kappa^2\text{-}H_2\text{-}H_2Si_2Ph_4)$.[26] Both of these complexes react with H_2 to form the diphenylsilane adduct, $Mo(PMe_3)_3H_4(\sigma\text{-}HSiHPh_2)$ (Scheme 12).

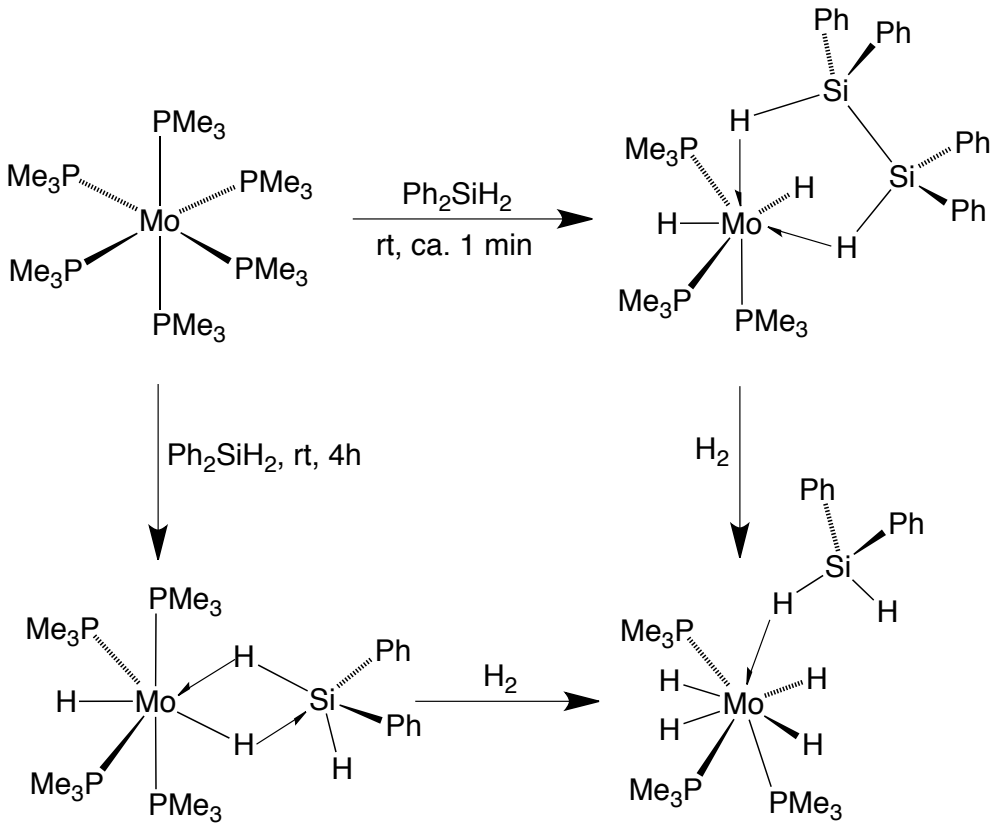

Scheme 12. Reactivity of $Mo(PMe_3)_6$ towards Ph_2SiH_2

1.4.2 Structure and Dynamics of $Mo(PMe_3)_4H(\kappa^2\text{-}H_2\text{-}H_2SiPh_2H)$

$Mo(PMe_3)_4H(\kappa^2\text{-}H_2\text{-}H_2SiPh_2H)$, the major product at room temperature, is the first structurally characterized complex with a hypervalent $\kappa^2\text{-}H_2\text{-}H_2SiPh_2H$ ligand (Figure 9); for example, the Si-H [1.69(3) Å, 1.74(3) Å] and Mo-H [1.62(3), 1.88(3) Å] distances are reflective of two 3-center, 2-electron interactions between the silicon, molybdenum, and bridging hydride ligands.[1a] A number of complexes of the type $M[H_2SiR_3]$ have been previously reported, and the bonding in these compounds has been described in terms of a number of models, including (*i*) silyl-dihydride, (*ii*) σ-silane-hydride, and (*iii*) symmetric hypervalent $[H_2SiR_3]$ formalisms. For example, another complex with a $[H_2SiPh_2H]$ moiety has been structurally characterized, namely $Cp^*W(CO)_2(SiHPh_2)H_2$[27]; however, this complex was reported as a silyl-dihydride, and the much longer Si-H distances [1.92 and 2.00 Å] indicate that this assignment is appropriate.

$Mo(PMe_3)_4H(\kappa^2\text{-}H_2\text{-}H_2SiPh_2H)$ is fluxional at room temperature, such that the terminal hydride and bridging hydrides appear as a single resonance at δ -4.88. The signal appears as a broad quintet at room temperature that sharpens upon heating. The unique Si-H appears much further downfield as a broad singlet at δ 6.58 (Figure 10).

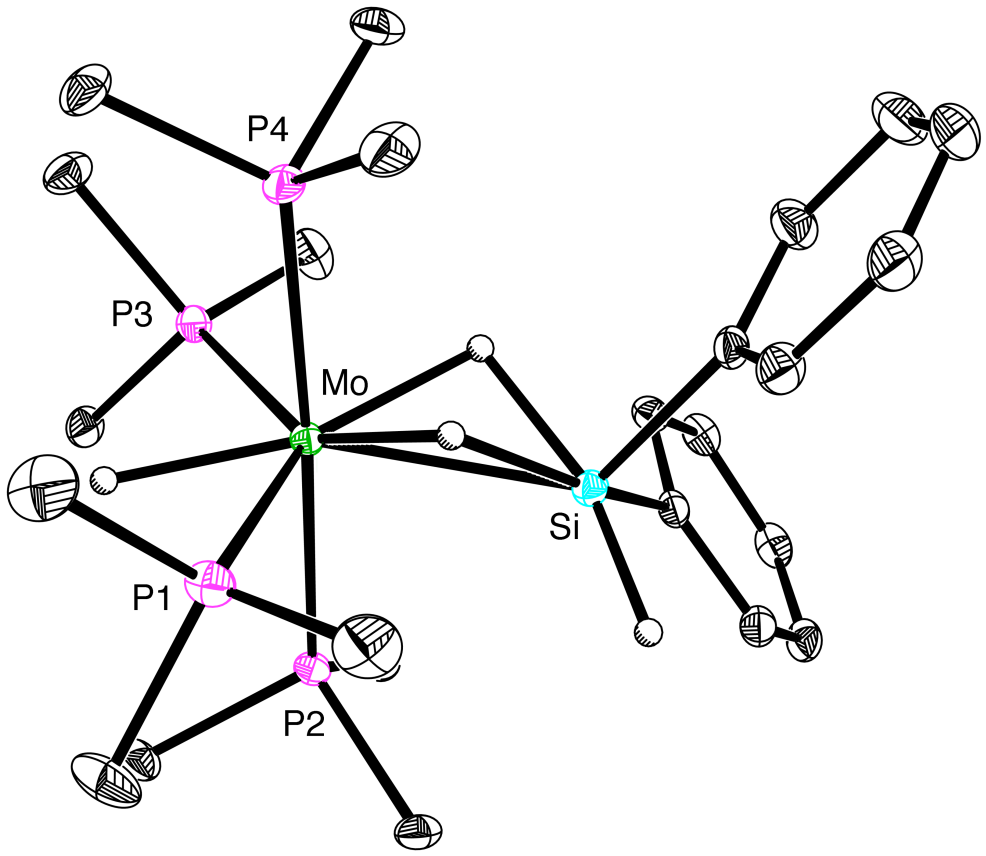

Figure 9. Molecular Structure of $Mo(PMe_3)_4H(\kappa^2\text{-}H_2\text{-}H_2SiPh_2H)$

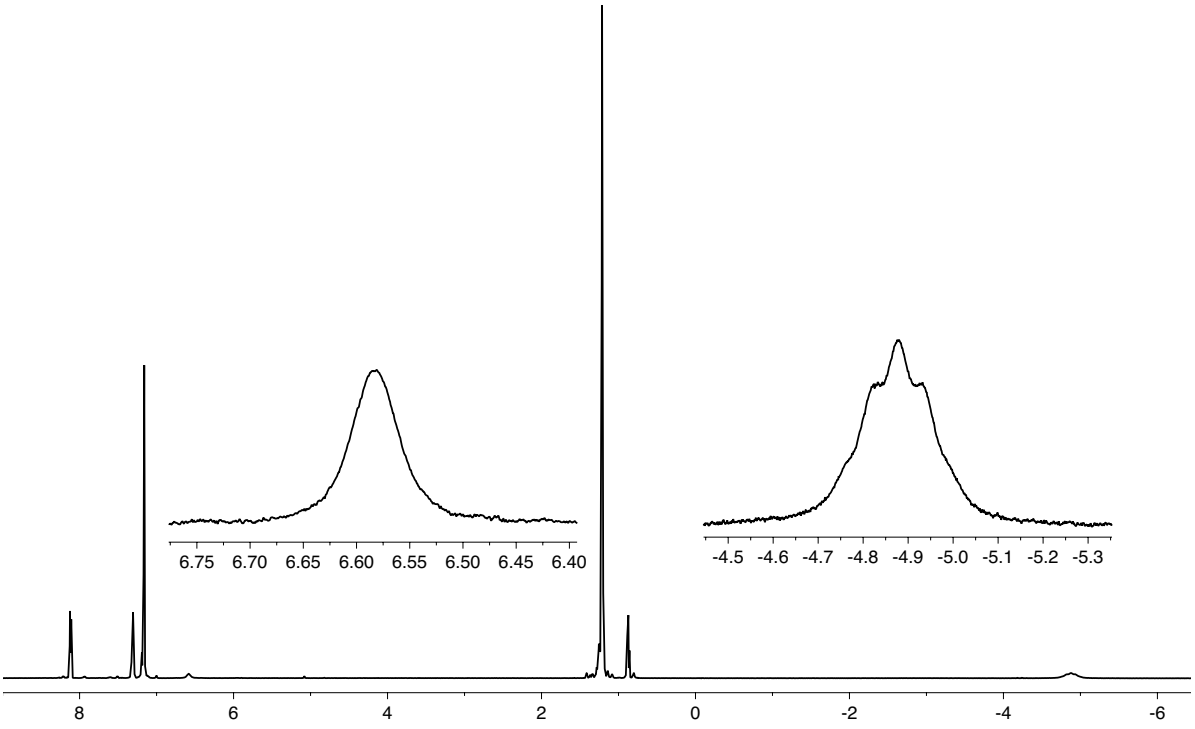

Figure 10. ^{1}H NMR Spectrum of Mo(PMe$_3$)$_4$H(κ^2-*H*$_2$-H$_2$SiPh$_2$H)

When the reaction of Mo(PMe$_3$)$_6$ with Ph$_2$SiH$_2$ is monitored by ^{1}H NMR spectroscopy, the formation of the signals attributable to Mo(PMe$_3$)$_4$H(κ^2-*H*$_2$-H$_2$SiPh$_2$H) is preceded by two quintets in the silyl and hydride regions, whose intensities decrease as Mo(PMe$_3$)$_4$H(κ^2-*H*$_2$-H$_2$SiPh$_2$H) is formed. It is proposed, therefore, that a species such as Mo(PMe$_3$)$_4$H$_3$(SiHPh$_2$) or Mo(PMe$_3$)$_4$H$_2$(σ-HSiHPh$_2$) may form initially and then isomerize to the observed product. In accord with this suggestion, the calculated energies of the geometry optimized structures of these species in the gas phase are all quite close in energy (Figure 11).

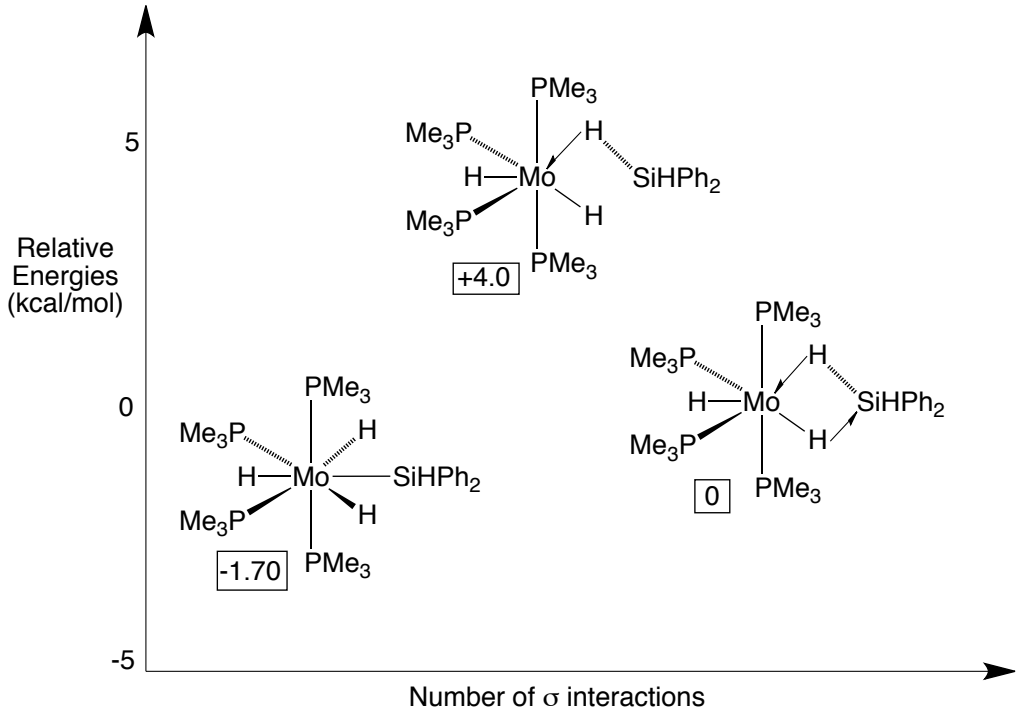

Figure 11. Relative Energies of Mo[H_2SiPh_2H] Species

1.4.3 $Mo(PMe_3)_4H_3(GeHPh_2)$: Comparison to $Mo(PMe_3)_4H(\kappa^2\text{-}H_2\text{-}H_2SiPh_2H)$

The reaction of $Mo(PMe_3)_6$ with Ph_2GeH_2 provides an interesting contrast to the reactivity described above. For example, the major product at room temperature is $Mo(PMe_3)_4H_3(GeHPh_2)$ (Figure 12), rather than a hypervalent germyl derivative. Interestingly, $Mo(PMe_3)_6$ appears to react with Ph_2GeH_2 in much the same manner as it does with Ph_2SiH_2, based on ^1H NMR spectroscopic analysis of the reaction; specifically, the initial product is characterized by a sharp quintet in the hydride region (δ -3.47), which becomes a broad resonance at δ -4.25 after a two hours at room temperature. However, the unique Ge-H hydrogen of the final product is characterized by a quintet at δ 5.63, which is in contrast to the broad singlet that is observed for the Si-H hydrogen in $Mo(PMe_3)_4H(\kappa^2\text{-}H_2\text{-}H_2SiPh_2H)$.

Furthermore, X-ray crystallographic analysis confirms that the final product is $Mo(PMe_3)_4H_3(GeHPh_2)$. As an example of the differences between the related silyl and germyl structures, the distance between the germanium and the closest hydride is 2.480

Å, which is substantially longer than the Si-$H_{hydride}$ distances observed in $Mo(PMe_3)_4H(\kappa^2\text{-}H_2\text{-}H_2SiPh_2H)$ [*i.e.* 1.69(3) Å and 1.74(3) Å]. Thus, the isolation of $Mo(PMe_3)_4H_3(GeHPh_2)$ supports the plausibility of silyl-hydride tautomers in the Ph_2SiH_2 system.

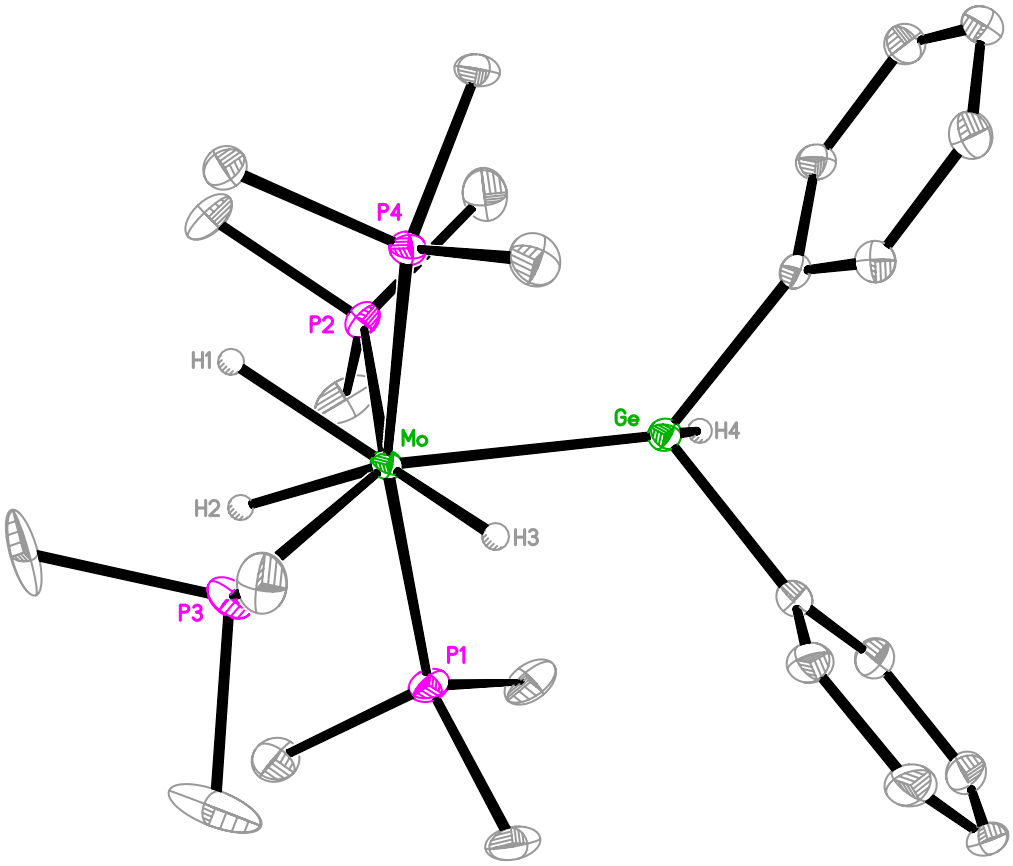

Figure 12. Molecular Structure of $Mo(PMe_3)_4H_3(GeHPh_2)$

1.4.4 Structure and Dynamics of $Mo(PMe_3)_3H_2(\kappa^2\text{-}H_2\text{-}H_2Si_2Ph_4)$

$Mo(PMe_3)_3H_2(\kappa^2\text{-}H_2\text{-}H_2Si_2Ph_4)$, which is formed as an initial product, is the first example of a structurally characterized disilane complex (Figure 13). The disilane chelates in an asymmetric fashion, with Mo-Si distances of 2.5322(8) Å and 2.7140(8) Å.[28] This complex decomposes rapidly at room temperature and is isolated only when the reaction is performed in pentane and immediately cooled to -15 ˚C. In addition to dehydrocoupling, this system is also capable of effecting redistribution; for example, $H_2PhSi\text{-}SiPh_3$[29] is produced over the course of the reaction but does not appear to

coordinate to the metal center, most likely due to steric bulk. Significantly, treatment of $Mo(PMe_3)_6$ with tetraphenyldisilane (Ph_2HSi-$SiHPh_2$) does *not* result in the formation of $Mo(PMe_3)_3H_2(\kappa^2$-H_2-$H_2Si_2Ph_4)$, which suggests that coordination of the disilane is contingent upon Si-Si bond formation at the metal center.

Like $Mo(PMe_3)_4H(\kappa^2$-H_2-$H_2SiPh_2H)$, $Mo(PMe_3)_3H_2(\kappa^2$-H_2-$H_2Si_2Ph_4)$ is fluxional and produces a ^1H NMR spectrum in which the terminal and bridging hydrides appear as a single resonance. This signal at δ -4.62 is a broad singlet that becomes a sharp quartet at 250 K. Interestingly, this signal broadens again upon further cooling to form a broad singlet at 193 K (Figure 14). We postulate that the broadening at high temperature is due to phosphine dissociation, while the broadening at low temperature is due to slow intramolecular exchange.

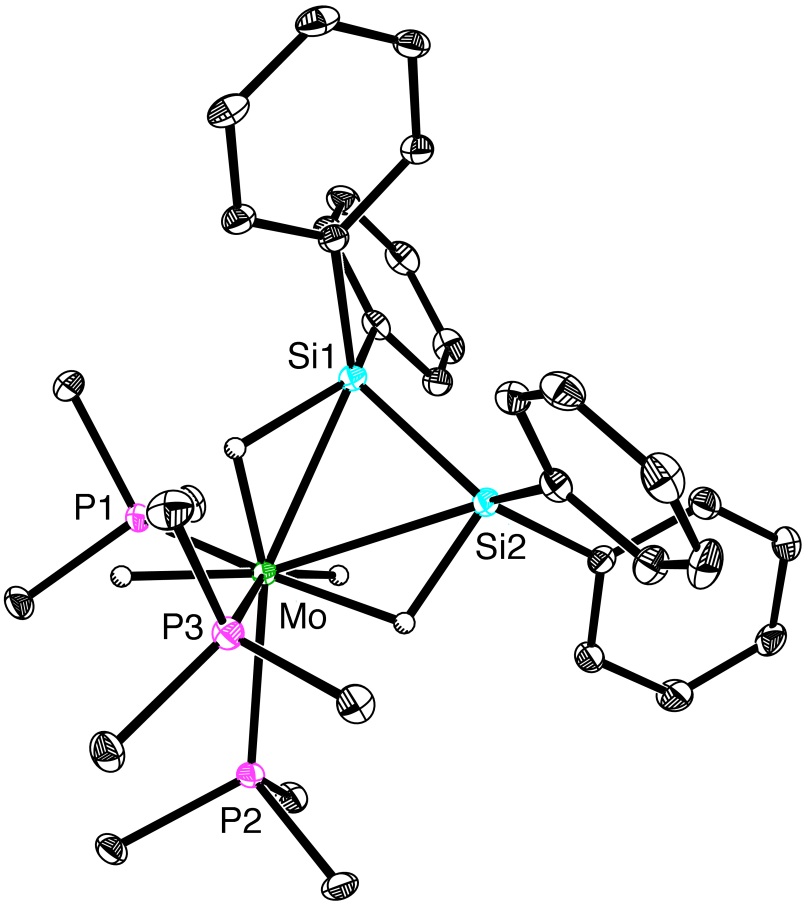

Figure 13. Molecular Structure of $Mo(PMe_3)_3H_2(\kappa^2$-H_2-$H_2Si_2Ph_4)$

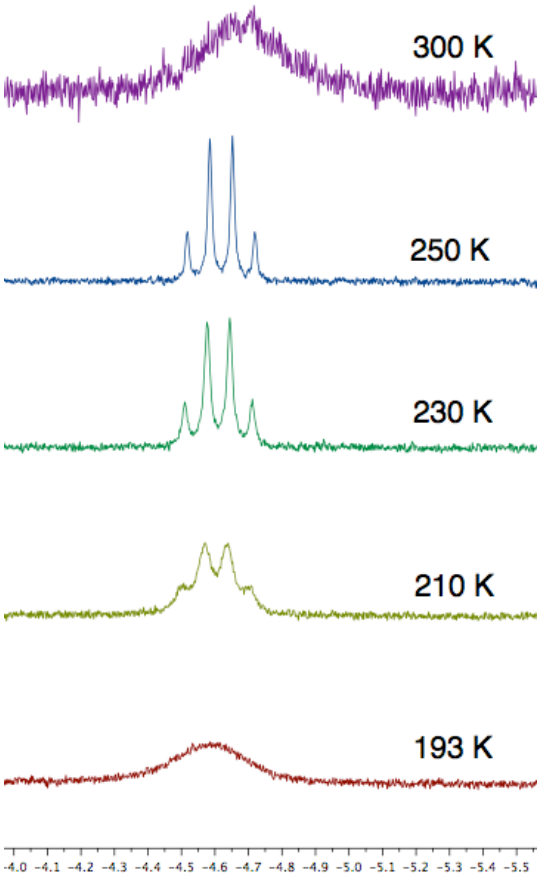

Figure 14. Low Temperature NMR of $Mo(PMe_3)_3H_2(\kappa^2\text{-}H_2\text{-}H_2Si_2Ph_4)$

1.4.5 Preparation and Discussion of $Mo(PMe_3)_3H_4(\sigma\text{-}HSiHPh_2)$

Both $Mo(PMe_3)_4H(\kappa^2\text{-}H_2\text{-}H_2SiPh_2H)$ and $Mo(PMe_3)_3H_2(\kappa^2\text{-}H_2\text{-}H_2Si_2Ph_4)$ react with H_2 to form the σ-complex $Mo(PMe_3)_3H_4(\sigma\text{-}HSiHPh_2)$. While the reaction of the disilane complex proceeds rapidly and quite cleanly at room temperature to form $Mo(PMe_3)_3H_4(\sigma\text{-}HSiHPh_2)$, the reaction of $Mo(PMe_3)_4H(\kappa^2\text{-}H_2\text{-}H_2SiPh_2H)$ with H_2 produces a substantial amount of $Mo(PMe_3)_4H_4$ in addition to $Mo(PMe_3)_3H_4(\sigma\text{-}HSiHPh_2)$.

The molecular structure of $Mo(PMe_3)_3H_4(\sigma\text{-}HSiHPh_2)$ (Figure 15) is characterized by Mo-Si [2.500(1) Å], Mo-H [1.64(5) Å], and Si-H [1.74(4) Å] distances that are in accord with its assignment as a diphenylsilane adduct.[30] For example, the Si–H bond length is

within the range accepted for σ-complexes (1.7 – 1.8 Å).[1a] Significantly, the Mo–Si bond length [2.500(1) Å] in this complex is slightly shorter than the Mo–SiR_3 bond lengths for the silyl compounds reported herein (2.56 Å – 2.58 Å). Thus, although it may be expected that an M–Si distance could correlate with the degree of activation of an Si–H bond, it is evident that this relationship may not always be true.[30b,31,32]

For comparison, a similar species, namely $Mo(depe)_2(CO)(\sigma\text{-}HSiHPh_2)$ [depe = (diethylphosphino)ethane] has previously been isolated by Kubas et al.[6] While the solid-state structures of $Mo(PMe_3)_3H_4(\sigma\text{-}HSiHPh_2)$ and $Mo(depe)_2(CO)(\sigma\text{-}HSiHPh_2)$ share important similarities[6a] with respect to the diphenylsilane ligand,[33] their properties in solution are decidedly different.[6b] Specifically, NMR spectroscopic analysis of $Mo(depe)_2(CO)(\sigma\text{-}HSiHPh_2)$ indicates that the compound is structurally static on the NMR timescale, which is expected for an octahedral compound.[6b] The bridging Mo-H-Si hydrogen demonstrates coupling to the phosphorus nuclei, the silicon nucleus, and the uncoordinated Si-H proton; furthermore, the $^{31}P\{^1H\}$ NMR spectrum shows four resonances corresponding to inequivalent phosphorus nuclei. $Mo(PMe_3)_3H_4(\sigma\text{-}HSiHPh_2)$, on the other hand, is fluxional on the NMR timescale, such that the phenyl groups, phosphine ligands, and hydrides are all equivalent. Furthermore, the Si-H proton that interacts with the metal center exchanges with the other hydrides, resulting in a single resonance at δ -4.21 corresponding to five hydrogens. In addition, the Si-H hydrogens do not couple to each other, and the terminal Si-H hydrogen appears much further downfield at δ 6.48.

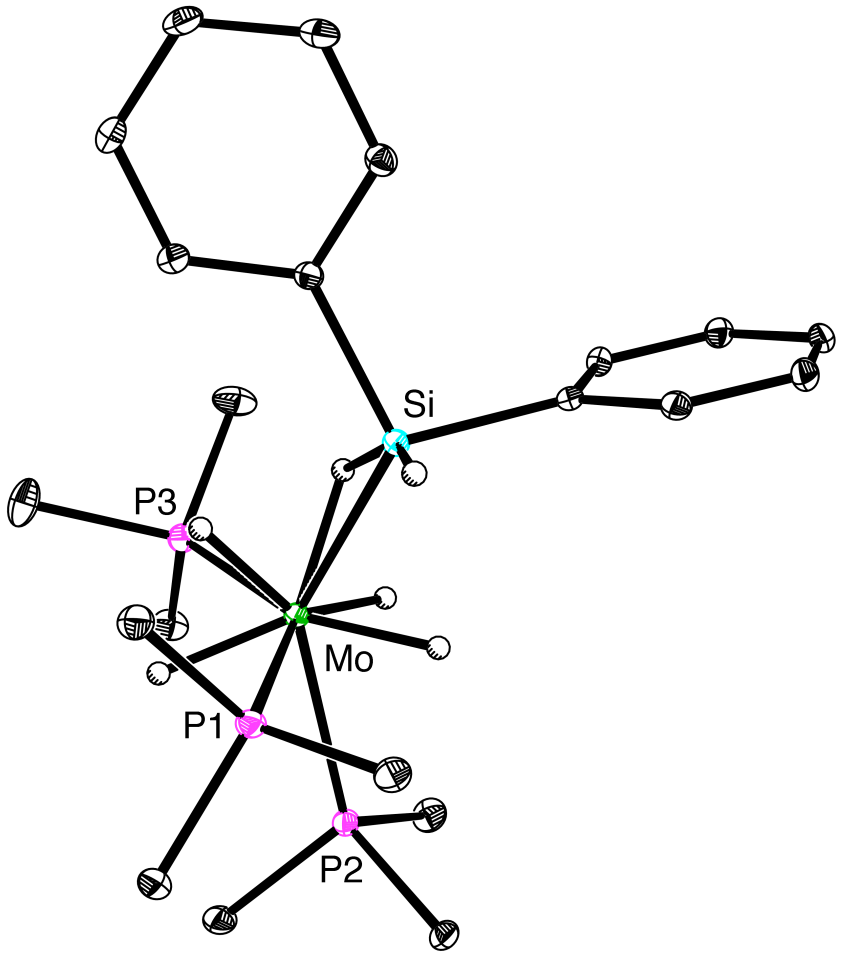

Figure 15. Molecular Structure of $Mo(PMe_3)_3H_4(\sigma\text{-}HSiHPh_2)$

1.4.5 Use of NBO Calculations towards Bonding Analysis

While $Mo(PMe_3)_4H(\kappa^2\text{-}H_2\text{-}H_2SiPh_2H)$, $Mo(PMe_3)_3H_2(\kappa^2\text{-}H_2\text{-}H_2Si_2Ph_4)$, and $Mo(PMe_3)_3H_4(\sigma\text{-}HSiHPh_2)$ all feature delocalized bonding in their solid-state structures, the fluxionality of these compounds in solution precludes further investigation of their bonding motifs. For example, the coupling constant between silicon and hydrogen, $J_{Si\text{-}H}$, has often been used to characterize σ-complexes. $J_{Si\text{-}H}$ coupling constants for coordinated Si-H bonds are typically between 30-70 Hz, compared to $^1J_{Si\text{-}H}$ values of > 150 Hz for non-coordinated Si-H silyl ligands and $^2J_{Si\text{-}H}$ values of < 20 Hz for the 2-bond coupling between silyl and hydride ligands.[1a] Since these complexes are fluxional, any significant $J_{Si\text{-}H}$ coupling for the σ-SiH hydrogen is averaged with the much smaller $^2J_{Si\text{-}H}$ of the hydride ligands.[34]

Furthermore, IR spectroscopy is not particularly helpful in analyzing these complexes. Specifically, the $\nu_{Mo\text{-}H\text{-}Si}$ stretching frequencies for $Mo(PMe_3)_4H(\kappa^2\text{-}H_2\text{-}H_2SiPh_2H)$ and $Mo(PMe_3)_3H_2(\kappa^2\text{-}H_2\text{-}H_2Si_2Ph_4)$ appear at 1601 cm^{-1} and 1704 cm^{-1}, respectively, which are within the range of previously reported values.[1a] However, these stretches overlap with the non-bridging Mo-H moiety stretches and thus do not provide additional information about the uniqueness of these hydrides.

In order to support the bonding description derived from the crystal structures of these compounds, geometry optimization calculations were performed, and Natural Bond Orbital (NBO) analysis was used to further probe the delocalized bonding that appears to be present in each structure. NBO analysis provides insight into bonding by producing orbitals that are localized primarily on one atom (lone pair), two atoms (bond pair), or three atoms (3-center, 2-electron interactions). In addition to Natural Bonding Orbitals, NBO analysis also generates Natural Localized Molecular Orbitals, which take into account the interaction between bonding (or non-bonding) and antibonding orbitals (*e.g.* backbonding.) The geometry optimizations for these compounds accurately reproduce the solid state structures, and the results of NBO analysis indicate that there is, in fact, delocalized bonding in each complex (Figure 16). $Mo(PMe_3)_4H(\kappa^2\text{-}H_2\text{-}H_2SiPh_2H)$ is defined by two 3-center, 2-electron interactions between the molybdenum, silicon, and two bridging hydrides. $Mo(PMe_3)_3H_2(\kappa^2\text{-}H_2\text{-}H_2Si_2Ph_4)$ also features two 3-center, 2-electron interactions for the coordinating disilane. Interestingly, the percent contribution of molybdenum is much smaller in one orbital than it is in the other, which reflects the asymmetry of the disilane chelation. Finally, the Mo-H-Si interaction of $Mo(PMe_3)_3H_4(\sigma\text{-}HSiHPh_2)$ is composed of both donation of the Si-H bonding electrons towards the metal center and backbonding of a molybdenum d-orbital into the Si-H antibonding orbital (Figure 16).

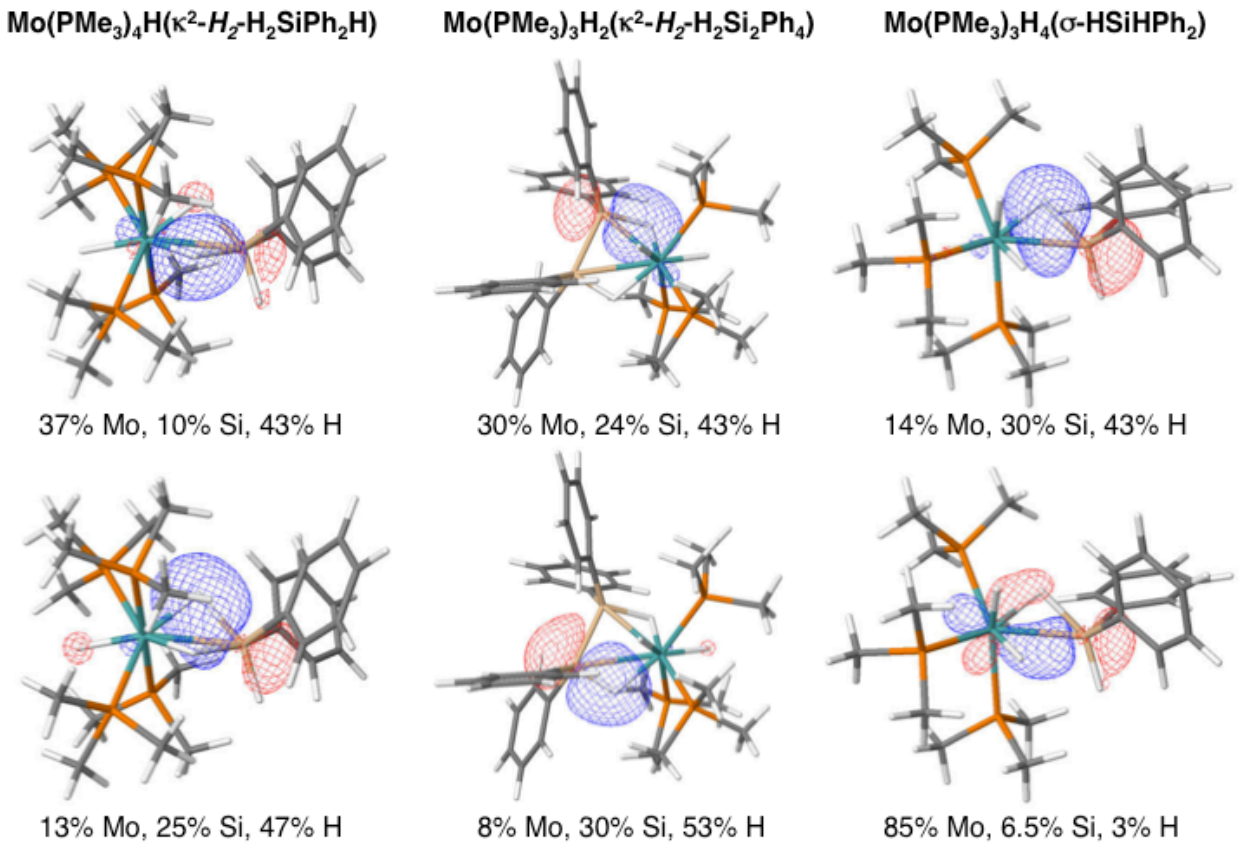

Figure 16. Relevant NLMOs for $Mo(PMe_3)_4H(\kappa^2\text{-}H_2\text{-}H_2SiPh_2H)$, $Mo(PMe_3)_3H_2(\kappa^2\text{-}H_2\text{-}H_2Si_2Ph_4)$, and $Mo(PMe_3)_3H_4(\sigma\text{-}HSiHPh_2)$. The percent contributions of each atom are listed below the orbital.

1.5 $Mo(PMe_3)_6 + Ph_3SiH$

In contrast to the reactivity of $Mo(PMe_3)_6$ towards SiH_4, $PhSiH_3$, and Ph_2SiH_2, which involves the cleavage of Si-H bonds, the reaction of $Mo(PMe_3)_6$ with Ph_3SiH results in coordination of Ph_3SiH through a phenyl group to produce the η^6-arene complex, $(\eta^6\text{-}C_6H_5SiPh_2H)Mo(PMe_3)_3$ (Scheme 13). Coordination of Ph_3SiH through a phenyl group is rare – there is only one other structurally characterized complex featuring such coordination, namely $(\eta^6\text{-}C_6H_5SiPh_2H)W(CO)_3$,[35] reported in the Cambridge Structural Database. The molecular structure is shown in Figure 17.

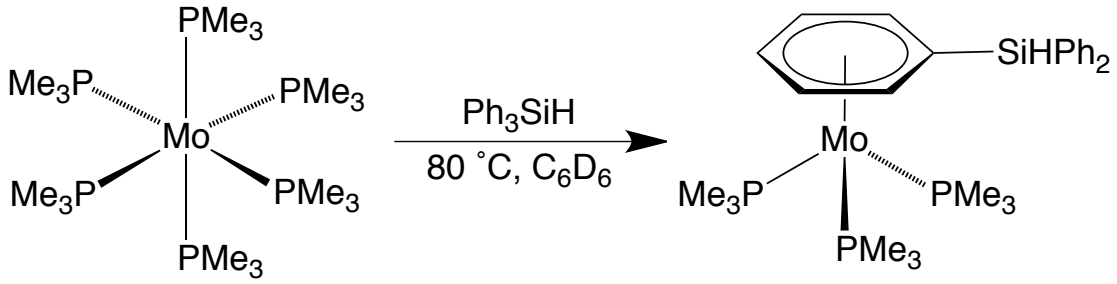

Scheme 13. Reaction of $Mo(PMe_3)_6$ with Ph_3SiH

It is worth noting that this conversion occurs to the almost complete exclusion of the benzene adduct, $(\eta^6\text{-}C_6D_6)Mo(PMe_3)_3$, when the reaction is performed in benzene. Since the coordination of benzene would be expected to compete kinetically with Ph_3SiH under these conditions, it was considered that the benzene adduct $(\eta^6\text{-}C_6D_6)Mo(PMe_3)_3$ could be an intermediate en route to the Ph_3SiH complex. Several observations, however, suggest that benzene coordination does not precede coordination of Ph_3SiH. Specifically, *(i)* $Mo(PMe_3)_6$ does not react with C_6D_6 sufficiently rapidly at 80 ˚C to allow $(\eta^6\text{-}C_6D_6)Mo(PMe_3)_3$ to be a viable intermediate;[36] *(ii)* $(\eta^6\text{-}C_6D_6)Mo(PMe_3)_3$ does not react readily with Ph_3SiH to give $(\eta^6\text{-}C_6H_5SiPh_2H)Mo(PMe_3)_3$ at 80 ˚C; *(iii)* arene exchange between $(\eta^6\text{-}C_6H_6)Mo(PMe_3)_3$ and C_6D_6 is not facile at 80 ˚C; and *(iv)* $Mo(PMe_3)_6$ does not react with Ph_4Si at 80 ˚C. On the basis of these observations, it is postulated that the mechanism for formation of $(\eta^6\text{-}C_6H_5SiPh_2H)Mo(PMe_3)_3$ involves the initial generation of a silane σ–complex that facilitates access to the η^6-arene complex.

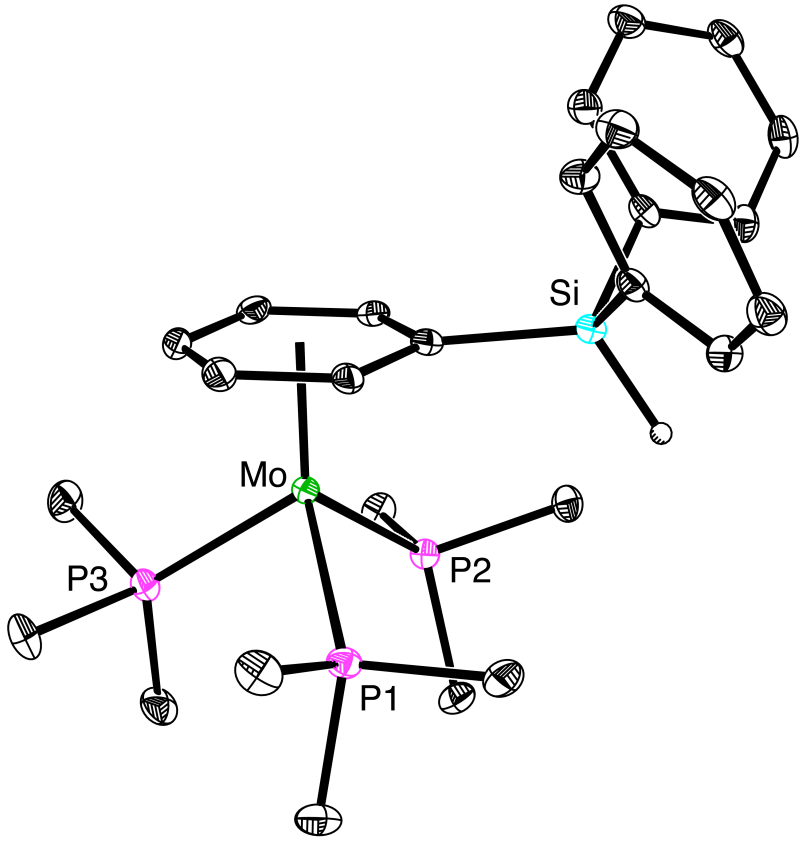

Figure 17. Molecular Structure of (η^6-$C_6H_5SiPh_2H$)$Mo(PMe_3)_3$

1.6 $Mo(PMe_3)_5H_2$ + Ph_xSiH_{4-x}

The reactivity of $Mo(PMe_3)_5H_2$ was examined with SiH_4, $PhSiH_3$, and Ph_2SiH_2. While the products of these reactions are, for the most part, species that are also produced in the reactions of $Mo(PMe_3)_6$ with silanes, the dihydride shows some interesting modes of reactivity. For example, when $Mo(PMe_3)_5H_2$ is treated with SiH_4, a mixture of $Mo(PMe_3)_4H_4$, $Mo(PMe_3)_4H_3(SiH_3)$, and $Mo(PMe_3)_4H_2(SiH_3)_2$ is produced in an approximately 1:4:2 ratio (Scheme 14). The overall product distribution appears to be relatively independent of the stoichiometry of the reaction. One plausible mechanism for this reactivity would involve initial generation of $Mo(PMe_3)_4H_3(SiH_3)$ followed by rapid redistribution to form $Mo(PMe_3)_4H_4$ and $Mo(PMe_3)_4H_2(SiH_3)_2$. However, since this process occurs neither in the presence of $Mo(PMe_3)_6$ nor when $Mo(PMe_3)_4H_3(SiH_3)$ is left

alone in solution, it is likely that such a redistribution process is unique to this reaction specifically.

Also of interest is the fact that the reaction of $Mo(PMe_3)_5H_2$ with $PhSiH_3$ produces the exact same product distribution – $Mo(PMe_3)_4H_4$, $Mo(PMe_3)_4H_3(SiH_3)$, and $Mo(PMe_3)_4H_2(SiH_3)_2$ – in approximately the same ratio (Scheme 14). This is presumably due to facile redistribution of $PhSiH_3$ into Ph_2SiH_2 and SiH_4, which then reacts with $Mo(PMe_3)_5H_2$ to form the observed products. In accord with this hypothesis, bubbling is observed upon treatment of $Mo(PMe_3)_5H_2$ with $PhSiH_3$, and Ph_2SiH_2 and SiH_4 are observed by ^1H NMR spectroscopy.

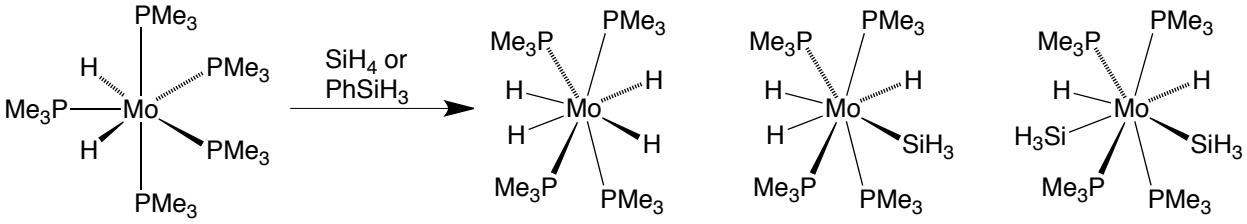

Scheme 14. Reaction of $Mo(PMe_3)_5H_2$ with SiH_4 and $PhSiH_3$

Finally, $Mo(PMe_3)_5H_2$ reacts with Ph_2SiH_2 to form primarily $Mo(PMe_3)_4H(\kappa^2\text{-}H_2\text{-}H_2SiPh_2H)$. This is a rational mode of reactivity given that the generation of $Mo(PMe_3)_4H(\kappa^2\text{-}H_2\text{-}H_2SiPh_2H)$ formally requires an equivalent of H_2, which is provided by the dihydride complex.

1.7 $Mo(PMe_3)_4H_4 + Ph_xSiH_{4-x}$

$Mo(PMe_3)_4H_4$, unlike $Mo(PMe_3)_6$ and $Mo(PMe_3)_5H_2$, does not react with silanes to form complexes; instead, it causes catalytic redistribution. For example, treatment of $Mo(PMe_3)_4H_4$ with Ph_2SiH_2 results in the formation of Ph_3SiH and $PhSiH_3$. Likewise, treatment of the metal complex with $PhSiH_3$ yields Ph_2SiH_2 and SiH_4. Although it is

clear that no redistribution may occur with SiH_4, $Mo(PMe_3)_4H_4$ does react with SiD_4 to form the isotopologues SiH_xD_{4-x}.

1.8 Reactivity of $Mo(PMe_3)_6$ in Hydrosilation

The reactivity of $Mo(PMe_3)_6$ towards silanes is defined by facile redistribution and dehydrocoupling. Thus, it was considered of interest to see if this complex is also active in hydrosilation reactions. Hydrosilation involves the addition of Si-H groups across unsaturated bonds, including C=C and C=O bonds. A series of alkenes, namely 1-hexene, cyclohexene, and 3,3-dimethyl-1-butene, were tested as substrates for olefin hydrosilation; acetone, acetophenone, and 3-pentanone were used to test the reactivity of carbonyl groups. $PhSiH_3$ and Ph_2SiH_2 were examined as silylating agents, and $Mo(PMe_3)_6$ was added as a catalyst.

Although $Mo(PMe_3)_6$ did not produce any hydrosilation products with alkenes, it was found to be an effective agent for the hydrosilation of carbonyl groups (Scheme 15). Specifically, the hydrosilation of acetone and 3-pentanone with $PhSiH_3$ was achieved at 80 ˚C after approximately 12 hours. However, the product distribution derived from these reactions is complex; this is presumably due to the fact that $Mo(PMe_3)_6$ can cause not only hydrosilation across multiple Si-H bonds of silanes, but also redistribution of $PhSiH_3$ into Ph_2SiH_2 and SiH_3. Therefore, the products of hydrosilation in this system are not restricted to derivatives of $PhSiH_x(OCHR_2)_{3-x}$ but may include products of the type $Ph_2SiH_x(OCHR_2)_{2-x}$ and $SiH_x(OCHR_2)_{4-x}$ as well.

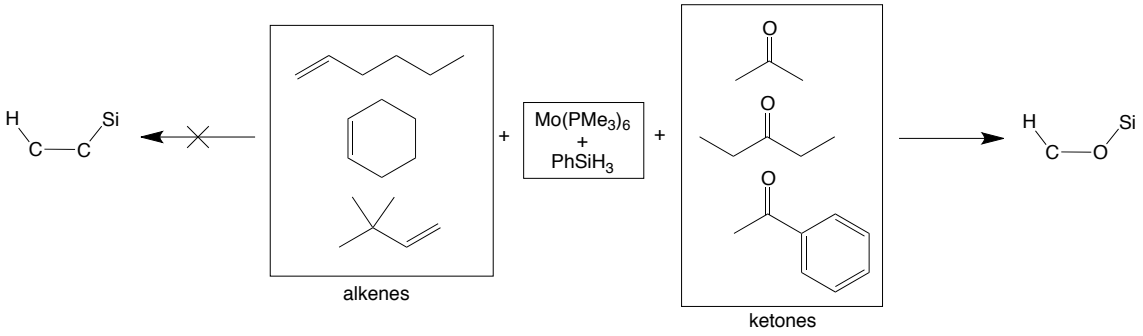

Scheme 15. Substrate scope examined for $Mo(PMe_3)_6$-promoted hydrosilation

1.9 Summary and Conclusions

In summary, $Mo(PMe_3)_6$ exhibits diverse reactivity towards SiH_4, $PhSiH_3$ and Ph_2SiH_2 to afford a variety of novel silyl, hypervalent silyl, silane, and disilane complexes, whereas Ph_3SiH simply forms the η^6-arene complex $(\eta^6\text{-}C_6H_5SiPh_2H)Mo(PMe_3)_3$. While the reactions of non-d^0 metal phosphine hydride compounds are often interpreted in terms of sequences that involve oxidative addition and reductive elimination, NMR spectroscopic analysis of the isotope exchange reaction between $Mo(PMe_3)_4(SiH_3)_2H_2$ and SiD_4 indicates that the reaction does not occur *via* initial reductive elimination of SiH_4, but rather by a metathesis pathway. The validity of the transition states (*i.e.* complexes with hypervalent silyl and σ-silane ligands) proposed for such a pathway are supported by the isolation of similar complexes from the reaction of $Mo(PMe_3)_6$ with Ph_2SiH_2.

Thus, in examining the reactivity of $Mo(PMe_3)_6$ with hydrosilanes, we have isolated a series of novel complexes that exhibit redistribution and dehydrocoupling, which are both significant reactions in silane chemistry. The unique binding modes of the silyl ligands in these complexes provide insight into the interaction of hydrosilanes with metal complexes, which may prove useful in the mechanistic exploration of silane chemistry and in the development of new catalysts for these reactions.

1.10 Experimental Details

1.10.1 General Considerations

All manipulations were performed using a combination of glovebox, high vacuum, and Schlenk techniques under an argon atmosphere.[37] Solvents were purified and degassed by standard procedures. NMR spectra were measured on Bruker 300 DRX, Bruker 300 DPX, Bruker 400 Avance III, Bruker 400 Cyber-enabled Avance III, and Bruker 500 DMX spectrometers. ^1H chemical shifts are reported in ppm relative to $SiMe_4$ ($\delta = 0$) and were referenced internally with respect to the protio solvent impurity ($\delta = 7.16$ for C_6D_5H,

2.08 for C_7D_7H).[38] ^{31}P chemical shifts are reported in ppm relative to 85% H_3PO_4 ($\delta = 0$) and were referenced using $P(OMe)_3$ ($\delta = 141.0$) as an external standard.[39] ^{29}Si chemical shifts are reported in ppm relative to external 1% $SiMe_4$ in $CDCl_3$ ($\delta = 0$). Coupling constants are given in hertz. Infrared spectra were recorded on a PerkinElmer Spectrum Two spectrometer and are reported in cm^{-1}. $Mo(PMe_3)_6$[40], $Mo(PMe_3)_5H_2$[41], and $Mo(PMe_3)_4H_4$[42] were prepared by the literature methods, while SiD_4[43] and $PhSiD_3$[44] were prepared *via* the literature method used for the protio counterparts.

1.10.2 X-ray Structure Determinations

Single crystal X-ray diffraction data were collected on a Bruker Apex II diffractometer, and crystal data, data collection and refinement parameters are summarized in Table 1. The structures were solved using direct methods and standard difference map techniques and were refined by full-matrix least-squares procedures on F^2 with SHELXTL (Version 2008/4).[45]

1.10.3 Computational Details

Calculations were carried out using DFT as implemented in the Jaguar 7.7 suite of *ab initio* quantum chemistry programs.[46] Geometry optimizations (Table 2) were performed with the B3LYP density functional[47] using the 6-31G** (C, H, Si and P) and LACVP** (Mo) basis sets.[48] NBO analyses were performed using Jaguar NBO 5.0.[49]

1.10.4 Synthesis of $Mo(PMe_3)_4H_2(SiH_3)_2$

$Mo(PMe_3)_6$ (100 mg, 0.18 mmol) was treated with a solution of $PhSiH_3$ (300 mg, 2.8 mmol) in C_6H_6 (5 mL). The solution was transferred to an ampoule, degassed, and allowed to stand at room temperature for 3 days. After this period, the brown solution was lyophilized, washed with pentane (4 mL), and dried *in vacuo* to afford $Mo(PMe_3)_4H_2(SiH_3)_2$ as a pale brown solid (44 mg, 52% yield). Pale yellow crystals of $Mo(PMe_3)_4H_2(SiH_3)_2$ suitable for X-ray diffraction were obtained from a solution in

toluene/pentane (50:50) at -15 ˚C. Analysis calcd. for $Mo(PMe_3)_4H_2(SiH_3)_2$: C, 31.0 %; H, 9.6 %. Found: C, 31.3 %; H, 9.2 %. ^1H NMR (C_6D_6): -4.80 [quint, $^2J_{P-H}$ = 26, 2H of $Mo\underline{H}_2$], 1.29 [s, 36H of $Mo(P\underline{Me}_3)_4$], 4.02 [quint, $^3J_{P-H}$ = 8, $^1J_{Si-H}$ = 157, 6H of $Mo(Si\underline{H}_3)_2$]. $^{31}P\{^1H\}$ NMR at 300 K (C_6D_6): -4.3 [s, 4P of $Mo(\underline{P}Me_3)_4$]. $^{31}P\{^1H\}$ NMR at 210 K (C_7D_8): -12.3 [br. s, 2P of $Mo(\underline{P}Me_3)_4$], 5.4 [br. s, 2P of $Mo(\underline{P}Me_3)_4$]. ^1H-^{29}Si HMQC NMR (C_6D_6): -61.5 [s, 2 Si of $Mo(\underline{Si}H_3)_2$]. IR Data (ATR, cm^{-1}): 2989 (w), 2969 (m), 2905 (m), 2800 (w), 2042 (s) [ν_{Si-H}], 1794 (m) [ν_{Mo-H}], 1425 (m), 1296 (m), 1278 (m), 1122 (w), 965 (m), 921 (vs), 851 (s), 736 (w), 697 (s), 656 (s), 598 (s), 566 (m), 523 (m).

1.10.5 Synthesis of $Mo(PMe_3)_4H_3(SiH_3)$

A solution of $Mo(PMe_3)_4H_2(SiH_3)_2$ (5 mg, 0.011 mmol) in C_6D_6 (0.7 mL) in an NMR tube equipped with a J. Young valve was degassed and charged with H_2 (*ca*. 1 atm). The solution was heated at 60 ˚C for 1 day and monitored by ^1H NMR spectroscopy, thereby demonstrating the conversion to $Mo(PMe_3)_4H_3(SiH_3)$. The dark brown solution was lyophilized to give $Mo(PMe_3)_4H_3(SiH_3)$ as a brown solid (2.5 mg, 53 % yield). Colorless crystals of $Mo(PMe_3)_4H_3(SiH_3)$ suitable for X-ray diffraction were obtained from a solution in pentane at -15 ˚C. Analysis calcd. for $Mo(PMe_3)_4H_3(SiH_3)$: C, 33.2 %; H, 9.8 %. Found: C, 33.1 %; H, 9.6 %. ^1H NMR (C_6D_6): -4.39 (quint, $^2J_{P-H}$ = 34, 3H of $Mo\underline{H}_3$)], 1.33 [d, $^2J_{P-H}$ = 6, 36H of $Mo(P\underline{Me}_3)_4$], 3.83 [quint of quart, $^3J_{P-H}$ = 9, $^3J_{H-H}$ = 2, 3H of $Mo(Si\underline{H}_3)^1$]. $^{31}P\{^1H\}$ NMR at 370 K (C_6D_6): 3.3 [s, 4P of $Mo(\underline{P}Me_3)_4$]. $^{31}P\{^1H\}$ NMR at 240 K (C_7D_8): -3.8 [quart, $^2J_{P-P}$ = 17, 1P of $Mo(\underline{P}Me_3)_4$], 3.0 [t, $^2J_{P-P}$ = 20, 2P of $Mo(\underline{P}Me_3)_4$], 15.4 [quart, $^2J_{P-P}$ = 17, 1P of $Mo(\underline{P}Me_3)_4$]. ^1H-^{29}Si HMQC NMR (C_6D_6): -60.8 [s, 1 Si of $Mo(\underline{Si}H_3)$]. IR Data (ATR, cm^{-1}): 2968 (m), 2905 (m), 2189 (w), 2030 (br) [ν_{Si-H}], 1703 (w) [ν_{Mo-H}], 1421 (m), 1296 (m), 1276 (m), 1034 (br), 933 (vs), 850 (s), 703 (s), 662 (s), 577 (m), 436 (m).

1.10.6 Reaction of $Mo(PMe_3)_5H_2$ with SiH_4

A solution of $Mo(PMe_3)_5H_2$ (7 mg, 0.014 mmol) in C_6D_6 (0.7 mL) in an NMR tube equipped with a J. Young valve was degassed and charged with SiH_4. The reaction was monitored by ^1H NMR spectroscopy at room temperature for three days, thereby demonstrating the formation of $Mo(PMe_3)_4H_4$, $Mo(PMe_3)_4(SiH_3)H_3$, and $Mo(PMe_4)(SiH_3)_2H_2$ in an approximately 1:4:2 ratio.

1.10.7 Reaction of $Mo(PMe_3)_4H_2(SiH_3)_2$ with D_2

A solution of $Mo(PMe_3)_4H_2(SiH_3)_2$ (4 mg, 0.009 mmol) in C_6D_6 (0.7 mL) in an NMR tube equipped with a J. Young valve was degassed and charged with D_2 (*ca.* 1 atm). The reaction was monitored by ^1H NMR spectroscopy at room temperature, thereby demonstrating the formation of a mixture of silane isotopologues, including $SiHD_3$, SiH_2D_2, SiH_3D, and SiH_4; furthermore, HD is produced.

1.10.8 Equilibrium Constant for $Mo(PMe_3)_4H_2(SiH_3)_2 + H_2 \leftrightarrows Mo(PMe_3)_4H_3(SiH_3) + SiH_4$

A solution of $Mo(PMe_3)_4H_2(SiH_3)_2$ (5 mg, 0.011 mmol) in C_6D_6 (0.7 mL) was treated with mesitylene (3 μL, 0.022 mmol) as an internal standard. The solution was transferred to an NMR tube equipped with a J. Young valve, degassed, and charged with H_2 (1 atm). The reaction was monitored by ^1H NMR spectroscopy at room temperature for two weeks. Equilibrium was attained after approximately 9 days, and an equilibrium constant of 1.0(1) was derived from the resulting concentrations of $Mo(PMe_3)_4H_2(SiH_3)_2$, H_2, $Mo(PMe_3)_4H_3(SiH_3)$, and SiH_4.

1.10.9 Reaction of $Mo(PMe_3)_4H_2(SiH_3)_2$ with SiD_4

(i) A solution of $Mo(PMe_3)_4H_2(SiH_3)_2$ (5 mg, 0.011 mmol) in C_6D_6 (0.7 mL) in an NMR tube equipped with a J. Young valve was degassed and charged with SiD_4. The reaction was monitored by ^1H NMR spectroscopy at room temperature, thereby demonstrating

the formation of primarily $SiHD_3$. SiH_2D_2 and SiH_3D are produced as the reaction progresses, but only trace amounts of SiH_4 are observed.

(ii) A solution of $Mo(PMe_3)_4H_2(SiH_3)_2$ (5 mg, 0.011 mmol) in C_6H_6 (0.7 mL) in an NMR tube equipped with a J. Young valve was degassed and charged with SiD_4. The reaction was monitored by ^2H NMR spectroscopy, thereby demonstrating the incorporation of deuterium into the silyl and hydride moieties in an approximately 6:1 ratio, which further indicates that oxidative addition of SiD_4 to $[Mo(PMe_3)_4(SiH_3)H]$ is not the operative mechanism.

1.10.10 Synthesis of $Mo(PMe_3)_4D_2(SiD_3)_2$

$Mo(PMe_3)_6$ (5 mg, 0.009 mmol) was treated with a solution of $PhSiD_3$ (15 mg, 0.13 mmol) in C_6H_6 (0.7 mL). The solution was transferred to an NMR tube equipped with a J. Young valve and monitored by ^2H NMR spectroscopy for 4 days at room temperature, thereby demonstrating the formation of $Mo(PMe_3)_4D_2(SiD_3)_2$. The solution was lyophilized, and the solid obtained was washed with pentane (2 × 0.7 mL) and dried *in vacuo*.

1.10.11 Reaction of $Mo(PMe_3)_4D_2(SiD_3)_2$ with SiH_4

A solution of $Mo(PMe_3)_4D_2(SiD_3)_2$ (*ca*. 2 mg) in C_6D_6 (0.7 mL) in an NMR tube equipped with a J. Young valve was degassed and charged with SiH_4. The reaction was monitored by ^1H NMR spectroscopy at room temperature, thereby demonstrating the formation of SiH_3D as the main silane isotopologue formed. Trace amounts of SiH_2D_2 are also generated as the reaction progresses. In addition, the consecutive formation of Mo-$SiHD_2$, Mo-SiH_2D, and Mo-SiH_3 moieties is observed.

1.10.12 Synthesis of $Mo(PMe_3)_4H_2(SiH_2Ph)_2$

$Mo(PMe_3)_6$ (21 mg, 0.038 mmol) was treated with a solution of $PhSiH_3$ (12 mg, 0.11 mmol) in pentane (0.7 mL). The solution was stirred for 1 minute, resulting in the

formation of a pale brown solution. The solution was filtered and placed at -15 ˚C, thereby depositing $Mo(PMe_3)_4H_2(SiH_2Ph)_2$ as yellow crystals suitable for X-ray diffraction (15 mg, 64 % yield). Analysis calcd. for $Mo(PMe_3)_4H_2(SiH_2Ph)_2$: C, 46.7 %; H, 8.5 %H. Found: C, 46.6 %; H, 8.3 %. ^{1}H NMR (C_6D_6): -4.28 [quint, $^2J_{P-H}$ = 26, 2H of $Mo\underline{H}_2$], 1.22 [s, 36H of $Mo(P\underline{Me}_3)_4$], 5.25 [br quint, $^3J_{P-H}$ = 10, 4H of $Mo(Si\underline{H}_2Ph)_2$], 7.26 (t, $^3J_{H-H}$ = 7, 2H of $Mo(SiH_2\underline{Ph})_2$], 7.37 [t, $^3J_{H-H}$ = 7, 4H of $Mo(SiH_2\underline{Ph})_2$], 8.25 [d, $^3J_{H-H}$ = 7, 4H of $Mo(SiH_2\underline{Ph})_2$]. $^{31}P\{^1H\}$ NMR (C_6D_6): -5.5 [s, 4P of $Mo(\underline{P}Me_3)_4$]. ^{1}H-^{29}Si HMQC NMR (C_6D_6): -6.5 [s, 2Si of $Mo(\underline{Si}H_2Ph)_2$]. IR Data (ATR, cm^{-1}): 3056 (w), 2969 (m), 2909 (m), 2806 (w), 2054 (m) [ν_{Si-H}], 2009 (m) [ν_{Si-H}], 1994 (m) [ν_{Si-H}], 1772 (w) [ν_{Mo-H}], 1562 (w),1476 (w), 1424 (m), 1300 (m), 1276 (m), 1062 (w), 938 (vs), 838 (vs), 720 (m), 696 (vs), 663 (s), 581 (m), 539 (m), 516 (m), 463 (w).

1.10.13 Synthesis of $Mo(PMe_3)_4H_2(SiH_2Ph)(SiH_3)$

$Mo(PMe_3)_6$ (25 mg, 0.045 mmol) was treated with a solution of $PhSiH_3$ (26 mg, 0.24 mmol) in C_6D_6 (0.7 mL). The solution was transferred to an NMR tube equipped with a J. Young valve and monitored by ^{1}H NMR spectroscopy for 2 hours. After this period, the clear, brown solution was lyophilized, washed with pentane, and dried *in vacuo* to afford $Mo(PMe_3)_4H_2(SiH_2Ph)(SiH_3)$ as a light brown powder (24 mg, 98 % yield). Pale yellow crystals of $Mo(PMe_3)_4H_2(SiH_2Ph)(SiH_3)$ suitable for X-ray diffraction were obtained from a solution in pentane at -15 ˚C. Analysis calcd. for $Mo(PMe_3)_4H_2(SiH_2Ph)(SiH_3)$: C, 40.0 %; H 9.0 %. Found: C, 40.2 %; H, 8.8 %. ^{1}H NMR (C_6D_6): -4.58 [br quint, $^2J_{P-H}$ = 26, 2H of $Mo\underline{H}_2$], 1.25 [s, 36H of $Mo(P\underline{Me}_3)_4$], 4.01 [quint, $^3J_{P-H}$ = 8, $^1J_{Si-H}$ = 157, 3H of $Mo(Si\underline{H}_3)$], 5.25 [quint, $^3J_{P-H}$ = 10, $^1J_{Si-H}$ = 158, 2H of $Mo(Si\underline{H}_2Ph)$], 7.25 [t, $^3J_{H-H}$ = 7, 1H of $Mo(SiH_2\underline{Ph})$], 7.35 [t, $^3J_{H-H}$ = 7, 2H of $Mo(SiH_2\underline{Ph})$], 8.20 [d, $^3J_{H-H}$ = 7, 2H of $Mo(SiH_2\underline{Ph})$]. $^{31}P\{^1H\}$ NMR (C_6D_6): -5.2 [s, 4P of $Mo(\underline{P}Me_3)_4$]. ^{1}H-^{29}Si HMQC NMR (C_6D_6): -62.4 [1Si of $Mo(\underline{Si}H_3)$], -8.2 [1Si of $Mo(\underline{Si}H_2Ph)$]. IR Data (ATR, cm$^{=1}$): 3064 (w), 3037 (w), 2999 (w), 2972 (m), 2910 (m), 2810 (w), 2065 (m) [ν_{Si-H}], 2033 (s) [ν_{Si-H}], 2007 (s) [ν_{Si-H}], 1798 (w) [ν_{Mo-H}], 1477 (w), 1426 (m), 1300 (m), 1280 (m), 1123 (w), 1093 (w), 1064

(w), 973 (m), 932 (vs), 852 (s), 838 (s), 798 (s), 723 (m), 698 (s), 659 (s), 588 (m), 570 (m), 508 (m).

1.10.14 Reaction of $Mo(PMe_3)_5H_2$ with $PhSiH_3$

$Mo(PMe_3)_5H_2$ (10 mg, 0.021 mmol) was treated with a solution of $PhSiH_3$ (15 mg, 0.14 mmol) in C_6D_6 (0.7 mL). The solution was transferred to an NMR tube equipped with a J. Young valve (some bubbling was observed), heated at 40 ˚C and monitored by ^1H NMR spectroscopy for 18 hours, thereby demonstrating the formation of $Mo(PMe_3)_4H_4$, $Mo(PMe_3)_4(SiH_3)H_3$, and $Mo(PMe_4)(SiH_3)_2H_2$ in an approximately 1:4:2 ratio.

1.10.15 Synthesis of $Mo(PMe_3)_4H(\kappa^2\text{-}H_2\text{-}H_2SiPh_2H)$

$Mo(PMe_3)_6$ (25 mg, 0.045 mmol) was treated with a solution of Ph_2SiH_2 (30 mg, 0.16 mmol) in C_6D_6 (0.7 mL). The solution was transferred to an NMR tube equipped with a J. Young valve and allowed to stand for four hours at room temperature. After this point, the yellow solution was lyophilized, washed with pentane (2 × 0.7 mL), and dried *in vacuo* to afford $Mo(PMe_3)_4H(\kappa^2\text{-}H_2\text{-}H_2SiPh_2H)$ as a mustard yellow powder (6 mg, 23 %). Yellow crystals of $Mo(PMe_3)_4H(\kappa^2\text{-}H_2\text{-}H_2SiPh_2H)$ suitable for X-ray diffraction (Figure S7) were obtained from a solution in pentane at -15 ˚C. Analysis calcd. for $Mo(PMe_3)_4H(\kappa^2\text{-}H_2\text{-}H_2SiPh_2H)$: C, 49.1 %; H, 8.6 %. Found: C, 48.9 %; H, 8.3 %. ^1H NMR at 300 K (C_6D_6): -4.88 [br quint, $^2J_{P\text{-}H}$ = 27, 3H of $Mo(\underline{H}_2SiPh_2H)\underline{H}$], 1.21 [filled in d, "J" = 5, 36H of $Mo(P\underline{Me}_3)_4$], 6.58 [br s, 1H of $Si\underline{H}Ph_2$], 7.18 [t, $^3J_{H\text{-}H}$ = 7, 2H of $SiH\underline{Ph}_2$], 7.31 [t, $^3J_{H\text{-}H}$ = 7, 4H of $SiH\underline{Ph}_2$], 8.12 [d, $^3J_{H\text{-}H}$ = 7, 4H of $SiH\underline{Ph}_2$]. ^1H NMR at 320 K (C_6D_6): -4.86 [quint, $^2J_{P\text{-}H}$ = 29, 3H of $Mo(\underline{H}_2SiPh_2H)\underline{H}$], 1.22 [s, 36H of $Mo(P\underline{Me}_3)_4$], 6.52 [br s, 1H of $Si\underline{H}Ph_2$], 7.16 [signal obscured by solvent signal, 2H of $SiH\underline{Ph}_2$], 7.29 [t, $^3J_{H\text{-}H}$ = 7, 4H of $SiH\underline{Ph}_2$], 8.09 [d, $^3J_{H\text{-}H}$ = 7, 4H of $SiH\underline{Ph}_2$]. $^{31}P\{^1H\}$ NMR (C_6D_6): 0.05 [s, 4P of $Mo(\underline{P}Me_3)_4$]. IR Data (ATR, cm^{-1}): 3056 (w), 2970 (w), 2905 (m), 1968 (m) [$\nu_{Si\text{-}H}$], 1601 (m) [$\nu_{Mo\text{-}H}$], 1425 (m), 1299 (m), 1276 (m), 1097 (w), 938 (vs), 852 (s), 824 (s), 737 (m), 700 (s), 650 (s), 496 (s), 467 (m).

1.10.16 Reaction of $Mo(PMe_3)_5H_2$ with Ph_2SiH_2 $Mo(PMe_3)_5H_2$ (10 mg, 0.021 mmol) was treated with a solution of Ph_2SiH_2 (15 mg, 0.081 mmol) in C_6D_6 (0.7 mL). The solution was transferred to an NMR tube equipped with a J. Young valve, heated at 40 ˚C, and monitored by ^1H NMR spectroscopy for one day, thereby demonstrating conversion primarily to $Mo(PMe_3)_4H(\kappa^2\text{-}H_2\text{-}H_2SiPh_2H)$, together with a small amount of $Mo(PMe_3)_4H_4$ (*ca*. 5%).

1.10.17 Synthesis of $Mo(PMe_3)_3H_2(\kappa^2\text{-}H_2\text{-}H_2Si_2Ph_4)$

$Mo(PMe_3)_6$ (10 mg, 0.018 mmol) was treated with a solution of Ph_2SiH_2 (10 mg, 0.054 mmol) in pentane (0.7 mL). The solution was stirred for *ca*. one minute to give a dark red solution. The solution was filtered and placed at -15 ˚C, thereby depositing $Mo(PMe_3)_3H_2(\kappa^2\text{-}H_2\text{-}H_2Si_2Ph_4)$ as bright red-orange crystals (3 mg, 24 %) suitable for X-ray diffraction (Figure S8). Analysis calcd. for $Mo(PMe_3)_3H_2(\kappa^2\text{-}H_2\text{-}H_2Si_2Ph_4)$: C, 57.2 %; H, 7.4 %. Found: C, 56.2 %; H, 6.8 %. ^1H NMR at 300 K (C_6D_6): -4.62 [br s, 4H of $Mo(\kappa^2\text{-}H_2\text{-}\underline{H_2}Si_2Ph_4)\underline{H_2}$], 1.14 [vt, "J" = 5, 27H of $Mo(P\underline{Me_3})_3$], 7.10 [t, $^3J_{H\text{-}H}$ = 7, 4H of $Mo(Si_2\underline{Ph_4})$], 7.16 [t, obscured by solvent signal, $^3J_{H\text{-}H}$ = 7, 8H of $Mo(Si_2\underline{Ph_4})$], 7.93 [d, $^3J_{H\text{-}H}$ = 7, 8H of $Mo(Si_2\underline{Ph_4})$]. ^1H NMR at 250 K (C_7D_8): -4.62 [quart, $^2J_{P\text{-}H}$ = 27, 4H of $Mo(\kappa^2\text{-}H_2\text{-}\underline{H_2}Si_2Ph_4)\underline{H_2}$], 1.10 [s, 27H of $Mo(P\underline{Me_3})_3$], 7.13 [m, partially obscured by solvent signal, 12H of $Mo((\kappa^2\text{-}H_2\text{-}H_2Si_2\underline{Ph_4})$], 7.89 [d, $^3J_{H\text{-}H}$ = 7, 8H of $Mo(Si_2\underline{Ph_4})$]. $^{31}P\{^1H\}$ NMR at 210 K (C_7D_8): 4.1 [br s, 3P of $Mo(\underline{P}Me_3)_3$]. $^{31}P\{^1H\}$ NMR at 300K (C_7D_8): 3.3 [br s, 3P of $Mo(\underline{P}Me_3)_3$]. IR Data (ATR, cm^{-1}): 3053 (w), 3005 (w), 2967 (m), 2902 (m), 2806 (w), 1704 (w) [$\nu_{Mo\text{-}H}$], 1581 (w), 1480 (w), 1424 (m), 1293 (m), 1264 (m), 1115 (w), 1092 (w), 921 (vs), 847 (s), 734 (m), 697 (s), 663 (s), 633 (s), 565 (w), 520 (w), 467 (m), 424 (m).

1.10.18 Synthesis of $Mo(PMe_3)_3H_4(\sigma\text{-}HSiHPh_2)$

A suspension of $Mo(PMe_3)_3H_2(\kappa^2\text{-}H_2\text{-}H_2Si_2Ph_4)$ (3 mg, 0.004 mmol) in C_6D_6 (0.7 mL) in an NMR tube equipped with a J. Young valve was degassed and charged with H_2 (*ca*. 1 atm). The solution turned from a red-orange to a pale yellow color over the course of

one hour at room temperature, and $Mo(PMe_3)_3H_4(\sigma\text{-}HSiHPh_2)$was observed as the major product (85 %) by ^1H NMR spectroscopy. The solution was lyophilized to give a pale yellow powder (2 mg). Yellow crystals of $Mo(PMe_3)_3H_4(\sigma\text{-}HSiHPh_2)$ suitable for X-ray diffraction (Figure S9) were obtained from a solution in pentane at -15 ˚C. ^1H NMR (C_6D_6): -4.21 [quart, $^2J_{P\text{-}H}$ = 30, 5H of $Mo(\sigma\text{-}\underline{H}SiHPh_2)\underline{H}_4$], 1.21 [filled in d, "J" = 6, 27H of $Mo(P\underline{Me}_3)_3$], 6.48 [quart, $^3J_{P\text{-}H}$ = 8, $^1J_{Si\text{-}H}$ = 172, 1H of $Mo(\sigma\text{-}HSi\underline{H}Ph_2)$], 7.19 [t, partially obscured by solvent signal, $^3J_{H\text{-}H}$ = 7, 2H of $Mo(\sigma\text{-}HSiH\underline{Ph}_2)$], 7.35 [t, $^3J_{H\text{-}H}$ = 7, 4H of $Mo(\sigma\text{-}HSiH\underline{Ph}_2)$], 8.18 [d, $^3J_{H\text{-}H}$ = 7, 4H of $Mo(\sigma\text{-}HSiH\underline{Ph}_2)$]. $^{31}P\{^1H\}$ NMR (C_6D_6): 1.5 [s, 3P of $Mo(\underline{P}Me_3)_3$]. $^1H\text{-}^{29}Si$ HMQC NMR (C_6D_6): 15.4 [s, 1Si of Mo $Mo(\sigma\text{-}H\underline{Si}HPh_2)$].

1.10.19 Reaction of $Mo(PMe_3)_4H(\kappa^2\text{-}\eta^2\text{-}H_2SiPh_2H)$ with H_2

A solution of $Mo(PMe_3)_4H(\kappa^2\text{-}\eta^2\text{-}H_2SiPh_2H)$ (5 mg, 0.01 mmol) in C_6D_6 (0.7 mL) in an NMR tube equipped with a J. Young valve was degassed and charged with H_2. The reaction was heated at 40 ˚C and monitored by ^1H NMR spectroscopy, thereby demonstrating the formation of $Mo(PMe_3)_3H_4(\sigma\text{-}HSiHPh_2)$ accompanied by $Mo(PMe_3)_4H_4$, the ratio of which changes as the reaction progresses. For example, the ratio of $Mo(PMe_3)_3H_4(\sigma\text{-}HSiHPh_2)$ to $Mo(PMe_3)_4H_4$ is approximately 2:1 after heating for *ca*. 0.5 hours, at which point a substantial amount of $Mo(PMe_3)_4H(\kappa^2\text{-}\eta^2\text{-}H_2SiPh_2H)$ is still present. After *ca*. 2 days at 40 ˚C, when the $Mo(PMe_3)_4H(\kappa^2\text{-}\eta^2\text{-}H_2SiPh_2H)$ has been consumed, the ratio of $Mo(PMe_3)_3H_4(\sigma\text{-}HSiHPh_2)$ to $Mo(PMe_3)_4H_4$ is approximately 1:50. The formation of $Mo(PMe_3)_4H_4$ is also accompanied by release of Ph_2SiH_2.

1.10.20 Synthesis of $(\eta^6\text{-}C_6H_5SiPh_2H)Mo(PMe_3)_3$

$Mo(PMe_3)_6$ (15 mg, 0.027) was treated with a solution of Ph_3SiH (35 mg, 0.13 mmol) in C_6D_6 (0.7 mL) and transferred to an NMR tube equipped with a J. Young valve. The reaction was heated for 1 day at 80 ˚C and monitored by ^1H NMR spectroscopy, thereby demonstrating the formation of $(\eta^6\text{-}C_6H_5SiPh_2H)Mo(PMe_3)_3$. The dark brown solution was lyophilized, washed with pentane, and dried *in vacuo* to afford (η^6-

$C_6H_5SiPh_2H)Mo(PMe_3)_3$ as a pale brown solid (11 mg, 69 % yield). Orange crystals of $(\eta^6\text{-}C_6H_5SiPh_2H)Mo(PMe_3)_3$ suitable for X-ray diffraction (Figure S10) were obtained from a solution in pentane at -15 ˚C. Analysis calcd. for $(\eta^6\text{-}C_6H_5SiPh_2H)Mo(PMe_3)_3$: C, 55.5 %; H, 7.4 %. Found: C, 53.4 %; H, 6.1 %. ^{1}H NMR (C_6D_6): 1.12 [vt, "J" = 5, 27H of $Mo(P\underline{Me}_3)_3$], 3.64 [m, 2H of $Mo(\eta^6\text{-}C_6\underline{H}_5SiPh_2SiH)$], 3.85 [m, 1H of $Mo(\eta^6\text{-}C_6\underline{H}_5SiPhSiH)$], 4.13 [m, 2H of $Mo(\eta^6\text{-}C_6\underline{H}_5SiPh_2H)$], 5.73 [s, $^1J_{Si\text{-}H}$ = 196, 1H of $Mo(\eta^6\text{-}C_6H_5SiPh_2Si\underline{H})$], 7.16 [m, obscured by solvent signal, 6H of $Mo(\eta^6\text{-}C_6H_5Si(C_6\underline{H}_5)_2SiH)$], 7.87 [dd, $^3J_{H\text{-}H}$ = 8, $^4J_{H\text{-}H}$ = 2, 4H of $Mo(\eta^6\text{-}C_6H_5Si(C_6\underline{H}_5)_2SiH)$]. $^{31}P\{^1H\}$ NMR (C_6D_6): 2.5 [s, 3P of $Mo(\underline{P}Me_3)_3$]. ^{1}H-^{29}Si HMQC NMR (C_6D_6) -11.8 [s, 1Si of $Mo(\eta^6\text{-}C_6H_5\underline{Si}Ph_2H)$].

1.10.21 Mechanism for Formation of $(\eta^6\text{-}C_6H_5SiPh_2H)Mo(PMe_3)_3$

The possible involvement of $(\eta^6\text{-}C_6H_6)Mo(PMe_3)_3$ in the formation of $(\eta^6\text{-}C_6H_5SiPh_2H)Mo(PMe_3)_3$ was investigated by monitoring four samples that were prepared in NMR tubes equipped with J. Young valves, namely *(i)* a solution of $Mo(PMe_3)_6$ (8 mg, 0.014 mmol) in C_6D_6 (0.7 mL), *(ii)* a mixture of $Mo(PMe_3)_6$ (8 mg, 0.014 mmol) and Ph_3SiH (4 mg, 0.015 mmol) in C_6D_6 (0.7 mL), *(iii)* a mixture of $(\eta^6\text{-}C_6D_6)Mo(PMe_3)_3$ (8 mg, 0.196 mmol) and Ph_3SiH (5 mg, 0.019 mmol) in C_6D_6, and *(iv)* a solution of $(\eta^6\text{-}C_6H_6)Mo(PMe_3)_3$ (7 mg, 0.017 mmol) in C_6D_6 (0.7 mL). All of the samples were heated at 80 ˚C for 1 day and examined by NMR spectroscopy. Sample *(i)* converted primarily to $Mo(PMe_3)_4(\eta^2\text{–}CH_2PMe_2)H$, with only a small amount of formation of $(\eta^6\text{-}C_6D_6)Mo(PMe_3)_3$. Sample *(ii)* demonstrated primarily conversion to $(\eta^6\text{-}C_6H_5SiPh_2H)Mo(PMe_3)_3$; small amounts of $Mo(PMe_3)_4(\eta^2\text{–}CH_2PMe_2)H$ and $(\eta^6\text{-}C_6D_6)Mo(PMe_3)_3$ were also formed. Sample *(iii)* resulted in only minimal formation of $(\eta^6\text{-}C_6H_5SiPh_2H)Mo(PMe_3)_3$, along with other unidentified products. Finally, sample *(iv)* did not undergo any observable arene exchange between C_6H_6 and C_6D_6. These observations indicate that $(\eta^6\text{-}C_6H_5SiPh_2H)Mo(PMe_3)_3$ is not preferentially formed *via* $(\eta^6\text{-}C_6H_6)Mo(PMe_3)_3$ as a potential intermediate. In addition, $Mo(PMe_3)_6$ does not react with Ph_4Si at 80 ˚C; therefore, we postulate that the mechanism for formation of $(\eta^6\text{-}$

$C_6H_5SiPh_2H)Mo(PMe_3)_3$ involves the initial generation of a silane σ–complex that facilitates access to the η^6-arene complex.

1.10.22 Synthesis of $Mo(PMe_3)_4H_3(GeHPh_2)$

$Mo(PMe_3)_6$ (10 mg, 0.018 mmol) was treated with a solution of Ph_2GeH_2 (16 mg, 0.071 mmol) in C_6D_6 (0.7 mL). The solution was transferred to an NMR tube equipped with a J. Young valve and monitored by ^1H NMR spectroscopy for two hours, thereby demonstrating conversion to $Mo(PMe_3)_4H_3(GeHPh_2)$. The solution was lyophilized, redissolved in pentane, and placed at -30 ˚C, thereby affording red crystals of $Mo(PMe_3)_4H_3(GeHPh_2)$ suitable for X-ray diffraction (3 mg, 27 %). ^1H NMR (C_6D_6): -4.25 [br s, 3H of $Mo\underline{H}_3$], 1.24 [d, $^2J_{P-H}$ = 6, 36H of $Mo(P\underline{Me}_3)_4$], 5.63 [quint, $^3J_{H-H}$ = 9, 1H of $Mo(Ge\underline{H}Ph_2)$], 7.29 [t, $^3J_{H-H}$ = 7, 4H of $Mo(GeH\underline{Ph}_2)$], 8.17 [d, $^3J_{H-H}$ = 7, 4H of $Mo(GeH\underline{Ph}_2)$]. 2H of $Mo(GeH\underline{Ph}_2)$ obscured by residual Ph_2GeH_2 signals.

1.10.23 Reactivity of $Mo(PMe_3)_6$ in Hydrosilation

$Mo(PMe_3)_6$ (5 mg, 0.010 mmol) was treated with a solution of $PhSiH_3$ (10 mg, 0. 090 mmol) and 3-pentanone (0.27 mmol) in C_6D_6 (0.7 mL). The solution was transferred to an NMR tube equipped with a J. Young valve, heated at 80 ˚C, and monitored by ^1H NMR spectroscopy, thereby demonstrating the complete consumption of 3-pentanone and the apparent generation of multiple hydrosilation products. Redistribution of $PhSiH_3$ to Ph_2SiH_2 and SiH_4 was also observed. Reactions with other substrates were performed in the same fashion.

1.11 Crystallographic Data

Table 1. Crystal, intensity collection and refinement data.

	$Mo(PMe_3)_4H_2(SiH_2Ph)_2$	$Mo(PMe_3)_4H_2(SiH_2Ph)(SiH_3)$
lattice	Monoclinic	Monoclinic
formula	$C_{24}H_{52}Si_2P_4Mo$	$C_{18}H_{48}Si_2P_4Mo$
formula weight	616.65	540.56
space group	$P2_1/n$	$P2_1/c$
a / Å	16.2394(18)	15.8327(10)
b / Å	11.0517(12)	12.3924(8)
c / Å	19.390(3)	14.3996(9)
α / °	90	90
β / °	114.633(2)	101.1112(9)
γ / °	90	90
V / Å^3	3163.3(7)	2772.3(3)
Z	4	4
temperature (K)	150(2)	130(2)
radiation (λ, Å)	0.71073	0.71073
ρ (calcd.), g cm^{-3}	1.295	1.295
μ (Mo Ka), mm^{-1}	0.704	0.793
θ max, deg.	30.75	32.99
no. of data collected	50335	48917
no. of data	9812	10031
no. of parameters	316	266
R_1 [$I > 2\sigma(I)$]	0.0496	0.0282
wR_2 [$I > 2\sigma(I)$]	0.0881	0.0630
R_1 [all data]	0.1079	0.0388
wR_2 [all data]	0.1071	0.0685
GOF	1.007	1.041

Table 1 (cont). Crystal, intensity collection and refinement data.

	$Mo(PMe_3)_4H_2(SiH_3)_2$	**$Mo(PMe_3)_4H_3(SiH_3)$**
lattice	Orthorhombic	Orthorhombic
formula	$C_{12}H_{44}Si_2P_4Mo$	$C_{12}H_{42}SiP_4Mo$
formula weight	464.47	434.36
space group	$P2_12_12$	$Cmc2_1$
a/Å	9.6486(16)	13.8563(13)
b/Å	12.613(2)	13.5078(13)
c/Å	9.6355(16)	12.3440(12)
α/°	90	90
β/°	90	90
γ/°	90	90
V/Å^3	1172.6(3)	2310.4(4)
Z	2	4
temperature (K)	150(2)	150(2)
radiation (λ, Å)	0.71073	0.71073
ρ (calcd.), g cm^{-3}	1.316	1.249
μ (Mo Ka), mm^{-1}	0.925	0.885
q max, deg.	32.66	32.75
no. of data collected	20217	19670
no. of data	4108	4236
no. of parameters	110	112
R_1 [$I > 2\sigma(I)$]	0.0384	0.0318
wR_2 [$I > 2\sigma(I)$]	0.0862	0.0569
R_1 [all data]	0.0420	0.0421
wR_2 [all data]	0.0880	0.0604
abs. struct. param.	0.3568(17)	-0.02(4)
GOF	1.091	1.034

Table 1 (cont). Crystal, intensity collection and refinement data.

	$Mo(PMe_3)_3H_4(\sigma\text{-}HSiHPh_2)$	**$Mo(PMe_3)_4H(\kappa^2\text{-}H_2\text{-}H_2SiPh_2H)$**
lattice	Monoclinic	Monoclinic
formula	$C_{21}H_{43}SiP_3Mo$	$C_{24}H_{50}SiP_4Mo$
formula weight	512.49	586.55
space group	$P2_1/c$	$C2/c$
a / Å	9.5132(11)	38.441(3)
b / Å	9.3963(11)	9.6368(8)
c / Å	29.385(3)	16.7191(15)
α / °	90	90
β / °	91.339(2)	99.461(1)
γ / °	90	90
V / Å^3	2626.0(5)	6109.3(9)
Z	4	8
temperature (K)	130(2)	150(2)
radiation (λ, Å)	0.71073	0.71073
ρ (calcd.), g cm^{-3}	1.296	1.275
μ (Mo Ka), mm^{-1}	0.732	0.688
θ max, deg.	30.65	32.87
no. of data collected	40598	51554
no. of data	8068	10770
no. of parameters	268	299
R_1 [$I > 2\sigma(I)$]	0.0576	0.0408
wR_2 [$I > 2\sigma(I)$]	0.1161	0.0871
R_1 [all data]	0.0702	0.0716
wR_2 [all data]	0.1199	0.0997
GOF	1.256	1.023

Table 1 (cont). Crystal, intensity collection and refinement data.

	$Mo(PMe_3)_3H_2(\kappa^2\text{-}H_2\text{-}H_2Si_2Ph_4)$	$(\eta^6\text{-}C_6H_5SiPh_2H)Mo(PMe_3)_3$
lattice	Monoclinic	Monoclinic
formula	$C_{33}H_{51}Si_2P_3Mo$	$C_{27}H_{43}MoP_3Si$
formula weight	692.76	584.55
space group	$P2_1/n$	$P2_1/c$
a / Å	11.5384(11)	13.762(2)
b / Å	16.2583(16)	9.4136(15)
c / Å	19.1670(19)	23.238(4)
α / °	90	90
β / °	102.975(1)	106.705(2)
γ / °	90	90
V / Å^3	3503.8(6)	2883.5(8)
Z	4	4
temperature (K)	150(2)	130(2)
radiation (λ, Å)	0.71073	0.71073
ρ (calcd.), g cm^{-3}	1.313	1.347
μ (Mo Ka), mm^{-1}	0.601	0.677
θ max, deg.	30.67	30.81
no. of data collected	56240	45989
no. of data	10809	8994
no. of parameters	377	302
R_1 [$I > 2\sigma(I)$]	0.0434	0.0512
wR_2 [$I > 2\sigma(I)$]	0.1066	0.1002
R_1 [all data]	0.0627	0.0952
wR_2 [all data]	0.1195	0.1169
GOF	1.029	1.014

Table 1 (cont). Crystal, intensity collection and refinement data.

	$Mo(PMe_3)_3H_3(GeHPh_2)$
lattice	Monoclinic
formula	$C_{24}H_{50}GeMoP_4$
formula weight	631.05
space group	$P2_1/c$
a / Å	9.913(2)
b / Å	16.588(4)
c / Å	18.725(5)
α / °	90
β / °	91.564(3)
γ / °	90
V / Å^3	3077.8(13)
Z	4
temperature (K)	130(2)
radiation (λ, Å)	0.71073
ρ (calcd.), g cm^{-3}	1.362
μ (Mo Ka), mm^{-1}	1.602
θ max, deg.	30.71
no. of data collected	48666
no. of data	9502
no. of parameters	299
R_1 [$I > 2\sigma(I)$]	0.0526
wR_2 [$I > 2\sigma(I)$]	0.1305
R_1 [all data]	0.0563
wR_2 [all data]	0.1319
GOF	1.235

1.12 Computational Data

Table 2. Cartesian coordinates for geometry optimized structures.

$Mo(PMe_3)_4H_2(SiH_3)_2$

-2495.80174713530 Hartrees

Atom	x	y	z
Mo	0	0	-0.062326897
P	1.857494034	0.320316194	1.717763445
P	1.689684099	-0.647092679	-1.817322302
Si	-0.213697008	2.572486428	0.414791148
C	2.780566652	-1.085040109	2.513495172
H	3.566467678	-0.690470683	3.166241137
H	3.231974418	-1.730197848	1.757342154
H	2.098816208	-1.699192927	3.105181453
C	3.320159148	1.323997818	1.146220446
H	4.013598174	1.51171951	1.973098141
H	2.975158522	2.278611322	0.745292037
H	3.855941247	0.789160485	0.358427181
C	1.459128894	1.273534523	3.272327361
H	2.359976511	1.419998161	3.878106109
H	0.725680306	0.727613342	3.869717441
H	1.041235468	2.250512122	3.021465148
C	2.559369088	0.730351556	-2.713495566
H	3.237154189	0.342279422	-3.481757136
H	3.132399998	1.322080885	-1.995213895
H	1.82666541	1.391778151	-3.180308894
C	3.18529717	-1.669023355	-1.364469192

H	3.815219441	-1.845619777	-2.243142397
H	2.87011182	-2.63255261	-0.958029259
H	3.780725127	-1.153476178	-0.607555992
C	1.112049504	-1.652453877	-3.275335562
H	1.950926164	-1.920888148	-3.92650274
H	0.386773744	-1.082156937	-3.860695633
H	0.631314115	-2.565930702	-2.918057711
H	-1.19372828	3.064192905	1.44598952
H	1.03268582	3.282621778	0.857047885
H	0.850337449	1.352916871	-0.71790694
H	-0.614699379	3.391442382	-0.778483832
P	-1.857494034	-0.320316194	1.717763445
P	-1.689684099	0.647092679	-1.817322302
Si	0.213697008	-2.572486428	0.414791148
C	-2.780566652	1.085040109	2.513495172
H	-3.566467678	0.690470683	3.166241137
H	-3.231974418	1.730197848	1.757342154
H	-2.098816208	1.699192927	3.105181453
C	-3.320159148	-1.323997818	1.146220446
H	-4.013598174	-1.51171951	1.973098141
H	-2.975158522	-2.278611322	0.745292037
H	-3.855941247	-0.789160485	0.358427181
C	-1.459128894	-1.273534523	3.272327361
H	-2.359976511	-1.419998161	3.878106109
H	-0.725680306	-0.727613342	3.869717441
H	-1.041235468	-2.250512122	3.021465148
C	-2.559369088	-0.730351556	-2.713495566
H	-3.237154189	-0.342279422	-3.481757136

H	-3.132399998	-1.322080885	-1.995213895
H	-1.82666541	-1.391778151	-3.180308894
C	-3.18529717	1.669023355	-1.364469192
H	-3.815219441	1.845619777	-2.243142397
H	-2.87011182	2.63255261	-0.958029259
H	-3.780725127	1.153476178	-0.607555992
C	-1.112049504	1.652453877	-3.275335562
H	-1.950926164	1.920888148	-3.92650274
H	-0.386773744	1.082156937	-3.860695633
H	-0.631314115	2.565930702	-2.918057711
H	1.19372828	-3.064192905	1.44598952
H	-1.03268582	-3.282621778	0.857047885
H	-0.850337449	-1.352916871	-0.71790694
H	0.614699379	-3.391442382	-0.778483832

$Mo(PMe_3)_4H_3(SiH_3)$

-2205.10374367303 Hartrees

Atom	x	y	z
Mo	0.005643768	2.998014735	10.27757113
P	2.488914863	2.96729899	10.78881371
P	-0.008684324	0.811196992	9.144718505
P	0.008789185	5.495721069	9.733247656
C	3.176514989	1.595398917	11.83951641
H	4.244897037	1.744028609	12.03081337
H	3.036082147	0.635952601	11.33954387
H	2.63965626	1.572562568	12.78990254
C	3.264308042	4.408889885	11.68480747

H	4.347622869	4.275320138	11.77809695
H	2.832884241	4.496245036	12.684404
H	3.071198667	5.339880356	11.1469201
C	1.423512702	6.095878067	8.680393694
H	1.296543374	7.147610734	8.401136868
H	1.468738969	5.484640791	7.775429632
H	2.372236977	5.987663181	9.211019939
C	3.652664872	2.886808974	9.339420744
H	4.697486108	2.834215722	9.664923558
H	3.513659303	3.775459892	8.718837
H	3.425283724	2.013962148	8.723305348
C	-0.034536918	6.859211866	10.99509126
H	-0.037574889	7.840062574	10.50746869
H	-0.926216254	6.764121239	11.61902881
C	-1.357210256	-0.429379378	9.479495715
H	-1.223298432	-1.330630512	8.871073998
H	-2.337417504	-0.002241678	9.256593075
H	-1.333224853	-0.708086817	10.53637476
C	-0.11227801	0.885808036	7.291129908
H	-0.111780404	-0.113278736	6.841418688
H	0.736851855	1.458553039	6.910051439
H	-1.024933556	1.414370802	7.00498505
Si	0.018151253	3.613339843	12.8390721
H	0.070053458	5.062904787	13.24946783
H	1.157524018	3.04848969	13.64051238
H	0.915390852	3.217448811	8.831366471
H	0.00545249	1.706188712	11.45229391
C	1.42107686	-0.369556927	9.321185843

H	1.275914353	-1.257569353	8.696380076
H	2.356764779	0.112320582	9.029747016
H	1.501809232	-0.682556507	10.36533
C	-1.368729612	6.063098813	8.615914871
H	-1.258647174	7.119499115	8.347361371
H	-1.353477146	5.454949268	7.70800816
H	-2.337840259	5.923487492	9.100242924
H	0.832602283	6.787031496	11.65537761
H	-1.159084423	3.131046127	13.6393191
P	-2.471460292	2.966285576	10.79460961
C	-3.145040519	1.631252914	11.89997942
H	-4.217532108	1.770236568	12.07416238
H	-2.982257933	0.652974843	11.4457493
H	-2.618230866	1.660396395	12.85552027
C	-3.262850471	4.434498107	11.63106225
H	-4.342583609	4.287529985	11.74452268
H	-2.820766656	4.57448404	12.62008559
H	-3.093308627	5.342117162	11.04713608
C	-3.635413282	2.811880057	9.351143571
H	-4.67956152	2.763327002	9.679419404
H	-3.50512428	3.673520795	8.691544684
H	-3.400352387	1.914377161	8.774132426
H	-0.918472966	3.228363224	8.84610454

$Mo(PMe_3)_4H_2(SiH_2Ph)_2$

-2957.91197659791 Hartrees

Atom	x	y	z

Mo	5.047141652	8.663066699	2.215690689
P	5.892325664	6.23339662	2.663688164
P	5.217547274	11.17901109	2.011846646
P	4.28396639	8.945170079	4.610638836
Si	7.548026911	8.872880304	1.395943601
Si	2.795481556	7.292150005	2.130718646
P	4.769049122	8.375031282	-0.366071599
C	9.089671064	8.886445708	2.549944347
C	1.104407744	7.993871784	1.539358033
C	4.270565573	7.510744386	5.802582355
H	3.964969393	7.848252255	6.79869901
H	5.261958164	7.058697771	5.876633928
H	3.559519019	6.758334476	5.457115995
C	6.641020278	12.05881934	2.832517472
H	6.551285123	13.14202174	2.697306424
H	7.58522445	11.7282291	2.394518621
H	6.666718189	11.83670719	3.900387482
C	3.812734469	12.20853238	2.67166989
H	3.992997625	13.27385492	2.493289045
H	3.688035505	12.05507084	3.74520524
H	2.8855156	11.91577188	2.172271625
C	10.29984018	8.338227731	2.083310662
H	10.32980093	7.872721891	1.100443103
C	5.219744715	10.13775795	5.692087453
H	4.81106846	10.14562477	6.708053493
H	5.166392849	11.15158512	5.290963625
H	6.270335005	9.838808045	5.732869825
C	2.549123874	9.541211763	4.941802795

H	2.382488032	9.657620275	6.018051511
H	1.826908573	8.820884779	4.551472941
H	2.370906231	10.49916328	4.451012861
C	11.46693977	8.371573846	2.849927177
H	12.38261322	7.933897251	2.459036416
C	5.35401313	12.01103563	0.348273383
H	5.361486432	13.09967591	0.468006702
H	4.513054328	11.73675601	-0.292299118
H	6.284575614	11.70746851	-0.134272363
C	11.45923385	8.961364954	4.114665024
H	12.3650991	8.988293812	4.71473519
C	5.960861654	9.079719324	-1.616088626
H	5.617514864	8.818019053	-2.622146369
H	6.962178441	8.671477257	-1.468511019
H	6.017807058	10.1649427	-1.538437657
C	10.2722468	9.510643941	4.602323856
H	10.25091785	9.970187347	5.588156099
C	0.18828811	7.13119161	0.907016895
H	0.470697109	6.096970665	0.721533115
C	4.646080103	6.679459871	-1.130465403
H	4.286816358	6.759640867	-2.161768038
H	3.959416501	6.049887535	-0.562098741
H	5.632124977	6.211479262	-1.14253585
C	9.10891031	9.466421852	3.830706994
H	8.19294841	9.88526038	4.239550713
C	0.689106181	9.321214365	1.746015287
H	1.371589542	10.02609808	2.213889318
C	3.196666002	9.102418013	-1.045739268

H	3.191257523	9.044431831	-2.139629756
H	3.098734594	10.14648029	-0.7411734
H	2.330906276	8.564888841	-0.655764915
C	-0.575000633	9.765884568	1.354292754
H	-0.865446993	10.79914369	1.53131673
C	-1.463184762	8.889312123	0.730288772
H	-2.44572593	9.23383486	0.417992003
C	-1.075787003	7.568364336	0.505958359
H	-1.757183896	6.877105053	0.015501202
C	7.331933901	6.138525995	3.838391112
H	7.573531159	5.093993024	4.062932709
H	7.09649675	6.660182015	4.768393844
H	8.208463849	6.622077003	3.404380343
C	4.832774942	4.894065284	3.415918997
H	5.425335334	3.977629607	3.502936032
H	3.962337655	4.692006761	2.789170076
H	4.482195503	5.178276719	4.407534868
C	6.586203417	5.194888063	1.280436905
H	7.110576555	4.325911168	1.691429979
H	7.281934959	5.777109097	0.67396412
H	5.771385422	4.839910782	0.646667286
H	2.42370303	6.746934985	3.483437793
H	2.829671192	6.020286159	1.321823102
H	7.999264305	7.838664148	0.396037642
H	3.529175455	9.426035484	1.925706538
H	6.347379384	8.930019124	3.315727855
H	7.768600539	10.13419207	0.604906639

$Mo(PMe_3)_4H_2(SiH_2Ph)(SiH_3)$

-2726.85635785982 Hartrees

Atom	x	y	z
Mo	3.506383559	5.794809974	3.033321022
H	2.350698039	6.984561402	2.55511364
H	3.446090839	4.454997122	4.105640718
P	5.897560032	5.728747383	4.043814578
P	2.409292414	6.258081937	5.248419816
P	1.34997058	4.737247738	2.248571154
P	4.226797175	6.339804734	0.573015607
Si	4.352405175	3.412630115	2.264666733
H	3.577368417	2.781761555	1.141765802
H	4.349027372	2.298277713	3.270369648
H	5.761009597	3.322544505	1.735938685
Si	4.108031699	8.347196019	3.269786059
H	4.047905178	8.810542819	4.701202954
H	5.527167093	8.722918977	2.924694644
C	7.371020327	5.699561497	2.907656871
H	8.280308821	5.45809062	3.468094383
H	7.492455505	6.685427985	2.454206579
H	7.229179269	4.955886051	2.12195988
C	6.574004289	6.986640089	5.247466697
H	7.621650659	6.748804618	5.459176243
H	6.019263746	6.9662907	6.18504556
H	6.520076414	7.994570594	4.833008049
C	6.243338573	4.203368829	5.053189588
H	7.248464431	4.247508819	5.485981119

H	6.160816981	3.3050884	4.438345296
H	5.508246625	4.125602915	5.858395894
C	3.430995395	6.61895332	6.763496781
H	2.784173354	6.753689082	7.636793129
H	4.00682102	7.532439704	6.608802592
H	4.115741474	5.790212169	6.96110609
C	1.353543135	4.924086509	6.007910544
H	0.994839104	5.230802586	6.995999073
H	1.946591584	4.011342341	6.109949343
H	0.487191175	4.702931432	5.382297059
C	1.224773866	7.688927253	5.387382094
H	0.779486068	7.727587237	6.387215136
H	0.427997181	7.594866831	4.647345141
H	1.753293154	8.626308111	5.201890444
C	0.909875438	3.061549511	2.9347676
H	-0.091362087	2.759977482	2.60865827
H	0.947877697	3.066728468	4.024080803
H	1.631771964	2.323539581	2.576659752
C	-0.23606565	5.656860692	2.573095386
H	-1.096705378	5.105067266	2.180685722
H	-0.184785299	6.634544468	2.086200612
H	-0.384750799	5.816996945	3.642290003
C	1.023951601	4.341265718	0.454219255
H	0.026041684	3.90410081	0.341478523
H	1.761847024	3.620129015	0.098906371
H	1.079552153	5.240611509	-0.162118148
C	4.404036783	5.01675276	-0.726682575
H	4.687170811	5.477662506	-1.67852682

H	3.469674596	4.47276102	-0.864160465
H	5.175251651	4.299009696	-0.438696401
C	5.820628823	7.229914707	0.18850841
H	5.821692409	7.555682749	-0.8570117
H	6.666052115	6.556687016	0.342799879
H	5.945821657	8.101648233	0.833038273
C	3.060515304	7.479006905	-0.322802554
H	3.35624151	7.582512502	-1.372502731
H	3.067008103	8.461824097	0.150517396
H	2.040398231	7.094226853	-0.274534916
C	3.176020159	9.766770325	2.373342158
C	3.897753128	10.85662469	1.849352999
H	4.98377843	10.85595253	1.913391342
C	3.258707267	11.94471615	1.24839477
H	3.849318611	12.76631793	0.850014785
C	1.866470135	11.97725044	1.159424449
H	1.364843024	12.82130662	0.693446181
C	1.124692057	10.91025545	1.671160885
H	0.039109814	10.9220063	1.605345302
C	1.774121128	9.823742591	2.2605394
H	1.176319273	8.995060447	2.632271053

$Mo(PMe_3)_4H(\kappa^2\text{-}H_2\text{-}H_2SiPh_2H)$

-2667.20894678239 Hartrees

Atom	x	y	z
Mo	22.88656288	-3.931468151	7.464373417
P	21.85910395	-6.203772834	7.417026088

P	24.95048646	-4.850115742	8.582201723
P	24.35558794	-2.546022296	5.93607925
P	20.85058197	-2.993395387	6.288900797
Si	22.50246777	-3.046741365	9.887220493
C	20.81261223	-6.686722138	5.95287043
H	20.45803453	-7.71893383	6.047211708
H	21.41475446	-6.596561944	5.044742947
H	19.94627783	-6.030208087	5.859505224
C	20.69158292	-6.602119722	8.807202167
H	20.27866478	-7.612663182	8.715243016
H	19.87392573	-5.877303897	8.815442191
H	21.2242582	-6.513617361	9.758019196
C	22.89770848	-7.749601344	7.44264673
H	22.25703717	-8.637917509	7.426268233
H	23.52319732	-7.789257191	8.335925735
H	23.54384188	-7.763859878	6.561407122
C	26.01037917	-6.05556122	7.620847818
H	26.91294862	-6.315170248	8.185125858
H	26.30279162	-5.620553271	6.664449746
H	25.45237069	-6.968798897	7.413656993
C	26.31838132	-3.703196922	9.138120754
H	27.16263031	-4.274817973	9.539538858
H	25.9450958	-3.029901118	9.910408067
H	26.67719924	-3.093228255	8.305608735
C	24.81791071	-5.824378986	10.17174493
H	25.78173987	-6.273402589	10.43470115
H	24.07016889	-6.616235306	10.08132547
H	24.50327818	-5.164444723	10.98227347

C	24.87925824	-0.857367365	6.508171961
H	25.50202232	-0.354125464	5.760472682
H	25.43808512	-0.944888177	7.442581832
H	23.99127797	-0.249523174	6.701861305
C	23.74487243	-2.110783897	4.230323127
H	24.51183388	-1.557837619	3.677678054
H	22.84470177	-1.496362131	4.280512277
H	23.51115124	-3.03064186	3.688584638
C	26.00221905	-3.21963347	5.388483015
H	26.49777419	-2.515416695	4.711757073
H	25.83843097	-4.16395255	4.863159352
H	26.65980005	-3.405616552	6.238158432
C	19.18849052	-3.376763771	7.04074018
H	18.38551013	-2.856626033	6.506488928
H	19.18604738	-3.059552798	8.086020098
H	18.98585564	-4.450432951	7.008614749
C	20.42334108	-3.338433716	4.499707963
H	19.47652271	-2.85876333	4.227164504
H	20.33119251	-4.41427214	4.337419937
H	21.2053123	-2.96744471	3.836111859
C	20.67821453	-1.136241295	6.291902876
H	19.77865008	-0.814240486	5.755103873
H	21.54995014	-0.660362729	5.835973714
H	20.61137046	-0.799986596	7.32973924
C	20.86508194	-2.128788805	10.29522264
C	20.70184485	-0.740234645	10.14518032
H	21.53312822	-0.137466365	9.786019865
C	19.50260283	-0.101667362	10.47039036

H	19.41013821	0.97468655	10.34443566
C	18.42786164	-0.840866629	10.96690538
H	17.4945418	-0.346686072	11.22485926
C	18.56621814	-2.219077844	11.13874459
H	17.73949061	-2.804007184	11.53573049
C	19.76931071	-2.847359358	10.80665281
H	19.86097835	-3.921727724	10.9576747
C	23.79444771	-1.929817235	10.77937087
C	24.29944876	-0.736144866	10.23301317
H	24.01620477	-0.451207077	9.223003271
C	25.1560155	0.099608267	10.95308009
H	25.52241453	1.019178114	10.50182432
C	25.5427955	-0.243073692	12.2504568
H	26.21287496	0.40199259	12.8127216
C	25.05576969	-1.42148119	12.81774712
H	25.34487937	-1.698272673	13.82904564
C	24.19177116	-2.245613052	12.09160989
H	23.81101214	-3.152049641	12.55862063
H	22.77061027	-2.312105485	8.259858925
H	21.59992864	-3.97707153	8.650081738
H	23.51239277	-4.900532709	6.117871259
H	22.43081933	-4.175526335	10.88651776

$Mo(PMe_3)_3H_2(\kappa^2\text{-}H_2\text{-}H_2Si_2Ph_4)$

-2958.91316119233 Hartrees

Atom	x	y	z
Mo	3.000841094	2.664541617	14.79582672

P	5.140956825	3.227802146	15.87152615
P	2.737930692	0.525505285	16.06631695
P	2.470216654	1.525250173	12.55015488
Si	2.433259216	5.130386684	14.44532647
Si	0.471662909	3.969674695	14.79350615
H	3.549053529	3.973892703	13.72237717
H	1.085570381	2.497893314	14.95564537
H	4.427923936	2.012422486	14.07519347
H	2.613264567	3.206592318	16.40484584
C	5.171387607	3.885776023	17.60417207
H	6.193296317	4.113645449	17.92662361
H	4.736779841	3.146554155	18.28165079
H	4.564126906	4.791761092	17.65375925
C	6.158097929	4.516311409	15.00464221
H	7.139778499	4.631219149	15.47722244
H	5.63608769	5.475704824	15.0372502
H	6.289904471	4.223609278	13.95998112
C	6.424270384	1.887805426	16.006487
H	7.326406951	2.252638674	16.50916197
H	6.68327067	1.546163832	15.00087757
H	6.032493598	1.033948629	16.56482638
C	3.242964564	0.50328693	17.85955537
H	3.014182688	-0.458371134	18.33200675
H	2.709106204	1.298021347	18.38720107
H	4.314410143	0.694920696	17.95699422
C	3.60901922	-1.016217309	15.48800582
H	3.458731431	-1.851498744	16.18069957
H	4.679966567	-0.817388944	15.39323027

H	3.232378943	-1.309349696	14.50399441
C	1.011714239	-0.147620967	16.28025357
H	1.004838871	-1.079761318	16.85672687
H	0.557231455	-0.329940768	15.30342877
H	0.400743727	0.59651836	16.79922761
C	1.051841089	0.326990385	12.45401007
H	0.939302783	-0.06502856	11.43730818
H	0.125201191	0.829904619	12.74193214
H	1.220236199	-0.511853747	13.13436705
C	3.838064237	0.475721537	11.86379633
H	3.52985263	-0.024016848	10.9384885
H	4.139991047	-0.273413208	12.59878829
H	4.701985329	1.113457241	11.65994646
C	2.098659817	2.55281297	11.05062349
H	1.998138708	1.922028804	10.16011716
H	2.899991886	3.277082749	10.89180152
H	1.168685832	3.105363892	11.20193633
C	2.880183315	6.436430436	15.76961024
C	3.637939361	7.576353492	15.43738789
H	3.968726706	7.723629221	14.41245944
C	3.966669731	8.541727485	16.39345281
H	4.55852444	9.406704444	16.10282103
C	3.529761188	8.403848984	17.71035969
H	3.775639	9.157710361	18.45373266
C	2.766936247	7.286787761	18.061451
H	2.410258899	7.17032439	19.08225305
C	2.456438428	6.316833013	17.10796898
H	1.87086294	5.453403217	17.40952214

C	2.489504439	6.148111038	12.82302948
C	3.422551972	5.893407661	11.80376058
H	4.12363006	5.069167552	11.9188959
C	3.477925815	6.675104078	10.64607659
H	4.213357478	6.452903153	9.876198636
C	2.591891421	7.738585577	10.47823324
H	2.627842373	8.345367832	9.576922949
C	1.660307434	8.021411048	11.48017108
H	0.968833975	8.852313545	11.36212454
C	1.618052361	7.240021262	12.63528013
H	0.892511049	7.484351804	13.40886648
C	-0.822566744	3.727041075	13.41855588
C	-0.88719861	4.541443111	12.27395732
H	-0.155219752	5.330661269	12.13086495
C	-1.884394225	4.360141295	11.31136014
H	-1.91241457	5.005783983	10.43698503
C	-2.842125082	3.359643227	11.47188755
H	-3.619026164	3.219985114	10.7244473
C	-2.801414366	2.541901282	12.60319934
H	-3.548185057	1.763473957	12.74021362
C	-1.805725854	2.726998677	13.56251745
H	-1.802079369	2.091511096	14.44575025
C	-0.517484017	4.09370723	16.41136399
C	-0.113775859	3.49368001	17.61733307
H	0.815532963	2.930911724	17.64156175
C	-0.872193893	3.621975874	18.7835676
H	-0.535771124	3.14423879	19.70090086
C	-2.05716941	4.358802236	18.77458652

H	-2.648676016	4.459730669	19.6807296
C	-2.475611647	4.965079367	17.58821511
H	-3.396905987	5.542220886	17.56704969
C	-1.717072522	4.831700031	16.42513817
H	-2.070553036	5.304706045	15.51173559

$Mo(PMe_3)_3H_4(\sigma\text{-}HSiHPh_2)$

-2207.28689079504 Hartrees

Atom	x	y	z
Mo	4.817834908	3.685230717	18.34734918
P	6.480956341	5.592444537	18.59669406
P	3.169219018	5.159234645	17.09740325
Si	6.98489909	2.352588901	17.77453421
P	3.177017018	2.354461945	19.68474085
C	7.746714422	1.156030305	19.06713526
C	6.93094145	1.380488426	16.1396211
C	7.969823971	0.806488593	13.99909928
H	8.781702401	0.94269716	13.28845948
C	7.964424143	1.525856585	15.19725246
H	8.781209833	2.215419834	15.40154122
C	7.463745728	6.163598743	17.13313164
H	8.163207044	6.958501485	17.41291721
H	6.78829649	6.534978629	16.35908096
H	8.021657512	5.319302599	16.7238752
C	7.475589667	1.232036845	20.44436172
H	6.773377744	1.980638995	20.80347872
C	5.809289121	7.213323959	19.20923325

H	6.603519679	7.960597508	19.3122938
H	5.3367978	7.050899959	20.18132938
H	5.05050496	7.60091579	18.52472231
C	5.896851424	0.479862356	15.82658843
H	5.070116049	0.352373682	16.52131716
C	9.271120806	-0.696314887	19.55632483
H	9.967466215	-1.451381241	19.19890222
C	3.834431425	6.395446936	15.88011633
H	3.023830904	6.914673992	15.35724533
H	4.454850618	5.867516816	15.15119607
H	4.456546131	7.138944308	16.38413725
C	5.896495688	-0.245911663	14.63544453
H	5.084199072	-0.936854456	14.42138002
C	7.808753445	5.333909877	19.86152783
H	8.467959342	6.206224585	19.92923747
H	8.400798594	4.453324602	19.60464387
H	7.335901548	5.158262966	20.83100869
C	6.934979154	-0.084085572	13.71561656
H	6.934535337	-0.645865094	12.78479255
C	8.659482313	0.168645701	18.64771251
H	8.890906008	0.066178422	17.59028175
C	8.986084806	-0.597551767	20.91902458
H	9.459303534	-1.271815231	21.62858365
C	1.991302535	4.268640998	15.97802167
H	1.340026519	4.968667486	15.44298445
H	1.377488757	3.578241339	16.55993275
H	2.569902569	3.683261788	15.25932913
C	8.085933888	0.371890267	21.36105547

H	7.855397787	0.457629487	22.42071884
C	2.002359693	6.234987032	18.06059768
H	1.328693421	6.796265057	17.40386822
H	2.576406106	6.935304318	18.67280493
H	1.407445285	5.614569448	18.73605902
C	1.380417078	2.292985752	19.21840453
H	0.808826906	1.67429756	19.91880146
H	1.283354889	1.872071192	18.21413235
H	0.955839741	3.300718664	19.21513337
C	3.046192087	2.806761752	21.47498045
H	2.365839182	2.136924367	22.01216599
H	2.690213916	3.836400961	21.56239132
H	4.040394923	2.755836716	21.92479008
C	3.542150533	0.543877727	19.80154913
H	2.826767761	0.027851308	20.45116424
H	4.554317548	0.406364028	20.19053986
H	3.502418212	0.104032291	18.80125673
H	8.119113302	3.3052779	17.51985325
H	5.438938396	3.838319333	16.73116925
H	4.242637013	4.757920961	19.58082115
H	5.344698677	2.036914695	18.32177433
H	5.586937727	3.38101315	19.85944549
H	3.952536393	2.687960594	17.2365697

$(\eta^6\text{-}C_6H_5SiPh_2H)Mo(PMe_3)_3$

-2435.97127342100 Hartrees

Atom	x	y	z
Mo	5.554493205	2.487134833	4.072544465

P	3.649771376	1.223902855	3.129527125
Si	6.901777152	3.399179757	0.479277095
P	7.093493454	0.547829693	3.972181526
P	4.908771375	1.919318373	6.388931748
C	5.595090544	4.650203341	4.875549395
H	5.303239328	5.008791449	5.858144557
C	8.766752083	3.663176578	0.278267063
C	5.024510834	4.135259481	2.550060826
H	4.283840538	4.11214659	1.756316589
C	5.918551997	4.489642347	-0.717284141
C	10.77867909	5.023056882	0.553407882
H	11.24874496	5.935767512	0.911023801
C	9.561400121	2.689526861	-0.35293358
H	9.100982587	1.77051757	-0.709225474
C	7.311184299	3.794453519	3.345352527
H	8.34270868	3.503603017	3.17261996
C	5.448474537	3.96357565	-1.933924748
H	5.623180204	2.915349539	-2.168680713
C	4.519114464	6.103564008	-2.569435586
H	3.980633995	6.724421415	-3.280517838
C	3.852435502	0.586248099	1.387859485
H	2.927972394	0.139956232	1.003636113
H	4.645725753	-0.166682513	1.36216027
H	4.152699377	1.407394075	0.732208527
C	4.972986418	6.646819524	-1.365371957
H	4.787593544	7.693361461	-1.136598189
C	6.95363308	4.286442616	4.627879812
H	7.690805193	4.336084483	5.421290083

C	2.068430158	2.19432774	2.904765874
H	1.288385851	1.594383425	2.422286477
H	2.256684614	3.081287263	2.294600602
H	1.70619159	2.527892293	3.881538616
C	11.54812759	4.040135339	-0.073700871
H	12.61736087	4.183884729	-0.205121829
C	5.661086794	5.847689171	-0.452150984
H	5.99564378	6.286520039	0.485340403
C	6.56014647	-1.241299124	4.111209294
H	7.420110962	-1.921013516	4.101337407
H	5.912132224	-1.493696684	3.266250344
H	5.995100924	-1.401240714	5.032160265
C	2.882377002	-0.30396236	3.891481184
H	2.074711645	-0.703118236	3.267130714
H	2.468057828	-0.056013099	4.873208939
H	3.639420633	-1.080021249	4.027106144
C	4.636524418	4.63433496	3.826992633
H	3.61386932	4.945276738	4.009517555
C	8.456468083	0.537517582	5.24872356
H	9.170967931	-0.276911862	5.082132022
H	8.02981536	0.431200802	6.250211437
H	8.987433505	1.492762591	5.208825307
C	9.40712902	4.834637132	0.725720233
H	8.828733091	5.60972374	1.223815467
C	10.93518813	2.872022781	-0.527801181
H	11.52609704	2.100843453	-1.015761836
C	6.381566862	3.774430604	2.24039041
C	4.756835373	4.75765952	-2.851091466

H	4.402942851	4.325389017	-3.783784764
C	4.771852205	0.193382421	7.102816352
H	4.419082287	0.216135932	8.14041527
H	5.752276222	-0.291344217	7.083836891
H	4.082271762	-0.410825827	6.509215585
C	8.142582057	0.358207511	2.441326695
H	8.828444833	-0.492275932	2.528646489
H	8.728357854	1.263745123	2.26717685
H	7.496506332	0.204224135	1.572955208
C	3.258106805	2.579993813	6.961580517
H	3.098614676	2.421921124	8.034482747
H	2.453268937	2.085849974	6.409516954
H	3.204166948	3.650675572	6.745637354
C	5.99061559	2.635584204	7.736418361
H	5.596248702	2.411921606	8.734265582
H	6.066329903	3.719928386	7.624105342
H	6.998179618	2.218672122	7.652929344
H	6.653895364	2.004246297	0.010476032

Ph_2SiH_2

-754.009571580929 Hartrees

Atom	x	y	z
C	6.114992768	7.958547393	2.791567005
C	7.273813821	7.191668129	2.578253682
H	7.199031609	6.108890659	2.506804539
C	8.526583848	7.79413787	2.448599883
H	9.408050164	7.18083514	2.282016953

C	8.644959368	9.182479008	2.52634638
H	9.618218604	9.654045228	2.421953774
C	7.505984897	9.963802216	2.73182802
H	7.590788553	11.04585218	2.786747226
C	6.256651233	9.35677326	2.860604123
H	5.378335826	9.981743464	3.005675382
Si	4.431052816	7.138511398	2.994234285
C	3.068742843	8.149179329	2.181123491
C	2.978822017	8.255539863	0.780419771
H	3.690975527	7.727565209	0.149795161
C	2.126458594	8.849944258	2.954173741
H	2.163959769	8.785080324	4.039144365
C	1.135925005	9.630845257	2.354847305
H	0.418940634	10.16514351	2.972382016
C	1.066826902	9.722316371	0.964858886
H	0.296715772	10.32865568	0.495813147
C	1.990148379	9.031270307	0.176904949
H	1.93867805	9.098212234	-0.90647631
H	4.079146034	6.993151816	4.435507516
H	4.513833366	5.777470481	2.394183494

$PhSiH_3$

-522.947145422379 Hartrees

Atom	x	y	z
Si	2.727587972	7.278759691	2.129590635
C	1.069980408	7.965132235	1.567000655
C	0.109631151	7.136339172	0.960267088

H	0.331951047	6.085766859	0.787473129
C	0.744926106	9.320201118	1.755962934
H	1.468362146	9.992817649	2.211180876
C	-0.493940148	9.826988593	1.362105111
H	-0.723643227	10.87775596	1.516377998
C	-1.434572106	8.98567521	0.765987628
H	-2.398774749	9.379114004	0.45600395
C	-1.130641737	7.638564054	0.564554321
H	-1.857349452	6.980543574	0.09596923
H	2.68152213	6.797903221	3.538550159
H	3.118743408	6.13107438	1.267826
H	3.770388789	8.336331532	2.044443409

SiH_4

-291.886271758111 Hartrees

Atom	x	y	z
Si	2.783961881	7.303110883	2.114813207
H	2.455814051	6.856593574	3.492791531
H	2.88144102	6.1204049	1.221709834
H	4.082120176	8.024803298	2.124107716
H	1.716171746	8.209798203	1.620906501

1.13 References and Notes

(**1**) (a) Corey, J. Y. *Chem. Rev.* **2011**, *111*, 863-1071.
(b) Corey, J. Y.; Braddock-Wilking, J. *Chem. Rev.* **1999**, *99*, 175-292.

(**2**) (a) Kim, B.-H.; Woo, H.-G. *Adv. Organomet. Chem.* **2005**, *52*, 143-174.
(b) Roy, A. K. *Adv. Organomet. Chem.* **2008**, *55*, 1-59.
(c) Troegel, D.; Stohrer, J. *Coord. Chem. Rev.* **2011**, *255*, 1440-1459.
(d) Corey, J. Y. *Adv. Organomet. Chem.* **2004**, *51*, 1-52.
(e) Waterman, R. *Chem. Soc. Rev.* **2013**, *42*, 5629-5641.
(f) Gauvin, F.; Harrod, J. F.; Woo, H. G. *Adv. Organomet. Chem.* **1998**, *42*, 363-405.

(**3**) *Comprehensive Handbook on Hydrosilylation*, Marciniec, B. (Eds.), Pergamon Press, New York, 1992.

(**4**) (a) Miller, R. D.; Michl, J. *Chem. Rev.* **1989**, *89*, 1359-1410.
(b) West, R. in *PATAI's Chemistry of Functional Groups*, John Wiley & Sons, Ltd. 2009, pp 1-21.

(**5**) Luo, X.-L.; Kubas, G. J.; Burns, C. J.; Bryan, J. C.; Unkefer, C. J. *J. Am. Chem. Soc.* **1995**, *117*, 1159–1160.

(**6**) (a) Vincent, J. L.; Luo, S.; Scott, B. L.; Butcher, R.; Unkefer, C. J.; Burns, C. J.; Kubas, G. J.; Lledós, A.; Maseras, F.; Tomàs, J. *Organometallics* **2003**, *22*, 5307-5323.
(b) Luo, X.-L.; Kubas, G. J.; Bryan, J. C.; Burns, C. J.; Unkefer, C. J. *J. Am. Chem. Soc.* **1994**, *116*, 10312-10313.

(**7**) (a) Parkin, G.; Bunel, E.; Burger, B. J.; Trimmer, M. S.; van Asselt, A.; Bercaw, J. E. *J. Mol. Catal.* **1987**, *41*, 21-39.
(b) Green, M. L. H.; Parkin, G.; Chen, M.; Prout, K. *J. Chem. Soc., Dalton Trans.* **1986**, 2227–2236.
(c) Jiang, Q.; Carroll, P. J.; Berry, D. H. *Organometallics* **1991**, *10*, 3648–3655.
(d) Hao, L.; Lebuis, A.-M.; Harrod, J. F. *Chem. Commun.* **1998**, 1089–1090.
(e) Ebsworth, E. A. V.; Fraser, T. E.; Henderson, S. G.; Leitch, D. M.; Rankin, D. W. H. *J. Chem. Soc. Dalton Trans.* **1981**, 1010-1018 and references therein.
(f) Ebsworth, E. A. V.; Marganian, V. M.; Reed, F. J. S.; Gould, R. O. *J. Chem. Soc., Dalton Trans.* **1978**, 1167–1170.
(g) Ebsworth, E. A. V.; Fraser, T. E. *J. Chem. Soc. Dalton Trans.* **1979**, 1960-1964.
(h) Ebsworth, E. A.; Leitch, D. M. *J. Chem. Soc. Dalton Trans.* **1973**, 1287-1292.

(**8**) See, for example: Glaser, P. B.; Tilley, T. D. *Organometallics* **2004**, *23*, 5799-5812.

(**9**) For example, the reductive elimination of H_2 from $Mo(PMe_3)_4H_2X_2$ (X = Cl, Br, I) has been reported. See: Hascall, T.; Rabinovich, D.; Murphy, V. J.; Beachy, M. D.; Friesner, R. A.; Parkin, G. *J. Am. Chem. Soc.* **1999**, *121*, 11402-11417.

(**10**) A mechanism involving reversible α-H elimination could also explain the H/D scrambling between the silyl and hydride groups,[a] but we favor a σ–complex intermediate on the basis that the interconversion of silyl-hydride and σ–

complexes is precedented.[b] Additionally, σ–complex intermediates have been invoked to explain H/D exchange between methyl and hydride sites.[c-e]
(a) Minato, M.; Zhou, D.-Y.; Zhang, L.-B.; Hirabayashi, R.; Kakeya, M.; Matsumoto, T.; Harakawa, A.; Kikutsuji, G.; Ito, T.
(b) references 5 and 6
(c) Parkin, G. *Acc. Chem. Res.* **2009**, *42*, 315-325.
(d) Hall, C.; Perutz, R. N. *Chem. Rev.* **1996**, *96*, 3125-3146.
(e) Crabtree, R. H. *Chem. Rev.* **1995**, *95*, 987-1007.

(**11**) It is worth noting that the proposed transition state for the sigma bond metathesis step resembles a hypervalent silyl ligand, which are known; for example, $Mo(PMe_3)_4H(\kappa^2\text{-}H_2\text{-}H_2SiPh_2H)$, presented herein, has a hypervalent silyl ligand. The formation of σ-silane complexes, as proposed for the H/D scrambling transition state, is also well precedented and achieved in this system ($Mo(PMe_3)_3H_4(\sigma\text{-}HSiHPh_2)$, presented herein).

(**12**) *Comprehensive Handbook of Chemical Bond Energies*, Yu-Ran Luo, CRC Press, Boca Raton, 2007.

(**13**) National Institute of Standards and Technology, Material Measurement Laboratory (http://www.nist.gov/mml/).

(**14**) The relative bond strengths of the Mo-H and Mo-SiH_3 bonds were determined in the following manner:
ΔG = -RTln(K):
K = 1, so ΔG = -RTln(1) = 0, so ΔG = 0
ΔG = ΔH - TΔS:
if S is assumed to be the same for the metal complexes and $S^0(H_2)$ = 31.2 cal mol^{-1} K^{-1} and $S^0(SiH_4)$ = 48.9 cal mol^{-1} K^{-1}, then ΔS = [$S^0(Mo(PMe_3)_4(SiH_3)H_3)$ + $S^0(SiH_4)$] - $S^0(Mo(PMe_3)_4(SiH_3)_2H_2)$ + $S^0(H_2)$] = 17.7 cal mol^{-1} K^{-1}
Therefore, the term TΔS becomes (298 K)(0.0177 kcal mol^{-1} K^{-1}) = 5.27 kcal mol^{-1}
Therefore, ΔH must also be 5.27 kcal/mol
$\mathbf{\Delta H_{rxn}}$ **=** (Energy of bonds that are broken) – (Energy of bonds that are formed)
= ($D_{Mo\text{-}SiH3}$ + $D_{H\text{-}H}$) – ($D_{Mo\text{-}H}$ + $D_{Si\text{-}H}$)
= ($D_{Mo\text{-}SiH3}$ + 104.2) – ($D_{Mo\text{-}H}$ + 91.7)
= ($D_{Mo\text{-}SiH3}$ – $D_{Mo\text{-}H}$) + 12.5
5.27-12.5 = -7.23, so -7.23 kcal mol^{-1} = ($D_{Mo\text{-}SiH3}$ – $D_{Mo\text{-}H}$)

(**15**) HD is also formed over the course of the reaction.

(**16**) (a) Drew, M. G. B. *Coord. Chem. Rev.* **1977**, *24*, 179-275.
(b) Hlatky, G. G.; Crabtree, R. H. *Coord. Chem. Rev.* **1985**, *65*, 1-48.

(**17**) (a) Osipov, A. L.; Gerdov, S. M.; Kuzmina, L. G.; Howard, J. A. K.; Nikonov, G. I. *Organometallics* **2005**, *24*, 587–602.
(b) Schmitzer, S.; Weis, U.; Käb, H.; Buchner, W.; Malisch, W.; Polzer, T.; Posset, U.; Kiefer, W. *Inorg. Chem.* **1993**, *32*, 303–309.

(c) Malisch, W.; Möller, S.; Fey, O.; Wekel, H.-U.; Pikl, R.; Posset, U.; Kiefer, W. *J. Organomet. Chem.* **1996**, *507*, 117–124.
(d) Mitzenheim, C.; Braun, T. *Angew. Chem. Int. Edit.* **2013**, *52*, 8625-8628.

(**18**) For examples of other structurally characterized silyls, see: Gossage, R. A. *J. Organomet. Chem.* **2000**, *608*, 164-171.

(**19**) There are, however, a few examples of bridging μ–SiH_3 compounds formed from $PhSiH_3$ for the f-block metals. See, for example:
(a) Castillo, I.; Tilley, T. D. *Organometallics* **2000**, *19*, 4733–4739.
(b) Radu, N. S.; Hollander, F. J.; Tilley, T. D.; Rheingold, A. L. *Chem. Commun.* **1996**, 2459-2460.
(c) Korobkov, I.; Gambarotta, S. *Organometallics* **2009**, *28*, 5560-5567.

(**20**) For example, terminal M-SiH_3 complexes have been isolated by redistribution of other silanes:
(a) Woo, H.-G.; Heyn, R. H.; Tilley, T. D. *J. Am. Chem. Soc.* **1992**, *114*, 5698-5707.
(b) Li, Y.-H.; Huang, Z.-F.; Li, X.-A.; Lai, W.-Y.; Wang, L.-H.; Ye, S.-H.; Cui, L.-F.; Wang, S. *J. Organomet. Chem.* **2014**, *749*, 246-250.

(**21**) Perutz, R. N.; Sabo-Etienne, S. *Angew. Chem. Int. Edit.* **2007**, *46*, 2578-2592.

(**22**) Castillo, I.; Tilley, T. D. *J. Am. Chem. Soc.* **2001**, *123*, 10526-10534.

(**23**) (a) Sadow, A. D.; Tilley, T. D. *Organometallics* **2001**, *20*, 4457-4459.
(b) Sadow, A. D.; Tilley, T. D. *Organometallics* **2003**, *22*, 3577-3585.

(**24**) Perrin, L.; Maron, L.; Eisenstein, O.; Tilley, T. D. *Organometallics* **2009**, *28*, 3767-3775.

(**25**) Mechanisms involving α-R migration have also been invoked for silane redistribution in an iridium system.[a,b] In addition, $(Ph_3P)_3RhCl$ catalyzes redistribution of $PhSiH_3$.[c]
(a) Sangtrirutnugul, P.; Tilley, T. D. *Organometallics* **2007**, *26*, 5557-5568.
(b) Park, S.; Kim, B. G.; Göttker-Schnetmann, I.; Brookhart, M. *ACS Catal.* **2012**, *2*, 307-316.
(c) Ojima, I.; Inaba, S.; Kogure, T.; Nagai, Y. *J. Organomet. Chem.* **1973**, *55*, C7-C8.

(**26**) The κ^x notation refers to the number of hydrogen atoms attached to the metal. See: Green, J. C.; Green, M. L. H.; Parkin, G. *Chem. Commun.* **2012**, *48*, 11481-11503. See this reference also for a description of the half-arrow notation used herein.

(**27**) Sakaba, H.; Hirata, T.; Kabuto, C.; Kabuto, K. *Organometallics* **2006**, *25*, 5145-5150.

(**28**) Disilane coordination to a metal through a single Si-H bond and coordination to two metals have been proposed but not structurally characterized. See: Karch, R.; Schubert, U. *Inorg. Chim. Acta* **1997**, *259*, 151-160.

(**29**) Söllradl, H.; Hengge, E. *J. Organomet. Chem.* **1983**, *243*, 257-269.

(**30**) (a) Lin, Z. *Chem. Soc. Rev.* **2002**, *31*, 239-245.
(b) Nikonov, G. I. *Adv. Organomet. Chem.* **2005**, *53*, 217-309.
(c) Lachaize, S.; Sabo-Etienne, S. *Eur. J. Inorg. Chem.* **2006**, 2115-2127.
(d) Schubert, U. *Adv. Organomet. Chem.* **1990**, *30*, 151-187.
(e) Scherer, W.; Meixner, P.; Barquera-Lozada, J. E.; Hauf, C.; Obenhuber, A.; Brück, A.; Wolstenholme, D. J.; Ruhland, K.; Leusser, D.; Stalke, D. *Angew. Chem. Int. Edit.* **2013**, *52*, 6092-6096.
(f) Hauf, C.; Barquera-Lozada, J. E.; Meixner, P.; Eickerling, G.; Altmannshofer, S.; Stalke, D.; Zell, T.; Schmidt, D.; Radius, U.; Scherer, W. *Z. Anorg. Allg. Chem.* **2013**, *639*, 1996-2004.
(g) Scherer, W.; Eickerling, G.; Tafipolsky, M.; McGrady, G. S.; Sirsch, P.; Chatterton, N. P. *Chem. Commun.* **2006**, 2986-2988.
(h) McGrady, G. S.; Sirsch, P.; Chatterton, N. P.; Ostermann, A.; Gatti, C.; Altmannshofer, S.; Herz, V.; Eickerling, G.; Scherer, W. *Inorg. Chem.* **2009**, *48*, 1588-1598.

(**31**) Shorter Mo-SiR_3 bonds (*e.g.* 2.480 Å and 2.495 Å) have, however, been reported. See:
(a) Filippou, A. C.; Chernov, O.; Schnakenburg, G. *Angew. Chem. Int. Edit.* **2011**, *50*, 1122-1126.
(b) Khalimon, A. Y.; Simionescu, R.; Kuzmina, L. G.; Howard, J. A. K.; Nikonov, G. I. *Angew. Chem. Int. Edit.* **2008**, *47*, 7701-7704.

(**32**) Additionally, the Mn-Si bond length [2.254(1) Å] in the silane adduct, $(Cp^{Me})Mn(CO)_2(\sigma\text{-}HSiCl_3)$, is shorter than that in the silyl compound, $(Cp^{Me})Mn(SiCl_3)_2$ [2.320(2) Å]. See: Schubert, U.; Ackermann, K.; Kraft, G.; Wörle, B. *Z. Naturforsch. (B)* **1983**, *38*, 1488-1492.

(**33**) For example, the three-membered [Mo,H,Si] moiety of $Mo(depe)_2(CO)(\sigma\text{-}HSiHPh_2)$ is characterized by Mo-Si [2.563(3) Å], Mo-H [2.04(2) Å], and Si-H [1.66(6) Å] bond lengths.

(**34**) Also of relevance is that $J_{Si\text{-}H}$ coupling constants for σ-silane compounds are a composite of $^1J_{Si–H}$ and $^2J_{Si–H}$ values, which have opposite signs; therefore, small values of $J_{Si–H}$ cannot alone be taken as evidence for no degree of Si–H interaction. See, for example:
(a) Dubberley, S. R.; Ignatov, S. K.; Rees, N. H.; Razuvaev, A. G.; Mountford, P.; Nikonov, G. I. *J. Am. Chem. Soc.* **2003**, *125*, 642–643.
(b) Dioumaev, V. K.; Yoo, B. R.; Procopio, L. J.; Carroll, P. J.; Berry, D. H. *J. Am. Chem. Soc.* **2003**, *125*, 8936–8948.
(c) reference 30c

(**35**) Gadek, A.; Kochel, A.; Szymańska-Buzar, T. *J. Organomet. Chem.* **2005**, *690*, 685-690.

(**36**) The reaction of $Mo(PMe_3)_6$ with C_6H_6 to give $(\eta^6\text{-}C_6H_6)Mo(PMe_3)_3$ does proceed efficiently at 120˚C. See: Zhu, G.; Janak, K. E.; Figueroa, J. S.; Parkin, G. *J. Am. Chem. Soc.* **2006**, *128*, 5452-5461.

(**37**) (a) McNally, J. P.; Leong, V. S.; Cooper, N. J. in *Experimental Organometallic Chemistry*, Wayda, A. L.; Darensbourg, M. Y., Eds.; American Chemical Society: Washington, DC, 1987; Chapter 2, pp 6-23.
(b) Burger, B.J.; Bercaw, J. E. in *Experimental Organometallic Chemistry*; Wayda, A. L.; Darensbourg, M. Y., Eds.; American Chemical Society: Washington, DC, 1987; Chapter 4, pp 79-98.
(c) Shriver, D. F.; Drezdzon, M. A.; *The Manipulation of Air-Sensitive Compounds*, 2nd Edition; Wiley-Interscience: New York, 1986.

(**38**) (a) Gottlieb, H. E.; Kotlyar, V.; Nudelman, A. *J. Org. Chem.* **1997**, *62*, 7512-7515.
(b) Fulmer, G. R.; Miller, A. J. M.; Sherden, N. H.; Gottlieb, H. E.; Nudelman, A.; Stoltz, B. M.; Bercaw, J. E.; Goldberg, K. I. *Organometallics* **2010**, *29*, 2176-2179.

(**39**) "Nuclear Magnetic Resonance Spectroscopy" Nelson, J. H. Prentice Hall, New Jersey (2003), p 79.

(**40**) Murphy, V. J.; Parkin, G. *J. Am. Chem. Soc.* **1995**, *117*, 3522-3528.

(**41**) Lyons, D.; Wilkinson, G.; Thomton-Pett, M.; Hursthouse, M. B. *J. Chem. Soc., Dalton Trans.* **1984**, 695-700.

(**42**) Brookhart, M.; Cox, K.; Cloke, F. G. N.; Green, J. C.; Green, M. L. H.; Hare, P. M.; Bashkin, J.; Derome, A. E.; Grebenik, P. D. *J. Chem. Soc., Dalton Trans.* **1985**, 423-433.

(**43**) Speier, J. L.; Zimmerman, R. E. *J. Am. Chem. Soc.* **1955**, *77*, 6395-6396.

(**44**) Banovetz, J. P.; Suzuki, H.; Waymouth, R. M. *Organometallics* **1993**, *12*, 4700-4703.

(**45**) (a) Sheldrick, G. M. SHELXTL, An Integrated System for Solving, Refining and Displaying Crystal Structures from Diffraction Data; University of Göttingen, Göttingen, Federal Republic of Germany, 1981.
(b) Sheldrick, G. M. *Acta Cryst.* **2008**, *A64*, 112-122.

(**46**) Jaguar 7.7, Schrödinger, LLC, New York, NY 2010.

(**47**) (a) Becke, A. D. *J. Chem. Phys.* **1993**, *98*, 5648-5652.
(b) Becke, A. D. *Phys. Rev. A* **1988**, *38*, 3098-3100.
(c) Lee, C. T.; Yang, W. T.; Parr, R. G. *Phys. Rev. B* **1988**, *37*, 785-789.
(d) Vosko, S. H.; Wilk, L.; Nusair, M. *Can. J. Phys.* **1980**, *58*, 1200-1211.
(e) Slater, J. C. *Quantum Theory of Molecules and Solids, Vol. 4: The Self-Consistent Field for Molecules and Solids*; McGraw-Hill: New York, 1974.

(**48**) (a) Hay, P. J.; Wadt, W. R. *J. Chem. Phys.* **1985**, *82*, 270-283.
(b) Wadt, W. R.; Hay, P. J. *J. Chem. Phys.* **1985**, *82*, 284-298.
(c) Hay, P. J.; Wadt, W. R. *J. Chem. Phys.* **1985**, *82*, 299-310.

(**49**) NBO 5.0. Glendening, E. D.; Badenhoop, J. K.; Reed, A. E.; Carpenter, J. E.; Bohmann, J. A.; Morales, C. M.; Weinhold, F. Theoretical Chemistry Institute, University of Wisconsin, Madison, 2001.

CHAPTER 2

Si-Si and Si-C Bond Formation *via* Tungsten-Silylene Intermediates: Evidence for $W{=}SiR_2$ Species through the Isolation of a Bridging Silylene Complex

Table of Contents

2.1 Introduction

As discussed in Chapter 1, transition metal catalysts play an important role in a number of critical transformations of silanes.[1] Thus, it is valuable not only to examine the reactivity of transition metal complexes with silanes, but also to understand how the transformations effected by a metal center are related to the coordination and bonding of the silanes to that metal.[2] Accordingly, we have examined the reactivity of an electron rich tungsten trimethylphosphine complex, $W(PMe_3)_4(\eta^2\text{–}CH_2PMe_2)H$, towards the series of silanes Ph_xSiH_{4-x} ($x = 0 – 4$). The course of these reactions depends critically on the substitution of the silane, and the products range from simple oxidative addition compounds to novel disilanyl, metallacycle, and bridging silylene species. These complexes demonstrate the ability of $W(PMe_3)_4(\eta^2\text{–}CH_2PMe_2)H$ to cause redistribution and dehydrocoupling of hydrosilanes, including Si-C bond formation and bond cleavage.

2.2 $W(PMe_3)_4(\eta^2\text{–}CH_2PMe_2)H + SiH_4$

2.2.1 Preparation and Characterization of Tungsten Silyl Complexes

The reactivity of $W(PMe_3)_4(\eta^2\text{–}CH_2PMe_2)H$ with SiH_4 has been previously investigated,[3] and it was determined that $W(PMe_3)_4H_2(SiH_3)_2$ is the major product when $W(PMe_3)_4(\eta^2\text{–}CH_2PMe_2)H$ is treated with an excess of SiH_4 (Scheme 1). This reactivity is analogous to that of $Mo(PMe_3)_6$, which also reacts with SiH_4 to form a bis(silyl) complex; however, the reaction with $W(PMe_3)_4(\eta^2\text{–}CH_2PMe_2)H$ requires heating,[4] whereas the molybdenum system reacts at room temperature. The crystal structure of $W(PMe_3)_4H_2(SiH_3)_2$ has also now been obtained (Figure 1), and it was found to be isostructural to the molybdenum analogue.

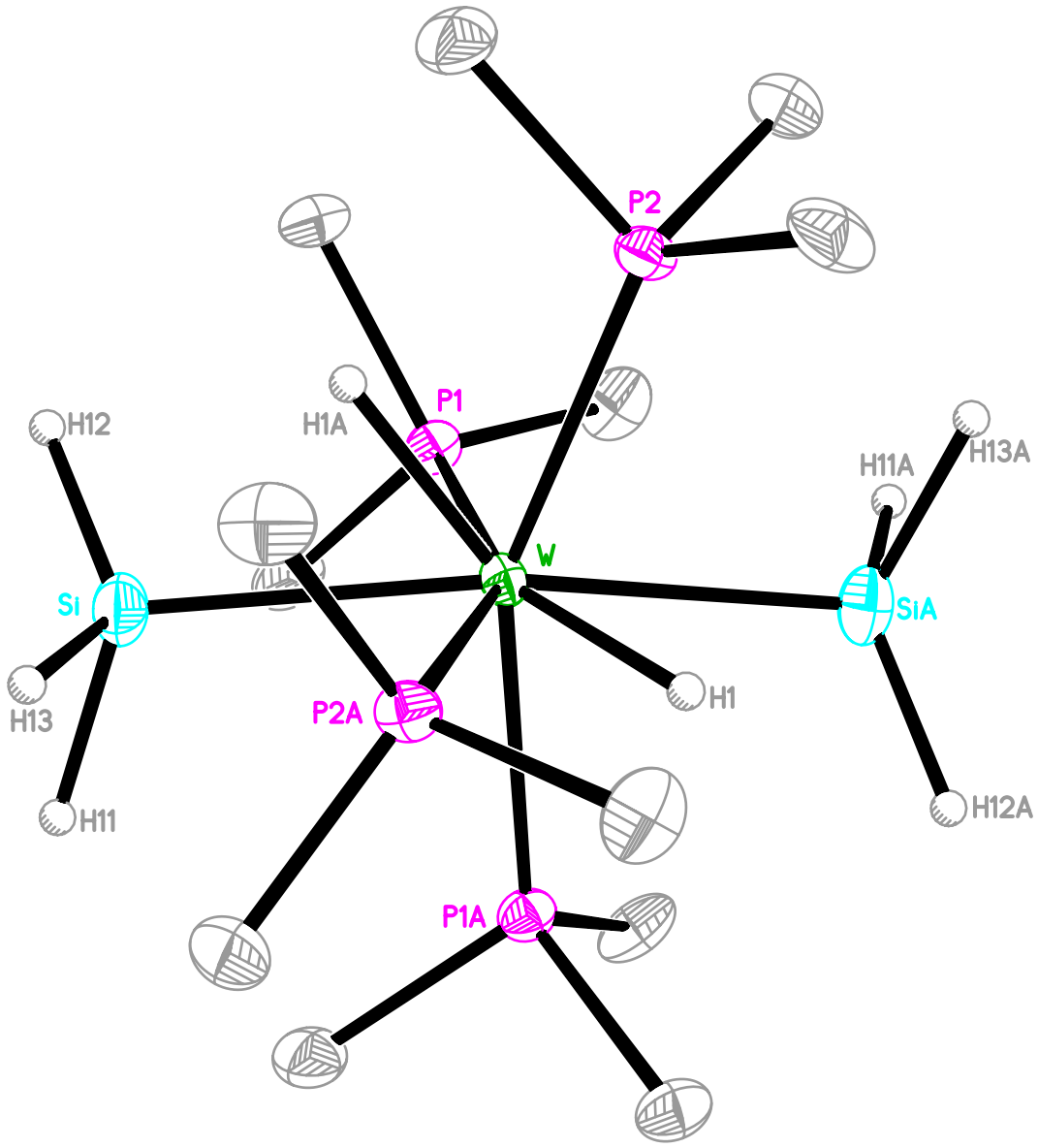

Figure 1. Molecular Structure of $W(PMe_3)_4H_2(SiH_3)_2$

In addition to this simple oxidative addition product, a metallacycle species, $W(PMe_3)_3H_3(\kappa^2\text{-}P,Si\text{-}PMe_2CH_2SiH_2SiH_2)$, is also obtained from the reaction of $W(PMe_3)_4(\eta^2\text{–}CH_2PMe_2)H$ with SiH_4 (Scheme 1). This complex is defined by a W-P-C-Si-Si five-membered ring; significantly, this M-P-C-Si-Si metallacycle motif is the first of its kind for any metal. The metallacycle fragment is defined by an acute Si-W-P angle of 83.15° and an "envelope" conformation. Although the mechanistic details regarding the formation of this product are unknown, the complex is formally derived from

$W(PMe_3)_4H_2(SiH_3)_2$ by removal of an equivalent of H_2. Thus, it is possible that $W(PMe_3)_3H_3(\kappa^2$-*P,Si*-$PMe_2CH_2SiH_2SiH_2)$ is formed when $W(PMe_3)_4H_2(SiH_3)_2$ reacts with unreacted $W(PMe_3)_4(\eta^2$–$CH_2PMe_2)H$ (to form $W(PMe_3)_5H_2$ and the metallacycle complex) under reaction conditions The molecular structure of $W(PMe_3)_3H_3(\kappa^2$-*P,Si*-$PMe_2CH_2SiH_2SiH_2)$ is shown in Figure 2.

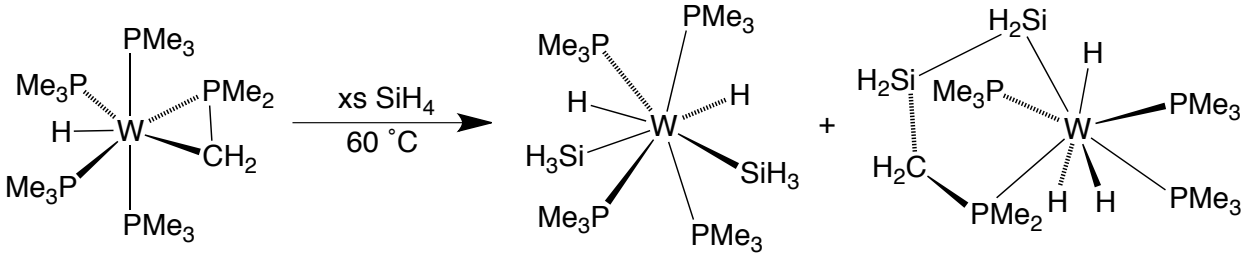

Scheme 1. Reaction of $W(PMe_3)_4(\eta^2$–$CH_2PMe_2)H$ with SiH_4

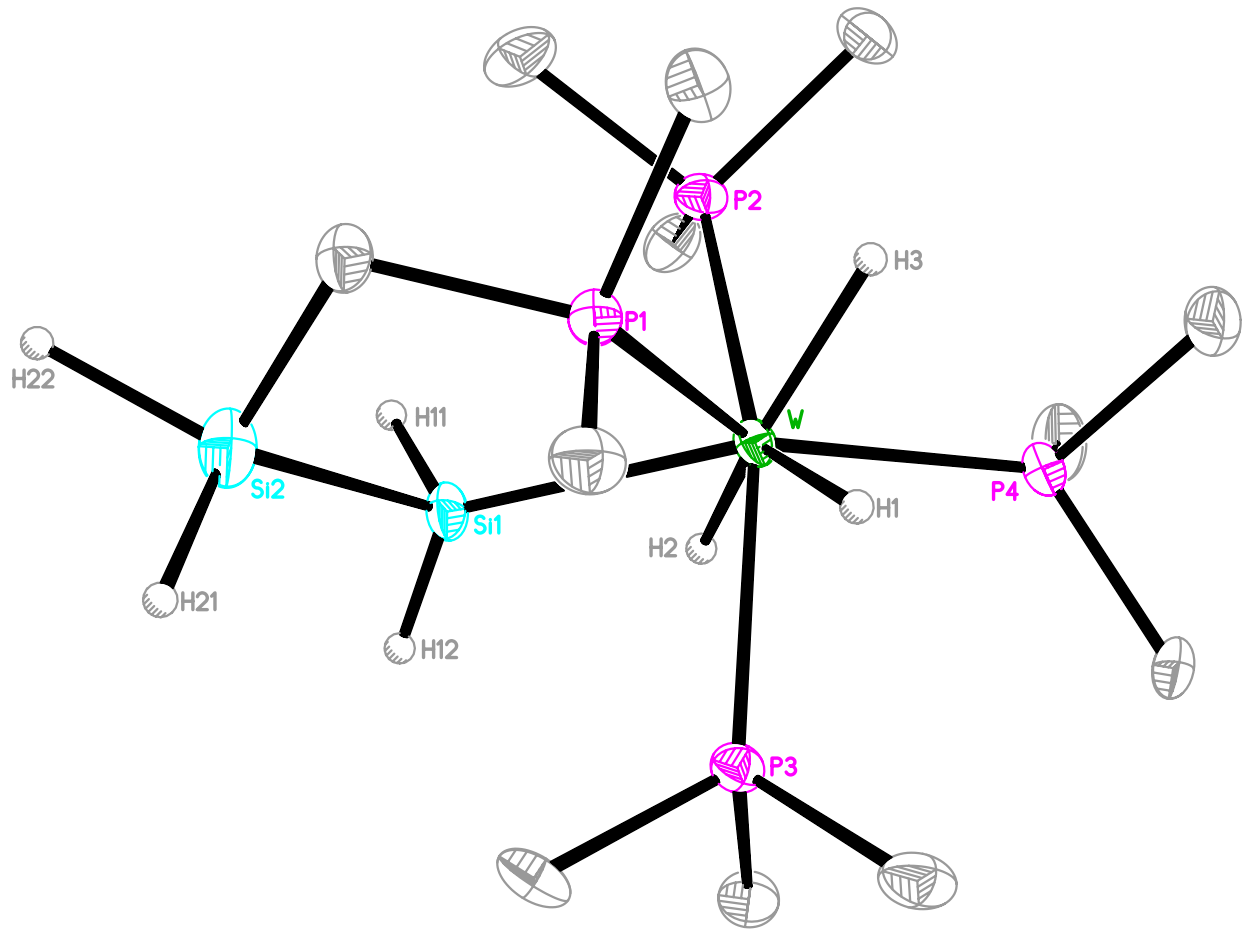

Figure 2. Molecular Structure of $W(PMe_3)_3H_3(\kappa^2$-*P,Si*-$PMe_2CH_2SiH_2SiH_2)$

2.2.2 Variable Temperature NMR Spectroscopy of $W(PMe_3)_4H_2(SiH_3)_2$

The ^1H NMR spectrum of $W(PMe_3)_4H_2(SiH_3)_2$ is similar to that of the molybdenum congener. For example, the silyl resonance demonstrates coupling to both silicon and phosphorus ($^3J_{P\text{-}H}$ = 8 Hz, $^1J_{Si\text{-}H}$ = 155 Hz), and the hydride signal exhibits coupling only to phosphorus ($^2J_{P\text{-}H}$ = 30 Hz). Unlike $Mo(PMe_3)_4H_2(SiH_3)_2$, however, $W(PMe_3)_4H_2(SiH_3)_2$ does not decompose at higher temperatures, such that variable temperature NMR spectroscopy was feasible. This was of particular interest since exchange of hydrogen between the silyl and hydride groups of $Mo(PMe_3)_4H_2(SiH_3)_2$ was invoked but not observable due to rapid decomposition upon heating. Significantly, the ^1H NMR spectrum of $W(PMe_3)_4H_2(SiH_3)_2$ does suggest that exchange may be occurring between the silyl and hydride groups since both resonances broaden at higher temperature (Figure 3).[6,7]

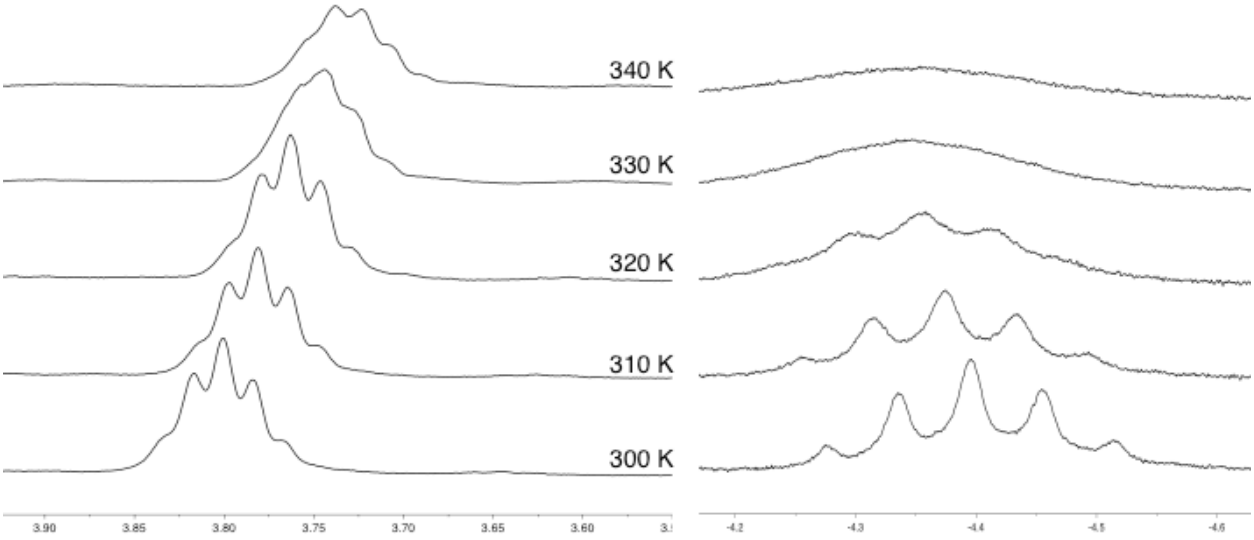

Figure 3. Variable Temperature ^1H NMR Spectra (silyl and hydride signals) of $W(PMe_3)_4H_2(SiH_3)_2$

2.3 $W(PMe_3)_4(\eta^2\text{–}CH_2PMe_2)H$ + $PhSiH_3$

2.3.1 Generation of Tungsten-Disilanyl Species from Monosilanes

The reactivity of $W(PMe_3)_4(\eta^2\text{–}CH_2PMe_2)H$ towards $PhSiH_3$ is substantially different than that of $Mo(PMe_3)_6$. At 80 °C, $W(PMe_3)_4(\eta^2\text{–}CH_2PMe_2)H$ reacts to form multiple

products simultaneously, and the product distribution depends on the amount of $PhSiH_3$ added. The major products of this reaction, two related disilanyl species, demonstrate the ability of $W(PMe_3)_4(\eta^2\text{–}CH_2PMe_2)H$ to cause redistribution and dehydrocoupling of hydrosilanes (Scheme 2).

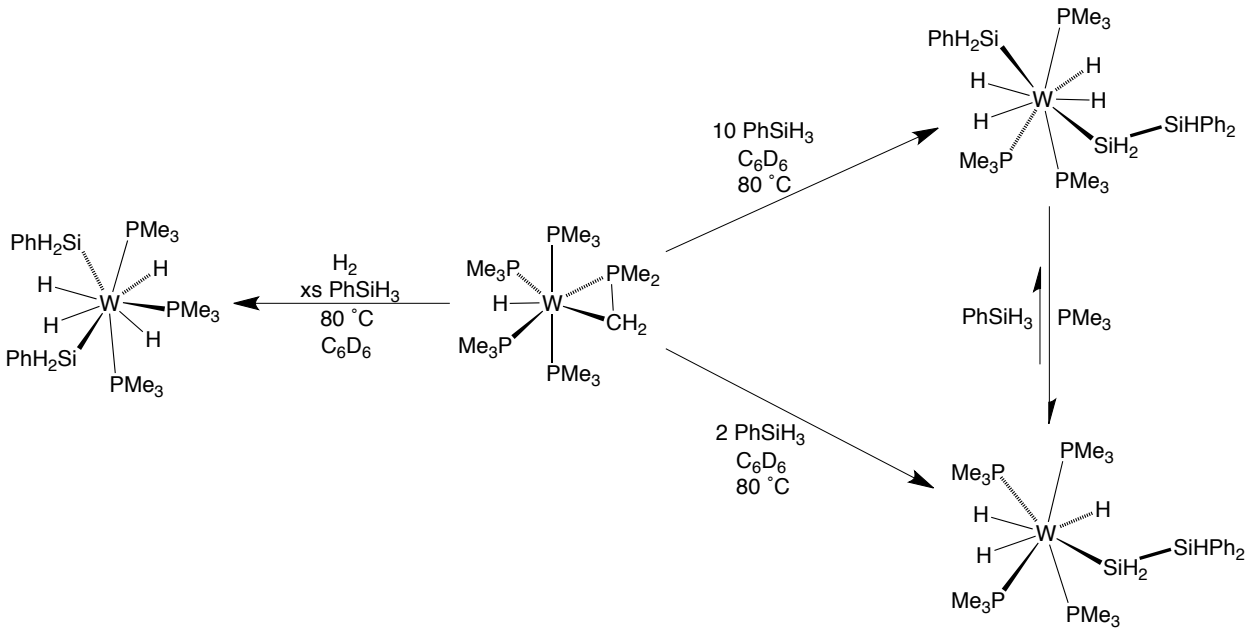

Scheme 2. Major products from $W(PMe_3)_4(\eta^2\text{–}CH_2PMe_2)H$ + $PhSiH_3$ at 80 ˚C

When $W(PMe_3)_4(\eta^2\text{–}CH_2PMe_2)H$ is treated with two equivalents of $PhSiH_3$ and heated at 80 ˚C, the major product is the tetravalent species, $W(PMe_3)_4H_3(SiH_2SiHPh_2)$ (Figure 4). The room temperature ^1H NMR spectrum of this complex is consistent with the solid state structure; for example, broad signals in a 1:2 ratio are observed for the hydrides by ^1H NMR spectroscopy (Figure 5), and the phosphine ligands resonate in a 1:2:1 ratio in the $^{31}P\{^1H\}$ NMR spectrum.[8] In the presence of a large excess (10x) of $PhSiH_3$, the major product at 80 ˚C is the hexavalent species, $W(PMe_3)_3H_4(SiH_2Ph)(SiH_2SiHPh_2)$ (Figure 6). This compound is fluxional at room temperature, such that all four hydrides and all three trimethylphosphine ligands appear equivalent. At -80 ˚C, however, four distinct signals are observed for the hydrides, and three unique signals are observed for the

W-PMe_3 groups in the ^1H NMR spectrum (Figure 7). The five unique Si-H hydrogens are also distinct at low temperature.

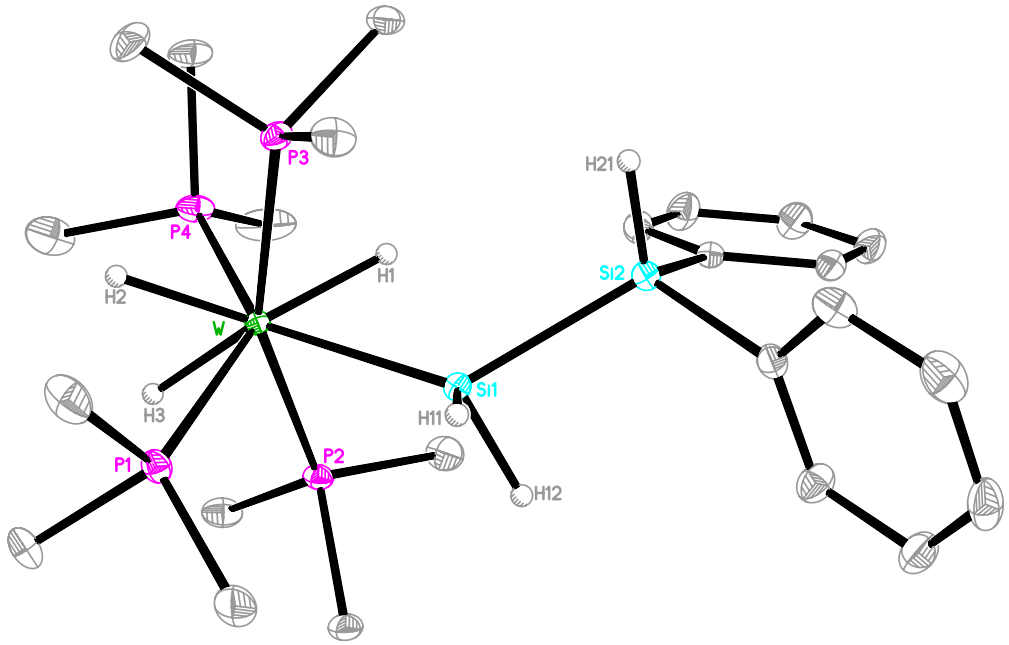

Figure 4. Molecular Structure of $W(PMe_3)_4H_3(SiH_2SiHPh_2)$

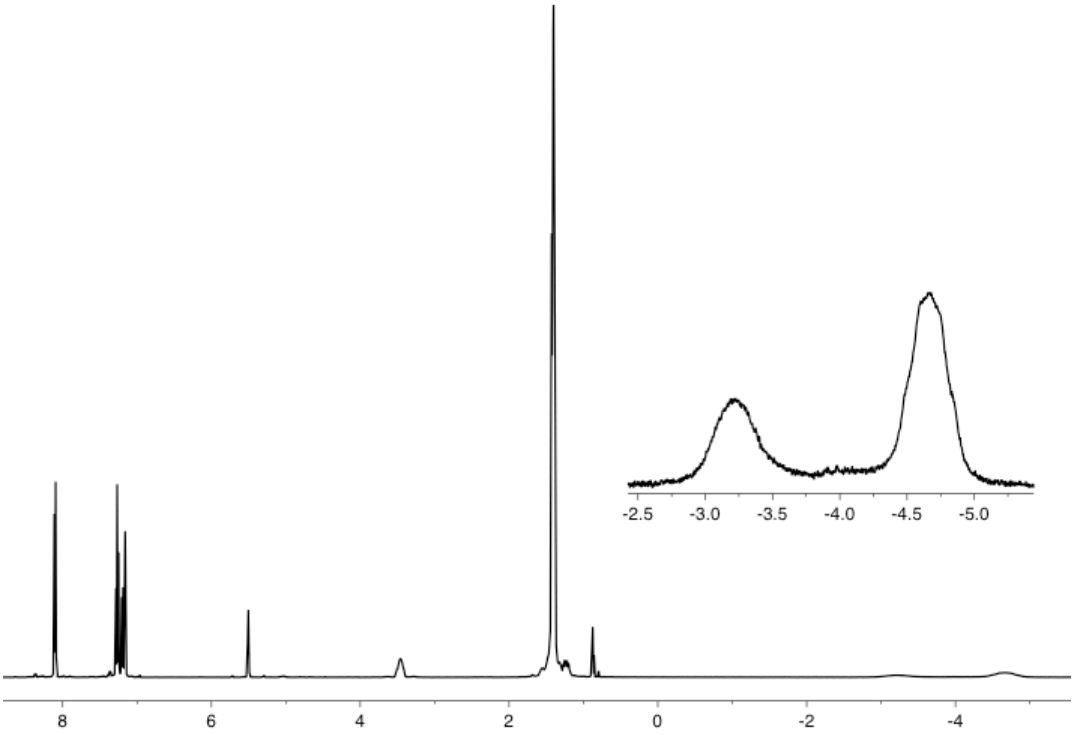

Figure 5. ^1H NMR Spectrum of $W(PMe_3)_4H_3(SiH_2SiHPh_2)$

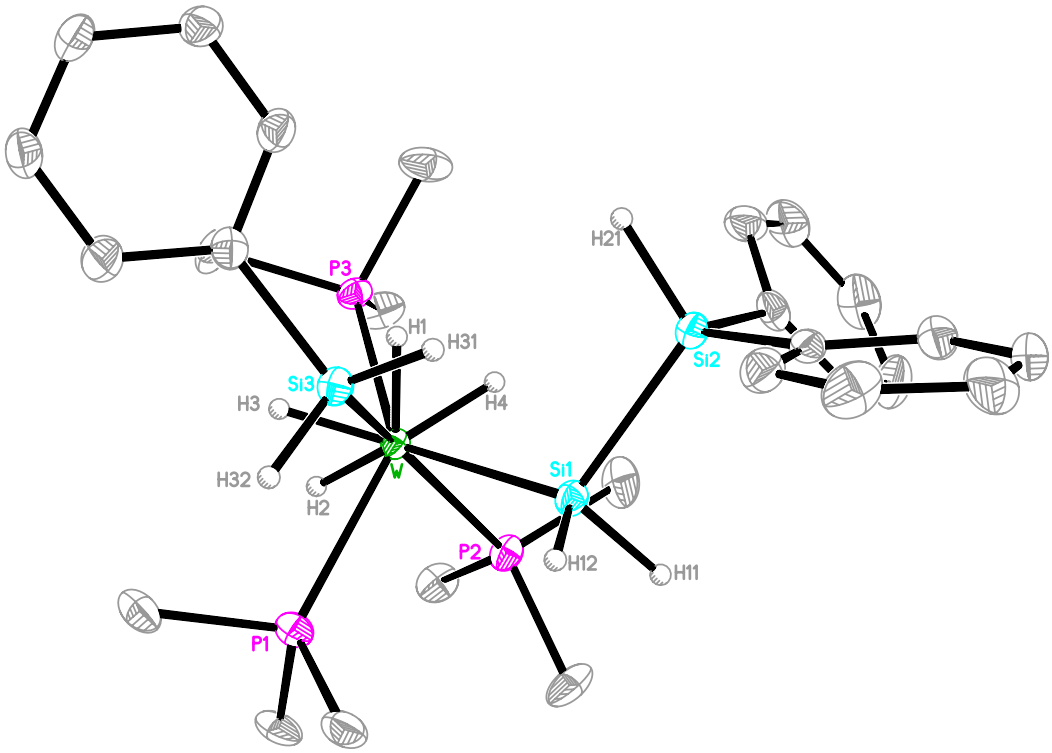

Figure 6. Molecular Structure of $W(PMe_3)_3H_4(SiH_2Ph)(SiH_2SiHPh_2)$

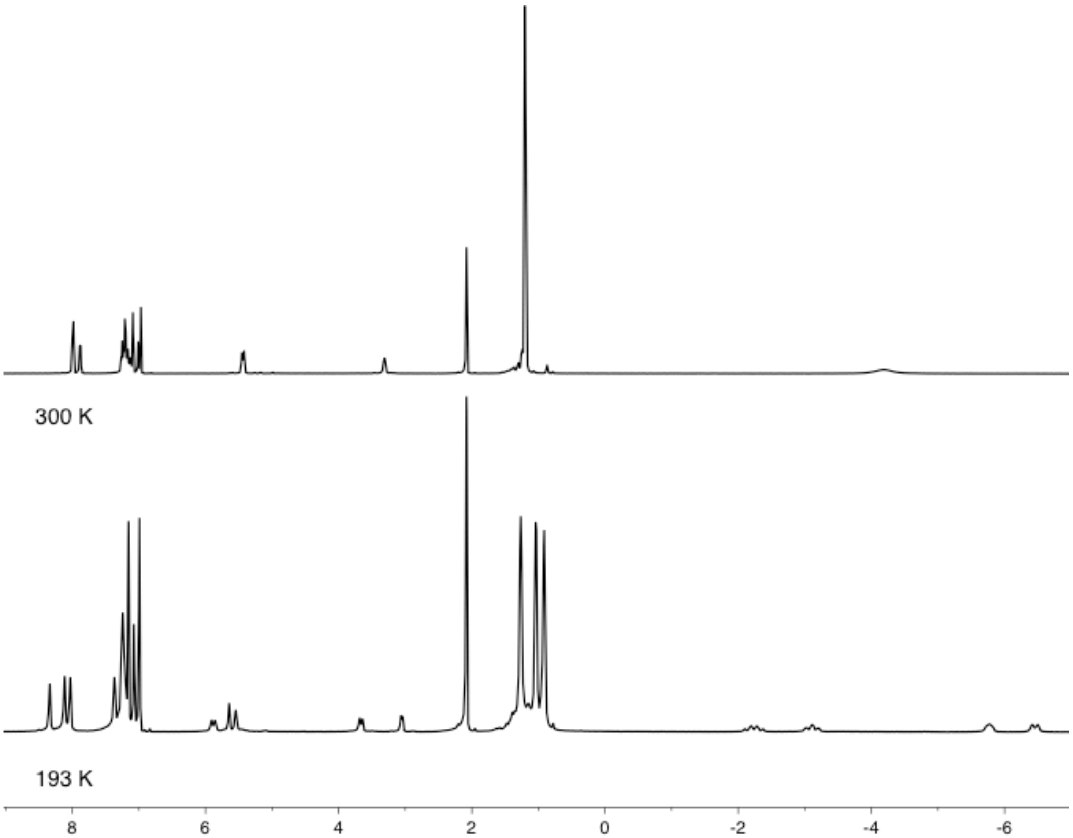

Figure 7. Variable Temp. ^1H NMR Spectra of $W(PMe_3)_3H_4(SiH_2Ph)(SiH_2SiHPh_2)$

One interesting feature of both of these compounds is the rare -SiH_2SiHPh_2 moiety; there are only three structurally characterized compounds in the Cambridge Structural Database of the type M(SiH_2SiR_3) (R = H, Ph).[9] All of these previously reported compounds were generated by treating a metal complex with a disilane; the Si-Si bond was not formed during the reaction with the metal. In this system, the existence of the -SiH_2SiHPh_2 ligand demonstrates that W(PMe_3)$_4$(η^2–CH_2PMe_2)H is capable of forming Si-Si bonds, which is necessary for forming disilanes, oligosilanes, and polysilanes. In addition, the -SiH_2SiHPh_2 unit shows the ability of W(PMe_3)$_4$(η^2–CH_2PMe_2)H to cause redistribution at silicon.

2.3.2 Mechanistic Insights into the formation of the W-SiH_2SiHPh_2 Moiety – Literature Precedent

Insight into the mechanism of the formation of W(PMe_3)$_3$$H_4$($SiH_2Ph$)($SiH_2SiHPh_2$) and W($PMe_3$)$_4$$H_3$($SiH_2SiHPh_2$) may be gained by examining previously reported studies on metal(silyl)silylene complexes. For example, iron complexes of the type $Cp^RFe(CO)_2Me$ (Cp^R = Cp or Cp*) may be photolyzed in the presence of a disilane, $HMe_2SiSiMes_2Me$, to generate iron(silyl)silylene complexes $Cp^RFe(CO)(=SiMes_2)(SiMe_3)$.[10] The Cp* derivative was structurally characterized.[10] The mechanism proposed for the formation of this product involves initial oxidative addition of the hydrodisilane, 1,2-silyl migration, and subsequent 1,3-migration of a methyl group (Scheme 3).[11] Such migratory steps have been proposed previously for the redistribution and deoligomerization of organosilanes.[12,13,14,15] When the iron(silyl)silylene complex was treated with Bu^{t}NC and heated, a disilanyl compound Cp*Fe(CO)(CN^{t}Bu)($SiMesMeSiMesMe_2$) was isolated as the main product.[10] Presumably, this product is formed *via* 1,3-migration of the methyl and mesityl groups followed by 1,2-silyl migration (Scheme 3). Analogous mechanistic steps are proposed for the formation of W(PMe_3)$_3$$H_4$($SiH_2Ph$)($SiH_2SiHPh_2$) and W($PMe_3$)$_4$$H_3$($SiH_2SiHPh_2$) (Scheme 4).

Specifically, initial oxidative addition of 2 equivalents of $PhSiH_3$ to the tungsten center would produce a bis(phenylsilyl) complex, which could undergo α-elimination of a W-SiH_2Ph hydrogen to produce a silylene intermediate of the type $W(PMe_3)_3H_3(=SiHPh)(SiH_2Ph)$. 1,3-migration of a phenyl group produces an isomeric silylene complex, $W(PMe_3)_3H_3(=SiH_2)(SiHPh_2)$, from which subsequent 1,2-silyl migration may occur. PMe_3 or $PhSiH_3$ may add to this coordinatively unsaturated disilanyl intermediate, producing the observed products. Support for the proposed $[W(PMe_3)_3H_2(SiH_2Ph)_2]$ intermediate is provided by the isolation of $W(PMe_3)_3H_4(SiH_2Ph)_2$ when the reaction of $W(PMe_3)_4(\eta^2\text{–}CH_2PMe_2)H$ with $PhSiH_3$ is performed under an atmosphere of H_2; the formation of $W(PMe_3)_3H_4(SiH_2Ph)_2$ is presumably due to the oxidative addition of H_2 to $[W(PMe_3)_3H_2(SiH_2Ph)_2]$. The molecular structure of $W(PMe_3)_3H_4(SiH_2Ph)_2$ is shown in Figure 8, and its formation is illustrated in Scheme 2.

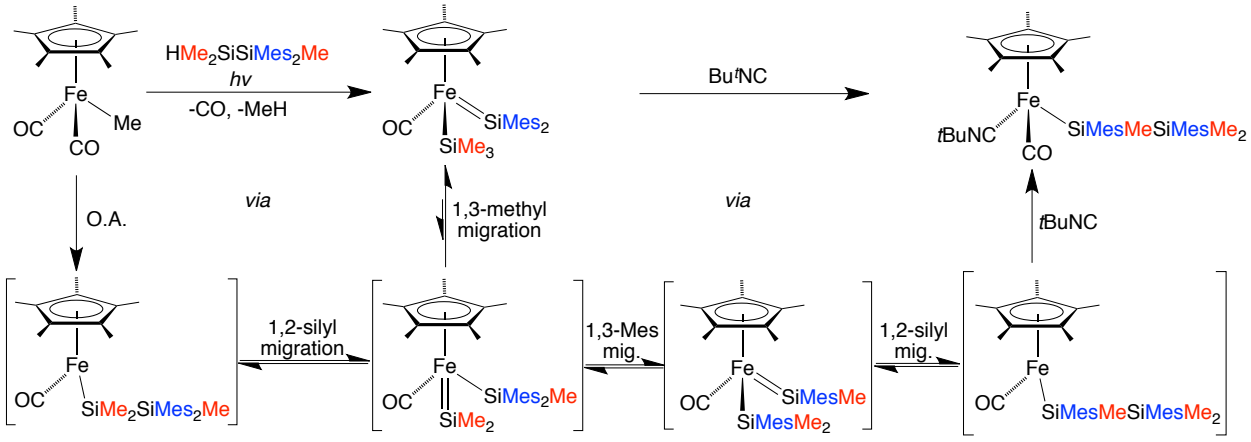

Scheme 3. Proposed literature mechanism involving silylene intermediates and disilanyl ligands

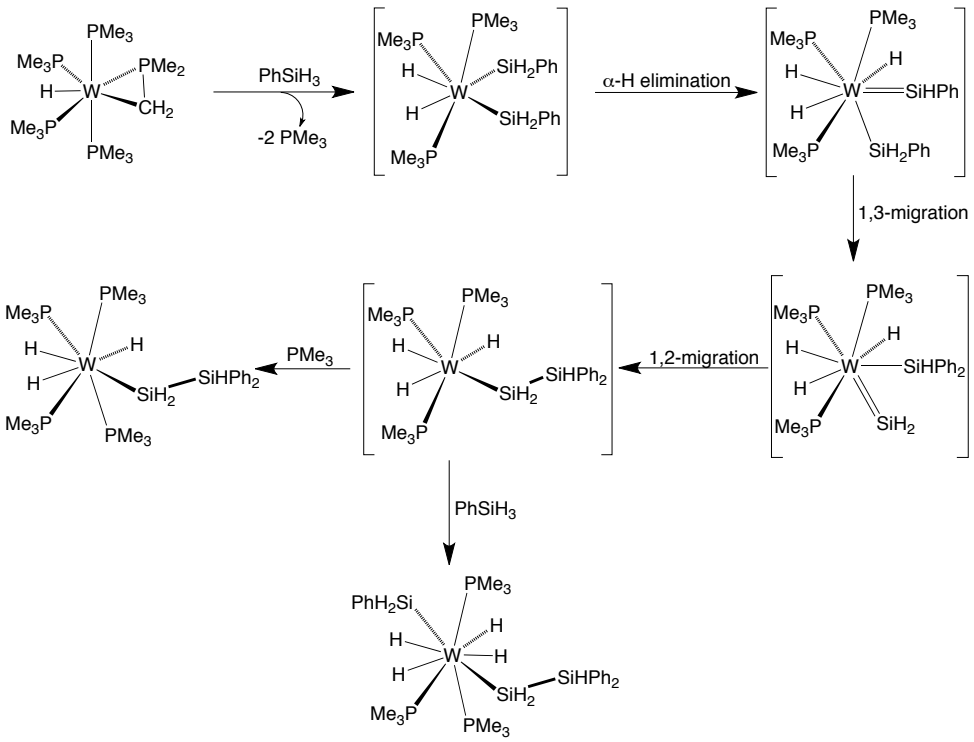

Scheme 4. Proposed mechanism for the formation of $W(PMe_3)_3H_4(SiH_2Ph)$-(SiH_2SiHPh_2) and $W(PMe_3)_4H_3(SiH_2SiHPh_2)$

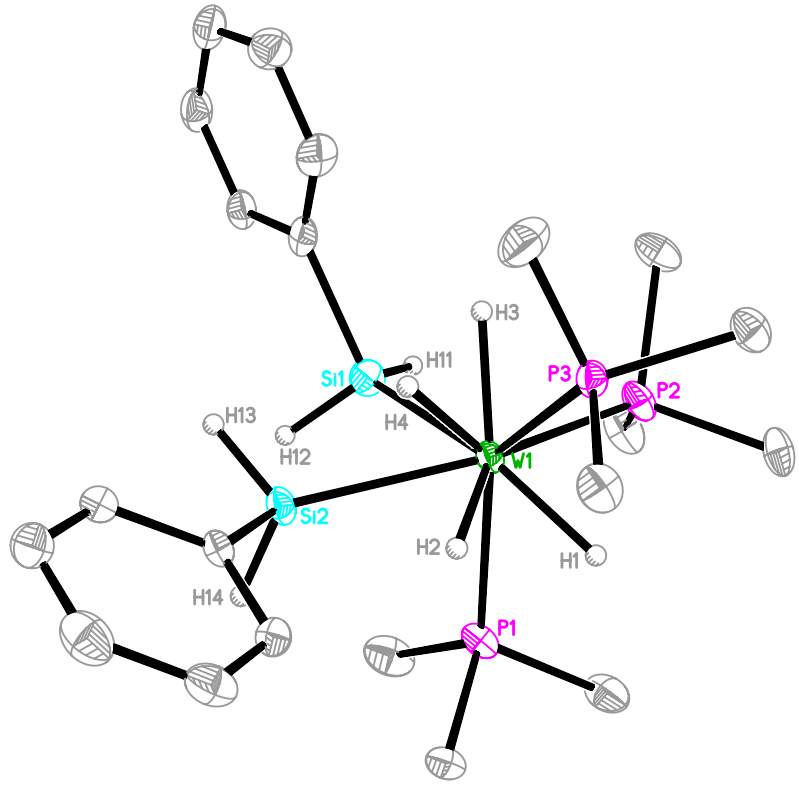

Figure 8. Molecular Structure of $W(PMe_3)_3H_4(SiH_2Ph)_2$

2.3.3 Mechanistic Insights into the formation of the W-SiH_2SiHPh_2 Moiety – DFT Calculations

Density Functional Theory (DFT) geometry optimization calculations of these proposed intermediates confirm that such a pathway is chemically rational, energetically accessible, and thermodynamically favorable. The energy profile for the mechanism is shown in Figure 9, where $W(PMe_3)_4H_3(SiH_2SiHPh_2)$ is the final product. The energy difference for the conversion of $W(PMe_3)_4H_3(SiH_2SiHPh_2)$ and $PhSiH_3$ to $W(PMe_3)_3H_4(SiH_2Ph)(SiH_2SiHPh_2)$ and PMe_3 is also calculated to be small and thermodynamically downhill (Scheme 5). This calculated energy difference is consistent with experimental results in which the disilanyl species interconvert, albeit not without decomposition, at 60 ˚C. Specifically, treatment of $W(PMe_3)_4H_3(SiH_2SiHPh_2)$ with $PhSiH_3$ and heating at 60 ˚C results in almost quantitative formation of $W(PMe_3)_3H_4(SiH_2Ph)(SiH_2SiHPh_2)$ and PMe_3, while the reverse process affords only small amounts of $W(PMe_3)_4H_3(SiH_2SiHPh_2)$ and $PhSiH_3$.

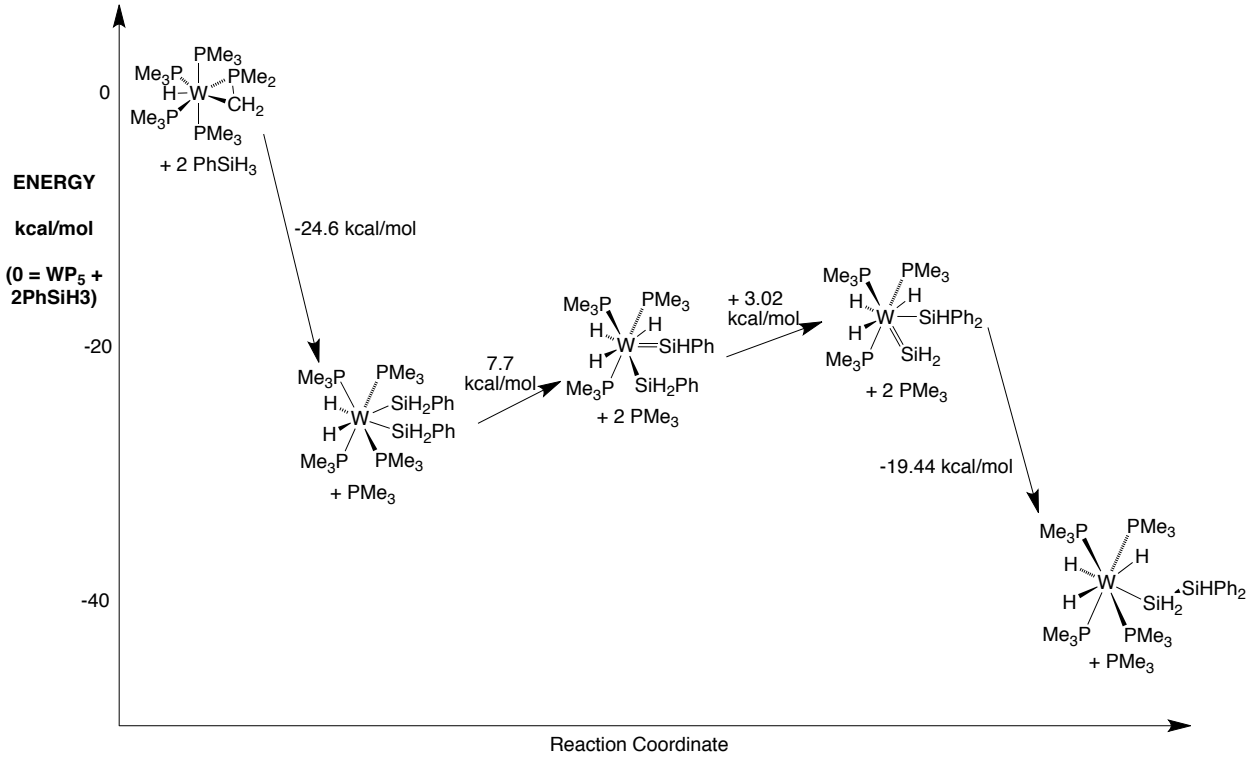

Figure 9. Proposed energy profile for $W(PMe_3)_4(\eta^2–CH_2PMe_2)H + PhSiH_3$

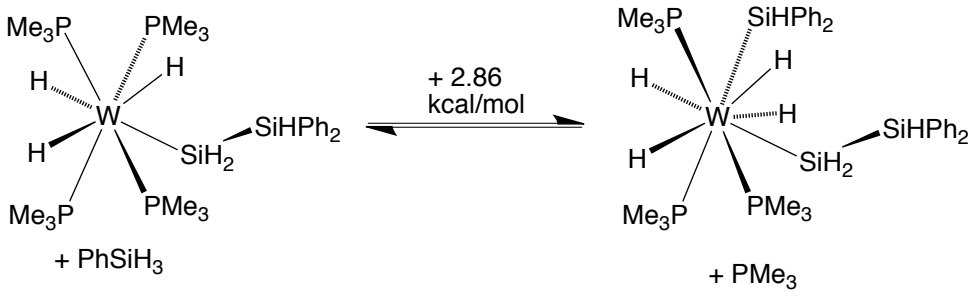

Scheme 5. Calculated energy difference and interconversion between $W(PMe_3)_4H_3(SiH_2SiHPh_2)$ and $W(PMe_3)_3H_4(SiH_2Ph)(SiH_2SiHPh_2)$

2.4 WSiW – A Dinuclear Complex with a Bridging Silylene Ligand

2.4.1 Isolation and Structural Characterization of WSiW

Perhaps the most convincing support for the presence of silylene intermediates in this reaction comes from the isolation of a complex with a bridging silylene ligand, $[W(PMe_3)_2(SiHPh_2)H_2](\mu\text{-}Si,P\text{-}SiHPhCH_2PMe_2)(\mu\text{-}SiH_2)[W(PMe_3)_3H_2]$ ("WSiW"). This complex is reproducibly made and isolated under the same conditions as $W(PMe_3)_4H_3(SiH_2SiHPh_2)$, albeit in low yields (i.e. < 5%) (Scheme 6). The two compounds may be separated by multiple crystallizations; specifically, the first crystallization process consistently affords crystals of WSiW, while the second crystallization yields $W(PMe_3)_4H_3(SiH_2SiHPh_2)$.

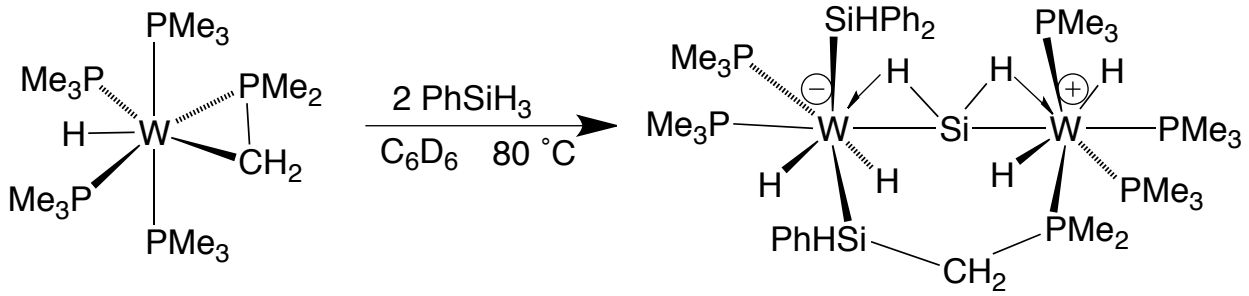

Scheme 6. Formation of WSiW (one resonance structure depicted)

The most noteworthy feature of the crystal structure of WSiW (Figure 10) is the unusually short W-Si bonds between the tungsten center and the bridging silicon. The W1-Si1 distance is 2.2813(13) Å, which is significantly shorter than the shortest previously reported W-Si distance in the Cambridge Structural Database (2.353 Å). The W2-Si1 distance is also notably short at 2.3651(13) Å. For comparison, the average W-Si distance in the CSD is 2.55 Å. The short W-Si distances observed in this complex may, in part, be due to the -SiHPhCH$_2$PMe$_2$- bridge that connects and therefore constrains the two tungsten centers; however, it is likely that these short distances, along with the near-linear geometry around the bridging silicon [W1-Si1-W2 = 176.16(6)°], are indicative of multiple-bond character between Si1 and the tungsten centers. The six hydride ligands, terminal Si-H hydrogens, and CH$_2$ hydrogen atoms of the bridge were located and freely refined isotropically. Selected bond lengths for WSiW are provided in Table 1.

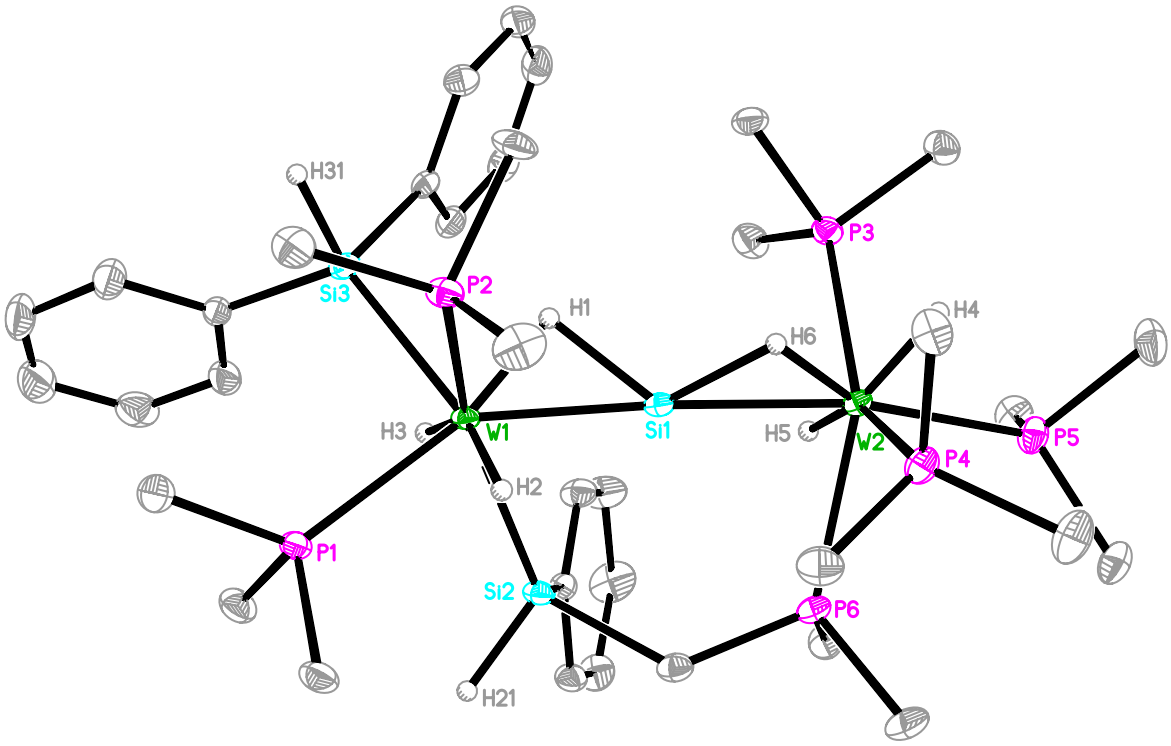

Figure 10. Molecular Structure of WSiW

Table 1. W-H and Si-H Distances of WSiW

Selected Distances	Bond Lengths/Å
W1-H1	1.59(4)
W1-H2	1.46(4)
W1-H3	1.54(4)
W2-H4	1.53(4)
W2-H5	1.53(4)
W2-H6	1.58(5)
Si1-H1	1.68(4)
Si1-H6	1.68(5)
Si2-H21	1.46(4)
Si3-H31	1.45(4)

2.4.2 DFT Calculations on WSiW

Additional support for the experimental structure of WSiW is provided by the fact that this complex is reproduced well by a geometry optimization calculation (Figure 11). The W-H distances in the geometry optimized structure are longer than those in the crystal structure (*i.e.* W-H_{avg} = 1.76 Å *vs*. W-H_{avg} = 1.54 Å), which is to be expected;[16] furthermore, the Si-H distances for the bridging silicon increase substantially to 1.720 Å (Si1-H1) and 1.942 Å (Si1-H6). The optimized structure accurately reflects the other structural traits of the molecule, including the W-Si1 distances (W1-Si1 = 2.300 Å, W2-Si1 = 2.424 Å).

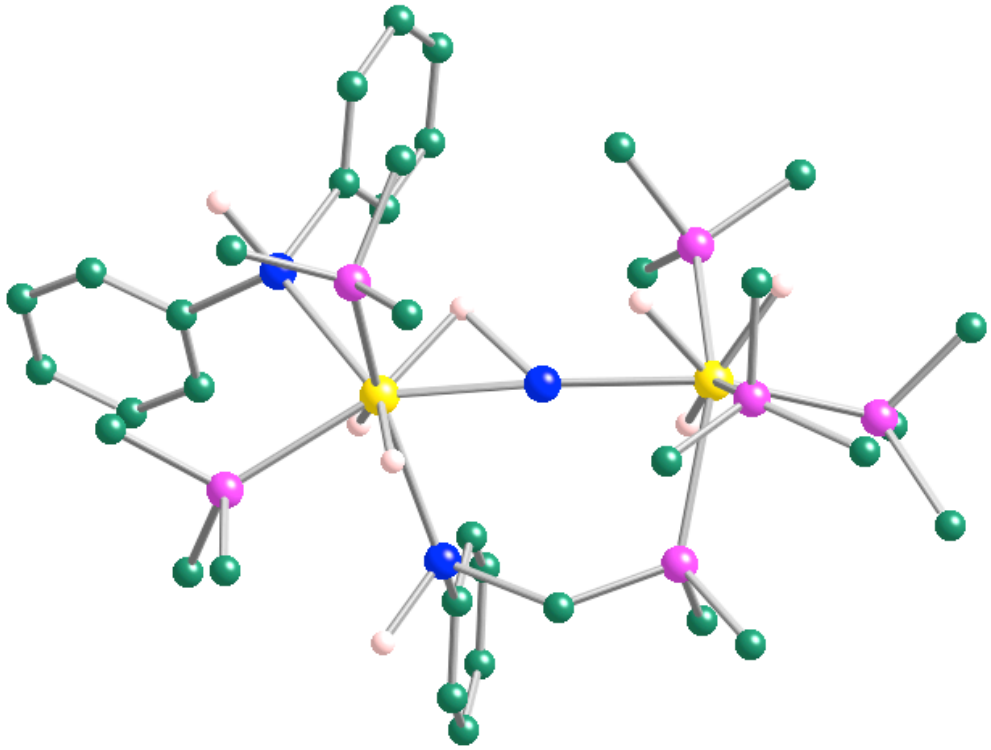

Figure 11. Geometry Optimized Structure of WSiW

Natural Bond Orbital (NBO) Analysis supports the presence of double bond character between the briding silicon and the tungsten centers. Specifically, there is significant double-bond character between W1 and Si1 and a small degree of double bond character between W2 and Si1. A 3-center, 2-electron interaction between W1, Si1, and the bridging hydride (H1) is evident; a similar interaction with a much smaller contribution from Si1 (*i.e.* 12.9% *vs.* 22.7%) is also present for W2, Si2, and H6. The relevant Natural Localized Molecular Orbitals (NLMOs) and primary atomic contributions are presented in Figures 12 and 13. Thus, the bonding description of WSiW presented in Scheme 6 represents a resonance structure that is most consistent with the experimentally determined Si-H distances for this molecule, and NBO analysis indicates that other resonance structures are likely also valid for this compound (Figure 14).

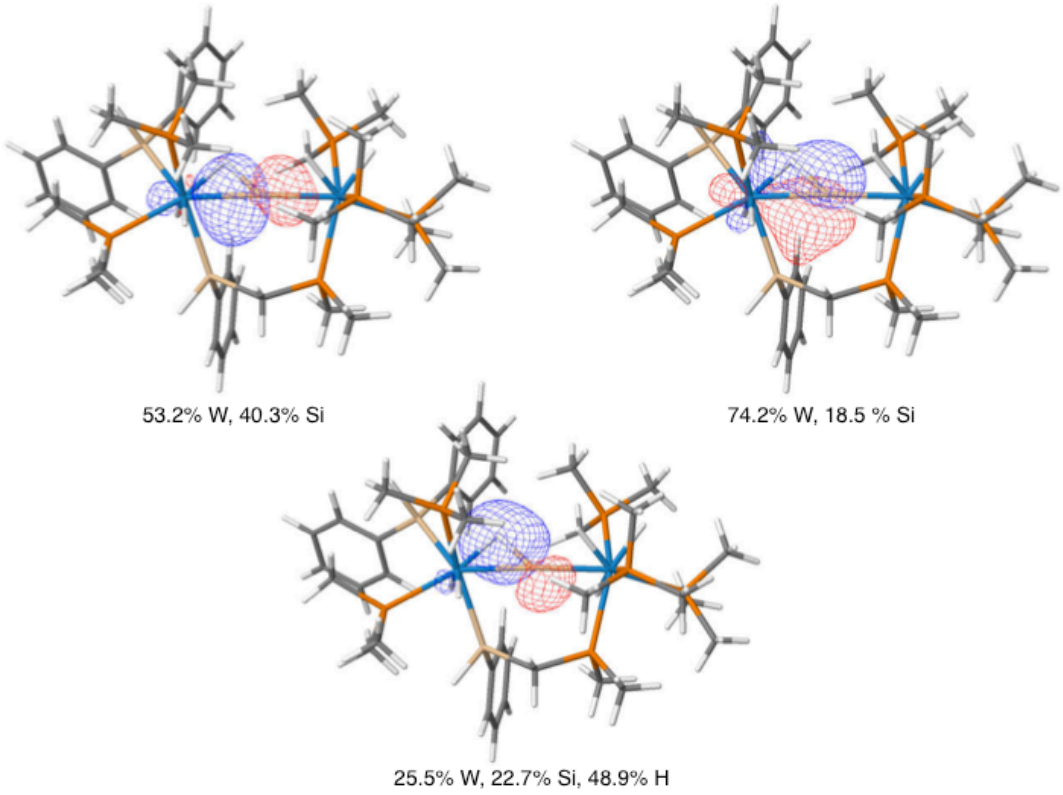

Figure 12. NLMOs for W1-Si1 bonding

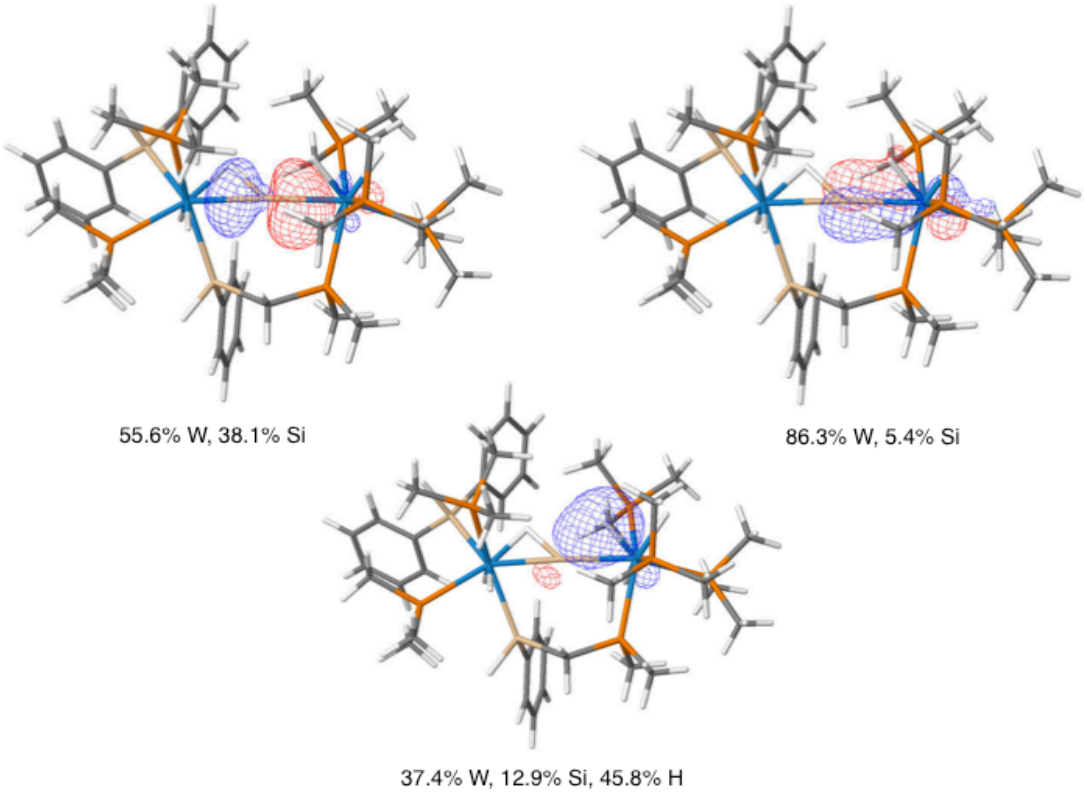

Figure 13. NLMOs for W2-Si1 bonding

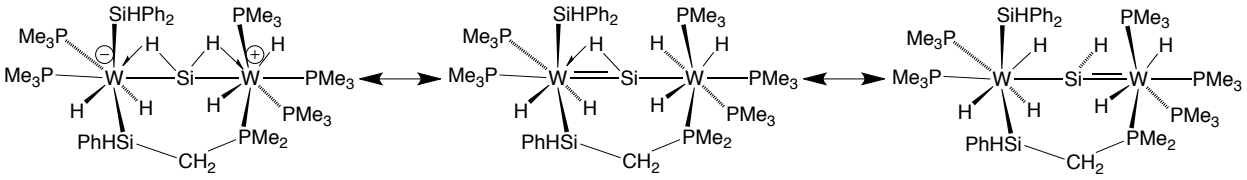

Figure 14. Resonance Structures for WSiW

DFT calculations also support a mechanism for the formation of WSiW (Figure 15) which shares the same intermediate, $[W(PMe_3)_3H_3(SiHPh_2)(=SiH_2)]$, that is invoked in the formation of $W(PMe_3)_3H_4(SiH_2Ph)(SiH_2SiHPh_2)$ and $W(PMe_3)_4H_3(SiH_2SiHPh_2)$. The energies of the geometry optimized structures of these intermediates demonstrate that such a mechanism is energetically feasible and that the reaction is thermodynamically favorable, with a net enthalpy change of approximately -35 kcal/mol.

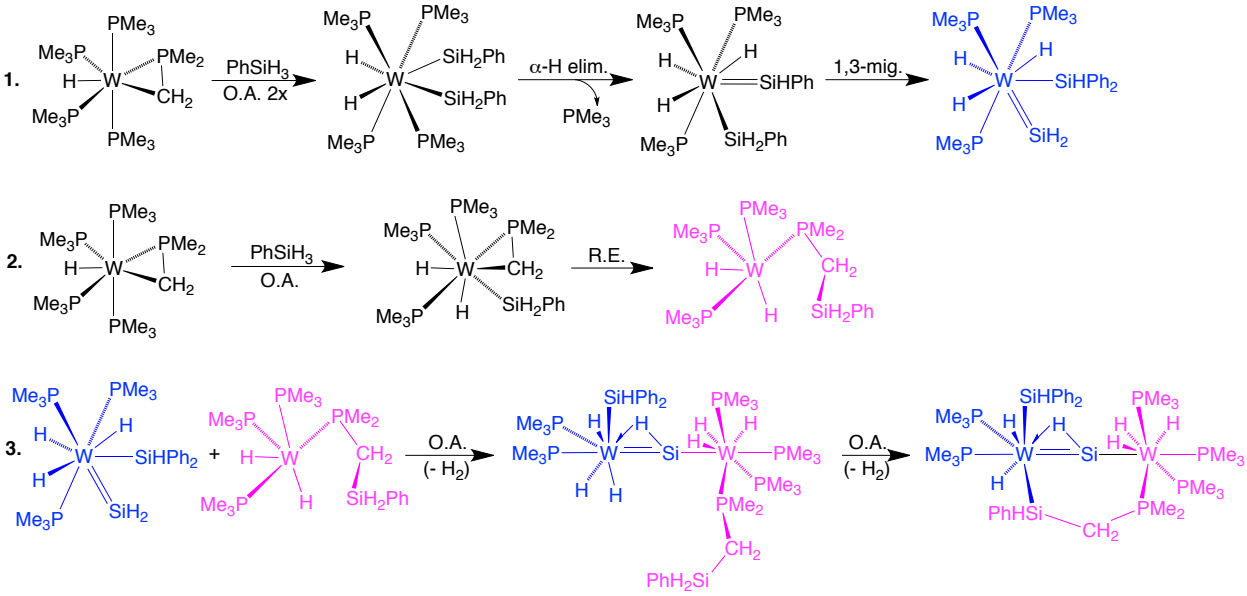

Figure 15. Proposed Mechanism for the Formation of WSiW

2.4.3 Spectroscopic Characterization of WSiW

WSiW has also been characterized spectroscopically. ^{1}H, $^{1}H\{^{31}P\}$, NOESY, $^{31}P\{^{1}H\}$, ^{31}P COSY, ^{29}Si, $^{29}Si\{^{1}H\}$ INEPT, ^{1}H-^{29}Si HMQC, and ^{1}H-^{29}Si HMBC NMR spectroscopic experiments have been performed on this compound. WSiW is fluxional at room

temperature, such that the ^{1}H NMR spectrum displays two broad hydride resonances, each corresponding to three hydrogens; the phosphine signals appear as two broad peaks, and the Si-H hydrogens of the -$SiHPh_2$ and -$SiHPhCH_2$- ligands overlap at room temperature (Figure 16, a). At 210 K, however, the presence of six unique hydride environments is revealed, although three of the resonances overlap, and the Si-H signals are resolved (Figure 16, b). The $^{31}P\{^{1}H\}$ NMR spectrum also transforms from two broad resonances at room temperature to six distinct signals at 210 K.

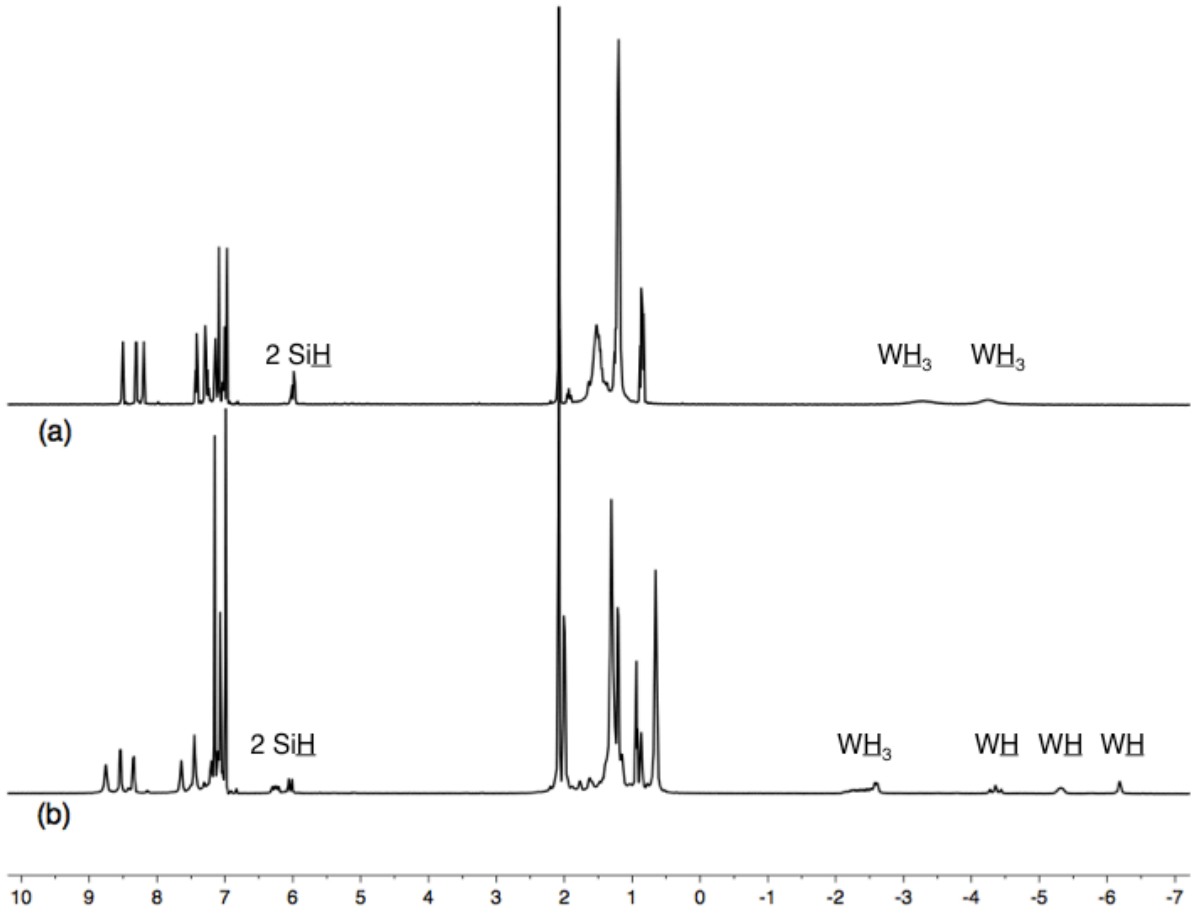

Figure 16. ^{1}H NMR of WSiW at (a) room temperature (300 K) and (b) low temperature (210 K)

Significantly, however, no ^{29}Si signal is observed for the bridging silicon. Two signals are observed in the ^{29}Si NMR spectrum, and their assignment as the -$SiHPh_2$ and -$SiHPhCH_2$- silicon atoms is confirmed by a ^{1}H-^{29}Si HMQC experiment. The notable

absence of a signal for the bridging silicon may be attributed to a number of factors. The ^{29}Si nucleus is not only low abundance (*ca*. 4.7 %) and low sensitivity, but it also has a negative gyromagnetic ratio and long relaxation time. Specifically, the negative gyromagnetic ratio results in a negative nuclear Overhauser effect for a ^{29}Si resonance under conditions of broad-band decoupling, such that the intensity of the signal may be diminished or depressed into the baseline if the ^{29}Si nucleus is in close proximity (< 3 Å) to any protons.[17]

A number of techniques were tried in order to avert these issues but were unsuccessful. $Cr(acac)_3$, a paramagnetic relaxation agent that has been used successfully in ^{29}Si NMR spectroscopy,[18,19] was added to a sample used for ^{29}Si NMR; although the signals in the ^{1}H NMR spectrum did broaden, as they are expected to with a shorter relaxation time, only two signals were observed in the ^{29}Si NMR spectrum. ^{1}H-^{29}Si HMQC spectroscopy may be used to characterize silyl compounds with terminal Si-H hydrogens; however, a significant (*i.e.* J = 120-215 Hz) coupling constant is required for this experiment. As such, the two silyl ligands with Si-H hydrogens are easily established by this method, but the bridging silicon is not. This is presumably due to the fact that it has only one 3-center 2-electron interaction with a bridging hydride, and that interaction is fluxional.[20] It was thus considered that an HMBC experiment, in which longer-range couplings (J = 2-15 Hz) are examined, might reveal the missing silicon. Unfortunately, no signal was observed using this technique over a wide range of coupling constants.

The observation of the bridging silicon was further hindered by the fact that ^{29}Si NMR spectra feature a large, broad glass peak ranging from *ca*. -50 to 150 ppm. Use of a PTFE tube did not help, however, since the probe of the NMR instrument also contains glass. WSiW is fairly insoluble in benzene and toluene (approximately 20 mg/mL), such that large amounts of the compound cannot be used for ^{29}Si NMR spectroscopic analysis. Thus, it is possible that the signal corresponding to the bridging silicon may be

obscured by the glass signal; alternatively, it may be absent all together due to the negative NOE.

2.4.4 Isomerization of WSiW to WSiW*

WSiW is thermally stable at room temperature and persists in solution for many days under an argon atmosphere; however, it is light sensitive and undergoes a facile transformation in ambient light. The ^{1}H NMR spectrum of the light-induced product (WSiW*) shares many features in common with the ^{1}H NMR spectrum of WSiW (Figure 17). For example, three chemically inequivalent phenyl groups are evident, as are two distinct Si-H resonances and a signal corresponding to a diastereotopic bridge C-H hydrogen. (For both WSiW and WSiW*, the second diastereotopic C-H hydrogen is obscured by a phosphine resonance). Although a total of six hydride ligands is retained in WSiW*, they are observed in a 4:2 ratio rather than the 3:3 ratio observed for WSiW. The hydride peaks of WSiW*, unlike WSiW, show coupling to phosphorus – the signal corresponding to four hydrides (δ -3.37) couples to two phosphine ligands ($^{2}J_{P\text{-}H}$ = 23 Hz), and the other two hydrides (δ -5.09) couple to four phosphines ($^{2}J_{P\text{-}H}$ = 32 Hz, $^{2}J_{P\text{-}H}$ = 19 Hz). Thus, WSiW* is formulated as an isomer of WSiW (Scheme 7).

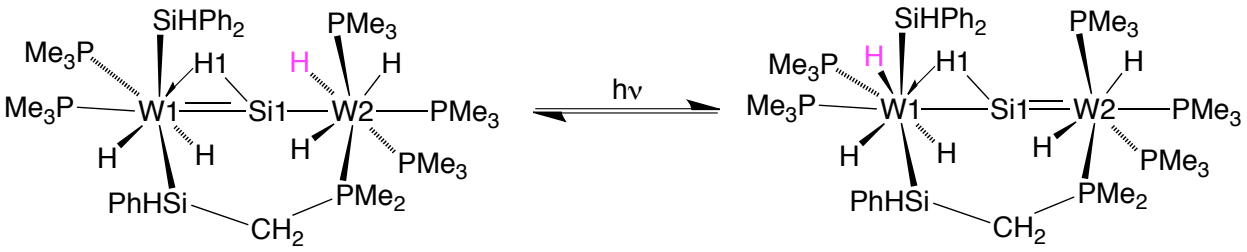

Scheme 7. Proposed Structure of WSiW*

The isolation of WSiW* as a pure compound is impeded by the fact that the conversion of WSiW appears to reach a photostationary state. After *ca*. 2 days in ambient light, the net change of WSiW to WSiW* ceases, and a mixture of WSiW:WSiW* results. Presumably, the frequencies of light required for the forward and reverse

transformations are both in the visible region, thereby resulting in a photochemical equilibrium. UV/Vis Spectrometry was used to characterize (*i*) WSiW and (*ii*) the light-induced mixture of WSiW and WSiW*, with the thought that distinct absorptions in the visible region could be apparent for these two complexes.[21] The absorption spectra (Figure 18) look very similar, however, which probably indicates either that these two complexes have near-identical absorptions or that WSiW* absorbs only very weakly. Attempts to crystallize WSiW* from mixtures of the two isomers produced only crystals of WSiW. This is most likely due to the greater propensity of WSiW to crystallize, which pushes the equilibrium towards WSiW as this complex comes out of solution.

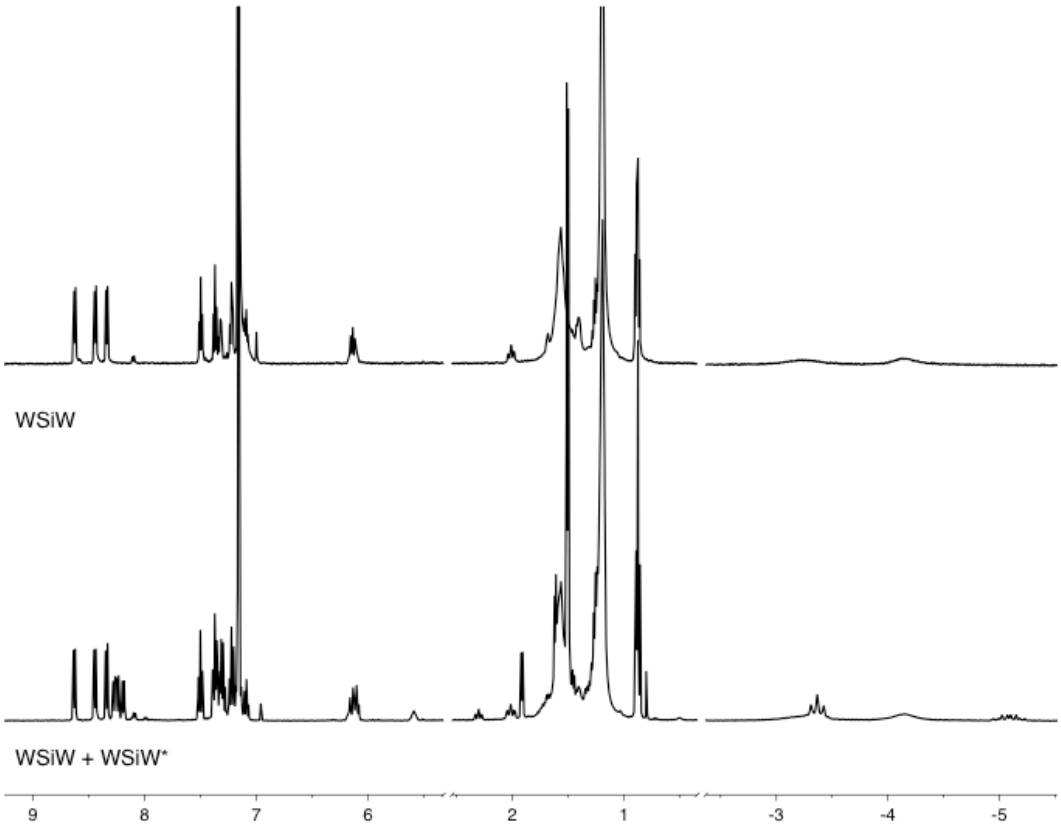

Figure 17. ^{1}H NMR Spectrum of (a) WSiW and (b) the WSiW/WSiW* equilibrium

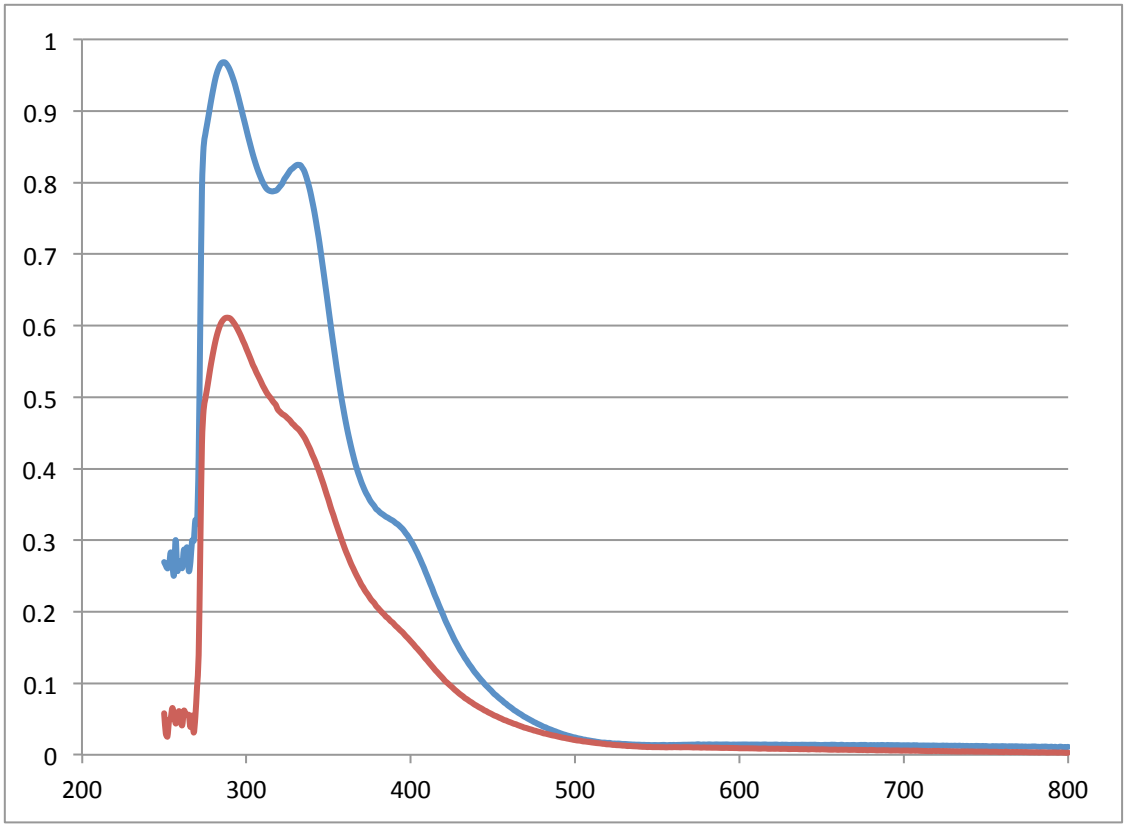

Figure 18. UV/Vis Absorption Spectra of WSiW (blue) and WSiW/WSiW* (red)

2.4.5 DFT Calculations on WSiW*

WSiW* is formally derived from WSiW *via* migration of a hydride and a shift of the double bond from W1=Si1 to W2=Si1. Accordingly, the structure of such an isomer is expected to have a W1-Si1 distance greater than that of WSiW and a W2-Si1 distance that is shorter. While WSiW* has not been characterized by X-ray diffraction, its proposed structure has been examined by a DFT geometry optimization calculation (Figure 19). These calculations support the proposal of this isomer and accurately reflect the expected change in bond distances; for example, the W1-Si1 distance in the geometry optimized structure is 2.479 Å, and the W2-Si1 distance is 2.323 Å. Key structural differences between the geometry optimized structures of WSiW and WSiW* are provided in Table 2.

Table 2. Structural differences between WSiW and WSiW*. Labels are specified in Scheme 7.

Selected Bond	WSiW Bond Lengths/Å	WSiW* Bond Lengths/Å
W1-Si1	2.300	2.480
W2-Si1	2.424	2.323
W1-H1	1.830	1.786
Si1-H1	1.719	1.915

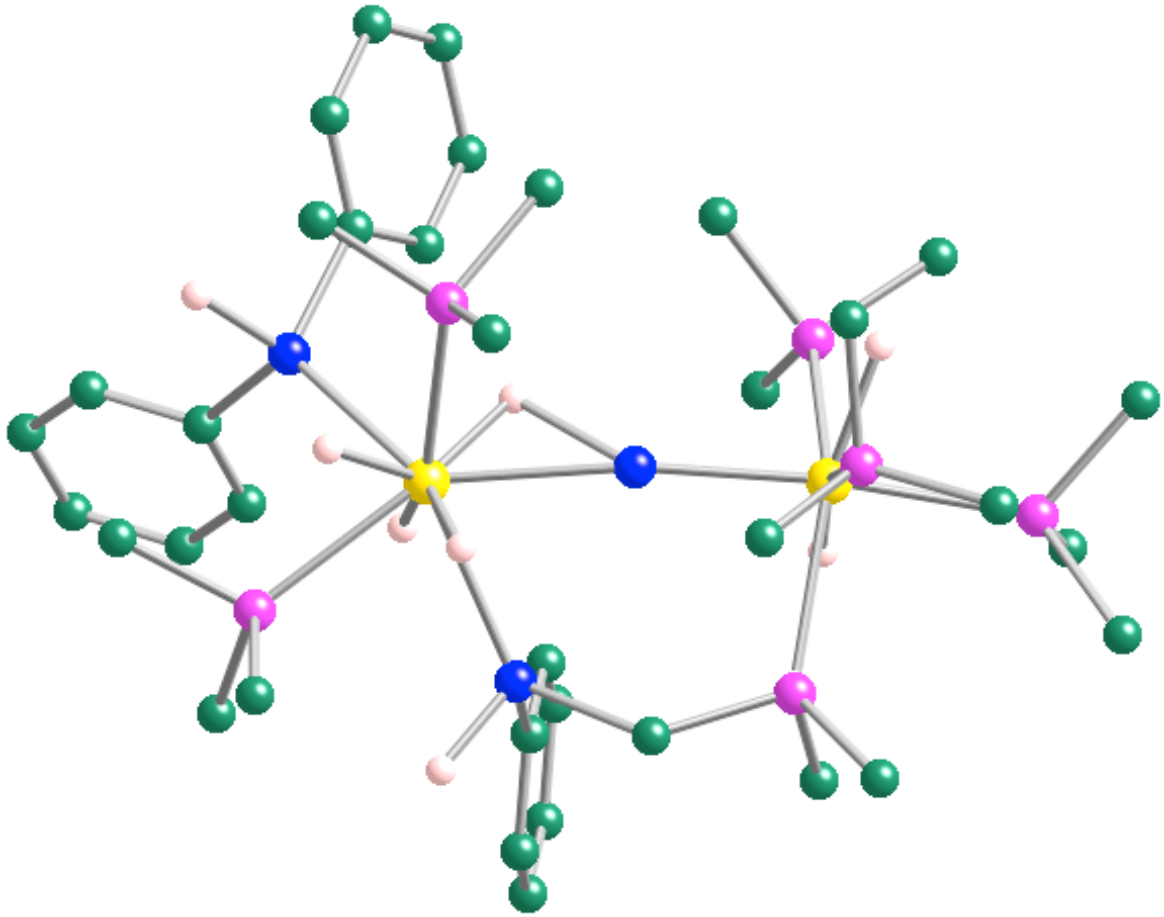

Figure 19. Geometry Optimized Structure of WSiW*

There is another hypothetical isomer of WSiW* (Scheme 8) whose structure would be consistent with the observed ^{1}H NMR spectrum. This alternative isomer formulation possesses a structure in which a hydride and a diphenylsilyl ligand migrate, resulting in

complex where W2 is coordinated to four phosphines and the –$SiHPh_2$ group. Attempts to geometry optimize this structure, however, reveal that it would be extremely sterically hindered. Therefore, it is not considered to be a likely option.

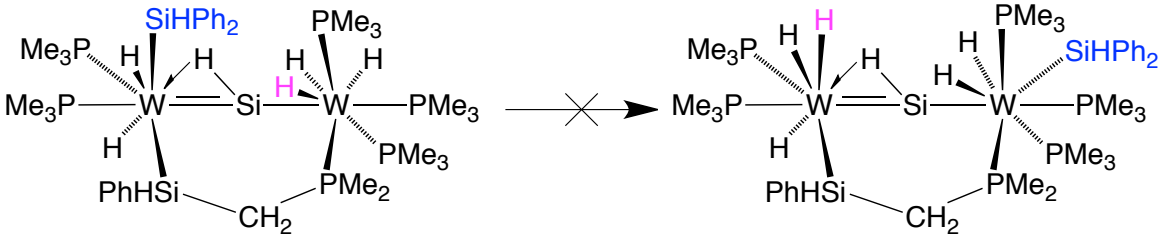

Scheme 8. Alternate (but unlikely) Structure of WSiW*

2.4.6 Isolation of WSiW#

Further support for the proposed formulation of WSiW* comes from the isolation and structural characterization of another analogous complex (WSiW#) (Figure 20), which is formally derived from WSiW or WSiW* by replacement of an equivalent of Ph_2SiH_2 by PMe_3. This compound was isolated from the decomposition of WSiW; however, there is evidence to support its formation from the reaction of WSiW* with PMe_3 (Scheme 9). Heating WSiW with PMe_3 at 80 ˚C in ambient light results in decomposition, and heating in the dark produces no reaction. When WSiW is allowed to isomerize to WSiW* and then treated with PMe_3 and heated in ambient light, decomposition occurs. However, when isomerization to WSiW* is followed by heating in the presence of PMe_3 in the dark, a relatively clean transformation of WSiW* is observed to a product whose ^1H NMR spectrum is consistent with WSiW# (Figure 21).

Specifically, the new compound that is generated lacks three inequivalent phenyl groups, has one Si-H proton, and features a hydride signal (δ = -5.70) that couples to four phosphines ($^2J_{P\text{-}H}$ = 27, 9). A second hydride resonance is also partially visible but is mainly obscured by the signal of residual WSiW. Furthermore, Ph_2SiH_2 is produced over this reaction, which supports the assignment of the product as WSiW#.

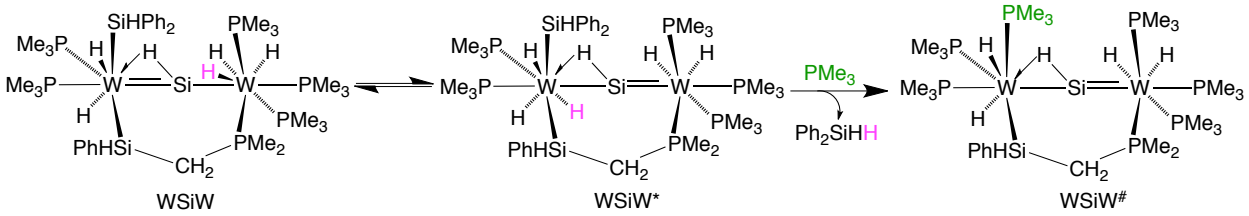

Scheme 9. Proposed formation of WSiW#

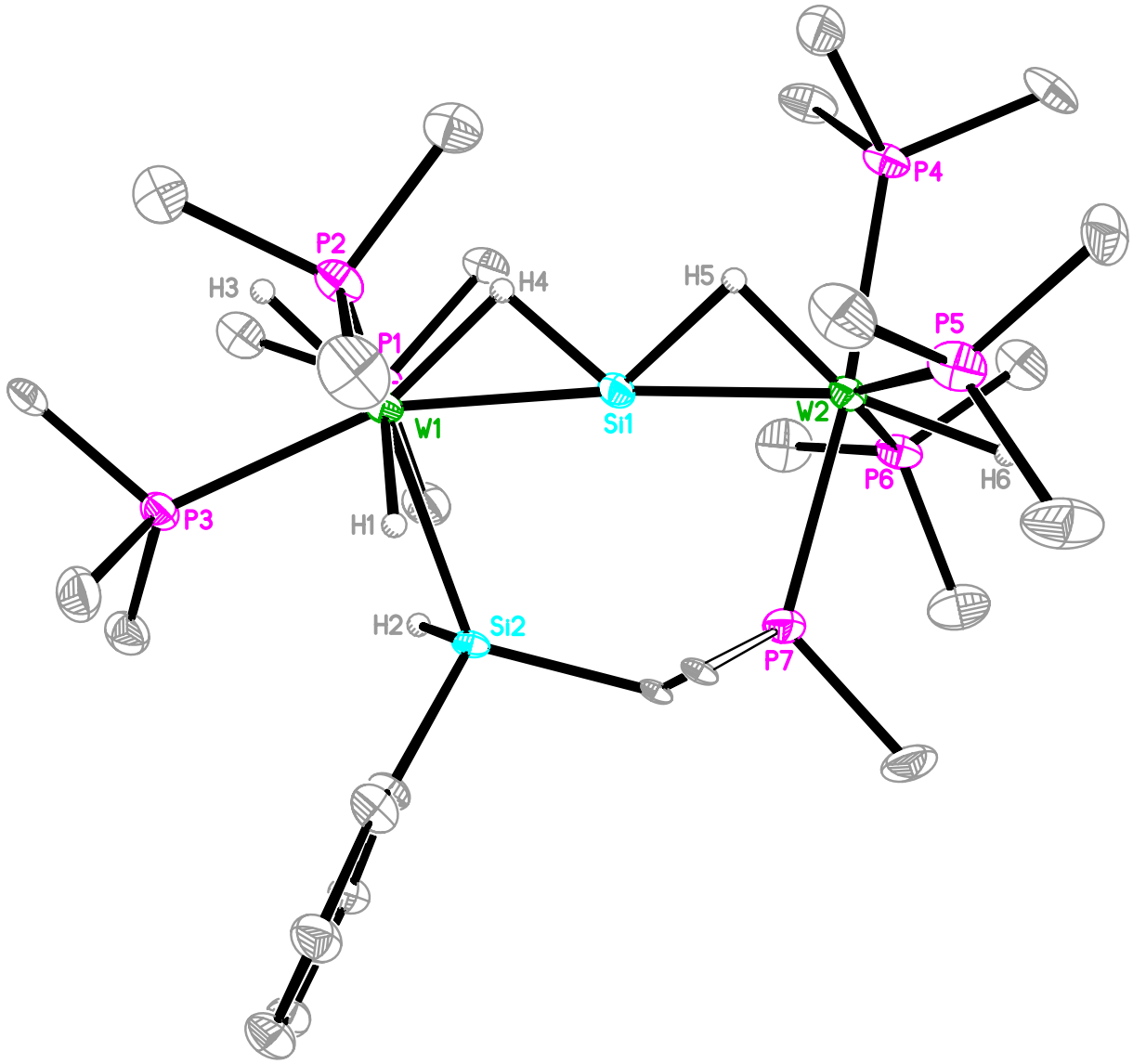

Figure 20. Molecular Structure of WSiW#

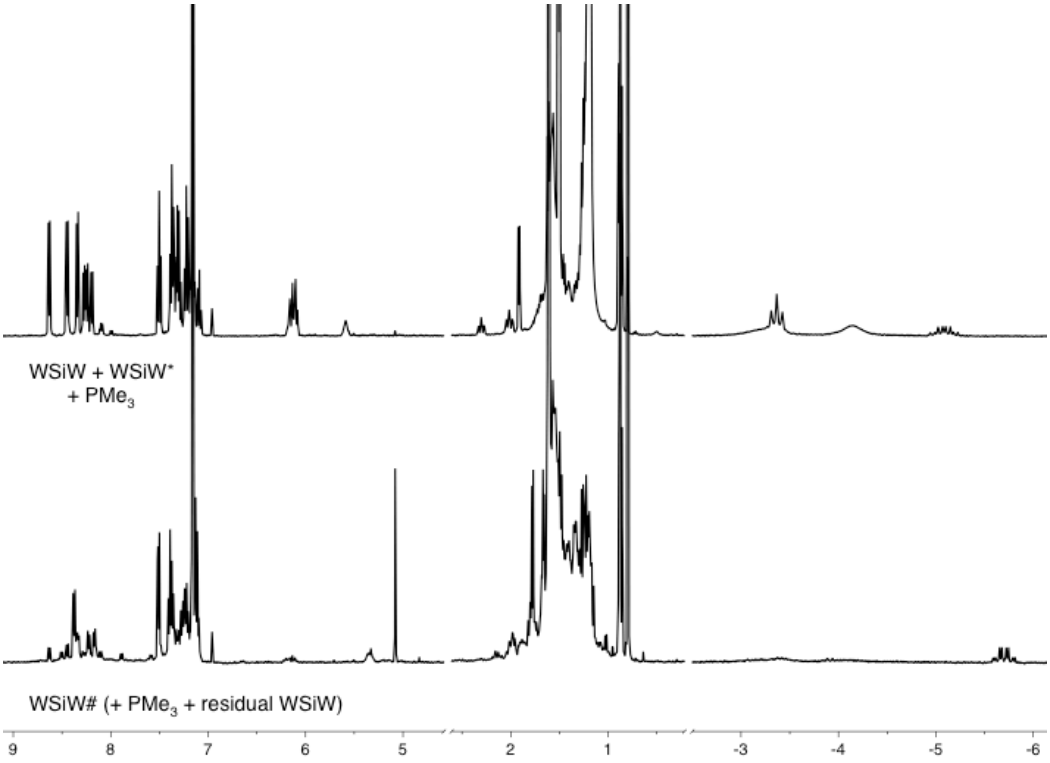

Figure 21. ^{1}H NMR spectrum of the reaction of WSiW* with PMe_3

2.5 $W(PMe_3)_4(\eta^2–CH_2PMe_2)H + Ph_2SiH_2$

2.5.1 Synthesis of $W(PMe_3)_3H_4(\sigma\text{-}HSiHPh_2)$

The reactivity of $W(PMe_3)_4(\eta^2–CH_2PMe_2)H$ towards SiH_4 and $PhSiH_3$ has been shown to be dramatically different, in most regards, than the reactivity of $Mo(PMe_3)_6$ towards these reagents (see Chapter 1). This divergence in reactivity is partially true for the reaction of $W(PMe_3)_4(\eta^2–CH_2PMe_2)H$ with Ph_2SiH_2 as well. For example, $Mo(PMe_3)_6$ reacts with Ph_2SiH_2 to form a disilane complex, $Mo(PMe_3)_3H_2(\kappa^2\text{-}H_2\text{-}H_2Si_2Ph_4)$, as the major initial product; $Mo(PMe_3)_4H(\kappa^2\text{-}H_2\text{-}H_2SiPh_2H)$, a hypervalent silyl species, is formed as the major final product at room temperature. Both of these complexes react with H_2 to form a diphenylsilane adduct, $Mo(PMe_3)_3H_4(\sigma\text{-}HSiHPh_2)$ (see Scheme 12 of Chapter 1). Although $W(PMe_3)_4(\eta^2–CH_2PMe_2)H$ does *not* form analogous disilane and hypervalent silyl complexes when treated with Ph_2SiH_2, it does form the diphenylsilane adduct, $W(PMe_3)_3H_4(\sigma\text{-}HSiHPh_2)$, as the only isolable product (Scheme 10) (Figure 23).

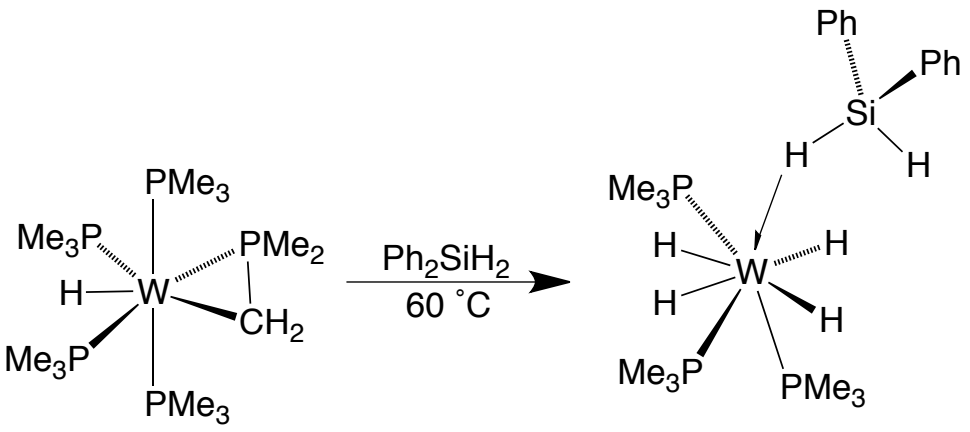

Scheme 10. Preparation of $W(PMe_3)_3H_4(\sigma\text{-}HSiHPh_2)$

Although $W(PMe_3)_3H_4(\sigma\text{-}HSiHPh_2)$ is the only product isolated, ^1H NMR spectroscopic analysis of the reaction indicates that treatment of $W(PMe_3)_4(\eta^2\text{–}CH_2PMe_2)H$ with Ph_2SiH_2 affords two major products whose ratio is determined by the amount of Ph_2SiH_2 added. The formation of $W(PMe_3)_3H_4(\sigma\text{-}HSiHPh_2)$ is favored by a large excess of Ph_2SiH_2. In addition, $W(PMe_3)_3H_4(\sigma\text{-}HSiHPh_2)$ may be formed as the exclusive product when the reaction of $W(PMe_3)_4(\eta^2\text{–}CH_2PMe_2)H$ with Ph_2SiH_2 is performed under an atmosphere of H_2. The ^1H NMR spectrum of $W(PMe_3)_3H_4(\sigma\text{-}HSiHPh_2)$ (Figure 22) features two sharp quartets in a 1:5 ratio corresponding to the terminal Si-H hydrogen (δ 6.74) and five hydrides (δ -3.34). The lack of distinction between the bridging hydride and the four terminal M-H hydride ligands was also observed in $Mo(PMe_3)_3H_4(\sigma\text{-}HSiHPh_2)$.

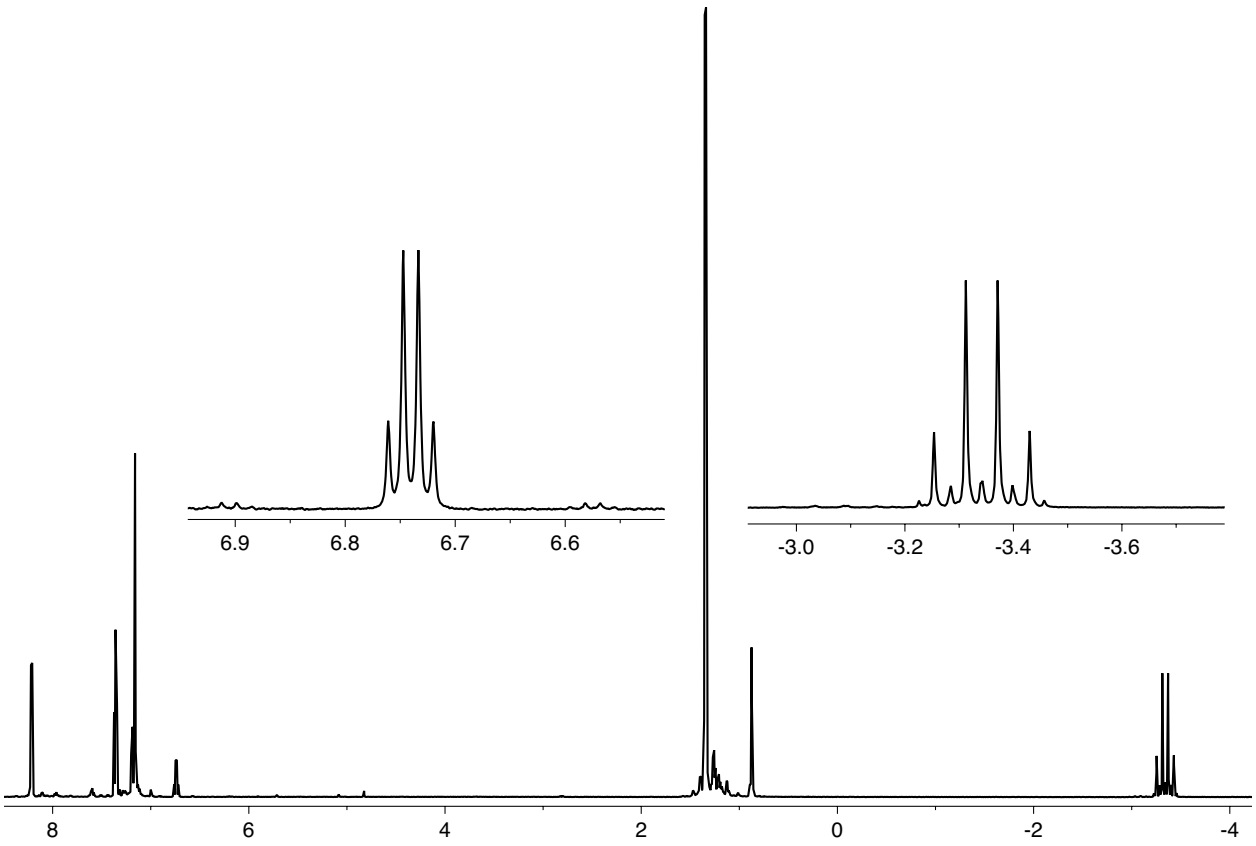

Figure 22. ^{1}H NMR Spectrum of W(PMe$_3$)$_3$H$_4$(σ-HSiHPh$_2$)

2.5.2 Tentative Assignment of W(PMe$_3$)$_3$H$_2$(κ^2-*H*$_2$-H$_2$SiHPh)

The other major product from the reaction of W(PMe$_3$)$_4$(η^2–CH$_2$PMe$_2$)H with Ph$_2$SiH$_2$ is characterized by a ^{1}H NMR spectrum that features doublet of triplet signals at δ 6.27 and -2.98 in a 1:4 ratio, presumably corresponding to a terminal silyl hydrogen ($^3J_{P\text{-}H}$ = 10, 7) and four hydrides ($^2J_{P\text{-}H}$ = 29, 25). One structure that is consistent with this ^{1}H NMR spectrum is the phenylsilane adduct W(PMe$_3$)$_3$H$_2$(κ^2-*H*$_2$-H$_2$SiHPh) (Scheme 11).[22,23] Support for this assignment is provided by the fact that Ph$_3$SiH is produced over the course of the reaction, but free PhSiH$_3$ is not observed by ^{1}H NMR spectroscopy. Since the redistribution of Ph$_2$SiH$_2$ to form Ph$_3$SiH will presumably also form PhSiH$_3$, the absence of free PhSiH$_3$ may be due to its coordination to tungsten.[24] Significantly, the reaction of W(PMe$_3$)$_4$(η^2–CH$_2$PMe$_2$)H with Ph$_2$SiH$_2$ in the presence of H$_2$, which does not

result in the formation of the proposed phenylsilane adduct, also does not result in the formation of Ph_3SiH.

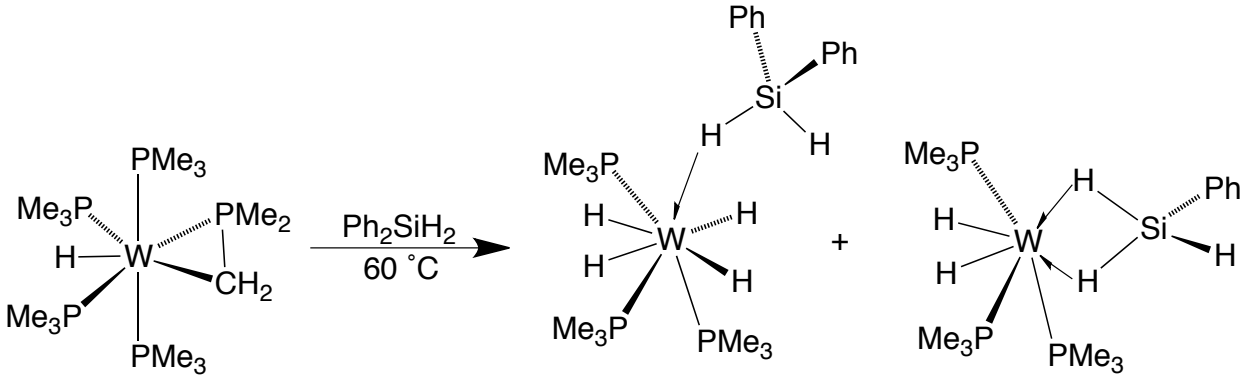

Scheme 11. Reaction of $W(PMe_3)_4(\eta^2–CH_2PMe_2)H$ with Ph_2SiH_2

The solid state structure of $W(PMe_3)_3H_4(\sigma\text{-}HSiHPh_2)$ is isostructural to $Mo(PMe_3)_3H_4(\sigma\text{-}HSiHPh_2)$; however, the four terminal W-H hydrides in this structure could not be freely refined and were therefore constrained to a W-H distance of 1.70 Å. The crystal structure of $W(PMe_3)_3H_4(\sigma\text{-}HSiHPh_2)$ is shown in Figure 23.

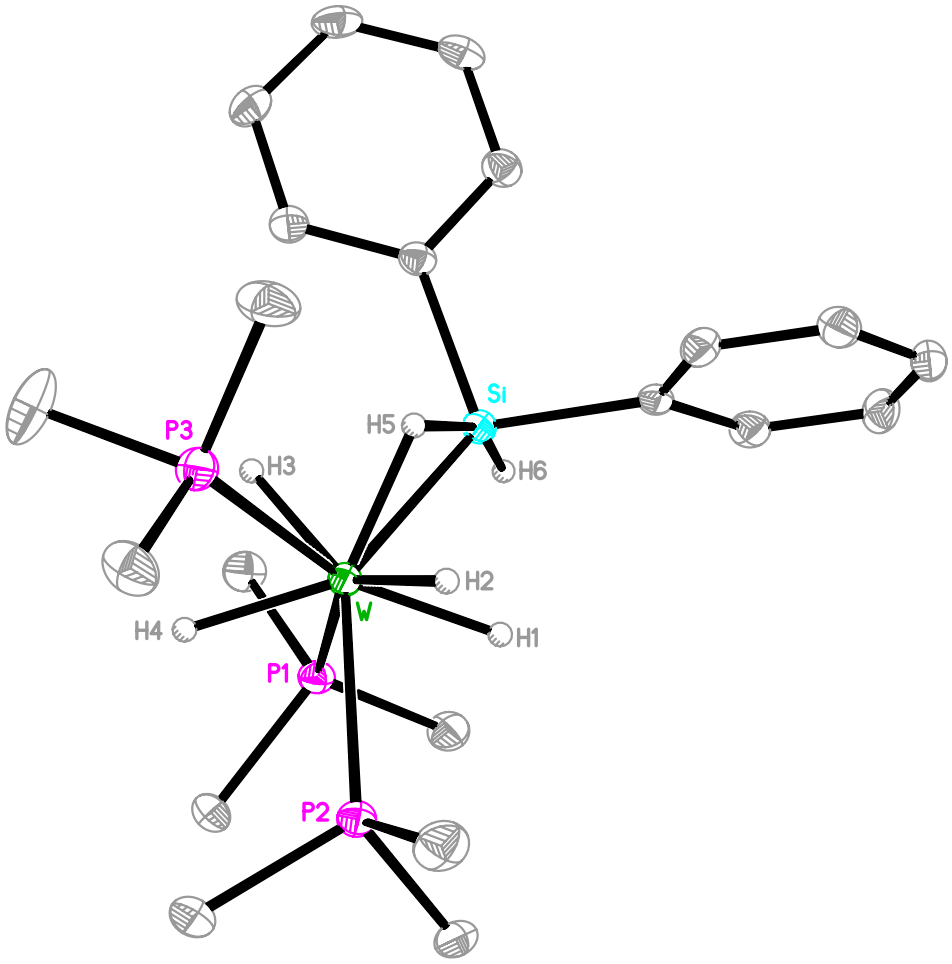

Figure 23. Molecular Structure of $W(PMe_3)_3H_4(\sigma\text{-}HSiHPh_2)$

2.6 Summary and Conclusions

$W(PMe_3)_4(\eta^2\text{–}CH_2PMe_2)H$ has been shown to effect a broad range of transformations of SiH_4, $PhSiH_3$, and Ph_2SiH_2, including Si-C bond cleavage and formation, Si-Si bond generation, and redistribution. The products of silane redistribution and dehydrocoupling are isolated as ligands at the tungsten center, thereby providing insight into how the coordination of hydrosilanes to transition metal complexes impacts their overall reactivity. Specifically, the products of these reactions range from simple oxidative addition products to novel disilanyl, metallacycle, and bridging silylene compounds.

Silylene intermediates are implicated in the formation of the disilanyl compounds, and support for such species is provided by the isolation of the unique bimetallic complex, "WSiW", which features a bridging silylene ligand. This coordination motif is unprecedented,[25] and the assignment of the bridging silicon as a silylene is corroborated by NBO analysis. In conclusion, the isolation and characterization of the complexes generated from the reactions of $W(PMe_3)_4(\eta^2\text{–}CH_2PMe_2)H$ with hydrosilanes demonstrate the multifaceted chemistry of this complex and represent new modes of reactivity in transition metal silane chemistry.

2.7 Experimental Details

2.7.1 General Considerations

All manipulations were performed using a combination of glovebox, high vacuum, and Schlenk techniques under an argon atmosphere.[26] Solvents were purified and degassed by standard procedures. NMR spectra were measured on Bruker 300 DRX, Bruker 300 DPX, Bruker 400 Avance III, Bruker 400 Cyber-enabled Avance III, and Bruker 500 DMX spectrometers. ^1H chemical shifts are reported in ppm relative to $SiMe_4$ ($\delta = 0$) and were referenced internally with respect to the protio solvent impurity ($\delta = 7.16$ for C_6D_5H, 2.08 for C_7D_7H).[27] ^{31}P chemical shifts are reported in ppm relative to 85% H_3PO_4 ($\delta = 0$) and were referenced using $P(OMe)_3$ ($\delta = 141.0$) as an external standard.[28] ^{29}Si chemical shifts are reported in ppm relative to external 1% $SiMe_4$ in $CDCl_3$ ($\delta = 0$). Coupling constants are given in hertz. Infrared spectra were recorded on a PerkinElmer Spectrum Two spectrometer and are reported in cm^{-1}. UV/Vis spectra were recorded on a Perkin-Elmer Lambda 950 spectrophotometer equipped with deuterium and tungsten halogen lamps. $W(PMe_3)_4(\eta^2\text{–}CH_2PMe_2)H$ was prepared *via* the literature method.[3]

2.7.2 X-ray Structure Determinations

Single crystal X-ray diffraction data were collected on a Bruker Apex II diffractometer, and crystal data, data collection and refinement parameters are summarized in Table 3. The structures were solved using direct methods and standard difference map techniques and were refined by full-matrix least-squares procedures on F^2 with SHELXTL (Version 2008/4).[29]

2.7.3 Computational Details

Calculations were carried out using DFT as implemented in the Jaguar 7.7 suite of *ab initio* quantum chemistry programs.[30] Geometry optimizations (Table 4) were performed with the B3LYP density functional[31] using the 6-31G** (C, H, N, and P) and LACVP** basis set.[32] NBO analyses were performed using Jaguar NBO 5.0.[33]

2.7.4 Synthesis and Structural Characterization of $W(PMe_3)_4H_2(SiH_3)_2$

A solution of $W(PMe_3)_4(\eta^2\text{–}CH_2PMe_2)H$ (10 mg, 0.02 mmol) in C_6D_6 (0.7 mL) in an NMR tube equipped with a J. Young valve was degassed and charged with SiH_4. The solution was heated for 3 days and monitored by ^1H NMR spectroscopy, thereby demonstrating the conversion to primarily $W(PMe_3)_4H_2(SiH_3)_2$. The orange solution was lyophilized, the residue was dissolved in pentane, and the solution was placed at -15 ˚C, thereby depositing yellow crystals of $W(PMe_3)_4H_2(SiH_3)_2$ suitable for X-ray diffraction.

2.7.5 Structural Characterization of $W(PMe_3)_3H_3(\kappa^2\text{-}P,Si\text{-}PMe_2CH_2SiH_2SiH_2)$

A solution of $W(PMe_3)_4(\eta^2\text{–}CH_2PMe_2)H$ (12 mg, 0.02 mmol) in C_6D_6 (0.7 mL) in an NMR tube equipped with a J. Young valve was degassed and charged with SiH_4. The solution was heated for 3 days and monitored by ^1H NMR spectroscopy, thereby demonstration the conversion to primarily $W(PMe_3)_4H_2(SiH_3)_2$, accompanied by a number of other products. The orange solution was lyophilized, the residue was

dissolved in pentane, and the solution was placed at -15 ˚C, thereby depositing colorless crystals of $W(PMe_3)_3H_3(\kappa^2\text{-}P,Si\text{-}PMe_2CH_2SiH_2SiH_2)$ suitable for X-ray diffraction.

2.7.6 Synthesis of $W(PMe_3)_3H_4(SiH_2Ph)(SiH_2SiHPh_2)$

A solution of $W(PMe_3)_4(\eta^2\text{-}CH_2PMe_2)H$ (30 mg, 0.05 mmol) in C_6D_6 (0.7 mL) was treated with $PhSiH_3$ (55 mg, 0.51 mmol) and transferred to an NMR tube equipped with a J. Young valve. The solution was heated at 80 ˚C for 3 hours and then lyophilized to afford a grainy, light orange residue. The residue was washed with pentane (2 × 0.7 mL) and dried *in vacuo* to afford a fine, white powder (8 mg, 21 %). Colorless crystals of $W(PMe_3)_3H_4(SiH_2Ph)(SiH_2SiHPh_2)$ suitable for X-ray diffraction were obtained from a toluene solution at -30 ˚C. Analysis calcd. for $W(PMe_3)_3H_4(SiH_2Ph)(SiH_2SiHPh_2)$: C, 44.02 %; H, 6.98 %; Found: C, 43.90 %, H, 6.74 %. ^{1}H NMR at 300 K (C_7D_8): -4.18 [br s, 4H of $W\underline{H}_4$], 1.20 [d, $^2J_{P\text{-}H}$ = 8, 27H of $W(P\underline{Me}_3)_3$], 3.31 [br s, 2H of $W(Si\underline{H}_2SiHPh_2)$], 5.43 [m, 3H, $W(Si\underline{H}_2Ph)$ and $W(SiH_2Si\underline{H}Ph_2)$], 7.19 [m, 9H of $W(SiH_2\underline{Ph})$ and $(W)SiH_2SiH\underline{Ph}_2$], 7.88 [d, $^3J_{H\text{-}H}$ = 7, 2H of $W(SiH_2\underline{Ph})$], 7.99 [d, $^3J_{H\text{-}H}$ = 7, 4H of $W(SiH_2SiH\underline{Ph}_2)$]. ^{1}H NMR at 193 K ($C_7D_8$): -6.46 [d, $^2J_{P\text{-}H}$ = 41, 1H of $W\underline{H}_4$], -5.77 [br s, 1H of $W\underline{H}_4$], -3.11 [t, $^2J_{P\text{-}H}$ = 45, 1H of $W\underline{H}_4$], -2.24 [quart, $^2J_{P\text{-}H}$ = 45, 1H of $W\underline{H}_4$], 0.91 [s, 9H of $(W(P\underline{Me}_3)_3$], 1.04 [s, 9H of $(W(P\underline{Me}_3)_3$], 1.27 [s, 9H of $(W(P\underline{Me}_3)_3$], 3.05 [d, $^3J_{P\text{-}H}$ = 12, 1H of $W(Si\underline{H}_2SiHPh_2)$], 3.66 [d, $^3J_{P\text{-}H}$ = 22, 1H of $W(Si\underline{H}_2SiHPh_2)$], 5.54 [br s, 1H of $W(Si\underline{H}_2Ph)$], 5.65 [s, 1H of $W(SiH_2Si\underline{H}Ph_2)$], 5.88 [d, $^3J_{P\text{-}H}$ = 26, 1H of $W(Si\underline{H}_2Ph)$], 7.24 [br m, 6H of $W(SiH_2SiH\underline{Ph}_2)$], 7.37 [br s, 3H of $W(SiH_2\underline{Ph})$], 8.03 [br s, 2H of $W(SiH_2SiH\underline{Ph}_2)$], 8.12 [br s, 2H of $W(SiH_2\underline{Ph})$], 8.34 [br s, 2H of $W(SiH_2SiH\underline{Ph}_2)$]. $^{31}P\{^1H\}$ NMR at 300 K (C_7D_8): -35.9 [br s, 3P of $W(\underline{P}Me_3)_3$]. $^{31}P\{^1H\}$ NMR at 210 K (C_7D_8): -43.7 [dd, $^2J_{P\text{-}P}$ = 36, $^2J_{P\text{-}P}$ = 24, $^1J_{W\text{-}P}$ = 116, 1P of $W(\underline{P}Me_3)_3$], -39.0 [dd, $^2J_{P\text{-}P}$ = 36, $^2J_{P\text{-}P}$ = 8, $^1J_{W\text{-}P}$ = 117, 1P of $W(\underline{P}Me_3)_3$], -22.6 [dd, $^2J_{P\text{-}P}$ = 24, $^2J_{P\text{-}P}$ = 8, $^1J_{W\text{-}P}$ = 130, 1P of $W(\underline{P}Me_3)_3$]. ^{1}H-^{29}Si HMQC NMR at 300 K (C_7D_8): -80.8 [s, 1Si of $W(\underline{Si}H_2SiHPh_2)$], -13.0 [s, 2Si of $W(\underline{Si}H_2Ph)$ and $W(SiH_2\underline{Si}HPh_2)$]. ^{1}H-^{29}Si HMQC NMR at 210 K (C_7D_8): -76.1 [s, 1Si of $W(\underline{Si}H_2SiHPh_2)$], -8.9 [s, 1Si of $W(SiH_2\underline{Si}HPh_2)$], -8.0 [s, 1Si of $W(SiH_2Ph)$].

2.7.7 Synthesis of $W(PMe_3)_4H_3(SiH_2SiHPh_2)$

A solution of $W(PMe_3)_4(\eta^2\text{-}CH_2PMe_2)H$ (30.0 mg, 0.05 mmol) in C_6D_6 (0.7 mL) was treated with $PhSiH_3$ (12 mg, 0.11 mmol) and transferred to an NMR tube equipped with a J. Young valve. The solution was heated overnight at 80 ˚C to afford a clear, dark orange solution. The volatile components were removed *in vacuo* to give a dark residue that was extracted into pentane, filtered, and placed at -30 ˚C. Crystals of WSiW formed initially; the solution was decanted from these crystals and placed at -30 ˚C, thereby depositing microcrystalline $W(PMe_3)_4H_3(SiH_2SiHPh_2)$ (7 mg, 19%). Yellow crystals of $W(PMe_3)_4H_3(SiH_2SiHPh_2)$ suitable for X-ray diffraction were obtained from a pentane solution at -30 ˚C. Analysis calcd. for $W(PMe_3)_4H_3(SiH_2SiHPh_2)$: C, 40.91; H, 7.44 %; Found: C, 41.19 %, H, 7.22 %. ^{1}H NMR (C_6D_6): -4.66 [br m, 2H of W$\underline{H}_3$], -3.21 [br s, 1H of W$\underline{H}_3$], 1.41 [m, 36H of W(P$\underline{Me}_3)_4$], 3.46 [br m, $^1J_{Si\text{-}H}$ = 136, 2H of W(Si$\underline{H}_2$SiHPh$_2$)], 5.51 [t, $^3J_{H\text{-}H}$ = 4, $^1J_{Si\text{-}H}$ = 172, 1H of W(SiH$_2$Si$\underline{H}$Ph$_2$)], 7.20 [d, $^3J_{H\text{-}H}$ = 7, 2H of W(SiH$_2$SiH$\underline{Ph}_2$) (para H)], 7.27 [t, $^3J_{H\text{-}H}$ = 7, 4H of W(SiH$_2$SiH$\underline{Ph}_2$) (meta H)], 8.10 [dd, $^3J_{H\text{-}H}$ = 8, $^4J_{H\text{-}H}$ = 1, 4H of W(SiH$_2$SiH$\underline{Ph}_2$) (ortho H)]. ^{31}P{^{1}H} NMR (C_6D_6): -39.5 [br s, 1P of W($\underline{P}$Me$_3)_4$], -37.3 [t, $^2J_{P\text{-}P}$ = 16, $^1J_{P\text{-}W}$ = 158, 2P of W($\underline{P}$Me$_3)_4$], -25.6 [br s, 1P of W($\underline{P}$Me$_3)_4$]. ^{29}Si NMR (C_6D_6): -87.5 [br m, 1 Si of W($\underline{Si}$H$_2$SiHPh$_2$)], -17.9 [s, 1Si of W(SiH$_2\underline{Si}$HPh$_2$)].

2.7.8 Interconversion of the Disilanyl Complexes

(*i*) $W(PMe_3)_3H_4(SiH_2Ph)(SiH_2SiHPh_2)$ (3 mg, 0.004 mmol) was treated with a solution of PMe_3 in C_6D_6 (0.7 mL) with mesitylene (2 μL) as an internal standard. The solution was transferred to an NMR tube equipped with a J. Young valve. Integration of the ^{1}H NMR spectrum indicated that the initial ratio of $W(PMe_3)_3H_4(SiH_2Ph)(SiH_2SiHPh_2)$ to PMe_3 was approximately 1:1. The solution was heated at 60 ˚C and monitored by ^{1}H NMR spectroscopy for 5 days, thereby demonstrating conversion to primarily $W(PMe_3)_3H_4(SiH_2Ph)(SiH_2SiHPh_2)$ (*ca*. 90 % conversion).

(*ii*) $W(PMe_3)_4H_3(SiH_2SiHPh_2)$ (6 mg, 0.009 mmol) was treated with a solution of $PhSiH_3$ (2 mg, 0.018 mmol) in C_6D_6 (0.7 mL) and transferred to an NMR tube equipped with a J.

Young valve. The sample was heated at 60 ˚C for five days and monitored by ^{1}H NMR spectroscopy, thereby demonstrating the formation of small amounts of $W(PMe_3)_3H_4(SiH_2Ph)(SiH_2SiHPh_2)$, along with decomposition.

2.7.9 Structural Characterization of $W(PMe_3)_3H_4(SiHPh_2)_2$

A solution of $W(PMe_3)_4(\eta^2\text{-}CH_2PMe_2)H$ (9 mg, 0.016 mmol) in C_6D_6 (0.7 mL) was treated with $PhSiH_3$ (9 mg, 0.08 mmol) and transferred to an NMR tube equipped with a J. Young valve. The solution was degassed, charged with H_2, and heated overnight at 60 ˚C. The reaction was monitored by ^{1}H NMR spectroscopy, thereby demonstrating conversion to a number of products, including $W(PMe_3)_3H_4(SiHPh_2)_2$, $W(PMe_3)_3H_4(SiH_2Ph)(SiH_2SiHPh_2)$, and $W(PMe_3)_5H_2$. The solution was lyophilized and redissolved in pentane, thereby affording colorless crystals of $W(PMe_3)_3H_4(SiHPh_2)_2$ suitable for X-ray diffraction. This complex is characterized by a hydride signal in the ^{1}H NMR spectrum at δ -3.39 ($^2J_{P\text{-}H}$ = 34).

2.7.10 Synthesis of WSiW

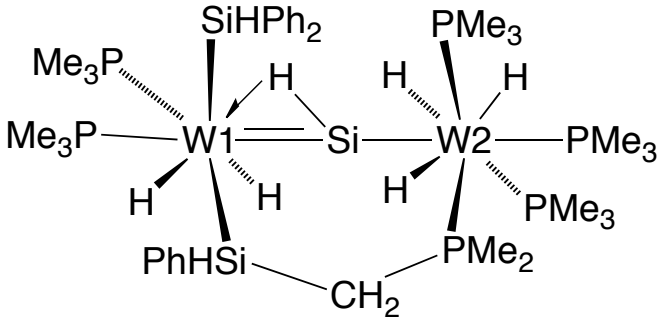

A solution of $W(PMe_3)_4(\eta^2\text{-}CH_2PMe_2)H$ (30.0 mg, 0.05 mmol) in C_6D_6 (0.7 mL) was treated with $PhSiH_3$ (12 mg, 0.11 mmol) and transferred to an NMR tube equipped with a J. Young valve. The solution was heated overnight at 80 ˚C to afford a clear, dark orange solution. The volatile components were removed *in vacuo* to give a dark residue that was extracted into pentane, filtered, and placed at -30 ˚C, thereby depositing crystals of WSiW co-crystallized with pentane ($2WSiW\bullet C_5H_{12}$) suitable for X-ray diffraction (1.2 mg, 4%). Analysis calcd. for WSiW crystals (2 molecules WSiW + 1

molecule pentane): C, 39.09 %; H, 6.99 %; Found: C, 39.36 %; H, 6.95 %. ^{1}H NMR at 300 K (C_6D_6) -4.14 [br s, 3H of W$\underline{H}_3$], -3.24 [br s, 3H of W$\underline{H}_3$], 1.20 [br m, 33H of W2(P$\underline{Me}_3$)$_3$(P$\underline{Me}_2$CH$_2$SiHPh)W1], 1.57 [br m, 18H of W1(PMe$_3$)$_2$], 2.01 [dt, $^{2}J_{P\text{-}H}$ = 13, $^{2}J_{H\text{-}H}$ = 13, $^{3}J_{H\text{-}H}$ = 3, 1H of -SiHPhC$\underline{H}_2$PMe$_2$-], 6.14 [m, 2H of -Si$\underline{H}$Ph$_2$ and -Si$\underline{H}$PhCH$_2$PMe$_2$-], 7.10 [m, partially obscured by solvent signal, 3H of -SiH$\underline{Ph}_2$) and -SiH$\underline{Ph}$CH$_2$PMe$_2$-], 7.22 [t, $^{3}J_{H\text{-}H}$ = 7, 2H of -Si$\underline{Ph}$], 7.37 [t, $^{3}J_{H\text{-}H}$ = 7, 2H of -Si$\underline{Ph}$], 7.50 [t, $^{3}J_{H\text{-}H}$ = 7, 2H of -Si$\underline{Ph}$], 8.34 [d, $^{3}J_{H\text{-}H}$ = 7, 2H of -Si$\underline{Ph}$], 8.44 [d, $^{3}J_{H\text{-}H}$ = 7, 2H of -Si$\underline{Ph}$], 8.63 [d, $^{3}J_{H\text{-}H}$ = 7, 2H of -Si$\underline{Ph}$]. (1H of 1H of -SiHPhC$\underline{H}_2$PMe$_2$- not observed.) ^{1}H NMR at 300 K (C_7D_8): -4.24 [br s, 3H of W$\underline{H}_3$], -3.28 [br s, 3H of W$\underline{H}_3$], 1.20 [m, 33H of W2(P$\underline{Me}_3$)$_3$(P$\underline{Me}_2$CH$_2$Si-)], 1.52 [br m, 18H of W1(PMe$_3$)$_2$], 1.56 [underneath broad signal at 1.52, 1H of -SiHPhC$\underline{H}_2$PMe$_2$-], 1.93 [t, $^{2}J_{P\text{-}H}$ = 13, $^{2}J_{H\text{-}H}$ = 13, 1H of -SiHPhC$\underline{H}_2$PMe$_2$-], 5.99 [m, 2H of -Si$\underline{H}$Ph$_2$ and -Si$\underline{H}$PhCH$_2$PMe$_2$-], 7.02 [peak partially obscured by solvent signal, 1H of -Si$\underline{Ph}$], 7.09 [peak partially obscured by solvent signal, 1H of -Si$\underline{Ph}$], 7.14 [t, $^{3}J_{H\text{-}H}$ = 7, 2H of -Si$\underline{Ph}$], 7.26 [t, $^{3}J_{H\text{-}H}$ = 7, 1H of -Si$\underline{Ph}$], 7.29 [t, $^{3}J_{H\text{-}H}$ = 7, 2H of -Si$\underline{Ph}$] 7.42 [t, $^{3}J_{H\text{-}H}$ = 7, 2H of -Si$\underline{Ph}$], 8.20 [d, $^{3}J_{H\text{-}H}$ = 7, 2H of -Si$\underline{Ph}$], 8.31 [d, $^{3}J_{H\text{-}H}$ = 7, 2H of -Si$\underline{Ph}$], 8.51 [d, $^{3}J_{H\text{-}H}$ = 7, 2H of -Si$\underline{Ph}$]. ^{1}H NMR at 210 K (C_7D_8): -6.19 [br s, 1H of W1$\underline{H}$], -5.32 [m, 1H of W2$\underline{H}$], -4.36 [t, $^{2}J_{P\text{-}H}$ = 40, 1H of W1$\underline{H}$], -2.60 [d, $^{2}J_{PH}$ = 19, 1H of W1$\underline{H}$], -2.50 [m, 1H of W2$\underline{H}$], -2.38 [m, 1H of W2$\underline{H}$], 0.65 [d, $^{2}J_{P\text{-}H}$ = 5, 15H of W2(P$\underline{Me}_3$)(P$\underline{Me}_2$CH$_2$-)], 1.21 [d, $^{2}J_{PH}$ = 6, 9H of W1(P$\underline{Me}_3$)], 1.31 [br. m,18H of W2(P$\underline{Me}_3$)$_2$], 2.00 [d, $^{2}J_{P\text{-}H}$ = 6, 9H of W1(P$\underline{Me}_3$)], 6.04 [d, $^{3}J_{P\text{-}H}$ = 23, 1H of W1(Si$\underline{H}$Ph$_2$)], 6.25 [dd, $^{3}J_{P\text{-}H}$ = 30, $^{3}J_{P\text{-}H}$ = 17, 1H of -Si$\underline{H}$PhCH$_2$PMe$_2$-], 7.10 [m, 2H of -Si$\underline{Ph}$, peaks partially obscured by toluene signals], 7.20 [t, $^{3}J_{H\text{-}H}$ = 7, 2H of –Si$\underline{Ph}$], 7.45 [m, 3H of -Si$\underline{Ph}$], 7.64 [br t, $^{3}J_{H\text{-}H}$ = 7, 2H of -Si$\underline{Ph}$], 8.35 [d, $^{3}J_{H\text{-}H}$ = 7, 2H of -Si$\underline{Ph}$], 8.54 [d, $^{3}J_{H\text{-}H}$ = 7, 2H of -Si$\underline{Ph}$], 8.75 [br s, 2H of -Si$\underline{Ph}$]. (2H of -SiHPhC$\underline{H}_2$PMe$_2$- not observed.) ^{31}P NMR at 210 K (C_7D_8): -41.6 [ddd, $^{2}J_{P\text{-}P}$ = 56, $^{2}J_{P\text{-}P}$ = 36, $^{2}J_{P\text{-}P}$ = 16, 1P of W2($\underline{P}$Me$_2$CH$_2$Si-)], -37.4 [m, 1P of W2($\underline{P}$Me$_3$)], -33.7 [m, 2P of W1($\underline{P}$Me$_3$) and W2($\underline{P}$Me$_3$)], -30.0 [d, $^{2}J_{P\text{-}P}$ = 26, 1P of W1($\underline{P}$Me$_3$)$_2$], -26.4 [t, $^{2}J_{P\text{-}P}$ = 16, 1P of W2($\underline{P}$Me$_3$)]. ^{1}H-^{29}Si HMQC at 300 K (C_6D_6): 10.7 [s, 1Si of W$\underline{Si}$], 25.0 [s, 1Si of W$\underline{Si}$]. ^{29}Si INEPT NMR at 210 K (C_7D_8): 18.0 [d, $^{2}J_{P\text{-}Si}$ = 21, 1Si of W($\underline{Si}$HPh$_2$)], 28.4 [dd, $^{2}J_{P\text{-}Si}$ = 21, $^{2}J_{P\text{-}Si}$ = 29, 1Si of W$_A$(SiHPhCH$_2$-)].

2.7.11 Generation of WSiW*

A solution of WSiW (6 mg, 0.005 mmol) in C_6D_6 (0.7 mL) was transferred to an NMR tube equipped with a J. Young valve. The solution was left in ambient light at room temperature and monitored by ^{1}H NMR spectroscopy, thereby demonstrating conversion to WSiW*. After an approximately 2:1 ratio of WSiW:WSiW* was achieved, no further change was noted. The conversion is driven to the right (towards WSiW*) under more dilute conditions. No conversion was observed when the NMR tube was wrapped in aluminum foil and left at room temperature. ^{1}H NMR (C_6D_6): -5.09 [d quart, $^2J_{P\text{-}H}$ = 32, $^2J_{P\text{-}H}$ = 19, 2H of W2$\underline{H}_2$], -3.37 [t, $^2J_{P\text{-}H}$ = 23, 4H of W1$\underline{H}_4$], 1.25 [m, 18H of W(P$\underline{Me}_3)_2$], 1.51 [d, $^2J_{P\text{-}H}$ = 6, 27 H of W(P$\underline{Me}_3)_3$], 1.62 [d, $^2J_{P\text{-}H}$ = 6, 3H of W2(P$\underline{Me}_2CH_2$-)], 1.92 [d, $^2J_{P\text{-}H}$ = 6, 3H of W2(P$\underline{Me}_2CH_2$-)], 2.30 [dt, $^2J_{P\text{-}H}$ = 12, $^2J_{H\text{-}H}$ = 12, $^3J_{H\text{-}H}$ = 3, 1H of W(PMe$_2$C$\underline{H}_2$Si-)], 5.59 [br m, 1H of W(Si$\underline{H}$PhCH$_2$-)], 6.10 [t, $^3J_{P\text{-}H}$ = 8, 1H of W(Si$\underline{H}$Ph$_2$)], 7.16-7.38 [9H of -Si$\underline{Ph}$], 8.19 [d, $^3J_{H\text{-}H}$ = 10, 2H of -Si$\underline{Ph}$], 8.24 [d, $^3J_{H\text{-}H}$ = 10, 2H of -Si$\underline{Ph}$], 8.27 [d, $^3J_{H\text{-}H}$ = 10, 2H of -Si$\underline{Ph}$]. (1H of W(PMe$_2$C$\underline{H}_2$Si-) not observed.)

2.7.12 Synthesis of WSiW#

A solution of WSiW (6 mg, 0.005 mmol) in C_6D_6 (0.7 mL) was transferred to an NMR tube equipped with a J. Young valve. The solution was left in ambient light at room temperature and monitored by ^{1}H NMR spectroscopy, thereby demonstrating conversion to WSiW*. After 2 days, when substantial conversion to WSiW* had been achieved, a small amount of PMe_3 was added (*ca*. 2 equiv relative to WSiW+WSiW*). The sample was covered in aluminum foil and heated for 1 day at 60 ˚C, until conversion to WSiW# was achieved, thereby producing a mixture of WSiW and WSiW#. This sequence (solution in ambient light at room temperature followed by heating in the dark at 60 ˚C) was repeated for 2 weeks, until WSiW# was the major species present.

2.7.13 Synthesis of $W(PMe_3)_3H_4(\sigma\text{-}HSiHPh_2)$

(*i*) A solution of $W(PMe_3)_4(\eta^2\text{-}CH_2PMe_2)H$ (10 mg, 0.02 mmol) in C_6D_6 (0.7 mL) was treated with Ph_2SiH_2 (4 mg, 0.02 mmol) and transferred to an NMR tube equipped with a J. Young valve. The solution was degassed and charged with H_2. The sample was heated at 40 ˚C overnight and monitored by ^1H NMR spectroscopy, thereby demonstrating conversion to exclusively $W(PMe_3)_3H_4(\sigma\text{-}HSiHPh_2)$. The golden-brown solution was lyophilized, affording $W(PMe_3)_3H_4(\sigma\text{-}HSiHPh_2)$ as a pale brown powder (8 mg, 75 %). Colorless crystals of $W(PMe_3)_3H_4(\sigma\text{-}HSiHPh_2)$ suitable for X-ray diffraction were obtained from a pentane solution at -15 ˚C. Analysis calcd. for $W(PMe_3)_3H_4(\sigma\text{-}HSiHPh_2)$: C, 42.01 %; H, 7.22 %. Found: C, 42.45 %; H, 6.79 %. ^1H NMR (C_6D_6): -3.34 [quart, $^2J_{P\text{-}H}$ = 29. 5H of $W\underline{H}_4(\sigma\text{-}\underline{H}SiHPh_2)$], 1.35 [filled in d, $^2J_{P\text{-}H}$ = 7, 27H of $W(P\underline{Me}_3)_3$], 6.74 [quart, $^3J_{P\text{-}H}$ = 7, $^1J_{Si\text{-}H}$ = 166, 1H of $W(\sigma\text{-}HSi\underline{H}Ph_2)$], 7.19 [t, $^3J_{H\text{-}H}$ = 7, 2H of $W(\sigma\text{-}HSiH\underline{Ph}_2)$], 7.36 [t, $^3J_{H\text{-}H}$ = 7, 4H of $W(\sigma\text{-}HSiH\underline{Ph}_2)$], 8.21 [t, $^3J_{H\text{-}H}$ = 7, 2H of $W(\sigma\text{-}HSiH\underline{Ph}_2)$].

(*ii*) A solution of $W(PMe_3)_4(\eta^2\text{-}CH_2PMe_2)H$ (20.0 mg, 0.035mmol) in C_6D_6 was treated with Ph_2SiH_2 (40.0 mg, 0.22 mmol) and transferred to an NMR tube equipped with a J. Young valve. The solution was heated for 7 hours at 80 ˚C and monitored by ^1H NMR spectroscopy, thereby demonstrating conversion to $W(PMe_3)_3H_4(\sigma\text{-}HSiHPh_2)$ and the complex tentatively assigned as $W(PMe_3)_3H_2(\kappa^2\text{-}H_2\text{-}H_2SiHPh)$ in an approximately 1:2 ratio. The dark orange solution was lyophilized, and the residue was extracted into pentane, filtered, and placed at -15 ˚C, thereby depositing X-ray quality crystals of $W(PMe_3)_3H_5(SiHPh_2)$ (2.3 mg, 10.8 %).

2.8 Crystallographic Data

Table 3. Crystal, intensity collection and refinement data.

	WSiW	**WSiW#**
lattice	Triclinic	Triclinic
formula	$C_{38.5}H_{82}Si_3P_6W_2$	$C_{26}H_{70}Si_2P_7W_2$
formula weight	1182.83	1023.49
space group	*P-1*	*P-1*
a / Å	11.276(2)	9.9109(13)
b / Å	13.112(2)	10.0461(13)
c / Å	18.316(3)	23.151(3)
α / °	75.844(3)	93.221(2)
β / °	81.307(3)	93.967(2)
γ / °	84.182(3)	111.378(2)
V / Å^3	2589.8(8)	2133.1(5)
Z	2	2
temperature (K)	130(2)	130(2)
radiation (λ, Å)	0.71073	0.71073
ρ (calcd.), g cm^{-3}	1.517	1.594
μ (Mo Kα), mm^{-1}	4.717	5.722
θ max, deg.	30.75	30.60
no. of data collected	41732	34388
no. of data	15992	13015
no. of parameters	528	426
R_1 [$I > 2\sigma(I)$]	0.0412	0.0816
wR_2 [$I > 2\sigma(I)$]	0.0582	0.1670
R_1 [all data]	0.0858	0.1517
wR_2 [all data]	0.0675	0.1940
GOF	1.005	1.033

Table 3 cont. Crystal, intensity collection and refinement data.

	$W(PMe_3)_4H_2(SiH_3)_2$	$W(PMe_3)_3H_3(PCSiSi)$
lattice	Orthorhombic	Monoclinic
formula	$C_{12}H_{44}Si_2P_4W$	$C_{12}H_{42}Si_2P_4W$
formula weight	552.38	550.37
space group	$P2_12_12$	$P2_1$
a/Å	9.5936(14)	9.613(2)
b/Å	12.5795(19)	12.753(3)
c/Å	9.5893(14)	9.806(2)
α/°	90	90
β/°	90	107.838(3)
γ/°	90	90
V/Å^3	1157.3(3)	1612.5(3)
Z	2	2
temperature (K)	130(2)	130(2)
radiation (λ, Å)	0.71073	0.71073
ρ (calcd.), g cm^{-3}	1.585	1.597
μ (Mo Kα), mm^{-1}	5.362	5.422
θ max, deg.	30.53	30.39
no. of data collected	18011	17361
no. of data	3550	6752
no. of parameters	110	212
R_1 [$I > 2\sigma(I)$]	0.0275	0.0531
wR_2 [$I > 2\sigma(I)$]	0.0603	0.0922
R_1 [all data]	0.0302	0.0917
wR_2 [all data]	0.0611	0.1042
abs. struct. param.	-0.009(9)	0.168(11)
GOF	1.121	1.051

Table 3 cont. Crystal, intensity collection and refinement data.

	$W(PMe_3)_3H_4(SiH_2Ph)(SiH_2SiHPh_2)$	$W(PMe_3)_4H_3(SiH_2SiHPh_2)$
lattice	Monoclinic	Monoclinic
formula	$C_{27}H_{51}Si_3P_3W$	$C_{24}H_{52}Si_2P_4W$
formula weight	736.71	704.56
space group	$P2_1/n$	$P2_1$
a / Å	9.6573(9)	9.7561(9)
b / Å	16.3977(15)	16.1203(15)
c / Å	21.2536(19)	10.2677(10)
α / °	90	90
β / °	94.398(1)	93.0754(13)
γ / °	90	90
V / Å^3	3355.8(5)	1612.5(3)
Z	4	2
temperature (K)	130(2)	130(2)
radiation (λ, Å)	0.71073	0.71073
ρ (calcd.), g cm^{-3}	1.458	1.451
μ (Mo Kα), mm^{-1}	3.707	3.866
θ max, deg.	30.98	30.92
no. of data collected	54687	28352
no. of data	10582	11341
no. of parameters	352	317
R_1 [$I > 2\sigma(I)$]	0.0524	0.0266
wR_2 [$I > 2\sigma(I)$]	0.0943	0.0586
R_1 [all data]	0.1062	0.0314
wR_2 [all data]	0.1118	0.0604
abs. struct. param.	–	-0.023(5)
GOF	1.012	1.051

Table 3 cont. Crystal, intensity collection and refinement data.

	$W(PMe_3)_3H_4(\sigma\text{-}HSiHPh_2)$	$W(PMe_3)_3H_4(SiH_2Ph)_2$
lattice	Monoclinic	Orthorhombic
formula	$C_{21}H_{43}SiP_3W$	$C_{21}H_{45}Si_2P_3W$
formula weight	600.40	630.51
space group	$P2_1/c$	$Pca2_1$
a / Å	9.5594(7)	18.1774(14)
b / Å	9.4055(7)	17.6309(13)
c / Å	29.378(2)	17.6303(13)
α / °	90	90
β / °	91.234(1)	90
γ / °	90	90
V / Å^3	2640.8(3)	5650.3(7)
Z	4	8
temperature (K)	150(2)	130(2)
radiation (λ, Å)	0.71073	0.71073
ρ (calcd.), g cm^{-3}	1.510	1.482
μ (Mo Kα), mm^{-1}	4.606	4.349
θ max, deg.	30.63	30.61
no. of data collected	41910	89421
no. of data	8150	17345
no. of parameters	268	566
R_1 [$I > 2\sigma(I)$]	0.0379	0.0423
wR_2 [$I > 2\sigma(I)$]	0.0788	0.0716
R_1 [all data]	0.0485	0.0738
wR_2 [all data]	0.0824	0.0821
GOF	1.086	1.005

2.9 Computational Data

Table 4. Cartesian coordinates for geometry optimized structures.

$W(PMe_3)_4H_2(SiH_3)_2$

-2496.09974977350 Hartrees

Atom	x	y	z
W	0	0	0.04831726
P	-1.864552626	-0.339908502	-1.693361766
P	-1.655351841	0.718887023	1.798483979
Si	0.246954737	-2.564879766	-0.498978882
C	-2.830855792	1.059510839	-2.446117026
H	-3.633898461	0.653237158	-3.069899288
H	-2.180694019	1.683057565	-3.062059126
H	-3.264096603	1.69642399	-1.673207583
C	-3.299829557	-1.369012936	-1.100207574
H	-3.828041626	-0.837803282	-0.304571713
H	-2.936208238	-2.317756134	-0.703381338
H	-4.004128428	-1.565438578	-1.915600037
C	-1.48485968	-1.246243157	-3.280035157
H	-2.40087583	-1.418397421	-3.85525907
H	-1.014147932	-2.208583237	-3.071231285
H	-0.802016776	-0.649805696	-3.889497595
C	-2.526600799	-0.626625247	2.739775857
H	-3.182376206	-0.208861653	3.511262719
H	-1.797799542	-1.290911723	3.207160175
H	-3.124259841	-1.222986641	2.04605188
C	-3.15985695	1.728219599	1.342351878
H	-3.765191927	1.939529751	2.230326906

H	-3.77541446	1.179090525	0.625970763
H	-2.858769809	2.674501325	0.88847363
C	-1.052999264	1.753221924	3.225699228
H	-1.88600551	2.072976331	3.860813942
H	-0.534192782	2.635505191	2.844926992
H	-0.356225651	1.171637668	3.834626477
H	1.213560224	-3.076473911	-1.531882078
H	0.905428621	1.300484151	0.746826626
H	0.631682862	-3.395506906	0.691982959
H	-1.011392943	-3.257378263	-0.933322172
P	1.864552626	0.339908502	-1.693361766
P	1.655351841	-0.718887023	1.798483979
Si	-0.246954737	2.564879766	-0.498978882
C	2.830855792	-1.059510839	-2.446117026
H	3.633898461	-0.653237158	-3.069899288
H	2.180694019	-1.683057565	-3.062059126
H	3.264096603	-1.69642399	-1.673207583
C	3.299829557	1.369012936	-1.100207574
H	3.828041626	0.837803282	-0.304571713
H	2.936208238	2.317756134	-0.703381338
H	4.004128428	1.565438578	-1.915600037
C	1.48485968	1.246243157	-3.280035157
H	2.40087583	1.418397421	-3.85525907
H	1.014147932	2.208583237	-3.071231285
H	0.802016776	0.649805696	-3.889497595
C	2.526600799	0.626625247	2.739775857
H	3.182376206	0.208861653	3.511262719
H	1.797799542	1.290911723	3.207160175

H	3.124259841	1.222986641	2.04605188
C	3.15985695	-1.728219599	1.342351878
H	3.765191927	-1.939529751	2.230326906
H	3.77541446	-1.179090525	0.625970763
H	2.858769809	-2.674501325	0.88847363
C	1.052999264	-1.753221924	3.225699228
H	1.88600551	-2.072976331	3.860813942
H	0.534192782	-2.635505191	2.844926992
H	0.356225651	-1.171637668	3.834626477
H	-1.213560224	3.076473911	-1.531882078
H	-0.905428621	-1.300484151	0.746826626
H	-0.631682862	3.395506906	0.691982959
H	1.011392943	3.257378263	-0.933322172

$W(PMe_3)_3H_3(\kappa^2\text{-}P,Si\text{-}PMe_2CH_2SiH_2SiH_2)$

-2494.91797494483 Hartrees

Atom	x	y	z
W	5.992681396	9.703438151	6.614902998
H	6.383652547	11.06114443	7.641021868
H	6.96712564	8.50647374	5.783004607
Si	5.110383416	7.235359062	6.90066322
Si	3.24133799	7.194832405	8.350513139
P	3.992928625	10.18813383	8.095606859
P	4.715152808	9.434812683	4.469986229
P	7.534293733	8.879900919	8.463020099
P	7.818456099	10.90873639	5.437892246
C	3.12009528	11.77867305	7.692557508
H	2.288234603	11.96386668	8.380753042

H	2.739741966	11.73787427	6.668728166
H	3.835523979	12.60293489	7.753966461
C	4.278027383	10.48977726	9.912205207
H	3.37770755	10.89133036	10.38986132
H	5.098788319	11.20014265	10.03959239
H	4.541611095	9.554031364	10.40912426
C	2.577515194	8.984003578	8.205083668
H	2.014643749	9.051252382	7.267575622
H	1.900560616	9.271340082	9.018095191
C	2.902335448	8.996974505	4.505796761
H	2.495811332	8.906366554	3.492662194
H	2.349048185	9.778010451	5.034766035
H	2.758071994	8.048946227	5.028345176
C	4.579555269	10.91003173	3.341964514
H	3.962069025	10.67842793	2.46768961
H	5.566874775	11.22241919	2.994714149
H	4.130495264	11.74313462	3.888842686
C	5.302915367	8.164765613	3.2453579
H	4.675565406	8.164504062	2.34736369
H	5.271635313	7.176060291	3.706032232
H	6.336306023	8.375137877	2.962898765
C	8.454189586	10.14636967	9.465085434
H	9.084476889	9.663614158	10.21928916
H	7.727928996	10.7913567	9.966454876
H	9.078303257	10.77111999	8.827933229
C	8.91553735	7.771262126	7.899608579
H	9.580790069	7.502374185	8.727280411
H	9.493679536	8.259794884	7.112879888

H	8.476817349	6.8631551	7.478921948
C	6.93986187	7.852316522	9.904366051
H	7.792930738	7.510903965	10.50068891
H	6.381027961	6.981967018	9.558826216
H	6.290485439	8.451587779	10.54553452
C	7.437393002	12.67206419	4.990192726
H	8.284345748	13.15369958	4.489333003
H	7.203366322	13.21503577	5.909633551
H	6.560031937	12.7183877	4.343831558
C	8.441938809	10.25304984	3.813369838
H	9.23805854	10.8850751	3.405925334
H	7.62992358	10.20106668	3.08545638
H	8.825963791	9.240541554	3.963635618
C	9.478368144	11.23904193	6.227266655
H	10.14317078	11.74917001	5.522019725
H	9.95761118	10.31194819	6.548545346
H	9.34100668	11.88355956	7.098730626
H	5.284984827	11.18622957	6.082687481
H	4.609675308	6.529276139	5.670443743
H	6.063369535	6.200513564	7.432455069
H	3.592840832	6.953018776	9.785575158
H	2.115590389	6.257437363	8.046103157

$W(PMe_3)_3H_4(SiH_2Ph)(SiH_2SiHPh_2)$

-3020.06249284297 Hartrees

Atom	x	y	z
W	7.834841619	0.798539181	16.56088834

P	6.299022323	2.013798438	18.28622563
Si	9.776358805	-0.740841114	15.78984026
P	9.856131832	2.266282689	17.23014637
Si	8.365875619	-0.721846468	18.65769208
P	6.109752131	0.705861663	14.75218542
Si	7.675964141	-2.978177858	18.45232072
C	8.558239022	-4.169182196	19.64475387
C	5.799499141	-3.099410689	18.73103407
C	9.640834025	-1.53941779	14.06330647
C	9.565824241	3.883297866	18.09825227
H	10.46567364	4.504453348	18.04233461
H	9.333851806	3.71422642	19.15109446
H	8.738027536	4.4206979	17.63001796
C	5.201304504	-2.707604585	19.94447927
H	5.825128867	-2.342466157	20.75776727
C	8.816600142	-3.331891841	12.61568941
H	8.260915696	-4.259688422	12.50018482
C	8.924006958	-2.736196845	13.87407444
H	8.450807192	-3.21797708	14.72794989
C	11.26748738	1.63302171	18.24646019
H	12.05189186	2.39356676	18.32063615
H	11.68241241	0.731969006	17.79166187
H	10.915222	1.376593653	19.24819538
C	7.858488254	-5.138497288	20.38611657
H	6.775622486	-5.19576655	20.3097793
C	5.571171165	3.641221873	17.76785455
H	4.914546531	4.041411816	18.54748538
H	4.999510674	3.525525428	16.84688235

H	6.37538914	4.356470663	17.57826786
C	9.958961825	-4.133230709	19.781248
H	10.53386672	-3.391554437	19.23134028
C	10.71792559	2.911444861	15.7226225
H	11.57058458	3.5388653	16.00322268
H	10.0052152	3.500680925	15.140522
H	11.06723275	2.080700597	15.1086832
C	4.61690842	1.811615965	14.76257088
H	3.988012266	1.612931173	13.88831787
H	4.937840438	2.856128662	14.73253545
H	4.01853927	1.652075261	15.66302734
C	3.819827682	-2.780081972	20.13225087
H	3.384826514	-2.476482403	21.08156292
C	10.256739	-0.972787521	12.93411628
H	10.83641556	-0.057548342	13.04100039
C	4.949041593	-3.56686205	17.71250328
H	5.376767364	-3.88716793	16.76508931
C	6.842143584	2.492350247	20.00028757
H	5.970021632	2.767838288	20.60217466
H	7.512201298	3.35230182	19.95700391
H	7.357676865	1.658837023	20.4787899
C	10.63138319	-5.031817818	20.61051253
H	11.7145186	-4.984315362	20.69302426
C	4.773036042	1.053135645	18.70345778
H	4.117593401	1.626300048	19.36815079
H	5.055600418	0.11713453	19.19063488
H	4.229788889	0.800340592	17.79032782
C	8.526385688	-6.035678465	21.22226042

H	7.959565043	-6.774963403	21.78327103
C	9.916245143	-5.987085572	21.33579132
H	10.43792061	-6.686195732	21.98426745
C	6.759828648	1.081873962	13.06309173
H	5.972052119	0.99769137	12.30655806
H	7.568866783	0.386298395	12.82791521
H	7.166427736	2.096596582	13.0543664
C	9.428549296	-2.742427769	11.50790393
H	9.347120477	-3.204054289	10.5270583
C	2.99687447	-3.242068387	19.10309104
H	1.920734576	-3.298118796	19.24676598
C	10.1522061	-1.560797865	11.67076512
H	10.6404871	-1.099577455	10.81541388
C	5.315160396	-0.940005988	14.4802929
H	4.568237614	-0.891445333	13.68106133
H	4.842602636	-1.280125179	15.40515553
H	6.088962025	-1.661408179	14.20523219
C	3.565238928	-3.635920032	17.89128377
H	2.932190697	-4.003975892	17.08723944
H	11.10591693	-0.045579969	15.70554592
H	10.07027492	-1.908870074	16.68062868
H	7.869524665	-3.503251331	17.06627743
H	7.627379622	-0.372427536	19.9283354
H	9.780306498	-0.782193669	19.15968988
H	8.660584502	0.980789622	15.05410831
H	7.805897543	-0.729500347	15.7772399
H	6.580872836	-0.272443952	17.06880489
H	7.643749503	2.422039988	15.93872524

$W(PMe_3)_4H_3(SiH_2SiHPh_2)$

-2958.22742092708 Hartrees

Atom	x	y	z
W	-8.934768204	4.077688297	-7.307465206
P	-10.19901081	5.55920648	-8.953423812
P	-6.947763379	5.656355154	-7.108162875
P	-8.93057158	3.47215609	-4.908974714
P	-10.18700919	1.980604298	-7.890228791
Si	-7.600003141	3.336219185	-9.500747594
Si	-5.452474515	2.313893433	-9.503282678
C	-7.768068778	4.258649447	-3.677223595
H	-8.039799066	3.969056367	-2.656511769
H	-7.804649378	5.347325223	-3.752945926
H	-6.744203648	3.928043078	-3.864644457
C	-4.868134803	1.939770166	-11.27344706
C	-11.12639085	1.846076675	-9.497278
H	-11.59562663	0.860834198	-9.591624993
H	-10.44924124	1.997761265	-10.33925987
H	-11.91036665	2.607818225	-9.530566892
C	-5.380279274	5.038095505	-6.318534846
H	-4.60939794	5.816206153	-6.322410752
H	-5.01228796	4.177634925	-6.880569952
H	-5.56418052	4.729291546	-5.289738252
C	-5.321542306	0.717399769	-8.467792168
C	-3.530481846	2.166154486	-11.6483907
H	-2.831269725	2.573231015	-10.92121327
C	-5.735515946	1.419882835	-12.25272598

H	-6.781261829	1.249372218	-12.00767591
C	-6.147208363	6.414740965	-8.614578486
H	-5.415481561	7.172811418	-8.315846416
H	-6.891414117	6.875095484	-9.265939851
H	-5.634364719	5.641460881	-9.189961493
C	-7.223837549	7.211150658	-6.128859716
H	-6.294027153	7.779156257	-6.018574755
H	-7.619125178	6.96968946	-5.140698612
H	-7.961973753	7.832043757	-6.641433309
C	-11.59564796	1.478911216	-6.779330744
H	-12.067939	0.559744729	-7.141414826
H	-12.33941817	2.280241168	-6.764983065
H	-11.25436789	1.314196063	-5.75594494
C	-5.28574829	1.127183117	-13.54194084
H	-5.977637123	0.724171983	-14.27754832
C	-3.953454632	1.356438917	-13.88878221
H	-3.602190707	1.132104176	-14.89254721
C	-9.828856908	7.386391835	-8.99247494
H	-10.54473887	7.918454786	-9.628348373
H	-8.823132208	7.571265454	-9.375780525
H	-9.892664898	7.784864075	-7.976682246
C	-3.076646979	1.880665505	-12.9374066
H	-2.037622518	2.066098031	-13.19880634
C	-9.238303406	0.385918928	-7.957495014
H	-9.902323631	-0.461194218	-8.161256352
H	-8.722177161	0.222938733	-7.009465378
H	-8.479502301	0.438750031	-8.740436672
C	-12.00970083	5.684265171	-8.549785878

H	-12.52370275	6.381950265	-9.220281479
H	-12.11571372	6.024121872	-7.516752018
H	-12.47689711	4.699866933	-8.629176787
C	-10.30044819	5.255313761	-10.78491408
H	-10.94961503	5.99795155	-11.26080483
H	-10.699368	4.258031318	-10.98030144
H	-9.30468991	5.311429808	-11.22969058
C	-5.401644217	-0.559169603	-9.053167114
H	-5.512670339	-0.649888156	-10.13124442
C	-5.149904604	0.777118069	-7.071264628
H	-5.071840078	1.743702588	-6.578920612
C	-5.324639532	-1.721068845	-8.281484841
H	-5.387264989	-2.693772473	-8.763450999
C	-5.067731453	-0.380742807	-6.295646785
H	-4.92408492	-0.302713041	-5.220272047
C	-5.158952861	-1.637082599	-6.898815365
H	-5.093219959	-2.540210274	-6.297743246
C	-10.51979642	3.819607404	-4.009434807
H	-10.46545849	3.517776149	-2.957883333
H	-11.34587689	3.297365665	-4.495036697
H	-10.7220701	4.892457601	-4.068386416
C	-8.609996216	1.70810908	-4.413088005
H	-8.624875563	1.592309346	-3.324016337
H	-7.630357196	1.409181067	-4.795578617
H	-9.356015032	1.038662667	-4.844878658
H	-7.339709734	4.391410604	-10.54649254
H	-4.404711157	3.225498923	-8.937986807
H	-8.2990132	2.308804683	-10.35860226

H	-9.4207089	5.525408399	-6.472984587
H	-7.678095417	2.914583323	-6.958270606
H	-10.58951752	4.10939092	-6.828156709

WSiW

-4470.06569988801 Hartrees

Atom	x	y	z
W	-6.799266484	-4.524043911	-4.487630005
W	-9.750872934	-1.049145426	-3.27117074
Si	-8.180528867	-2.816525824	-3.8039564
Si	-7.393147739	-3.209665396	-6.607564466
H	-6.297625146	-3.127237963	-7.648766537
Si	-7.31948091	-7.017593392	-3.745835359
H	-6.35696079	-7.638971614	-2.7537256
P	-5.032156455	-5.51313799	-6.072121422
P	-5.34320171	-4.525051023	-2.425887187
P	-11.17694198	-2.795240279	-2.201729005
P	-8.070513276	0.696510027	-2.460339556
P	-11.75691831	0.51183362	-3.531972163
P	-9.011298494	-0.383280839	-5.705128391
C	-7.58607287	-1.246466182	-6.497787208
H	-6.682820104	-0.908273368	-5.97223759
H	-7.52536585	-0.857616113	-7.523045337
C	-8.856610631	-3.739432359	-7.742241983
C	-8.848710891	-3.401445786	-9.109187708
H	-7.995371419	-2.863480365	-9.519855118
C	-9.899707318	-3.746539303	-9.962700132
H	-9.855625484	-3.474788468	-11.01524778

C	-11.00251019	-4.445454585	-9.467468597
H	-11.82194136	-4.719043031	-10.12749555
C	-11.0336305	-4.801246518	-8.117304194
H	-11.88056405	-5.357737753	-7.721254709
C	-9.972640005	-4.456397523	-7.274344243
H	-9.999582496	-4.760663037	-6.230913145
C	-4.011083948	-6.985138586	-5.569938277
H	-3.320245663	-7.257271149	-6.375479074
H	-4.665001774	-7.835903238	-5.366178106
H	-3.433615202	-6.765099547	-4.670916257
C	-5.590443073	-6.124453882	-7.731599563
H	-4.731272371	-6.440647675	-8.333584577
H	-6.131316164	-5.340003052	-8.263406598
H	-6.259725449	-6.975191487	-7.58781304
C	-3.676476987	-4.343183886	-6.551443547
H	-2.980050607	-4.80750514	-7.258140275
H	-3.131833624	-4.038455414	-5.653558034
H	-4.117124238	-3.453442932	-7.005492073
C	-8.971519304	-7.347502949	-2.805780446
C	-8.980888504	-7.616805379	-1.424144766
H	-8.039282623	-7.637239108	-0.878719162
C	-10.16232625	-7.89208349	-0.72938411
H	-10.12607691	-8.098211581	0.338408763
C	-11.38266178	-7.922105881	-1.406105781
H	-12.30285144	-8.150770909	-0.873977169
C	-11.40066996	-7.680272677	-2.78240579
H	-12.34065835	-7.723092179	-3.32895398
C	-10.21586904	-7.392770528	-3.463508427

H	-10.2599679	-7.221833469	-4.537070244
C	-3.910435102	-5.692037457	-2.191210957
H	-3.47994349	-5.588393831	-1.189036658
H	-3.132158993	-5.468935529	-2.92647502
H	-4.246332168	-6.721711519	-2.331898303
C	-6.203664054	-4.778590852	-0.7971862
H	-5.504915419	-4.708452364	0.044456278
H	-6.683818644	-5.759475847	-0.782205438
H	-6.981529352	-4.018489268	-0.684445078
C	-4.462427386	-2.930612534	-2.060040612
H	-3.844538583	-3.007656155	-1.158088388
H	-5.202636805	-2.139615308	-1.920762495
H	-3.833283355	-2.660884398	-2.91195679
C	-11.96424021	-4.037757545	-3.317629956
H	-12.50648982	-4.797148688	-2.746768046
H	-11.18510643	-4.528642518	-3.904006843
H	-12.64712111	-3.530768053	-4.004652917
C	-12.63142712	-2.321564346	-1.139408816
H	-13.10798538	-3.220549178	-0.735201922
H	-13.3803848	-1.7591049	-1.700620581
H	-12.28165685	-1.705330196	-0.30655355
C	-10.31230432	-3.874536482	-0.970976736
H	-11.00688594	-4.590205991	-0.520608599
H	-9.879074531	-3.243789094	-0.189383681
H	-9.51190313	-4.434007846	-1.458512212
C	-8.422117939	2.524277189	-2.529916077
H	-7.617324671	3.100684826	-2.060605781
H	-9.356450224	2.735586369	-2.001905672

H	-8.529258403	2.852929382	-3.566234871
C	-6.330895181	0.669323088	-3.10992175
H	-5.692224691	1.36619592	-2.556573192
H	-6.301648332	0.934044533	-4.168763332
H	-5.932550227	-0.343127513	-3.012909472
C	-7.727876434	0.522322715	-0.647965241
H	-6.965823973	1.238387184	-0.321575935
H	-7.385693101	-0.494077163	-0.440812095
H	-8.651140676	0.688610474	-0.088324906
C	-13.29713866	-0.216088065	-4.279761739
H	-14.12583596	0.500514731	-4.276174796
H	-13.59908734	-1.11192954	-3.734204376
H	-13.08550967	-0.513995722	-5.310010716
C	-11.74139028	2.110345043	-4.499738303
H	-12.70092596	2.628156979	-4.395037619
H	-11.56996616	1.920995154	-5.561592357
H	-10.94892458	2.765781308	-4.130662803
C	-12.40701332	1.204623359	-1.936511949
H	-13.32015219	1.785975052	-2.102458009
H	-11.64667498	1.85564141	-1.496454092
H	-12.61054871	0.402681394	-1.227683253
C	-8.568692175	1.390248464	-6.090814181
H	-8.391138376	1.490440332	-7.166581189
H	-7.654910709	1.685369515	-5.571122448
H	-9.367842209	2.074844305	-5.801974929
C	-10.352524	-0.62842736	-6.959331618
H	-9.994234304	-0.363126204	-7.959223457
H	-11.21903422	-0.007981736	-6.716620381

H	-10.65807185	-1.675472833	-6.963422644
C	-7.372553197	-8.416415787	-5.066792893
C	-8.096207814	-8.300004014	-6.269725215
H	-8.583109353	-7.357433725	-6.511556854
C	-8.195481766	-9.360642354	-7.174292045
H	-8.766297336	-9.235480497	-8.091823276
C	-7.557512352	-10.57410557	-6.908390969
H	-7.627750364	-11.39859612	-7.613383764
C	-6.828157757	-10.71524096	-5.726985849
H	-6.326052778	-11.65464879	-5.505669816
C	-6.744917487	-9.653172934	-4.82247408
H	-6.18363932	-9.789992584	-3.900109973
H	-8.254583437	-4.480195351	-3.379683963
H	-5.58962251	-3.286708514	-4.738490765
H	-7.87206607	-5.413009931	-5.523908256
H	-10.12487006	-0.578912603	-1.631201311
H	-10.66481946	-1.871165102	-4.496026944
H	-8.634722084	-1.845300923	-2.181735266

WSiW*

-4470.04592786220 Hartrees

Atom	x	y	z
W	-2.603779854	-1.26136286	-18.12632136
H	-3.932107043	-0.091402197	-17.88509076
H	-2.082881202	-2.579899032	-17.09043819
H	-1.976129125	0.303182453	-18.47148616
W	-4.768944968	0.047076971	-14.06001023
H	-6.461130017	-0.421634352	-14.15413829

H	-3.963971508	1.587057146	-14.07512359
Si	-3.861950386	-0.689428562	-16.06770693
Si	-0.964241341	-0.387508694	-16.2390487
H	0.386341955	-1.020784972	-16.431978
Si	-3.19905236	-0.284091758	-20.51889115
H	-3.335478494	-1.286717581	-21.63736311
P	-4.596826543	-2.794666031	-18.53658427
P	-0.314432238	-1.761078927	-19.15460259
P	-2.345487543	-0.162931708	-13.2276487
P	-5.50980342	1.122932771	-11.86330736
P	-5.108634026	-2.360186576	-13.28742217
P	-6.148949304	1.640500854	-15.37242498
C	-1.110585162	-0.929878236	-14.36953041
H	-0.11371785	-0.818614618	-13.92049704
H	-1.325987128	-2.00634587	-14.39636297
C	-4.782860659	-3.530070705	-20.22702125
H	-5.631987947	-4.221442352	-20.24485467
H	-3.869004891	-4.070346907	-20.48672694
H	-4.936722616	-2.750337023	-20.97303957
C	-6.339955474	-2.244651399	-18.24378948
H	-7.037875567	-3.070847374	-18.41689087
H	-6.577951927	-1.426931844	-18.92934328
H	-6.451143038	-1.88295897	-17.21915728
C	-4.531223541	-4.358258711	-17.54652082
H	-5.32600826	-5.04960265	-17.84859418
H	-4.638794282	-4.127793148	-16.4857194
H	-3.55777552	-4.831233299	-17.69578245
C	-0.329542524	-2.338087582	-20.91605412

H	0.679920865	-2.629299626	-21.22602731
H	-0.683744739	-1.541299215	-21.57278409
H	-1.000467477	-3.194807715	-21.01434997
C	0.992296811	-0.455861266	-19.27220202
H	1.896571827	-0.868396081	-19.73228166
H	1.238709142	-0.05891404	-18.28684518
H	0.613306374	0.359826533	-19.89245412
C	0.571515031	-3.18548935	-18.37431847
H	1.527730561	-3.372400235	-18.87414602
H	-0.062574222	-4.071799636	-18.45811001
H	0.746190848	-2.980938129	-17.31719363
C	-1.544716285	1.457100787	-12.82083253
H	-0.500902739	1.315147107	-12.52143435
H	-2.09012006	1.93426107	-12.00160721
H	-1.583487133	2.109748149	-13.69239197
C	-1.908519654	-1.071031372	-11.64853519
H	-0.826239226	-1.028281766	-11.48574528
H	-2.201813845	-2.121605935	-11.69967891
H	-2.408264526	-0.619803397	-10.78925677
C	-4.72957576	0.720375829	-10.21313456
H	-5.238582253	1.257457232	-9.405145917
H	-3.678873616	1.020624683	-10.21393
H	-4.784853091	-0.351138737	-10.01039901
C	-5.31145878	2.971410125	-11.75463705
H	-5.714405327	3.366953503	-10.81558292
H	-5.805840798	3.466119571	-12.59195987
H	-4.246040428	3.208912902	-11.816907
C	-7.289452411	0.918441896	-11.3511501

H	-7.515484931	1.491527114	-10.44519583
H	-7.48553913	-0.139898486	-11.15694093
H	-7.953650667	1.237555745	-12.15438083
C	-3.827733691	-3.667914808	-13.63015089
H	-4.208590498	-4.664180094	-13.37985244
H	-2.923726002	-3.48940491	-13.04386097
H	-3.548152131	-3.638859236	-14.68546114
C	-5.444583554	-2.766916592	-11.49619881
H	-5.657749537	-3.832986196	-11.36084842
H	-6.304709784	-2.191703862	-11.14291766
H	-4.57826378	-2.503760941	-10.8837931
C	-6.596743641	-3.168147804	-14.04155319
H	-6.681490163	-4.214101175	-13.72552222
H	-6.527984117	-3.11816856	-15.12929228
H	-7.490182378	-2.618847372	-13.73581795
C	-7.692718507	2.38490924	-14.62800027
H	-8.172488803	3.059827104	-15.34470359
H	-7.480892511	2.946155521	-13.71641018
H	-8.391341683	1.578649286	-14.38664964
C	-6.942579339	1.026413832	-16.92769334
H	-7.579408333	1.796860169	-17.3747587
H	-7.549839981	0.149074519	-16.69292043
H	-6.181015145	0.744314855	-17.65632379
C	-5.326553093	3.18225472	-15.99178347
H	-6.011675157	3.788288569	-16.5943187
H	-4.461849801	2.902975005	-16.59710597
H	-4.96655052	3.770661342	-15.143726
C	-0.456223315	1.464514831	-16.21414927

C	-1.296171488	2.501039997	-16.6562228
H	-2.282422734	2.252279989	-17.03817776
C	-0.890809492	3.838171755	-16.63037486
H	-1.567124682	4.61518387	-16.97959684
C	0.382346435	4.176706639	-16.16754056
H	0.704131711	5.214909283	-16.15338977
C	1.241236205	3.165687357	-15.73247095
H	2.239700074	3.414190861	-15.37952722
C	0.82340027	1.832996902	-15.75649302
H	1.514203887	1.061596177	-15.41918525
C	-4.86597812	0.657913979	-20.71360124
C	-5.06525426	1.930175506	-20.14446641
H	-4.268702217	2.384050978	-19.55818352
C	-6.249380539	2.643793423	-20.33211771
H	-6.361961873	3.632591661	-19.89217286
C	-7.287617177	2.094906055	-21.08859931
H	-8.212270672	2.647636536	-21.23576067
C	-7.119974534	0.835816154	-21.66407012
H	-7.915210647	0.401808972	-22.26646679
C	-5.922385571	0.137526889	-21.48404242
H	-5.80151121	-0.825209656	-21.97704682
C	-1.987062772	0.961409544	-21.35269013
C	-1.379118008	2.027983007	-20.66420845
H	-1.519441559	2.124120567	-19.59000824
C	-0.580473664	2.968368441	-21.32058967
H	-0.129970731	3.780667412	-20.75459492
C	-0.353763814	2.862286604	-22.69419639
H	0.271275161	3.589213947	-23.20671522

C	-0.937797667	1.809889843	-23.4008846
H	-0.769582329	1.712984084	-24.47133719
C	-1.74329122	0.880793098	-22.73763865
H	-2.199987628	0.076333446	-23.31105052
H	-2.414194186	-2.705968829	-19.05642088

WSiW#

-4177.16375599806 Hartrees

Atom	x	y	z
W	4.615954246	5.217288641	19.36627602
H	5.739271174	6.201757829	18.39427357
H	5.307553427	6.417561691	20.46897988
W	5.875632833	4.648652461	14.84332798
H	6.722307666	4.764799729	16.44315057
H	5.893496228	4.039154145	13.16257945
P	3.28357131	7.285121909	19.10029837
P	6.903534996	4.462326215	20.19962451
P	3.482711522	4.583204057	21.56900373
P	7.320723245	6.640748212	14.44342919
P	7.828347468	3.130863627	14.57994611
P	4.076199612	5.688723856	13.46592471
P	4.375491255	2.733230629	15.40953583
Si	5.124831784	5.175694563	17.0287273
C	2.560984064	3.099472483	15.66326769
H	2.035150638	2.219866286	16.04475946
H	2.092320097	3.402718076	14.72465488
Si	4.247908307	2.665341354	18.75043169

C	2.499978838	1.871005217	19.02979963
C	2.428041128	0.525978733	19.44570902
H	3.350447685	-0.019989523	19.63573843
C	1.209165474	-0.133070161	19.62709322
H	1.198277635	-1.170955	19.9528796
C	0.00806902	0.538153085	19.39317258
H	-0.943177909	0.030798966	19.53247182
C	0.045532466	1.871253321	18.98043835
H	-0.881804904	2.408790498	18.79374358
C	1.271802678	2.520204638	18.80753679
H	1.274370759	3.560988907	18.49284641
C	4.741786332	1.86791506	17.02051618
H	5.828619029	1.719471052	17.04691539
H	4.277915147	0.872125287	17.01053543
C	4.097045958	8.638767914	18.12207842
H	3.465403684	9.531903552	18.0588568
H	4.313180442	8.273544649	17.11489789
H	5.045368394	8.899761399	18.59999642
C	1.639603254	7.191966816	18.24747928
H	1.170401904	8.178279606	18.1603172
H	0.978308451	6.525895866	18.80812423
H	1.778765797	6.768916785	17.25005361
C	2.807678006	8.291722604	20.59426217
H	2.283785028	9.209279588	20.30445127
H	3.715119081	8.556058924	21.14356291
H	2.157813362	7.715449339	21.25740231
C	7.640234005	2.784893509	19.89767109
H	8.689757598	2.763688963	20.21028341

H	7.575244636	2.540685295	18.83535118
H	7.083460372	2.023139783	20.4468809
C	8.254954287	5.531451816	19.50981738
H	9.228901419	5.276103522	19.94208922
H	8.023184764	6.578153796	19.72041369
H	8.292798078	5.398143086	18.42612152
C	7.311553164	4.632219022	22.00892056
H	8.363840906	4.391802834	22.19617607
H	6.691540128	3.963335605	22.61124293
H	7.120021711	5.661694025	22.32176356
C	3.738077975	2.912196252	22.3511729
H	3.247630129	2.858039337	23.32949122
H	4.805354177	2.712998316	22.47781146
H	3.324247561	2.136584523	21.70303876
C	3.902894364	5.661075585	23.02528172
H	3.334079416	5.359818352	23.91193584
H	3.678951203	6.703025811	22.79070638
H	4.969214159	5.588845268	23.24571544
C	1.628000414	4.650867268	21.65666238
H	1.274865479	4.451502563	22.67445902
H	1.208224379	3.904661018	20.97943475
H	1.273318154	5.636587506	21.3449383
C	8.922564795	6.754883084	15.40233717
H	9.41700986	7.720471553	15.24698333
H	9.609648391	5.962101524	15.09533215
H	8.711337221	6.632504198	16.46775558
C	6.668139652	8.322143408	14.93879515
H	7.359239038	9.127814664	14.66347748

H	6.527389622	8.326886931	16.02288422
H	5.696852839	8.51360538	14.47726537
C	8.007439324	7.083100574	12.75759112
H	8.699885255	7.930079861	12.82051257
H	7.196187381	7.345815274	12.07711903
H	8.53412835	6.225465387	12.33360091
C	7.607455085	1.314175971	14.22661411
H	8.577703662	0.821110024	14.10151134
H	7.026168349	1.192493053	13.30974448
H	7.071848421	0.832231515	15.04792404
C	8.990244086	3.498825229	13.17131843
H	9.75873964	2.72336265	13.078105
H	9.483181427	4.461239857	13.32384325
H	8.413033942	3.550115064	12.24473465
C	9.050012723	2.982063599	15.97547294
H	9.904378111	2.356145843	15.69492749
H	8.552743582	2.531855664	16.8380989
H	9.409070261	3.970264793	16.26935937
C	2.642148308	6.562880535	14.27487861
H	1.916405397	6.928414894	13.53927398
H	3.024569828	7.408856664	14.85254478
H	2.140034502	5.880058742	14.96331882
C	4.481900392	6.97353036	12.17074548
H	3.57998611	7.260297834	11.61886266
H	5.203524058	6.550909974	11.46706714
H	4.91349892	7.870886756	12.6178338
C	3.165015004	4.551751836	12.30140344
H	2.37107642	5.08585838	11.76723824

H	2.72755763	3.704948401	12.83021714
H	3.886776508	4.160357752	11.57985542
C	4.118627778	1.275338682	14.25443179
H	3.308110812	0.63266703	14.61570436
H	5.024579212	0.675110737	14.1712353
H	3.864125065	1.645283091	13.25670067
H	2.444545351	3.910858984	16.38529057
H	5.034726186	1.70528757	19.60945972
H	3.01753882	4.784873593	18.84455538

$W(PMe_3)_3H_4(\sigma\text{-}HSiHPh_2)$

-2207.60119529505 Hartrees

Atom	x	y	z
C	2.388038082	-5.021384493	-5.260234824
C	4.056591579	-5.016669686	-0.400180384
C	2.573132665	-5.583573747	-2.264176934
C	0.714662069	-11.15558215	-1.718908458
C	3.362342864	-2.884384603	-5.958328028
C	3.228119525	-3.914616958	-5.026477456
C	2.654878999	-2.928785436	-7.161223257
C	1.55148798	-4.88018687	-1.600667129
C	3.828578602	-5.634508396	-1.633221754
C	1.686015474	-5.039847575	-6.477956687
C	-1.705323247	-11.248031	-3.223584559
C	3.027314678	-4.322023648	0.23476429
C	1.771124137	-4.255164583	-0.372970022
C	2.939067104	-9.015505578	-6.521341698
C	3.647870522	-10.05389554	-3.934405428

C	-1.419645782	-9.471205526	-0.989848587
C	1.815700254	-4.013108037	-7.417805832
C	1.640276442	-11.31297907	-5.528531037
C	-1.943535964	-5.305365623	-4.663665252
C	-3.397731787	-7.514808037	-3.631025699
C	-2.466457501	-7.574206843	-6.328211163
H	5.038894051	-5.078077337	0.062832457
H	0.2192609	-11.8702397	-1.052807504
H	1.423899975	-10.55610797	-1.142449339
H	1.272183052	-11.71337203	-2.474891525
H	4.017605581	-2.043435323	-5.743087168
H	3.783779109	-3.851668985	-4.093779046
H	2.756102197	-2.127098718	-7.888431167
H	0.561202109	-4.827476107	-2.047189218
H	4.646177944	-6.168566228	-2.113463685
H	1.029759467	-5.878832537	-6.695634917
H	-2.019785277	-11.98568868	-2.477493234
H	-1.233132498	-11.76394861	-4.063634883
H	-2.588334709	-10.72991295	-3.606552231
H	3.199793193	-3.83926399	1.193416775
H	0.960782172	-3.716556705	0.113356992
H	3.679012178	-9.729251662	-6.899476563
H	3.421388485	-8.051895595	-6.346584855
H	2.152415431	-8.876002932	-7.266863852
H	4.356789565	-10.66092184	-4.506959408
H	3.335804282	-10.60790582	-3.046273856
H	4.137589837	-9.133812328	-3.611000936
H	-1.719811302	-10.32839976	-0.377309255

H	-2.306040724	-8.898026119	-1.268419801
H	-0.762835404	-8.81787763	-0.410598088
H	1.258778007	-4.06131159	-8.351235678
H	2.48315063	-11.86726971	-5.954963845
H	0.862320589	-11.19841165	-6.287697805
H	1.223486511	-11.89301361	-4.701366898
H	-2.918198175	-4.943525915	-5.008501905
H	-1.157670697	-4.930641949	-5.324239767
H	-1.750843404	-4.920924277	-3.658384642
H	-4.276435091	-7.016245714	-4.053960207
H	-3.249493564	-7.1613891	-2.607069922
H	-3.586795988	-8.591387458	-3.60300053
H	-3.399017963	-7.053344416	-6.57047058
H	-2.621840195	-8.653747672	-6.399232038
H	-1.694294966	-7.297611639	-7.049622248
H	3.658035541	-7.086762936	-4.143231614
P	-0.516504126	-10.01264254	-2.512881145
P	2.164508373	-9.624068678	-4.954709236
P	-1.872914009	-7.152886169	-4.62720375
Si	2.313072869	-6.432440595	-3.954163101
W	0.347166561	-8.127312421	-3.991190223
H	-0.372384377	-9.240049971	-5.123682744
H	-0.333253787	-7.429550788	-2.552124573
H	0.537519298	-7.546699545	-5.614800327
H	0.451874606	-6.400153332	-3.915793661
H	1.460921587	-8.274823195	-2.652941781

$W(PMe_3)_3H_4(SiHPh_2)_2$

-2498.29733411405 Hartrees

Atom	x	y	z
W	-11.54520968	9.315919814	-8.095743937
P	-12.01040007	9.867907882	-5.617508218
P	-9.82387002	7.489241528	-7.375981959
P	-10.18202441	10.23988226	-9.968733216
Si	-13.17624213	7.235312134	-7.930792592
H	-12.47533087	5.964959736	-7.521784616
H	-14.28832031	7.293728039	-6.922251922
Si	-13.96133375	10.2393561	-8.319339931
H	-14.98503916	9.287654149	-8.840634066
H	-14.55416042	10.67893981	-7.008728366
C	-13.39159209	9.09716068	-4.658874117
H	-13.45538489	9.535251846	-3.657445553
H	-13.22502603	8.02057651	-4.571958878
H	-14.33603705	9.252758351	-5.182883468
C	-12.31087658	11.67725342	-5.357960904
H	-12.43746209	11.89636494	-4.29263554
H	-13.20320552	11.99386882	-5.898164522
H	-11.45047006	12.22929278	-5.743822594
C	-10.61570098	9.67386894	-4.404089564
H	-10.881064	10.13648262	-3.44805399
H	-9.723810853	10.16542955	-4.800213559
H	-10.38769575	8.6231875	-4.221882363
C	-9.480607058	6.239790059	-8.699570226
H	-8.697756015	5.540144594	-8.388055396
H	-9.171320225	6.744144886	-9.617578842

H	-10.3985403	5.684921086	-8.907046839
C	-8.107554337	8.061699956	-6.962679941
H	-7.459114096	7.214188389	-6.716730279
H	-8.148324339	8.739772307	-6.106810996
H	-7.677614566	8.60543442	-7.804276448
C	-10.08509343	6.333889789	-5.939223029
H	-9.311360391	5.559197412	-5.940580387
H	-11.06433585	5.860028336	-6.015662459
H	-10.02466986	6.873545663	-4.992850504
C	-8.377320728	9.841649677	-10.16471146
H	-7.972909086	10.32098812	-11.06258358
H	-8.223084057	8.762714123	-10.24713829
H	-7.826931289	10.210393	-9.295206222
C	-10.79690512	9.864387285	-11.67162142
H	-10.16117538	10.32548997	-12.43481527
H	-11.81665115	10.24454629	-11.77197261
H	-10.82214003	8.782399583	-11.82327127
C	-10.09683295	12.08534819	-10.01259231
H	-9.51173952	12.43588239	-10.86977785
H	-9.637924555	12.44308541	-9.087163043
H	-11.11024872	12.48939296	-10.07006217
C	-14.08098779	6.66927354	-9.51960161
C	-15.45684497	6.37737444	-9.489695869
H	-16.01395977	6.529644141	-8.568415053
C	-16.13143555	5.900553376	-10.61626268
H	-17.19697684	5.690559509	-10.5589162
C	-15.44263382	5.696334248	-11.81248371
H	-15.96423652	5.32598002	-12.6913318

C	-14.07590612	5.976144379	-11.86858947
H	-13.52666633	5.821946841	-12.79485536
C	-13.41232088	6.458313432	-10.73862259
H	-12.34946562	6.680243254	-10.81049811
C	-14.22911165	11.75691564	-9.448559847
C	-14.91936257	11.61612494	-10.66566939
H	-15.29628873	10.63741412	-10.95528821
C	-15.14201423	12.70623723	-11.51161993
H	-15.67704531	12.56498742	-12.44778709
C	-14.68601691	13.97449816	-11.15263275
H	-14.86150798	14.82566142	-11.80575496
C	-14.00477212	14.1434874	-9.945114934
H	-13.65094052	15.12984179	-9.653502506
C	-13.77868231	13.04663126	-9.111373489
H	-13.23879716	13.20150505	-8.178922492
H	-11.83671662	11.01510595	-8.118862023
H	-11.46963822	8.111410465	-9.334393127
H	-10.20314824	10.18984289	-7.389635644
H	-12.49637568	9.658202832	-9.485334327

2.10 References and Notes

(**1**) (a) Kim, B.-H.; Woo, H.-G. *Adv. Organomet. Chem.* **2005**, *52*, 143-174.
(b) Roy, A. K. *Adv. Organomet. Chem.* **2008**, *55*, 1-59.
(c) Troegel, D.; Stohrer, J. *Coord. Chem. Rev.* **2011**, *255*, 1440-1459.
(d) Corey, J. Y. *Adv. Organomet. Chem.* **2004**, *51*, 1-52.
(e) Waterman, R. *Chem. Soc. Rev.* **2013**, *42*, 5629-5641.
(f) Gauvin, F.; Harrod, J. F.; Woo, H. G. *Adv. Organomet. Chem.* **1998**, *42*, 363-405.

(**2**) (a) Corey, J. Y. *Chem. Rev.* **2011**, *111*, 863-1071.
(b) Corey, J. Y.; Braddock-Wilking, J. *Chem. Rev.* **1999**, *99*, 175-292.

(**3**) Green, M. L. H.; Parkin, G.; Chen, M.; Prout, K. *J. Chem. Soc., Dalton Trans.* **1986**, 2227–2236.

(**4**) The preparation of $W(PMe_3)_4H_2(SiH_3)_2$ reported in reference 3 involves heating $W(PMe_3)_4(\eta^2\text{–}CH_2PMe_2)H$ with SiH_4 in light petroleum (b.p. 40-60 ˚C) at 45 ˚C; for this work, $W(PMe_3)_4(\eta^2\text{–}CH_2PMe_2)H$ was heated with SiH_4 in C_6D_6 at 60 ˚C.

(**5**) $W(PMe_3)_3H_2$ is observed by ^1H NMR spectroscopy; however, there are small amounts of $W(PMe_3)_3H_2$ present in the starting material, so it is not known whether this compound is being produced under these conditions as well.

(**6**) Hore, P. J. *Nuclear Magnetic Resonance*; Compton, R. G.; Davies, S. G.; Evans, J.; Gladden, L. F., Eds.; Oxford University Press: Oxford, 1995; Chapter 4, pp 44-55.

(**7**) An EXSY experiment at room temperature was performed in order to provide further support for this suggestion, but no exchange peak was observed.

(**8**) The structure of $W(PMe_3)_4H_3(SiH_2SiHPh_2)$ is based on a dodecahedral arrangement, where the PMe_3 ligands adopt a flattened tetrahedral array that interpenetrates the elongated tetrahedral array of the disilanyl and hydride ligands. Thus, the PMe_3 ligands of $W(PMe_3)_4H_3(SiH_2SiHPh_2)$ comprise an AMX_2 set, which produces the observed $^{31}P\{^1H\}$ NMR spectrum.

(**9**) (a) Glaser, P.B.; Tilley, T.D. *Organometallics* **2004**, *23*, 5799-5812.
(b) Sadow, A.D.; Tilley, T.D. *J. Am. Chem. Soc.* **2005**, *127*, 643-656.
(c) Malisch, W.; Jehle, H.; Möller, S.; Thum, G.; Reising, J.; Gbureck, A.; Nagel, V.; Fickert, C.; Kiefer, W.; Nieger, M. *Eur. J. Inorg. Chem.* **1999**, 1597-1605.

(**10**) Tobita, H.; Matsuda, A.; Hashimoto, H.; Ueno, K.; Ogino, H. *Angew. Chem., Int. Ed.* **2004**, *43*, 221-224.

(**11**) In this terminology, a 1,2-silyl migration refers to the migration of the silyl ligand from the metal center to the silicon atom of the silylene ligand, thus producing a disilanyl ligand. A 1,3-alkyl or aryl migration refers to the migration of the alkyl or aryl group from the silyl ligand to the silylene ligand; the result is still a silyl(silylene) complex, but substitution of each ligand is altered.

(**12**) (a) Pannell, K. H.; Cervantes, J.; Hernandez, C.; Cassias, J.; Vincenti, S. *Organometallics* **1986**, *5*, 1056-1057.
(b) Tobita, H.; Ueno, K.; Ogino, H. *Chem. Lett.* **1986**, 1777-1780.

(**13**) Ogino, H. *Chem. Rec.* **2002**, *2*, 291-306.

(**14**) Sharma, H. K.; Pannell, K. H. *Chem. Rev.* **1995**, *95*, 1351-1374.

(**15**) Okazaki, M.; Tobita, H.; Ogino, H. *Dalton Trans.* **2003**, 493-506.

(**16**) The W-H distances derived from X-ray diffraction are shorter than the computed W-H distances because the distances derived from X-ray diffraction refer to the separation between positions of electron density maxima and not between nuclei. Specifically, nuclear positions and electron density maxima for hydrogen atoms do not necessarily coincide in a compound, such that bond lengths determined by X-ray diffraction are shorter than the internuclear value. For example, see:
(a) Coppens, P. *Angew. Chem. Int. Edit. Engl.* **1977**, *16*, 32-40.
(b) Cotton, F. A.; Luck, R. L. *Inorg. Chem.* **1989**, *28*, 3210-3213.

(**17**) Krentz, R.; Pomeroy, R. K. *Inorg. Chem.* **1985**, *24*, 2976-2980.

(**18**) Levy, G. C.; Cargioli, J. D. *J. Mag. Res.* **1973**, *10*, 231-234.

(**19**) (a) Levy, G. C.; Cargioli, J. D.; Juliano, P. C.; Mitchell, T. D. *J. Mag. Res.* **1972**, *8*, 399-401.
(b) Levy, G. C.; Cargioli, J. D.; Juliano, P. C.; Mitchell, T. D. *J. Am. Chem. Soc.* **1973**, *95*, 3445-3454.

(**20**) As discussed in Chapter 1, the $J_{Si\text{-}H}$ coupling constant for 3-center, 2-electron interactions is typically 30-70 Hz,[a,b] which is significantly lower than the $^{1}J_{Si\text{-}H}$ values observed for terminal Si-H hydrogens (> 150 Hz).[a] Furthermore, the observed coupling constant in this system is the average of the 3-center, 2-electron $J_{Si\text{-}H}$ value and the $^{2}J_{Si\text{-}H}$ coupling constants for the other hydrides , which are expected to be less than 20 Hz.[a] Thus, no appreciable J-coupling between the bridging silicon and the hydrides is expected. See: (a) reference 2a
(b) Luo, X.-L.; Kubas, G. J.; Burns, C. J.; Bryan, J. C.; Unkefer, C. J. *J. Am. Chem. Soc.* **1995**, *117*, 1159-1160.

(**21**) Thanks to Nick Anderson for help in acquiring these spectra on the Owen group's spectrophotometer!

(**22**) The bridging W-H-Si hydrides and terminal W-H hydrides are expected to be equivalent on the NMR timescale if the compound is fluxional, which is consistent with its formulation as a seven-coordinate complex. For example, see: Luo, X.-L.; Kubas, G. J.; Burns, C. J.; Bryan, J. C.; Unkefer, C. J. *J. Am. Chem. Soc.* **1995**, *117*, 1159-1160.

(**23**) While κ^2-*H*$_2$-H_2SiR_2 coordination of silanes to metal centers is much less common than σ-$HSiHR_2$ coordination, it is, nonetheless, precedented. See, for example:

(a) Thomas, C. M.; Peters, J. C. *Angew. Chem., Int. Ed.* **2006**, *45*, 776-780.
(b) Lipke, M. C.; Tilley, T. D. *J. Am. Chem. Soc.* **2011**, *133*, 16374-16377.

(**24**) Ph_3SiH, on the other hand, does not react with $W(PMe_3)_4(\eta^2–CH_2PMe_2)H$; Ph_4Si is also unreactive towards $W(PMe_3)_4(\eta^2–CH_2PMe_2)H$.

(**25**) A linear M-Si-M motif has been observed before, but this complex is best described as having a "trapped" SiH_4 in between two ruthenium centers. See: Atheaux, I.; Donnadieu, B.; Rodriguez, V.; Sabo-Etienne, S.; Chaudret, B.; Hussein, K.; Barthelat, J.-C. *J. Am. Chem. Soc.* **2000**, *122*, 5664-5665.

(**26**) (a) McNally, J. P.; Leong, V. S.; Cooper, N. J. in *Experimental Organometallic Chemistry*, Wayda, A. L.; Darensbourg, M. Y., Eds.; American Chemical Society: Washington, DC, 1987; Chapter 2, pp 6-23.
(b) Burger, B.J.; Bercaw, J. E. in *Experimental Organometallic Chemistry*; Wayda, A. L.; Darensbourg, M. Y., Eds.; American Chemical Society: Washington, DC, 1987; Chapter 4, pp 79-98.
(c) Shriver, D. F.; Drezdzon, M. A.; *The Manipulation of Air-Sensitive Compounds*, 2nd Edition; Wiley-Interscience: New York, 1986.

(**27**) (a) Gottlieb, H. E.; Kotlyar, V.; Nudelman, A. *J. Org. Chem.* **1997**, *62*, 7512-7515.
(b) Fulmer, G. R.; Miller, A. J. M.; Sherden, N. H.; Gottlieb, H. E.; Nudelman, A.; Stoltz, B. M.; Bercaw, J. E.; Goldberg, K. I. *Organometallics* **2010**, *29*, 2176-2179.

(**28**) "Nuclear Magnetic Resonance Spectroscopy" Nelson, J. H. Prentice Hall, New Jersey (2003), p 79.

(**29**) (a) Sheldrick, G. M. SHELXTL, An Integrated System for Solving, Refining and Displaying Crystal Structures from Diffraction Data; University of Göttingen, Göttingen, Federal Republic of Germany, 1981.
(b) Sheldrick, G. M. *Acta Cryst.* **2008**, *A64*, 112-122.

(**30**) Jaguar 7.7, Schrödinger, LLC, New York, NY 2010.

(**31**) (a) Becke, A. D. *J. Chem. Phys.* **1993**, *98*, 5648-5652.
(b) Becke, A. D. *Phys. Rev. A* **1988**, *38*, 3098-3100.
(c) Lee, C. T.; Yang, W. T.; Parr, R. G. *Phys. Rev. B* **1988**, *37*, 785-789.
(d) Vosko, S. H.; Wilk, L.; Nusair, M. *Can. J. Phys.* **1980**, *58*, 1200-1211.
(e) Slater, J. C. *Quantum Theory of Molecules and Solids, Vol. 4: The Self-Consistent Field for Molecules and Solids*; McGraw-Hill: New York, 1974.

(**32**) (a) Hay, P. J.; Wadt, W. R. *J. Chem. Phys.* **1985**, *82*, 270-283.
(b) Wadt, W. R.; Hay, P. J. *J. Chem. Phys.* **1985**, *82*, 284-298.
(c) Hay, P. J.; Wadt, W. R. *J. Chem. Phys.* **1985**, *82*, 299-310.

(**33**) NBO 5.0. Glendening, E. D.; Badenhoop, J. K.; Reed, A. E.; Carpenter, J. E.; Bohmann, J. A.; Morales, C. M.; Weinhold, F. Theoretical Chemistry Institute, University of Wisconsin, Madison, 2001.

CHAPTER 3

Preparation of New Ruthenaboratrane Complexes: Synthesis, Structure, Bonding, and Reactivity of $[\kappa^4\text{-B(mim}^{\text{But}})_3]\text{Ru(CO)(PPh}_3)$ and $[\kappa^4\text{-B(mim}^{\text{But}})_3]\text{Ru(CO)(PMe}_3)$

Table of Contents

3.1 Introduction

Metallaboratranes are a unique class of compounds with an atrane structure[1] that features a metal-to-ligand, M→B σ-dative bond. This bonding motif is noteworthy since the majority of metal complexes feature ligands that act as one-electron (X) or two-electron (L) donors. Metallaboratranes, in contrast, are formed with ligands that possess a bridgehead boron that acts as a two-electron acceptor ligand (Z) towards the metal center (Figure 1)[2]. While the coordination of BX_3 ligands to metal centers has been proposed for years[3], structural verification of this bonding mode was provided for the first time in 1999 by Hill *et al.*, who prepared the ruthenaboratrane complex [κ^4-$B(mim^{Me})_3$]Ru(CO)(PPh_3) (mim = 2-mercapto-1-methylimidazole)[4].

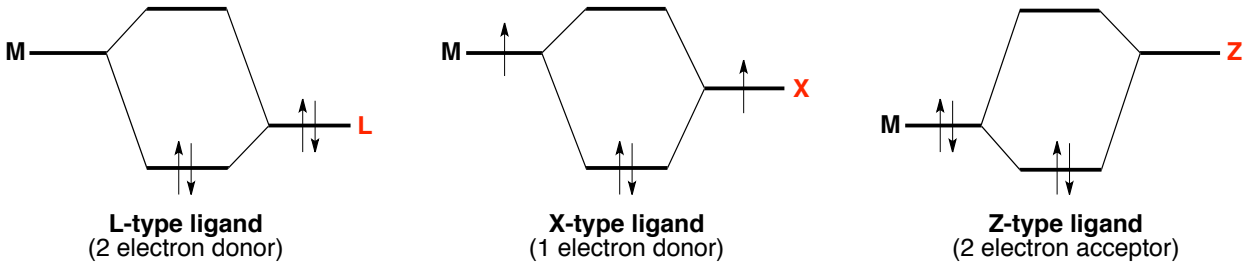

Figure 1. Covalent Bond Classification of L, X, and Z ligands

Since this initial report, metallaboratrane complexes have been prepared for all of the late transition metals (Groups 8 - 11)[5,6,7,8]. Many of these boratrane complexes were prepared using the tris(2-mercapto-1-methylimidazolyl)hydroborato ligand [Tm^{Me}][9]. This [S_3] donor ligand serves as a complement to the tris(pyrazolyl)hydroborato ligand, [$Tp^{RR'}$][10]; however, these ligands differ not only in their donor atoms (*i.e.* sulfur vs. nitrogen), but also in their geometry. The greater flexibility of the Tm ligand allows for the coordination of the boron to the metal center to form five-membered rings, whereas the four-membered metallacycle rings that would be formed in a Tp boratrane would be prohibitively strained. A [P_3] donor ligand, namely tris(phosphine)borane (TPB), has also been used in the preparation of metallaboratrane complexes[8a] (Figure 2).

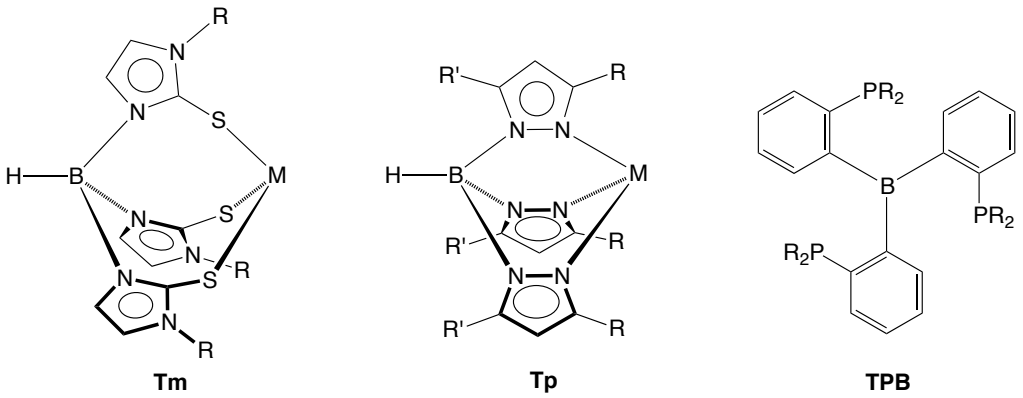

Figure 2. Common Tripodal Ligand Scaffolds

While the structures of metallaboratranes have been described in detail, their reactivity has been explored comparatively little. Furthermore, many of the initial metallaboratranes derived from the Tm ligand were restricted to those of the parent [$HB(mim^{Me})_3$] derivative. Therefore, we sought to prepare a boratrane that incorporates more sterically demanding substituents into the ligand scaffold and to explore the reactivity of the resulting boratrane. Here we present the synthesis, structure, bonding, and reactivity of two new ruthenaboratranes, [κ^4-$B(mim^{But})_3$]$Ru(CO)(PPh_3)$ and [κ^4-$B(mim^{But})_3$]$Ru(CO)(PMe_3)$.

3.2 Preparation and Characterization of [κ^4-$B(mim^{But})_3$]$Ru(CO)(PR_3)$ (R = Ph, Me)

The new ruthenaboratrane [κ^4-$B(mim^{But})_3$]$Ru(CO)(PPh_3)$ is analogous to the first reported boratrane, [κ^4-$B(mim^{Me})_3$]$Ru(CO)(PPh_3)$, and differs only in the functionalization of the Tm ligand. The synthesis of [κ^4-$B(mim^{But})_3$]$Ru(CO)(PPh_3)$, however, proved to be much more straightforward than that of the analogous methyl-substituted derivative. For example, [κ^4-$B(mim^{Me})_3$]$Ru(CO)(PPh_3)$ was prepared by first converting $RuHCl(CO)(PPh_3)_3$ to $Ru(CH{=}CHCPh_2OH)Cl(CO)(PPh_3)_2$, followed by subsequent treatment with $Na[Tm^{Me}]$.[4] [κ^4-$B(mim^{But})_3$]$Ru(CO)(PPh_3)$, on the other hand, was prepared simply by heating $RuHCl(CO)(PPh_3)_3$ with $K[Tm^{But}]$ (Scheme 1). Significantly, treatment of $RuHCl(CO)(PPh_3)_3$ with $Na[Tm^{Me}]$ did *not* result in the formation of [κ^4-$B(mim^{Me})_3$]$Ru(CO)(PPh_3)$, but rather [κ^3-*H,S,S*-$B(mim^{Me})_3$]-

$RuH(CO)(PPh_3)$ (Scheme 1).[11,] This difference in reactivity highlights the significance of the substitution of the ligand, which clearly influences the overall course of the reaction.

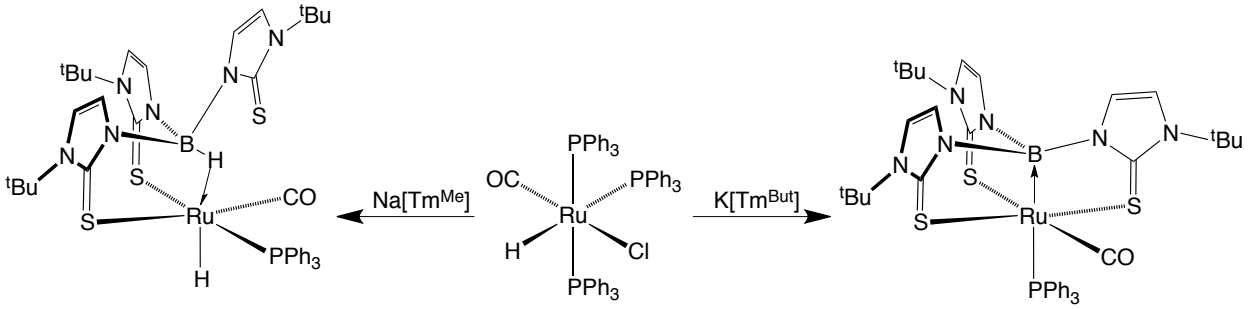

Scheme 1. Preparation of $[\kappa^4\text{-B(mim}^{\text{But}})_3]\text{Ru(CO)(PPh}_3)$

It is worth noting, however, that the reaction conditions for these procedures are different. $[\kappa^3\text{-}H,S,S\text{-B(mim}^{\text{Me}})_3]\text{RuH(CO)(PPh}_3)$ was prepared by reflux in THF for 3 minutes, whereas $[\kappa^4\text{-B(mim}^{\text{But}})_3]\text{Ru(CO)(PPh}_3)$ was synthesized by heating $\text{RuHCl(CO)(PPh}_3)_3$ with $K[\text{Tm}^{\text{But}}]$ in benzene at 80 °C for 1-2 days. However, reflux of $\text{RuHCl(CO)(PPh}_3)_3$ with $Na[\text{Tm}^{\text{Me}}]$ in toluene for 2 hours was reported to produce only a mixture of $[\kappa^3\text{-}H,S,S\text{-B(mim}^{\text{Me}})_3]\text{RuH(CO)(PPh}_3)$ and $[\kappa^4\text{-B(mim}^{\text{Me}})_3]\text{Ru(CO)(PPh}_3)$, and in our hands, $[\kappa^4\text{-B(mim}^{\text{Me}})_3]\text{Ru(CO)(PPh}_3)$ was not generated by heating in benzene.

The crystal structure of $[\kappa^4\text{-B(mim}^{\text{But}})_3]\text{Ru(CO)(PPh}_3)$, although poor quality, establishes its assignment as a boratrane complex (Figure 3). The ^{1}H NMR spectrum of this complex is also in accord with a boratrane formulation – the presence of two imidazolyl environments in a 2:1 ratio and a coordinated PPh_3 ligand are evident (Figure 4).

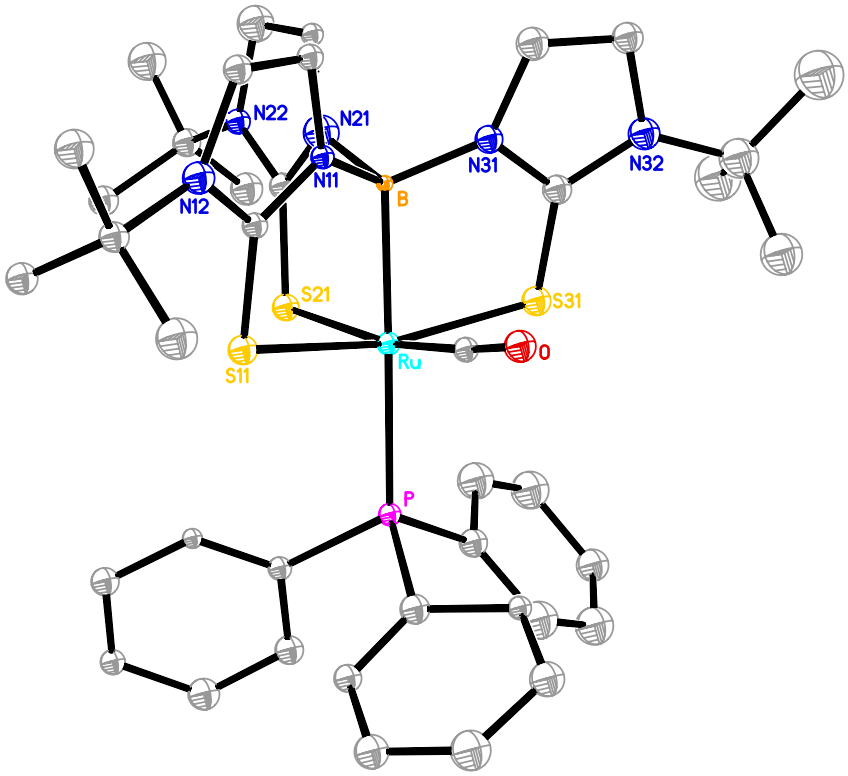

Figure 3. Molecular Structure of [κ⁴-B(mim$^{Bu^t}$)$_3$]Ru(CO)(PPh$_3$)

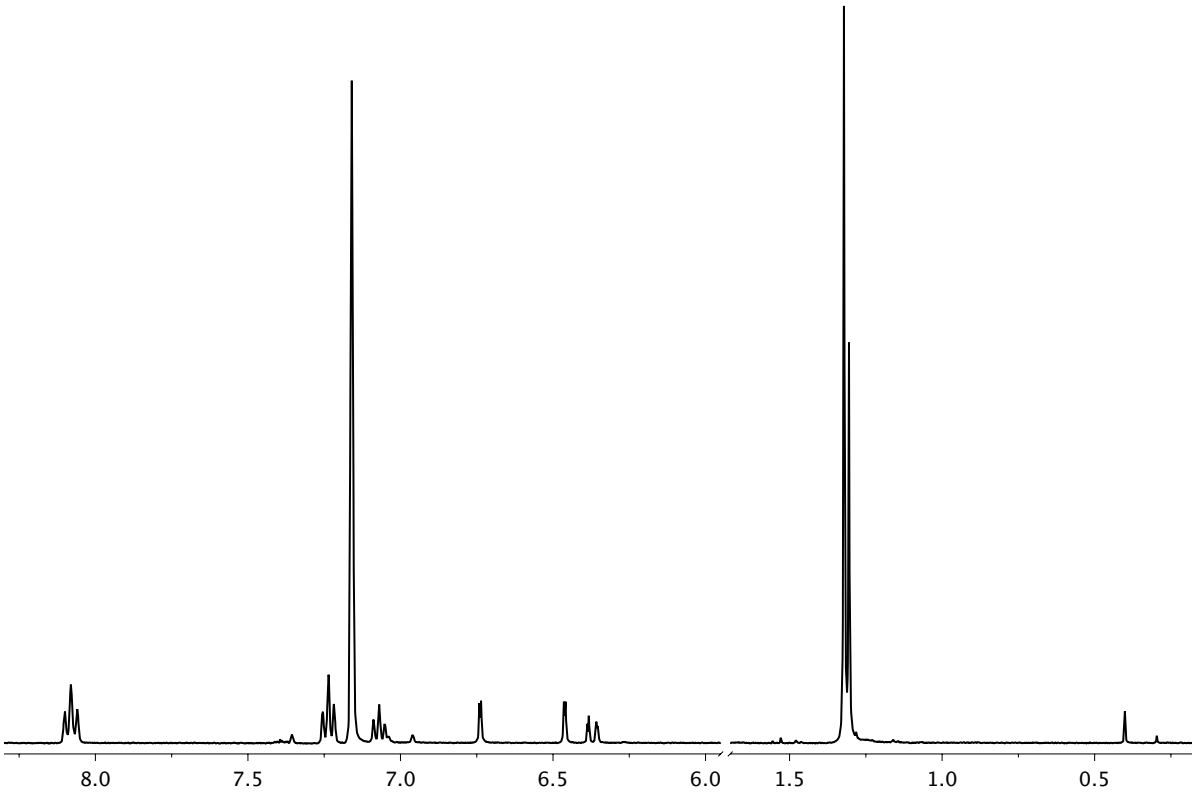

Figure 4. ^{1}H NMR Spectrum of [κ⁴-B(mim$^{Bu^t}$)$_3$]Ru(CO)(PPh$_3$)

Addition of excess PMe_3 to [κ^4-B(mim^{But})$_3$]Ru(CO)(PPh_3) results in facile displacement of PPh_3 to form [κ^4-B(mim^{But})$_3$]Ru(CO)(PMe_3) (Scheme 2), which has also been structurally characterized (Figure 5). The ^{1}H NMR spectrum of [κ^4-B(mim^{But})$_3$]Ru(CO)(PMe_3) is indicative of a structure that features two imidazolyl environments in a 2:1 ratio and a coordinated PMe_3 ligand (Figure 6). The PPh_3 liberated by this reaction may be washed away with pentane to afford [κ^4-B(mim^{But})$_3$]Ru(CO)(PMe_3) as a fairly pure, pale green solid. The removal of excess PPh_3 is important, since decomposition of [κ^4-B(mim^{But})$_3$]Ru(CO)(PMe_3) occurs in the presence of PPh_3. Specifically, treatment of [κ^4-B(mim^{But})$_3$]Ru(CO)(PMe_3) with PPh_3 results in the formation of some [κ^4-B(mim^{But})$_3$]Ru(CO)(PPh_3), but liberated PMe_3 is *not* observed by ^{1}H NMR spectroscopy. Instead, the displaced PMe_3 ligand appears to react with unreacted [κ^4-B(mim^{But})$_3$]Ru(CO)(PMe_3) to form [κ^3-*B,S,S*-B(mim^{But})$_3$]Ru(CO)(PMe_3)$_2$ (Scheme 3). In accord with this suggestion, the product of the reaction of [κ^4-B(mim^{But})$_3$]Ru(CO)(PMe_3) with PMe_3 possesses the same ^{1}H NMR spectrum as the decomposition product described here.

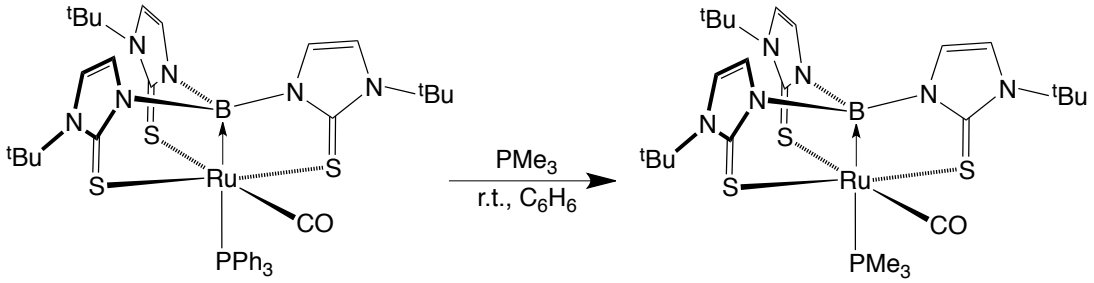

Scheme 2. Preparation of [κ^4-B(mim^{But})$_3$]Ru(CO)(PMe_3)

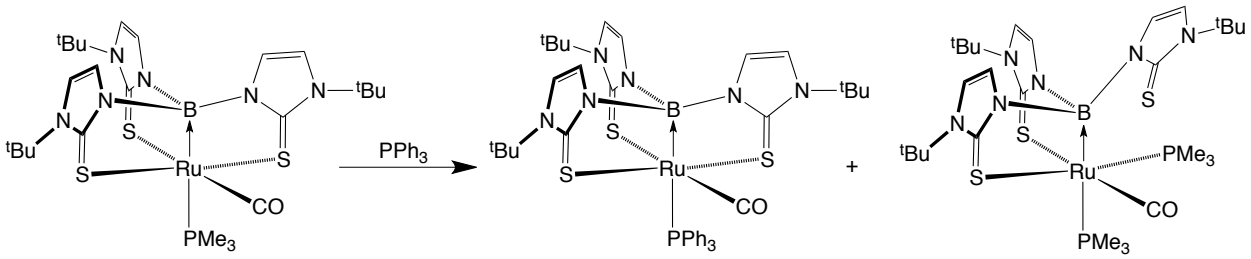

Scheme 3. Reaction of [κ^4-B(mim^{But})$_3$]Ru(CO)(PMe_3) with PPh_3

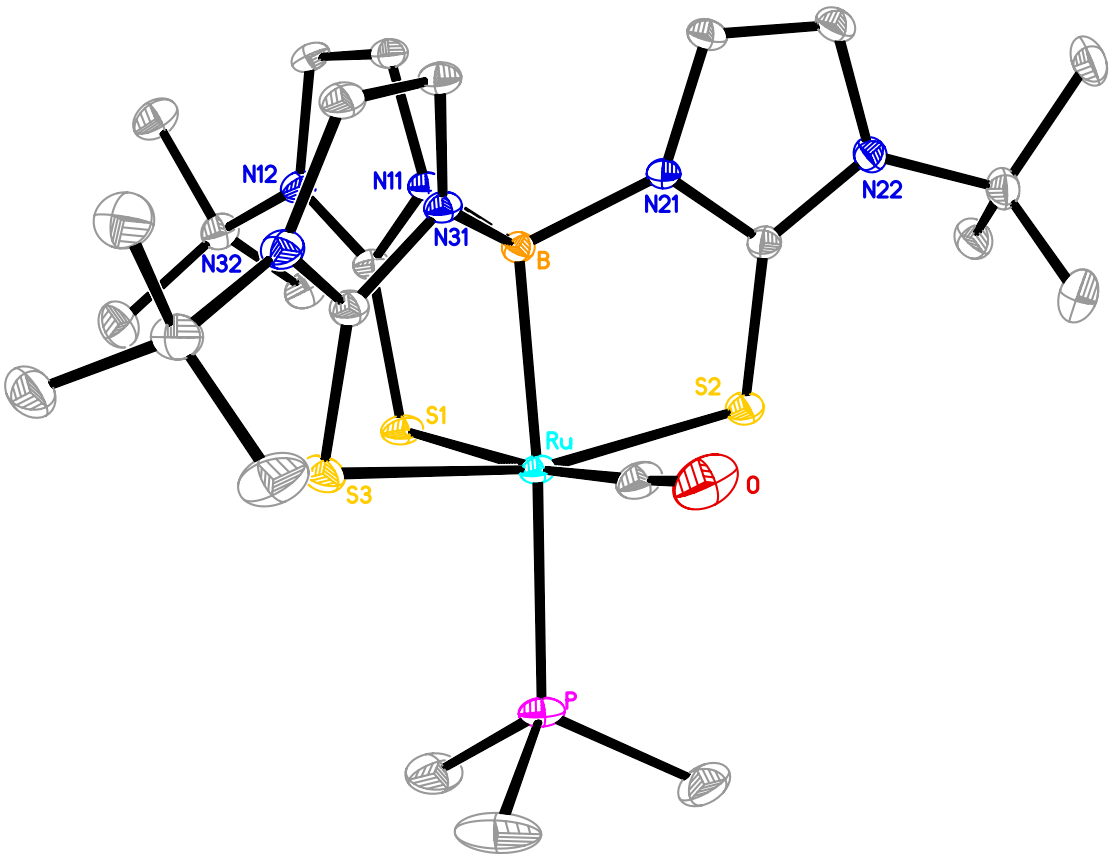

Figure 5. Molecular Structure of [κ⁴-B(mim^{But})$_3$]Ru(CO)(PMe$_3$)

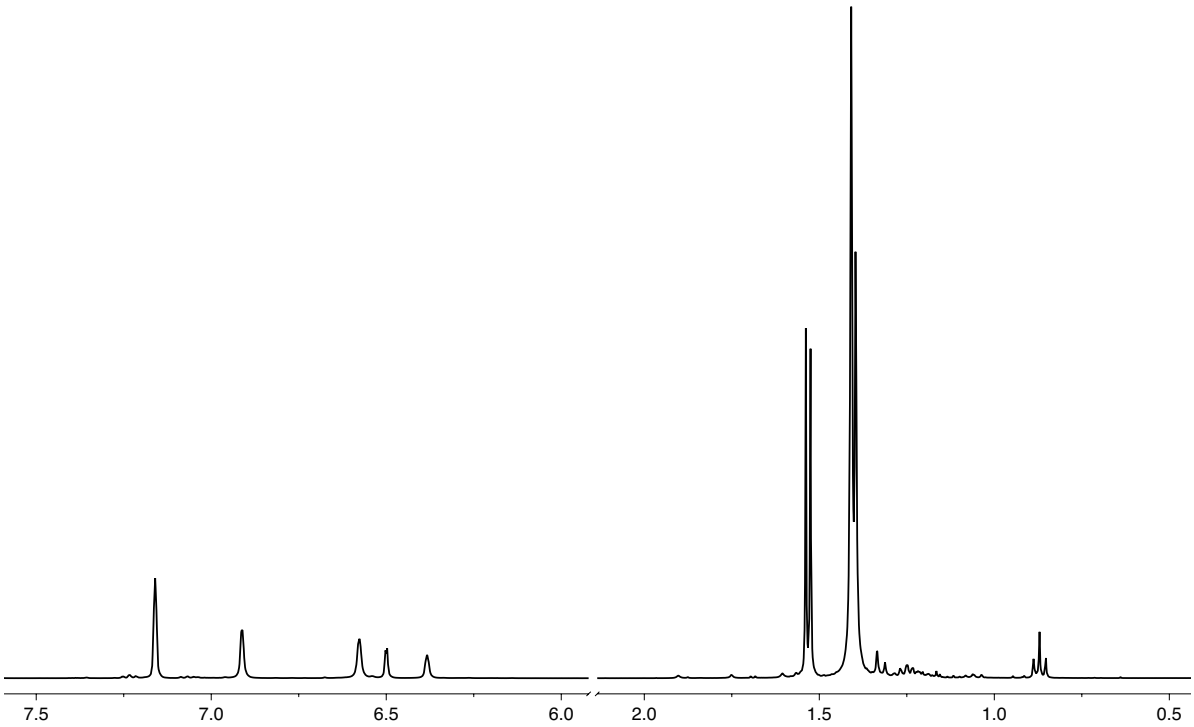

Figure 6. ^{1}H NMR Spectrum of [κ⁴-B(mim^{But})$_3$]Ru(CO)(PMe$_3$)

3.3 Structure and Bonding Analysis of [κ⁴-B(mim^{But})$_3$]Ru(CO)(PR$_3$) (R = Ph, Me)

The solid state structures of [κ⁴-B(mim^{But})$_3$]Ru(CO)(PPh$_3$) and [κ⁴-B(mim^{But})$_3$]Ru(CO)(PMe$_3$) feature Ru-B distances, respectively 2.149(18) Å and 2.148(2) Å, that support the presence of a Ru→B retrodative interaction.[5b,12] The geometry around each ruthenium center in [κ⁴-B(mim^{But})$_3$]Ru(CO)(PPh$_3$) and [κ⁴-B(mim^{But})$_3$]Ru(CO)(PMe$_3$) is nearly octahedral – for example, the B-Ru-P angles in these complexes are respectively 173.5(5) ° and 175.07(6) °, and the Ru-P distances are considerably longer than the average Ru-P bond length (2.332 Å) reported in the Cambridge Structural Database. The elongation of bonds *trans*- to the M→B bond in metallaboratrane complexes has been observed in other systems as well.[6b] The Ru-S distance for the bond *trans* to the carbonyl group in each structure is longer by *ca*. 0.06 Å than the *trans* S-Ru-S bonds. Select structural parameters for a series of ruthenaboratranes are presented in Table 1, from which it is evident that the elongation of the Ru→P bond is a general feature. These complexes all feature phosphine ligands that are *trans* to the Ru→B bond. Density functional theory geometry optimization calculations of [κ⁴-B(mim^{But})$_3$]Ru(CO)(PPh$_3$) and [κ⁴-B(mim^{But})$_3$]-Ru(CO)(PMe$_3$) accurately reproduce the experimentally determined structures (Figure 7).

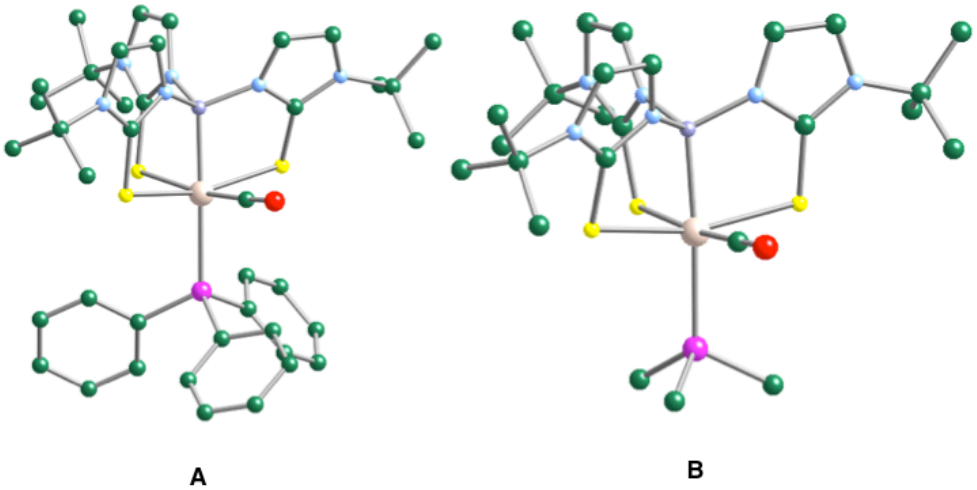

Figure 7. Geometry Optimized structures of (A) [κ⁴-B(mim^{But})$_3$]Ru(CO)(PPh$_3$) and (B) [κ⁴-B(mim^{But})$_3$]Ru(CO)(PMe$_3$)

Table 1. Comparison of Structural Parameters for [κ⁴-B(mim^{R})$_3$]Ru(L)(PR$_3$)

Complex	Ru-B (Å)	Ru-P$_{trans}$ (Å)	Reference
[κ⁴-B(mim^{But})$_3$]Ru(CO)(PPh$_3$)	2.149(18)	2.413(5)	This work
[κ⁴-B(mim^{But})$_3$]Ru(CO)(PMe$_3$)	2.148(2)	2.4090(6)	This work
[κ⁴-B(mim^{Me})$_3$]Ru(CO)(PPh$_3$)[a]	2.161	2.435	4
[κ⁴-B(mim^{Me})$_3$]Ru(CS)(PPh$_3$)	2.154(5)	2.4569(12)	5b
[κ⁴-B(mim^{PhCl})$_3$]Ru(CO)(PPh$_3$)	2.166(14)	2.424(4)	**13**

a – ESDs were not provided for this structure

The bonding in metallaboratrane complexes has been described in conflicting ways; for example, the appropriate d-electron count for metals involved in M→B bonding has been debated. Some have favored a d^n configuration, since the formal oxidation number of the metal is not impacted upon interaction with the neutral boron center,[7c] while others have argued that the M→B retrodative interaction will increase the valence of the metal by two, resulting in a d^{n-2} configuration.[6d] The validity of the d^{n-2} configuration has been confirmed by molecular orbital calculations for the iridaboratrane [κ⁴-B(mim^{H})$_3$]Ir(PH$_3$)Cl[6d] and the palladaboratrane [κ⁴-B(mim^{But})$_3$]Pd(PMe$_3$);[7b] therefore, it seemed like a worthy objective to determine the most accurate bonding descriptions of the ruthenaboratranes, the results of which are shown here for [κ⁴-B(mim^{But})$_3$]Ru(CO)(PMe$_3$).

As has been previously described,[6d] the molecular orbital description for a complex in which the apical boron does not interact with the metal center (*i.e.* a "pro-boratrane")[1] would be significantly different than that for a complex with a M→B retrodative bond. For example, the hypothetical complex [κ³-*S*,*S*,*S*-B(mim^{But})$_3$]Ru(CO)(PMe$_3$) would be expected to have a d^8 configuration, where the HOMO of the molecule possesses d_{z^2} character and is the σ-antibonding component of the Ru-P bond. The boron p_z orbital would be empty and non-coordinating (Figure 8, **A**). Upon forming [κ⁴-

$B(mim^{But})_3]Ru(CO)(PMe_3)$, however, the boron interacts with the metal and results in a 3-center, 4-electron B-Ru-P bonding description. This interaction produces B-Ru-P bonding, non-bonding, and anti-bonding orbitals, and the metal center possesses a d^6 configuration (Figure 8, **B**). Specifically, the two highest energy d electrons (*i.e.* those in the d_{z^2} orbital) go from being metal-based in description **A** to being ligand-based in description **B**, resulting in a d^6 metal center. Molecular orbital analysis of [κ^4-$B(mim^{But})_3]Ru(CO)(PMe_3)$ using Fenske-Hall calculations supports the latter bonding description, in which the metal is engaged in a 3-center, 4-electron interaction and has six electrons in non-bonding orbitals. The results of these calculations are shown in Figure 9.

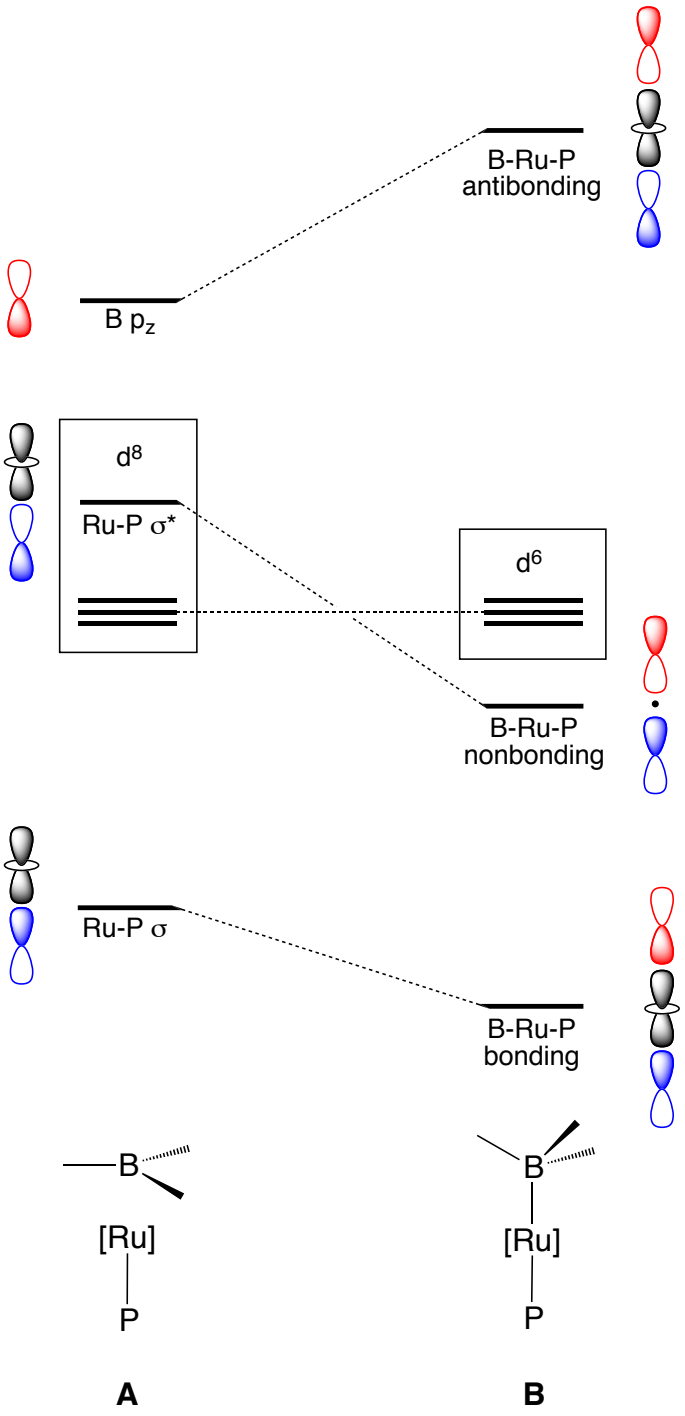

Figure 8. Molecular Orbital description for the hypothetical species [κ^3-S_3-B(mim^{But})$_3$]Ru(CO)(PMe$_3$) (A) and for [κ^4-B(mim^{But})$_3$]Ru(CO)(PMe$_3$)

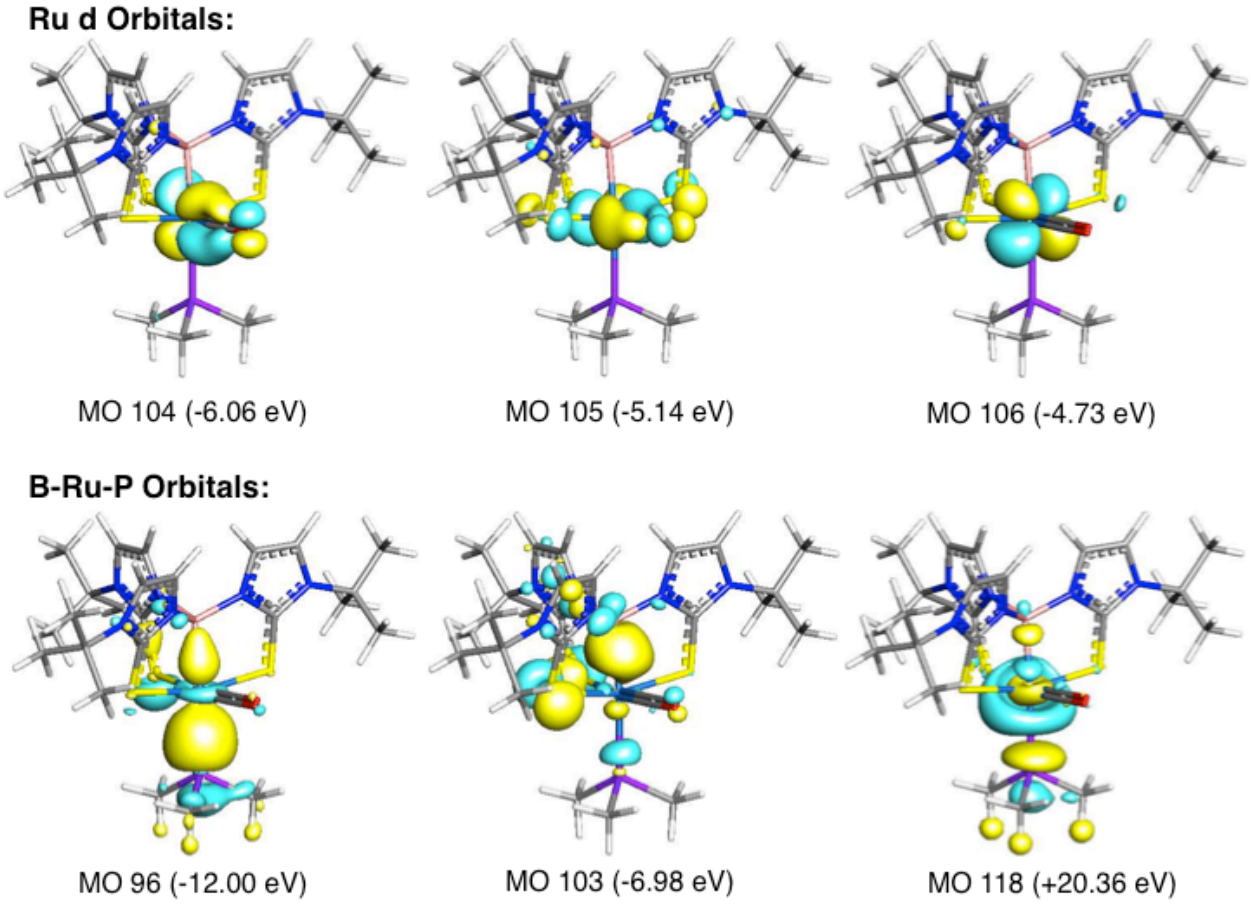

Figure 9. Selected Molecular Orbitals (MOs) of [κ⁴-B(mim$^{Bu^t}$)$_3$]Ru(CO)(PMe$_3$)

Natural Bond Orbital (NBO) Analysis also confirms the presence of a Ru→B bond and a d^6 configuration of the metal center. Unlike the molecular orbital analysis detailed above, NBO analysis presents a bonding description in which orbitals are localized on one atom (lone pair), two atoms (bond pair), or three atoms (3-center, 2-electron interaction). Thus, the 3-center, 4-electron bonding description is not explicitly reproduced by NBO calculations; nonetheless, Ru-P and Ru-B bonding interactions are evident, as is the antibonding component of the B-Ru-P interaction. The results of these calculations are shown in Figure 10.

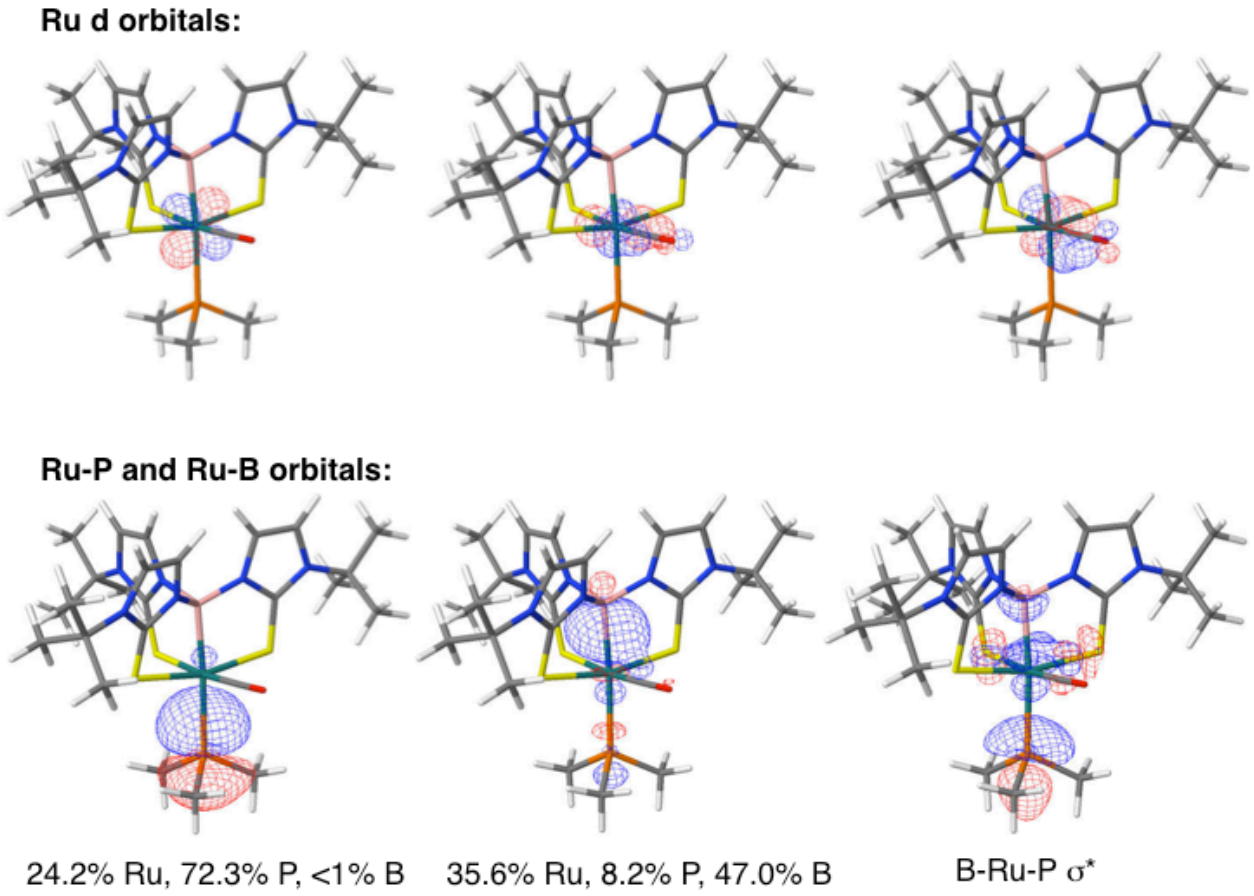

Figure 10. NBO Analysis of [κ⁴-B(mim^{But})$_3$]Ru(CO)(PMe$_3$). Orbital contributions are listed where necessary.

3.4 Reactivity of [κ⁴-B(mim^{But})$_3$]Ru(CO)(PR$_3$) (R = Ph, Me)

In addition to the structure and bonding of [κ⁴-B(mim^{But})$_3$]Ru(CO)(PPh$_3$) and [κ⁴-B(mim^{But})$_3$]Ru(CO)(PMe$_3$), we were also interested in the reactivity of these complexes. Some reactivity of metallaboratranes has been explored – for example, the ferraboratrane [κ⁴-B(mim^{But})$_3$]Fe(CO)$_2$[5a] and nickel boratranes of the type of [κ⁴-B(mim^{But})$_3$]NiX[7a] were shown to undergo addition across the M→B bond in the presence of a number of substrates. The addition of H_2 across M→B bonds has also been reported.[14,15] Addition reactions of this type are of interest because the ligand is directly involved in the reaction rather than simply acting as a scaffold for the metal center.[16] Ligand substitution reactions of ruthenaboratranes and rhodaboratranes have been

explored,[5b,6b] and the reactivity of a TPB-based ferraboratrane towards nitrogen fixation has also been studied.[17] Therefore, we were interested in investigating the reactivity of [κ^4-B(mim^{But})$_3$]Ru(CO)(PPh$_3$) and [κ^4-B(mim^{But})$_3$]Ru(CO)(PMe$_3$) towards addition and substitution reactions.

Under a number of conditions, [κ^4-B(mim^{But})$_3$]Ru(CO)(PPh$_3$) was found to be rather unreactive. When heated in the presence of carbon dioxide, for example, no change was observed by ^{1}H NMR spectroscopy. Photolysis of the ruthenaboratrane led to complete decomposition. Reactions with chloroform, trityl chloride, and water were equally unfruitful, all leading to decomposition after heating. Reaction of [κ^4-B(mim^{But})$_3$]Ru(CO)(PPh$_3$) with CO did proceed, presumably to form [κ^4-B(mim^{But})$_3$]Ru(CO)$_2$, but not to completion; the reversible formation of a bis(carbonyl) boratrane has been reported previously.[5b]

[κ^4-B(mim^{But})$_3$]Ru(CO)(PMe$_3$) was found to be more reactive than [κ^4-B(mim^{But})$_3$]-Ru(CO)(PPh$_3$). For example, [κ^4-B(mim^{But})$_3$]Ru(CO)(PMe$_3$) transforms cleanly in the presence of CO. The ^{1}H NMR spectrum of this product suggests that it may be an isomeric boratrane in which the CO ligand is *trans* to the boron and the PMe$_3$ ligand is *cis* (Scheme 4) (Figure 11). For example, the presence of two imidazolyl environments in a 2:1 ratio and a resonance corresponding to a coordinated PMe$_3$ ligand are present in both [κ^4-B(mim^{But})$_3$]Ru(CO)(PMe$_3$) and its product with CO. Alternatively, a structure in which another equivalent of CO has coordinated to the metal, displacing the imidazolyl arm *trans* to the carbonyl group, would be consistent with this ^{1}H NMR spectrum (Scheme 5); however, a [κ^3-*B*,*S*,*S*-B(mim^R)$_3$] configuration in which the two coordinated imidazolyl arms are *trans* to each other is rare and has only been observed in dimeric species.[7b] IR spectroscopic analysis could, in principle, distinguish between these two possibilities. The product of this reaction does not revert back to [κ^4-B(mim^{But})$_3$]Ru(CO)(PMe$_3$) in the absence of CO.

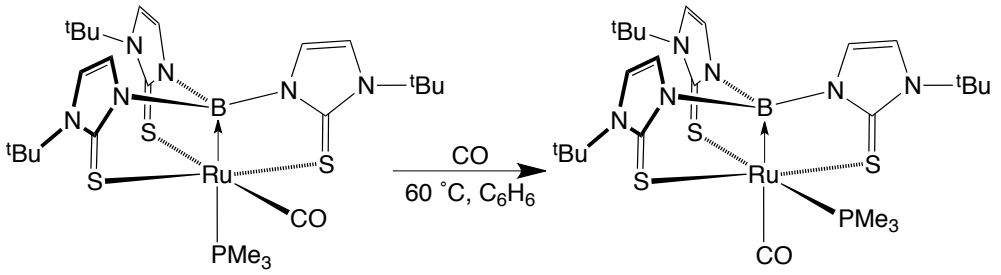

Scheme 4. Reactivity of [κ⁴-B(mim^{But})$_3$]Ru(CO)(PMe$_3$) towards CO

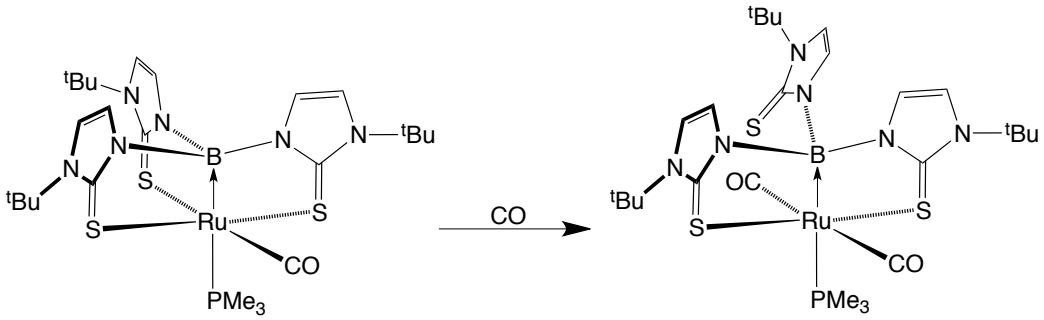

Scheme 5. Alternate explanation for the reactivity of [κ⁴-B(mim^{But})$_3$]Ru(CO)(PMe$_3$) towards CO

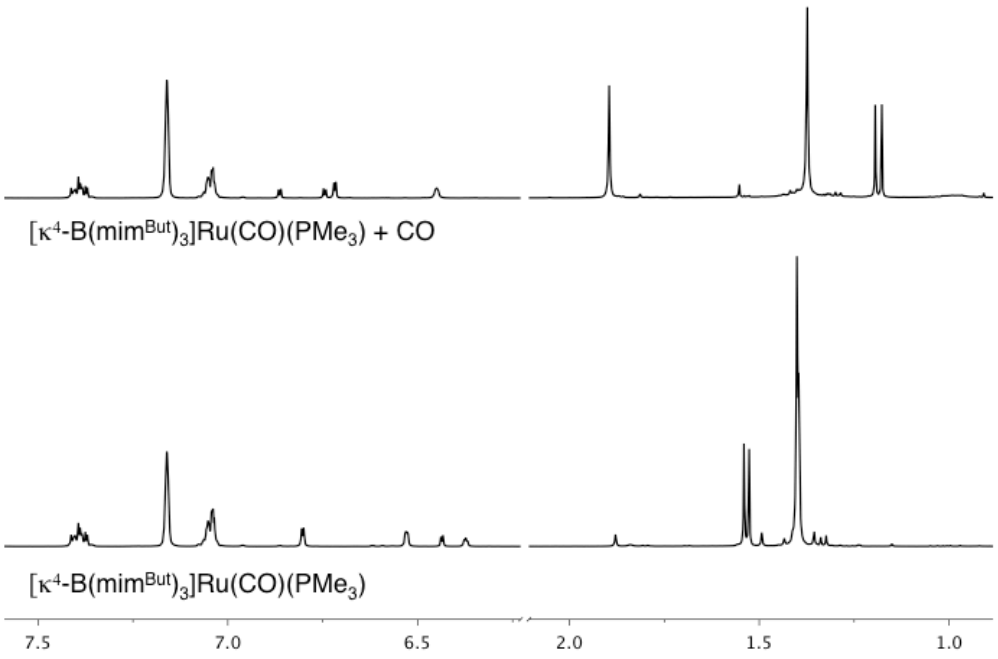

Figure 11. ^{1}H NMR spectroscopic analysis of [κ⁴-B(mim^{But})$_3$]Ru(CO)(PMe$_3$) + CO (some free PPh$_3$ is present but does not appear to affect the course of this reaction)

$[\kappa^4\text{-B(mim}^{\text{Bu}^t}\text{)}_3]\text{Ru(CO)(PMe}_3\text{)}$ also reacts quite cleanly with MeI; ^{1}H NMR spectroscopic analysis of the reaction is suggestive of a product in which the MeI has added across the Ru→B bond (Scheme 6). For example, three unique imidazolyl environments are observed, which is consistent with a product in which each imidazolyl arm is *trans* to a different ligand (PMe_3, CO, X). However, the overall configuration (*i.e.* whether the methyl group is attached to the boron or the ruthenium) is not known, and no coupling of the methyl group to phosphorus or boron is observed. The ^{1}H NMR spectrum of this reaction (Figure 12) appears to contain a smaller set of peaks in addition to the major product, which may suggest that both isomers are formed in different amounts.

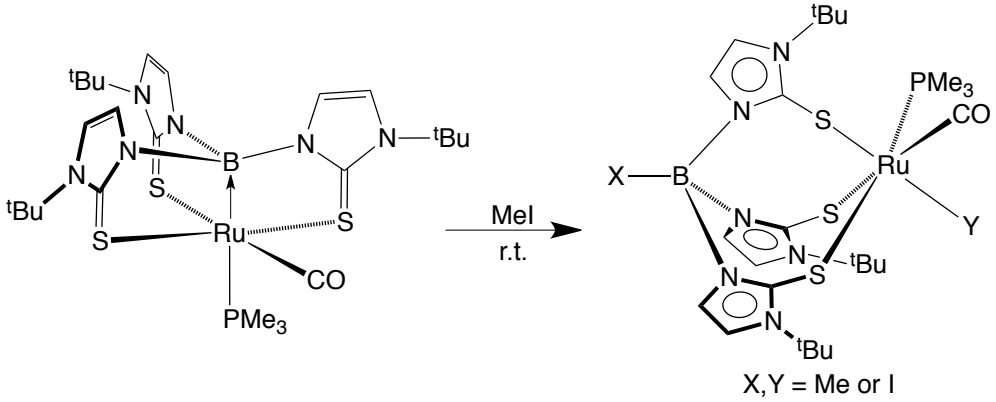

Scheme 6. Reaction of $[\kappa^4\text{-B(mim}^{\text{Bu}^t}\text{)}_3]\text{Ru(CO)(PMe}_3\text{)}$ with MeI

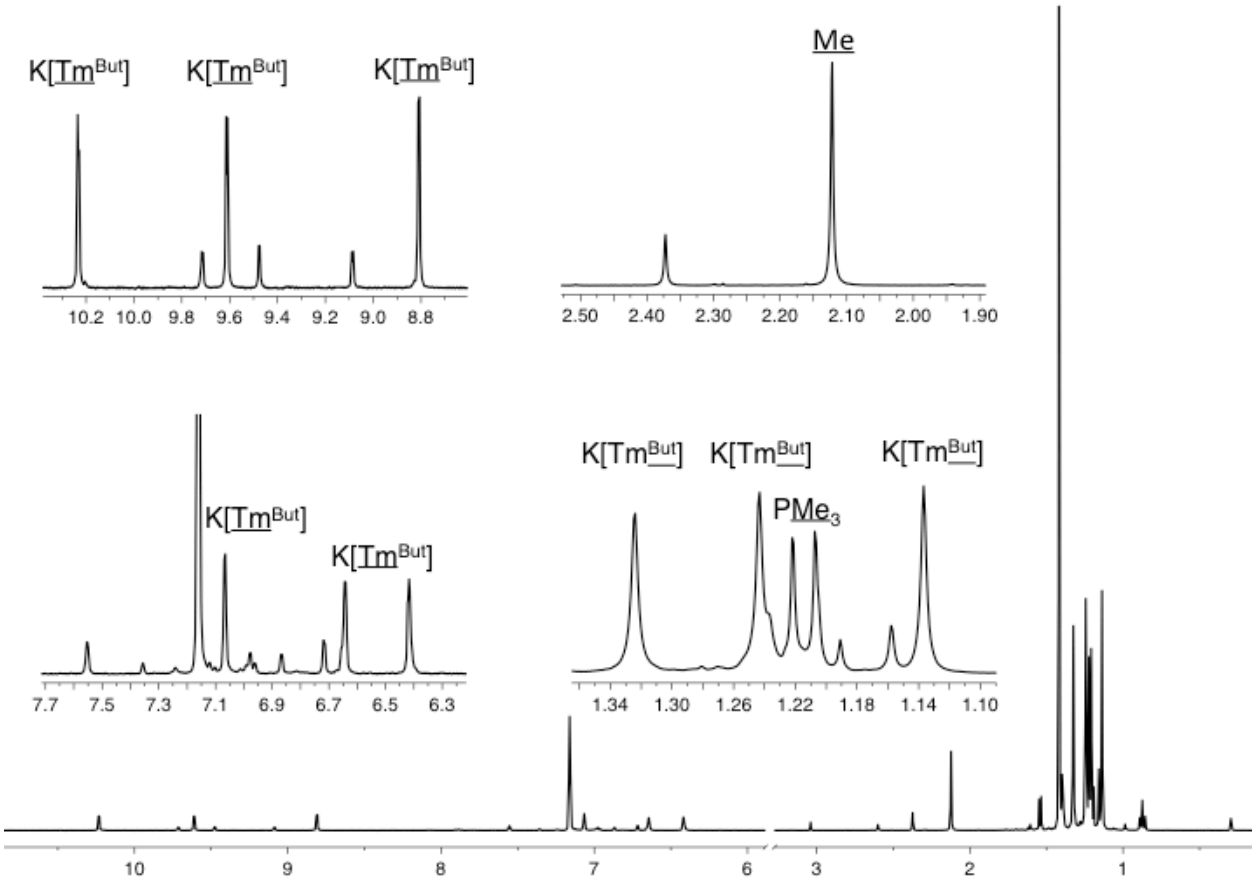

Figure 12. ^{1}H NMR Spectroscopic Analysis of [κ^4-B(mim^{But})$_3$]Ru(CO)(PMe$_3$) + MeI – signals are labeled for the major product

Reactions of [κ^4-B(mim^{But})$_3$]Ru(CO)(PMe$_3$) with C_2H_4, I_2, CO_2, $CHCl_3$, and XeF_2 resulted in a mixture of products, none of which was identified.

Numerous attempts were made at preparing the bis(PMe$_3$) boratrane, in which the carbonyl group is replaced with another phosphine ligand. Heating [κ^4-B(mim^{But})$_3$]Ru(CO)(PMe$_3$) with excess PMe$_3$ did result in the coordination of an additional PMe$_3$ ligand; however, the ^{1}H NMR spectrum of this product indicated that one of the arms of the Tm ligand dissociated instead of the CO ligand, producing the complex [κ^3-*B,S,S*-B(mim^{But})$_3$]Ru(CO)(PMe$_3$)$_2$ (*vide supra*). Chelating bis(phosphine) ligands were also considered as promising options due to entropic reasons. Treatment

of [κ⁴-B(mim^{But})$_3$]Ru(CO)(PMe$_3$) with 1,2-bis(diphenylphosphino)ethane (dppe) did result in the evolution of free PMe$_3$, but whether or not the CO ligand was also displaced is unclear. Photolysis of [κ⁴-B(mim^{But})$_3$]Ru(CO)(PMe$_3$) and treatment with trimethyl-amine-*N*-oxide and pyridine *N*-oxide were also unsuccessful in removing the carbonyl ligand. Ruthenium precursors that do not contain CO ligands, such as RuCl$_2$(PMe$_3$)$_4$, RuHCl(PPh$_3$)$_3$, and RuCl$_2$(DMSO)$_4$, did not result in the isolation of a boratrane complex. Specifically, the reaction of RuHCl(PPh$_3$)$_3$ with K[Tm^{But}] resulted in decomposition of the metal complex, and the reaction of RuCl$_2$(DMSO)$_4$ produces decomposition of the ligand, as evidenced by the formation of free imidazole in the ^{1}H NMR spectrum. RuCl$_2$(PMe$_3$)$_4$ does react with K[Tm^{But}] to afford multiple species, including a ruthenium hydride species; the nature of this complex is unknown, but the ^{1}H NMR spectrum does not indicate the presence of two imidazolyl environments that is indicative of a boratrane structure.

RuHCl(CO)(PMe$_3$)$_3$ was also considered as a boratrane precursor. This complex is synthesized by heating RuHCl(CO)(PPh$_3$)$_3$ with excess PMe$_3$ at 80 °C; when this reaction is monitored by ^{1}H NMR spectroscopy, stepwise replacement of the PPh$_3$ ligands is visible (Figure 13).

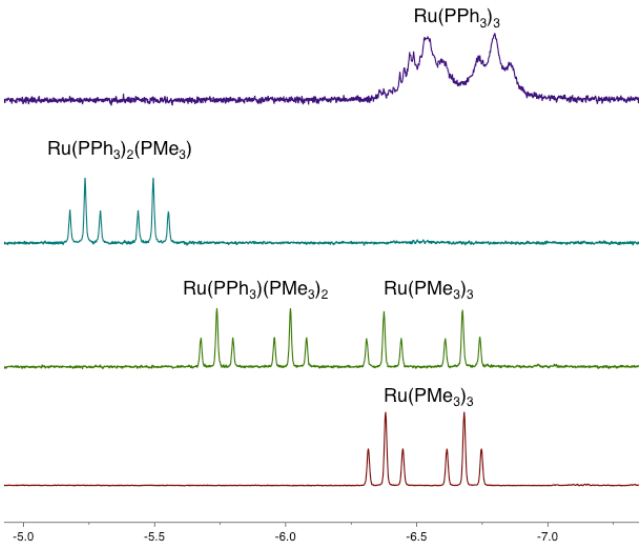

Figure 13. ^{1}H NMR spectra (hydride region) of RuHCl(CO)(PPh$_3$)$_3$ + PMe$_3$

$RuHCl(CO)(PMe_3)_3$, unlike $[\kappa^4\text{-}B(mim^{But})_3]Ru(CO)(PMe_3)$, is soluble in pentane; therefore, this complex could not be purified of the liberated PPh_3 by washing with pentane. As such, MeI was added to the reaction mixture of $RuHCl(CO)(PMe_3)_3$ and PPh_3 in order to generate $[PPh_3Me]I$ as an insoluble precipitate. Although this technique was successful in the removal of the free phosphine, it also converted the ruthenium hydride species into the iodide, $RuICl(CO)(PMe_3)_3$. Treatment of this complex with $K[Tm^{But}]$ resulted in a cationic species, $\{[\kappa^3\text{-}H,S,S\text{-}Tm^{But}]Ru(CO)(PMe_3)_2\}I$ (Scheme 7), as confirmed by X-ray crystallography (Figure 14). Treatment of $RuHCl(CO)(PMe_3)_3$ with $K[Tm^{But}]$ in the presence of free PPh_3 resulted primarily in decomposition. One interesting structural feature of $\{[\kappa^3\text{-}H,S,S\text{-}Tm^{But}]Ru(CO)(PMe_3)_2\}I$ is that the Ru-P bond *trans* to the B-H interaction is significantly shorter than the Ru-P bonds of the boratrane complexes; specifically, Ru-P1 in $\{[\kappa^3\text{-}H,S,S\text{-}Tm^{But}]Ru(CO)(PMe_3)_2\}I$ is 2.292(3) Å, compared to the values of 2.413(5) Å and 2.4090(6) Å in the boratrane complexes. This difference provides further evidence that the Ru→B retrodative bond has a marked impact on the overall bonding of a boratrane complex. The B-H bond could not be freely refined.

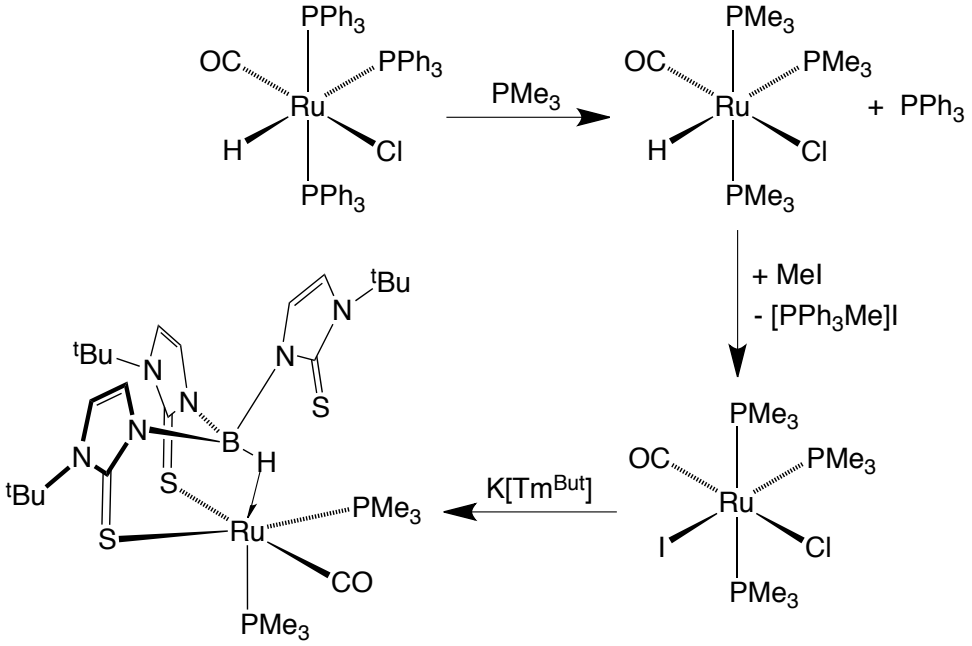

Scheme 7. Reactivity of $RuHCl(CO)(PMe_3)$ towards MeI and $K[Tm^{But}]$

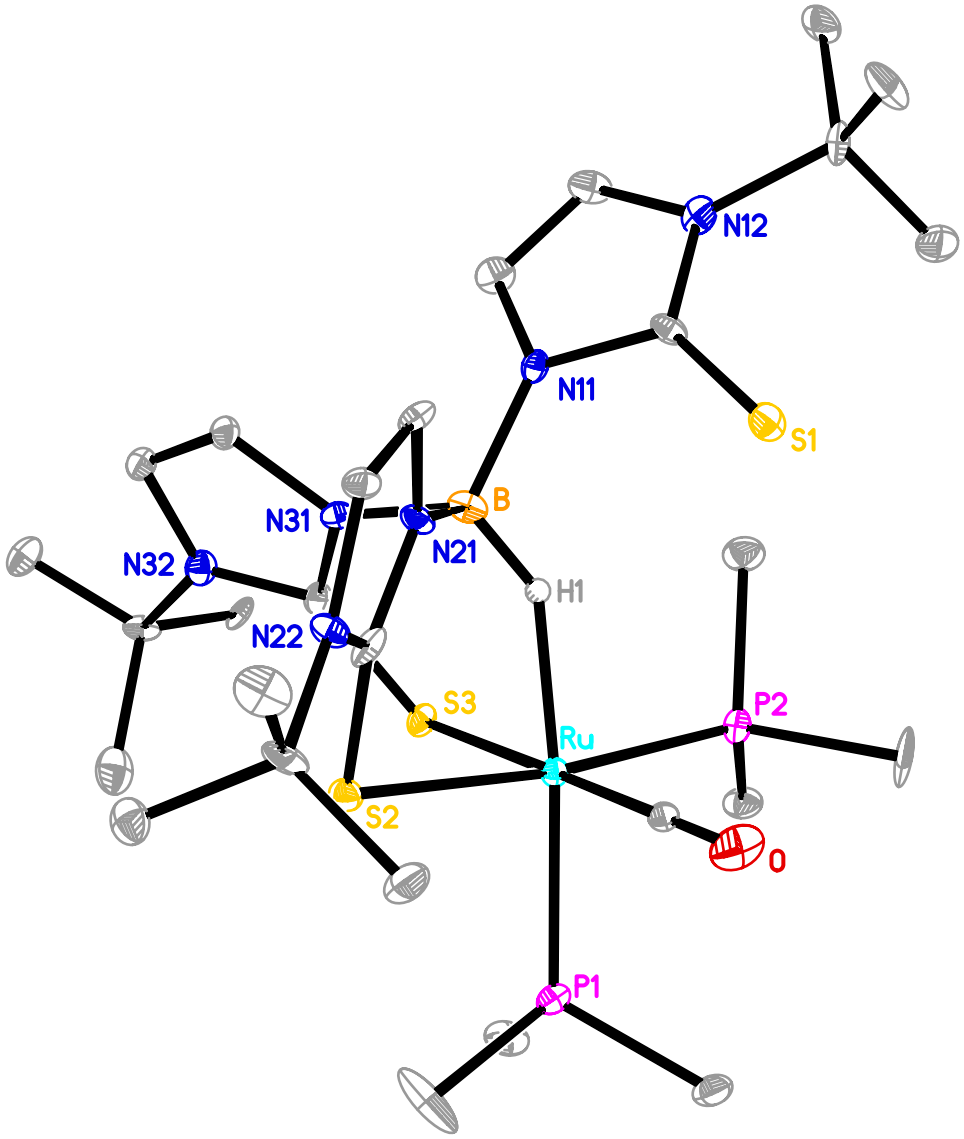

Figure 14. Molecular Structure of {[κ³-*H,S,S*-Tm^{But}]Ru(CO)(PMe$_3$)$_2$}I. The anion (I$^-$) and a molecule of co-crystallized acetonitrile are omitted for clarity.

3.5 Summary and Conclusions

In conclusion, two new ruthenaboratranes, namely [κ^4-B(mim^{But})$_3$]Ru(CO)(PPh$_3$) and [κ^4-B(mim^{But})$_3$]Ru(CO)(PMe$_3$), have been prepared. These complexes have been spectroscopically and structurally characterized, and their bonding has been investigated computationally. The reactivities of [κ^4-B(mim^{But})$_3$]Ru(CO)(PPh$_3$) and [κ^4-B(mim^{But})$_3$]Ru(CO)(PMe$_3$) have also been examined. While [κ^4-B(mim^{But})$_3$]Ru(CO)(PPh$_3$)

was found to decompose under a number of conditions, the reactions of [κ^4-B(mim^{But})$_3$]Ru(CO)(PMe$_3$) proceeded smoothly with some substrates such as CO and MeI. Finally, the reaction of a non-hydride ruthenium compound afforded an ionic Tm complex, {[κ^3-*H,S,S*-Tm^{But}]Ru(CO)(PMe$_3$)$_2$}I. Computational results support the notion that the M→B interaction reduces the d-electron count of the ruthenium by two, resulting in a d^6 metal configuration.

3.6 Experimental Details

3.6.1 General Considerations

All manipulations were performed using a combination of glovebox, high vacuum, and Schlenk techniques under a nitrogen atmosphere unless otherwise specified.[18] Solvents were purified and degassed by standard procedures. ^{1}H NMR spectra were measured on Bruker Avance III 400 and Bruker Avance III 400 SL spectrometers. ^{1}H chemical shifts are reported in ppm relative to SiMe$_4$ (δ = 0) and were referenced internally with respect to the protio solvent impurity (δ 7.16 for C_6D_5H).[19] ^{31}P chemical shifts are reported in ppm relative to 85% H_3PO_4 (δ = 0) and were referenced using P(OMe)$_3$ (δ = 141.0) as an external standard.[20] RuHCl(CO)(PPh$_3$)$_3$ was prepared by the literature method,[21] and K[Tm^{But}] was prepared by a method analogous to that used for Na[Tm^{But}].[6a]

3.6.2 X-ray Structure Determinations

X-ray diffraction data were collected on a Bruker Apex II diffractometer. Crystal data, data collection and refinement parameters are summarized in Section 3.7, Table 1. The structures were solved using direct methods and standard difference map techniques, and were refined by full-matrix least-squares procedures on F^2 with SHELXTL (Version 6.10).[22]

3.6.3 Computational Details

Calculations were carried out using DFT as implemented in the Jaguar 7.7 (release 107) suite of ab initio quantum chemistry programs.[23] Geometry optimizations (Section 3.8, Table 2) were performed with the B3LYP density functional[24] using the LACVP** basis set.[25] Molecular orbital analyses were performed with the aid of JIMP2,[26] which employs Fenske-Hall calculations and visualization using MOPLOT.[27] NBO calculations were performed using Jaguar NBO 5.0.[28]

3.6.4 Synthesis of [κ^4-B(mim$^{Bu^t}$)$_3$]Ru(CO)(PPh$_3$)

A suspension of RuHCl(CO)(PPh$_3$)$_3$ (0.23 g, 0.24 mmol) and K[Tm$^{Bu^t}$] (0.28 g, 0.25 mmol) in C_6H_6 (*ca.* 20 mL) was heated for *ca.* 36 hours at 80 ˚C in an ampoule under an argon atmosphere. After this time, a white powder was observed to have precipitated from the reaction mixture. The contents of the ampoule were filtered, the filtrate was concentrated to approximately 10 mL, and hexane (*ca*. 5 mL) was added to the solution to effect precipitation of the product. This process was repeated, and the precipitates were combined to afford [κ^4-B(mim$^{Bu^t}$)$_3$]Ru(CO)(PPh$_3$) as a light brown powder (0.12 g, 57 % yield). Single crystals of [κ^4-B(mim$^{Bu^t}$)$_3$]Ru(CO)(PPh$_3$) suitable for X-ray diffraction were obtained from a solution in C_6H_6 layered with hexane. ^{1}H NMR (C_6D_6): 1.31 [s, 9H of κ^4-B(mim$^{\underline{Bu^t}}$)$_3$], 1.32 [s, 18H of κ^4-B(mim$^{\underline{Bu^t}}$)$_3$], 6.36 [d, $^3J_{H\text{-}H}$ = 2, 1H of κ^4-B(mim$^{\underline{Bu^t}}$)$_3$], 6.39 [d, $^3J_{H\text{-}H}$ = 2, 1H of κ^4-B(mim$^{\underline{Bu^t}}$)$_3$], 6.46 [d, $^3J_{H\text{-}H}$ = 2, 2H of κ^4-B(mim$^{\underline{Bu^t}}$)$_3$], 6.74 [d, $^3J_{H\text{-}H}$ = 2, 2H of κ^4-B(mim$^{\underline{Bu^t}}$)$_3$], 7.07 [t, $^3J_{H\text{-}H}$ = 8, 3H of Ru(P$\underline{Ph_3}$)], 7.24 [t, $^3J_{H\text{-}H}$ = 8, 6H of Ru(P$\underline{Ph_3}$)], 8.08 [t, $^3J_{H\text{-}H}$ = 8, $^3J_{P\text{-}H}$ = 8, 6H of Ru(P$\underline{Ph_3}$)]. ^{31}P{^{1}H} NMR (C_6D_6): 26.6.

3.6.5 Synthesis of [κ^4-B(mim$^{Bu^t}$)$_3$]Ru(CO)(PMe$_3$) A solution of [κ^4-B(mim$^{Bu^t}$)$_3$]Ru(CO)(PPh$_3$) (0.15 g, 0.17 mmol) was dissolved in C_6H_6 (*ca*. 15 mL) and treated with PMe$_3$ (*ca*. 0.1 mL) in an ampoule. The solution was allowed to sit at room temperature overnight, at which point the solution had turned a vivid green color. The solution was lyophilized and washed with pentane (2 × 20 mL) to afford [κ^4-

B(mim^{But})$_3$]Ru(CO)(PMe$_3$) as a sea-green powder (0.11g, 92 % yield). Crystals of [κ^4-B(mim^{But})$_3$]Ru(CO)(PMe$_3$) suitable for X-ray diffraction were obtained from a solution in C_6D_6 layered with pentane at room temperature. Analysis calcd. for [κ^4-B(mim^{But})$_3$]-Ru(CO)(PMe$_3$): C, 44.05%; H, 6.21 %. Found: C, 46.31%; H, 6.08 %. ^{1}H NMR (C_6D_6): 1.39 [s, 9H of κ^4-B(mim$^{\underline{But}}$)$_3$], 1.40 [s, 18H of κ^4-B(mim$^{\underline{But}}$)$_3$], 1.53 [d, $^2J_{P-H}$ = 5, 9H of Ru(P$\underline{Me}_3$)], 6.37 [filled in d, J_{H-H} = 2, 1H of κ^4-B($\underline{mim}^{But}$)$_3$], 6.44 [d, $^3J_{H-H}$ = 2, 1H of κ^4-B($\underline{mim}^{But}$)$_3$], 6.52 [d, $^3J_{H-H}$ = 2, 2H of κ^4-B($\underline{mim}^{But}$)$_3$], 6.80 [d, $^3J_{H-H}$ = 2, 2H of κ^4-B($\underline{mim}^{But}$)$_3$]. ^{31}P{^{1}H} NMR (C_6D_6): -26.6 [br s, 1P of Ru-$\underline{P}$Me$_3$]. ^{11}B NMR (C_6D_6): -1.3 [br d, J_{P-B} = 70].

3.6.6 Reaction of [κ^4-B(mim^{But})$_3$]Ru(CO)(PMe$_3$) with CO

A solution of [κ^4-B(mim^{But})$_3$]Ru(CO)(PMe$_3$) (8 mg, 0.01 mmol) in C_6D_6 in an NMR tube equipped with a J. Young valve was degassed and charged with CO (1 atm). The solution was heated at 60 ˚C for 3 days, thereby resulting in the putative isomeric product in which the CO ligand is *trans* to the Ru→B bond. ^{1}H NMR (C_6D_6): 1.19 [d, $^2J_{P-H}$ = 7, 9H of Ru(P$\underline{Me}_3$)], 1.37 [s, 18H of κ^4-B(mim$^{\underline{But}}$)$_3$], 1.90 [s, 9H of κ^4-B(mim$^{\underline{But}}$)$_3$], 6.45 [br s, 2H of κ^4-B($\underline{mim}^{But}$)$_3$], 6.72 [d, $^3J_{H-H}$ = 2, 2H of κ^4-B($\underline{mim}^{But}$)$_3$], 6.74 [d, $^3J_{H-H}$ = 2, 1H of κ^4-B($\underline{mim}^{But}$)$_3$], 6.86 [d, $^3J_{H-H}$ = 2, 1H of κ^4-B($\underline{mim}^{But}$)$_3$]. ^{1}H-^{31}P HMQC (C_6D_6): -29.6 [s, 1P of Ru-$\underline{P}$Me$_3$].

3.6.7 Reaction of [κ^4-B(mim^{But})$_3$]Ru(CO)(PMe$_3$) with MeI

A solution of [κ^4-B(mim^{But})$_3$]Ru(CO)(PMe$_3$) (10 mg, 0.01 mmol) in C_6D_6 in an NMR tube equipped with a J. Young valve was treated with excess MeI. After 15 minutes at room temperature, ^{1}H NMR spectroscopic analysis indicated that the [κ^4-B(mim^{But})$_3$]Ru(CO)(PMe$_3$) had completely reacted to form the putative addition product, [κ^3-XB(mim^{But})$_3$]Ru(CO)(PMe$_3$)Y (X,Y = Me or I). ^{1}H NMR (C_6D_6): 1.14 [s, 9H of κ^4-B(mim$^{\underline{But}}$)$_3$], 1.21 [d, $^2J_{P-H}$ = 6, 9H of Ru(P$\underline{Me}_3$)], 1.24 [s, 9H of κ^4-B(mim$^{\underline{But}}$)$_3$], 1.32 [s, 9H of κ^4-B(mim$^{\underline{But}}$)$_3$], 2.12 [s, 3H of M-$\underline{Me}$], 6.42 [filled in d, J_{H-H} = 2, 1H of κ^3-XB($\underline{mim}^{But}$)$_3$], 6.64 [d, $^3J_{H-H}$ = 2, 1H of κ^3-XB($\underline{mim}^{But}$)$_3$], 7.07 [d, $^3J_{H-H}$ = 2, 1H of κ^3-XB($\underline{mim}^{But}$)$_3$], 8.81 [d, $^3J_{H-H}$ =

2, 1H of κ^3-XB($\underline{\text{mim}}^{\text{But}}$)$_3$], 9.61 [d, $^3J_{H\text{-}H}$ = 2, 1H of κ^3-XB($\underline{\text{mim}}^{\text{But}}$)$_3$], 10.23 [d, $^3J_{H\text{-}H}$ = 2, 1H of κ^3-XB($\underline{\text{mim}}^{\text{But}}$)$_3$].

3.6.8 Synthesis of $RuHCl(CO)(PMe_3)_3$

A suspension of $RuHCl(CO)(PPh_3)_3$ (147 mg, 0.15 mmol) in benzene (10 mL) in an ampoule was treated with PMe_3 (0.15 mL, 1.5 mmol). The reaction was heated for 3 days at 80 ˚C, thereby resulting in the quantitative conversion of $RuHCl(CO)(PPh_3)_3$ to $RuHCl(CO)(PMe_3)_3$. The mixture of $RuHCl(CO)(PMe_3)_3$ and PPh_3 (*ca*. 1:4 ratio) was isolated (120 mg) and used for further reactions.

3.6.9 Structural Characterization of {[κ^3-*H,S,S*-Tm^{But}]$Ru(CO)(PMe_3)_2$}I

A suspension of $RuHCl(CO)(PPh_3)_3$ (10 mg, 0.01 mmol) in C_6D_6 in an NMR tube equipped with a J. Young valve was treated with an excess of PMe_3. The sample was heated at 80 ˚C overnight, thereby resulting in the complete conversion to $RuHCl(CO)(PMe_3)_3$. The sample was lyophilized, redissolved in C_6H_6, transferred to a schlenk tube, and treated with an excess of MeI, resulting in the formation of a precipitate. The reaction was filtered, and the filtrate was lyophilized, redissolved in C_6D_6, and treated with K[Tm^{But}]. The solution was transferred to an NMR tube equipped with a J. Young valve and heated at 80 ˚C, producing {[κ^3-*H,S,S*-Tm^{But}]$Ru(CO)(PMe_3)_2$}I. Crystals of {[κ^3-*H,S,S*-Tm^{But}]$Ru(CO)(PMe_3)_2$}I suitable for X-ray diffraction were obtained from a solution in CD_3CN and benzene at room temperature.

3.7 Crystallographic Data

Table 2. Crystal, intensity collection and refinement data.

	[κ⁴-B(mim^{But})$_3$]Ru(CO)(PPh$_3$)	**[κ⁴-B(mim^{But})$_3$]Ru(CO)(PMe$_3$)**
lattice	Orthorhombic	Monoclinic
formula	$C_{40}H_{48}BN_6OPRuS_3$	$C_{31}H_{48}BN_6OPRuS_3$
formula weight	867.87	759.78
space group	*Pbca*	$P2_1/c$
a / Å	23.115(8)	11.7923(8)
b / Å	12.892(5)	20.0398(13))
c / Å	28.947(10)	16.1630(11)
α / °	90	90
β / °	90	101.225(1)
γ / °	90	90
V / Å^3	8626(5)(3)	3746.5(4)
Z	8	4
temperature (K)	125(2)	125(2)
radiation (λ, Å)	0.71073	0.71073
ρ (calcd.), g cm^{-3}	1.337	1.347
μ (Mo Kα), mm^{-1}	0.584	0.661
θ max, deg.	30.61	32.64
no. of data collected	13269	13027
no. of data	2172	9248
no. of parameters	213	409
R_1 [$I > 2\sigma(I)$]	0.1637	0.0375
wR_2 [$I > 2\sigma(I)$]	0.4085	0.0789
R_1 [all data]	0.3204	0.0720
wR_2 [all data]	0.5438	0.0940
GOF	1.007	1.062

Table 2 (cont). Crystal, intensity collection and refinement data.

	{[κ³-*H,S,S*-Tm^{But}]Ru(CO)(PMe$_3$)$_2$}I
lattice	Triclinic
formula	$C_{30}H_{55}BIN_7OP_2RuS_3$
formula weight	926.71
space group	*P-1*
a / Å	11.242(6)
b / Å	13.514(7)
c / Å	14.531(8)
α / °	92.344(9)
β / °	111.741(8)
γ / °	98.896(8)
V / Å^3	2014.3(18)
Z	2
temperature (K)	125(2)
radiation (λ, Å)	0.71073
ρ (calcd.), g cm^{-3}	1.528
μ (Mo Kα), mm^{-1}	1.424
θ max, deg.	30.71
no. of data collected	12323
no. of data	5946
no. of parameters	418
R_1 [$I > 2\sigma(I)$]	0.1084
wR_2 [$I > 2\sigma(I)$]	0.2096
R_1 [all data]	0.2540
wR_2 [all data]	0.2921
GOF	1.051

3.8 Computational Data

Table 3. Cartesian coordinates for geometry optimized structures.

$[\kappa^4$-B(mim^{But})$_3$]Ru(CO)(PPh$_3$)

-3611.83743783376 Hartrees

Atom	x	y	z
Ru	2.440493543	0.765901611	3.350748647
P	1.168758292	2.948895793	3.396411535
S	2.951153624	0.695448669	0.945689908
S	0.266247456	-0.537198623	3.01531734
S	2.390560314	0.330456633	5.808016525
O	5.203411052	1.905892379	3.722389005
N	4.169758903	-1.460144424	2.075103017
N	4.702308512	-1.243904897	-0.06392463
N	2.243636475	-2.326102793	3.474040424
N	0.271103746	-3.315941515	3.392657136
N	4.206145674	-1.347694901	4.695213471
N	4.483662108	-1.213573642	6.885418282
B	3.338173093	-1.18218331	3.382872467
C	4.118696995	1.499786949	3.579696704
C	3.980229259	-0.692844088	0.969065785
C	5.325167967	-2.3945182	0.416959046
H	5.954537032	-3.013043263	-0.197622654
C	4.98637229	-2.524859643	1.720879284
H	5.253692821	-3.308223763	2.409523726
C	4.816906344	-0.72212868	-1.466524357
C	3.425503444	-0.736372433	-2.127378511
H	3.028652311	-1.756424653	-2.162770742

H	3.505644159	-0.362960028	-3.153488358
H	2.717412429	-0.108482289	-1.584148813
C	5.418696538	0.695333437	-1.432038229
H	4.795430653	1.381940639	-0.856892547
H	5.507283141	1.077598069	-2.454162555
H	6.41766091	0.676076184	-0.984198275
C	5.755225163	-1.636488138	-2.27229109
H	5.371612086	-2.658937694	-2.349211227
H	6.765282887	-1.663984154	-1.851305336
H	5.832625325	-1.23777006	-3.287426675
C	0.919214821	-2.104387744	3.295792116
C	1.230909926	-4.295387363	3.649910211
H	0.979651279	-5.33256896	3.782236363
C	2.435178336	-3.678696343	3.69914067
H	3.407974645	-4.095136565	3.906021768
C	-1.202792116	-3.564187391	3.275338062
C	-1.680485775	-3.126374053	1.878004367
H	-1.491893627	-2.065379659	1.706344935
H	-2.756145926	-3.309456079	1.786324894
H	-1.166493282	-3.701853805	1.100704609
C	-1.479475945	-5.06843904	3.441754503
H	-1.178240059	-5.43704893	4.427506656
H	-0.98419923	-5.666913311	2.670364818
H	-2.556274009	-5.232119565	3.344915258
C	-1.936906751	-2.799213548	4.392778265
H	-1.599681024	-3.143114422	5.376250743
H	-3.013585186	-2.982691393	4.314496729
H	-1.759245267	-1.725033359	4.321190747

C	3.724582501	-0.773705586	5.827742307
C	5.468331429	-2.061287721	6.379840157
H	6.220681906	-2.511283178	7.002567502
C	5.287597349	-2.141210114	5.038243853
H	5.884192997	-2.659162248	4.306658901
C	4.327378289	-0.831949826	8.327968809
C	2.925185972	-1.251552903	8.807597894
H	2.795212539	-2.334845508	8.711761136
H	2.140518715	-0.755631087	8.233411072
H	2.805265018	-0.983162021	9.86222934
C	5.379596143	-1.575823707	9.167632515
H	5.273805995	-2.662991224	9.093489757
H	5.237203293	-1.301506456	10.21646553
H	6.40118137	-1.296462348	8.891245675
C	4.550480437	0.684429283	8.479872871
H	3.826316442	1.25391171	7.895057143
H	5.557671639	0.958176472	8.149083467
H	4.446156967	0.963568659	9.533501053
C	2.175911628	4.465663116	3.044194268
C	1.905826643	5.3369989	1.979494025
H	1.043274892	5.165075048	1.343877263
C	2.737746088	6.430531094	1.725534472
H	2.51198297	7.091990351	0.892819622
C	3.846658045	6.677321346	2.533819564
H	4.491501598	7.529244226	2.335753176
C	4.125259725	5.815241655	3.597224825
H	4.989952271	5.991413448	4.231680974
C	3.304241661	4.716868025	3.844979156

H	3.543372798	4.04795543	4.666322306
C	-0.283361361	3.145393884	2.257353462
C	-1.328063775	4.047294931	2.519594503
H	-1.302562089	4.657679151	3.417319548
C	-2.406534616	4.160021516	1.643671161
H	-3.208921006	4.859628116	1.864163657
C	-2.459286498	3.373783403	0.490637751
H	-3.303525569	3.458349267	-0.188979751
C	-1.429716929	2.473330667	0.221867777
H	-1.467007622	1.849149896	-0.667214135
C	-0.350800049	2.35550691	1.100597813
H	0.431654925	1.631723539	0.89625887
C	0.377758322	3.350020139	5.026532567
C	-0.360650036	2.326429213	5.644344988
H	-0.428074806	1.350681207	5.16960858
C	-0.997618234	2.54756233	6.86394118
H	-1.564074415	1.743410405	7.326775343
C	-0.897934777	3.788978129	7.495185033
H	-1.387354932	3.95787054	8.451047502
C	-0.161473319	4.80892359	6.894226562
H	-0.076692765	5.778641363	7.378637685
C	0.468709448	4.594136168	5.665892437
H	1.034555549	5.399690135	5.209072094

$[\kappa^4$-B(mim$^{But})_3]$Ru(CO)(PMe$_3$)

-3036.64536104257 Hartrees

Atom	x	y	z

Ru	8.757887589	15.90924638	1.108875762
S	10.98609889	16.68548864	0.155761969
S	9.449091937	13.55517035	0.924166771
S	8.256807939	18.20132299	1.935623087
P	7.669103569	16.13672459	-1.113740808
B	9.824945907	15.83610557	2.972503948
C	7.221681342	15.31396924	1.944260154
O	6.264146922	14.92676083	2.490040699
N	11.26887809	16.48057505	2.839036331
N	13.09937277	17.28556742	1.900173491
N	10.05189631	14.35256186	3.45565534
N	10.37915841	12.17809419	3.185031416
N	9.078649995	16.72018947	4.054140015
N	8.105815525	18.59293985	4.721623483
C	11.82536875	16.82206262	1.650924684
C	12.18495778	16.74334594	3.843599322
H	11.95869335	16.58022708	4.884990054
C	13.31184262	17.2364922	3.27847884
H	14.23138515	17.55654262	3.734973927
C	14.09119474	17.78560855	0.894500064
C	13.51461287	19.02765529	0.189858106
H	12.57933809	18.79412946	-0.321397302
H	14.23527567	19.39886728	-0.546238407
H	13.32359151	19.824052	0.916731907
C	14.40872188	16.65905071	-0.106444495
H	14.84660307	15.79972495	0.412284684
H	15.13201087	17.01973062	-0.845137488
H	13.51064388	16.32690223	-0.629656817

C	15.39079872	18.183937	1.614976112
H	15.23457447	18.99951215	2.328180465
H	16.10469084	18.53573973	0.865165354
H	15.84956992	17.33740068	2.135859113
C	9.959379949	13.33170978	2.561835205
C	10.57199941	13.84028144	4.635878905
H	10.78345837	14.45246834	5.495715088
C	10.76427623	12.50949846	4.483205664
H	11.12974017	11.7804054	5.184052113
C	10.42212832	10.79644358	2.602036948
C	9.000271772	10.38203035	2.180110418
H	8.331351297	10.37447884	3.046854955
H	9.025542358	9.373027335	1.75601443
H	8.591625915	11.06455928	1.433213968
C	11.39937028	10.77836852	1.411827336
H	11.09173801	11.47517487	0.630453487
H	11.43653091	9.770449495	0.985823456
H	12.40792931	11.04961011	1.740981846
C	10.92676603	9.80986711	3.66910411
H	11.94438912	10.0420218	3.999081321
H	10.94513957	8.809340801	3.228576708
H	10.26740083	9.773375477	4.542054072
C	8.476180799	17.85781765	3.620063894
C	9.071927987	16.73121947	5.438827703
H	9.440393098	15.91033664	6.029646105
C	8.472963818	17.87289881	5.857325669
H	8.259939288	18.21467894	6.854326572
C	7.400490739	19.91679101	4.730869462

C	7.205428292	20.3799444	6.184688817
H	6.568700442	19.69585514	6.754386783
H	6.70898347	21.3540418	6.170028052
H	8.157969197	20.50281807	6.710070215
C	6.019006016	19.75951976	4.06928807
H	6.110634452	19.41792165	3.037001333
H	5.499511107	20.72328916	4.07580257
H	5.410595279	19.03641769	4.621982241
C	8.270166116	20.95324495	3.995334949
H	9.236584057	21.06758351	4.49753391
H	7.763661056	21.92386559	4.000095389
H	8.450602501	20.66130717	2.959247055
C	5.990224188	16.9258087	-1.073731891
H	6.07298753	17.91879129	-0.622182746
H	5.329256055	16.32743643	-0.439688865
H	5.545901008	17.01746259	-2.071352672
C	8.502860441	17.15214199	-2.424489098
H	7.906577251	17.21397071	-3.341980511
H	9.476937931	16.71318051	-2.659330676
H	8.677726548	18.16061591	-2.038863398
C	7.300971174	14.5797301	-2.055842872
H	6.695798782	13.91750294	-1.429750432
H	8.23993752	14.06343091	-2.277082205
H	6.768854612	14.77315633	-2.994353405

3.9 References and Notes

(**1**) Verkade, J. G. *Coord. Chem. Rev.* **1994**, *137*, 233-295.

(**2**) Green, M. L. H. *J. Organomet. Chem.* **1995**, *500*, 127-148.

(**3**) For example, the M→B adduct $Ir(PPh_3)_2(CO)Cl(BF_3)$ has been spectroscopically characterized. See: Scott, R. N.; Shriver, D. F.; Vaska, L. *J. Am. Chem. Soc.* **1968**, *90*, 1079–1080.

(**4**) Hill, A. F.; Owen, G. R.; White, A. J. P.; Williams, D. J. *Angew. Chem., Int. Ed.* **1999**, *38*, 2759–2761.

(**5**) (a) Figueroa, J. S.; Melnick, J. G.; Parkin, G. *Inorg. Chem.* **2006**, *45*, 7056–7058.
(b) Crossley, I. R.; Foreman, M. R. St.-J.; Hill, A. F.; Owen, G. R.; White, A. J. P.; Williams, D. J.; Willis, A. C. *Organometallics* **2008**, *27*, 381-386.
(c) Foreman, M. R. St.-J.; Hill, A. F.; White, A. J. P.; Williams, D. J. *Organometallics* **2004**, *23*, 913–916.

(**6**) (a) Mihalcik, D. J.; White, J. L.; Tanski, J. M.; Zakharov, L. N.; Yap, G. P. A; Incarvito, C. D.; Rheingold, A. L.; Rabinovich, D. *Dalton Trans.* **2004**, 1626–1634.
(b) Crossley, I. R.; Hill, A. F.; Willis, A. C. *Organometallics* **2006**, *25*, 289-299.
(c) Crossley, I. R.; Hill, A. F.; Willis, A. C. *Organometallics* **2005**, *24*, 1062-1064.
(d) Landry, V. K.; Melnick, J. G.; Buccella, D.; Pang, K.; Ulichny, J. C.; Parkin, G. *Inorg. Chem.* **2006**, *45*, 2588-2597.
(e) Crossley, I. R.; Hill, A. F.; Willis, A. C. *Organometallics* **2010**, *29*, 326-336.

(**7**) (a) Pang, K.; Tanski, J. M.; Parkin, G. *Chem. Commun.* **2008**, 1008–1010.
(b) Pang, K.; Quan, S. M.; Parkin, G. *Chem. Commun.* **2006**, 5015-5017.
(c) Crossley, I. R.; Hill, A. F. *Organometallics* **2004**, *23*, 5656-5658.

(**8**) (a) Sircoglou, M.; Bontemps, S.; Bouhadir, G.; Saffon, N.; Miqueu, K.; Gu, W.; Mercy, M.; Chen, C.-H.; Foxman, B. M.; Maron, L.; Ozerov, O. V.; Bourissou, D. *J. Am. Chem. Soc.* **2008**, *130*, 16729-16738.
(b) Nuss, G.; Saischek, G.; Harum, B. N.; Volpe, M.; Belaj, F.; Mösch-Zanetti, N. C. *Inorg. Chem.* **2011**, *50*, 12632-12640.

(**9**) Garner, M.; Reglinski, J.; Cassidy, I.; Spicer, M. D.; Kennedy, A. R. *Chem. Commun.* **1996**, 1975–1976.

(**10**) Trofimenko, S. *J. Am. Chem. Soc.* **1966**, *88*, 1842-1844.

(**11**) Foreman, M. R. St.-J.; Hill, A. F.; Owen, G. R.; White, A. J. P.; Williams, D. J. *Organometallics* **2003**, *22*, 4446-4450.

(**12**) The average Ru-B bond distance reported in the Cambridge Structural Database is 2.238 Å.

(**13**) Zhu, H.; Ma, Q.; Jia, A.-Q.; Chen, Q.; Leung, W.-H.; Zhang, Q.-F. *Inorg. Chim. Acta* **2013**, *405*, 427-436.

(**14**) Tsoureas, N.; Kuo, Y.-Y.; Haddow, M. F.; Owen, G. R. *Chem. Commun.* **2011**, *47*, 484-486.

(**15**) Fong, H.; Moret, M.-E.; Lee, Y.; Peters, J. C. *Organometallics* **2013**, *32*, 3053-3062.

(**16**) Owen, G. *Chem. Soc. Rev.* **2012**, *41*, 3535-3546.

(**17**) Moret, M.-E.; Peters, J. C. *Angew. Chem., Int. Ed.* **2011**, *50* 2063-2067.

(**18**) (a) McNally, J. P.; Leong, V. S.; Cooper, N. J. in *Experimental Organometallic Chemistry*; Wayda, A. L.; Darensbourg, M. Y., Eds.; American Chemical Society: Washington, DC, 1987; Chapter 2, pp 6-23.
(b) Burger, B.J.; Bercaw, J. E. in *Experimental Organometallic Chemistry*; Wayda, A. L.; Darensbourg, M. Y., Eds.; American Chemical Society: Washington, DC, 1987; Chapter 4, pp 79-98.
(c) Shriver, D. F.; Drezdzon, M. A.; *The Manipulation of Air-Sensitive Compounds*, 2nd Edition; Wiley-Interscience: New York, 1986.

(**19**) (a) Gottlieb, H. E.; Kotlyar, V.; Nudelman, A. *J. Org. Chem.* **1997**, *62*, 7512-7515.
(b) Fulmer, G. R.; Miller, A. J. M.; Sherden, N. H.; Gottlieb, H. E.; Nudelman, A.; Stoltz, B. M.; Bercaw, J. E.; Goldberg, K. I. *Organometallics* **2010**, *29*, 2176-2179.

(**20**) "Nuclear Magnetic Resonance Spectroscopy" Nelson, J. H. Prentice Hall, New Jersey (2003), p 79.

(**21**) Ahmad, N.; Levison, J. J.; Robinson, S. D.; Uttley, M. F. in *Inorganic Syntheses*; Parshall, G. W., Eds.; McGraw-Hill: New York, 1974; Chapter 3, pp 45-72.

(**22**) (a) Sheldrick, G. M. SHELXTL, An Integrated System for Solving, Refining and Displaying Crystal Structures from Diffraction Data; University of Göttingen, Göttingen, Federal Republic of Germany, 1981.
(b) Sheldrick, G. M. *Acta Cryst.* **2008**, *A64*, 112-122.

(**23**) Jaguar 7.7, Schrödinger, LCC, New York, NY 2010

(**24**) (a) Becke, A. D. *J. Chem. Phys.* **1993**, *98*, 5648-5652.
(b) Becke, A. D. *Phys. Rev. A* **1988**, *38*, 3098-3100.
(c) Lee, C. T.; Yang, W. T.; Parr, R. G. *Phys. Rev. B* **1988**, *37*, 785-789.
(d) Vosko, S. H.; Wilk, L.; Nusair, M. *Can. J. Phys.* **1980**, *58*, 1200-1211.
(e) Slater, J. C. *Quantum Theory of Molecules and Solids, Vol. 4: The Self-Consistent Field for Molecules and Solids*; McGraw-Hill: New York, 1974.

(**25**) (a) Hay, P. J.; Wadt, W. R. *J. Chem. Phys.* **1985**, *82*, 270-283.
(b) Wadt, W. R.; Hay, P. J. *J. Chem. Phys.* **1985**, *82*, 284-298.
(c) Hay, P. J.; Wadt, W. R. *J. Chem. Phys.* **1985**, *82*, 299-310.

(**26**) (a) Hall, M. B.; Fenske, R. F. *Inorg. Chem.* **1972**, *11*, 768.
(b) Bursten, B. E.; Jensen, J. R.; Fenske, R. F. *J. Chem. Phys.* **1978**, *68*, 3320.
(c) Manson, J.; Webster, C. E.; Pérez, L. M.; Hall, M. B.
http://www.chem.tamu.edu/jimp2/index.html.

(**27**) Version 2.0, June 1993; Lichtenberger, D. L. Department of Chemistry, University of Arizona, Tuscon, AZ 85721.

(**28**) NBO 5.0. Glendening, E. D.; Badenhoop, J. K.; Reed, A. E.; Carpenter, J. E.; Bohmann, J. A.; Morales, C. M.; Weinhold, F. Theoretical Chemistry Institute, University of Wisconsin, Madison, 2001.

CHAPTER 4

The Reactivity of Transition Metal Phosphine Complexes with Industrially Relevant Substrates: Some Insights into the Water Gas Shift Reaction, CO_2 Hydrogenation, Hydrodeoxygenation, and Hydrosilane Reactivity

Table of Contents

4.1 Introduction

Transition metal phosphine complexes are as diverse as they are numerous. Not only is there a multitude of structurally unique transition metal phosphine complexes, but these complexes have also found great utility in a number of catalytic processes. For example, (*i*) rhodium phosphine complexes are effective catalysts for alkene hydrogenation,[1] (*ii*) cobalt and rhodium phosphine complexes have been used industrially in hydroformylation processes,[2] and (*iii*) alkyne carbonylation may be facilitated by palladium phosphine complexes.[3]

One reason that tertiary phosphine ligands are so widely employed in transition metal complexes is that their steric and electronic properties may be readily tuned. The substituents on the phosphorus influence whether the ligand will be a strong σ-donor or a strong π-acceptor, sterically unencumbered or hindered, soluble in polar or non-polar solvents, and chiral or achiral; all of these properties ultimately serve to determine how a transition metal complex will behave.[4,5,6,7] For example, strongly electron-donating trialkylphosphine ligands such as PMe_3 have been used to prepare highly reactive, electron-rich metal complexes that are capable of effecting C-C, C-H, O-H, C-S, C-Si, and Si-H bond cleavage reactions.[8] PPh_3, the parent triarylphosphine ligand, is a component of of seminal metal complexes such as Wilkinson's catalyst, $RhCl(PPh_3)_3$, and Vaska's compound, $IrCl(CO)(PPh_3)_2$.[1,9]

Given the significance of these metal complexes and the transformations for which they are responsible, it is of interest to explore the reactivity of transition metal complexes featuring trimethylphosphine and triphenylphosphine ligands. Thus, the reactivity of $Ru(PMe_3)_4H_2$, $Mo(PMe_3)_6$, $W(PMe_3)_4(\eta^2\text{-}CH_2PMe_2)H$, $Mo(PMe_3)_4(\eta^2\text{-}CH_2PMe_2)H$, and $IrCl(CO)(PPh_3)_2$ towards a number of substrates was explored and is presented herein.

4.2 Reactivity of $Ru(PMe_3)_4H_2$

4.2.1 Background

Ruthenium is a valuable metal in transition metal catalysis. For example, ruthenium catalysts are critical to reactions such as olefin metathesis, the dehydrogenation of diols, and the hydrogenation of alkenes, aldehydes, and CO_2.[10,11,12] We were therefore interested in exploring the catalytic potential of a ruthenium phosphine complex, $Ru(PMe_3)_4H_2$. This species has been shown to be an active catalyst for the dehydrogenation of alcohols and the hydrogenation of CO_2.[11,13] $Ru(PMe_3)_4H_2$ was found to react with a number of other substrates here as well, including CS_2 and H_2S, and this complex exhibits catalytic potential in the water gas shift reaction.

4.2.2 Reactivity of $Ru(PMe_3)_4H_2$ in the Water Gas Shift Reaction

The water gas shift reaction (WGSR) is an industrially significant process in which carbon monoxide reacts with water to form hydrogen and carbon dioxide:

$CO + H_2O \leftrightarrows H_2 + CO_2$

This transformation is important in a number of different processes, including (*i*) the large-scale production of hydrogen for ammonia synthesis, (*ii*) the enrichment of synthesis gas ($CO + H_2$) in hydrogen, and (*iii*) the treatment of combustion exhaust gases for reducing noxious nitrogen and sulfur oxide gases.[14,15] The heterogeneous catalysis of this process in industry involves severe conditions (*i.e.* high pressure and temperatures greater than 300 °C).[16] The high temperature required to make this process proceed at a viable rate leads to an unfavorable shift in the equilibrium position for this reaction at high temperature.[16,17,18] As such, there is an incentive to perform the WGSR at reduced temperatures. Homogeneous catalysts, which are frequently active at significantly lower temperatures than heterogeneous ones, have therefore been investigated for this process and were first reported in 1977.[14,19,20] Many of these early reports utilize metal carbonyl complexes as homogeneous catalysts, and ruthenium carbonyl complexes in particular have been studied extensively as catalysts for this

reaction.[21,22] The vast majority of homogeneous WGS reactions proceed in aqueous alkaline solutions. However, another early report found that platinum phosphine complexes were capable of catalyzing the WGSR in aprotic solvents with no added base.[23] We therefore considered that $Ru(PMe_3)_4H_2$ might also be capable of effecting the WGSR.

Encouragingly, treatment of $Ru(PMe_3)_4H_2$ with $H_2O(l)$ and CO does produce H_2 and CO_2 when the reaction is performed in C_6D_6, as shown by ^1H, ^{13}C, and $^{13}C\{^1H\}$ NMR spectroscopy (Scheme 1). The evolution of H_2 and CO_2 is observed after mild heating at 60 ˚C, which is substantially lower than the temperatures reported in earlier examples of the homogeneous WGSR. It is also significant that this reaction proceeds in a neutral, non-polar solvent such as benzene. While attack of a hydroxide ion is frequently invoked as the first mechanistic step in systems that operate under alkaline conditions (Figure 1, **A**), it is likely that a modified mechanism involving neutral intermediates is operational when $Ru(PMe_3)_4H_2$ is used as a catalyst (Figure 1, **B**).

$$CO + H_2O \xrightarrow[60\ ^\circ C,\ C_6D_6]{Ru(PMe_3)_4H_2} CO_2 + H_2$$

Scheme 1. Reactivity of $Ru(PMe_3)_4H_2$ towards CO and H_2O

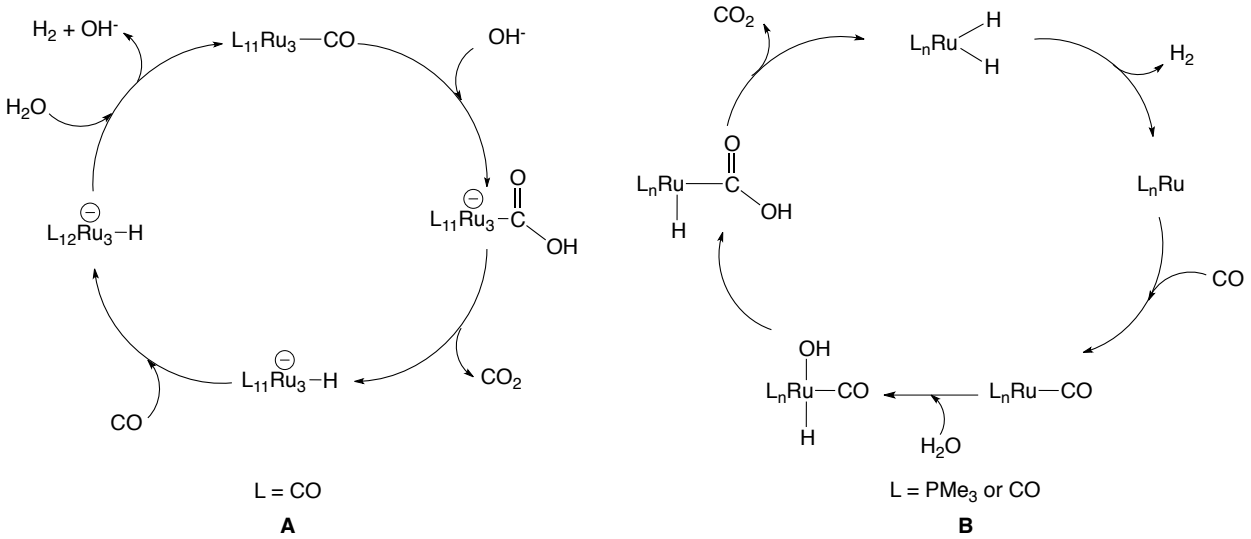

Figure 1. Catalytic cycles (A) proposed by Ford et al. for the WGSR catalyzed by ruthenium clusters in alkaline solution[21c,18] and (B) proposed for $Ru(PMe_3)_4H_2$ (analogous to the mechanism proposed by Yoshida et al.[23])

When the reaction solution is further heated at 60 ˚C, the production of a formate species is observed by ^1H (Figure 2) and ^{13}C NMR spectroscopy. When the reaction is performed with ^{13}C-enriched CO, the peak attributable to the formate moiety in the ^1H NMR spectrum (δ 8.70) exhibits coupling to both carbon ($^1J_{C\text{-}H}$ = 192 Hz) and phosphorus ($^4J_{P\text{-}H}$ = 2 Hz). A number of hydride signals are also evident, and these may correspond to species in which CO has replaced phosphine ligands, namely $Ru(PMe_3)_x(CO)_{4-x}H_2$. The ^1H NMR spectrum suggests that a formate species of the type *trans*-$Ru(PMe_3)_4[OC(O)H]X$ may be formed, in which X could be a hydroxo ligand or another formate moiety (Scheme 2). The presence of a formate complex may suggest the possibility of coupling the WGSR directly to the hydrogenation of CO_2.[24]

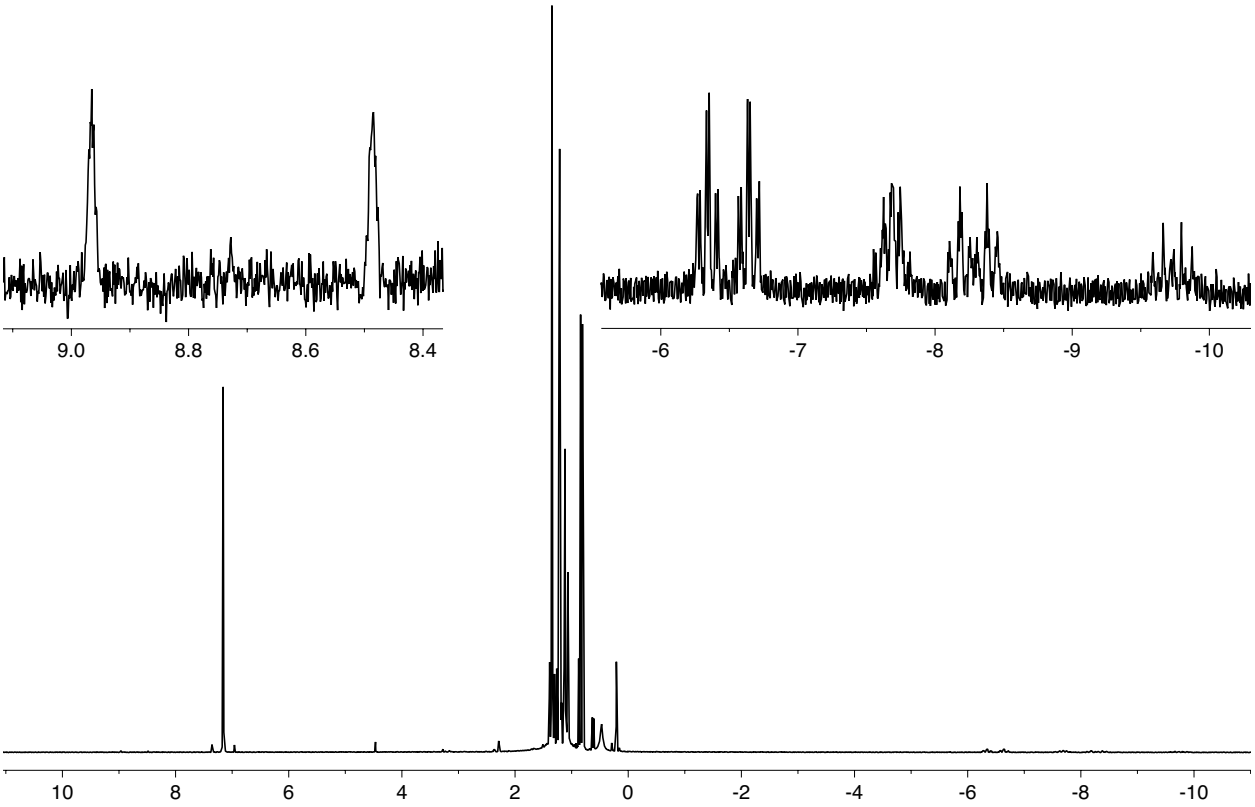

Figure 2. ^{1}H NMR Spectrum of a ^{13}C-Enriched Formate Species Generated *via* the WGSR

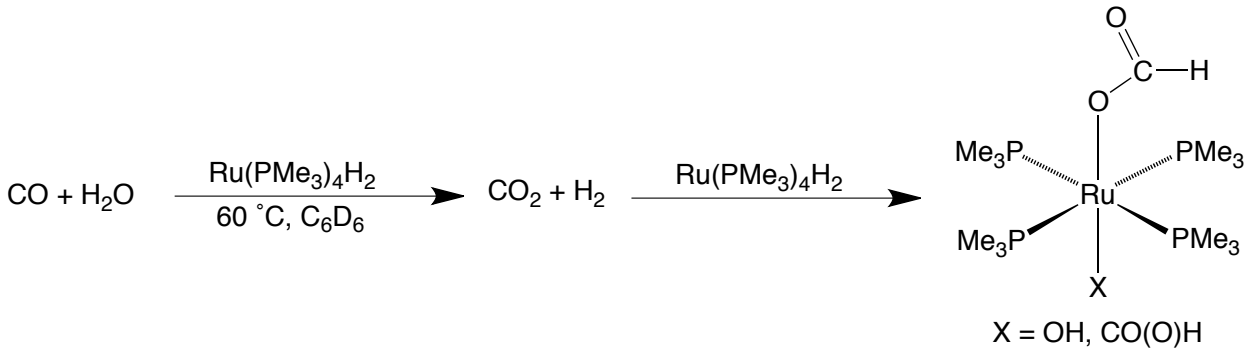

Scheme 2. Overall Reaction of $Ru(PMe_3)_4$ with CO and H_2O

Although the active catalyst species for the WGSR in this system is not known, prolonged heating of $Ru(PMe_3)_4H_2$ in the presence of CO and H_2 forms $Ru(PMe_3)_2(CO)_3$ as a final product, whose structure has been previously reported.[25] Isolation of this complex demonstrates the ability of CO to displace phosphine ligands, which is

significant since a plausible catalytic cycle presumably involves the attack of a coordinated carbonyl ligand by water in an inter- or intramolecular fashion.

Treatment of $Ru(PMe_3)_4H_2$ with CO alone results in the evolution of H_2 and PMe_3, which is consistent with the isolation of $Ru(PMe_3)_2(CO)_3$ described above. Some ruthenium hydride species are also generated, which likely correspond to complexes of the type $Ru(PMe_3)_x(CO)_{4-x}H_2$ (*vide supra*).

4.2.3 Reactivity of $Ru(PMe_3)_4H_2$ towards CO_2

The reactivity of $Ru(PMe_3)_4H_2$ with CO_2 was also examined. Not only is the reduction of CO_2 to form more valuable chemicals of longstanding interest, but it was also necessary to compare the reactivity of CO_2 alone with the *in situ*-generated CO_2 and H_2 described above. The reaction of $Ru(PMe_3)_4H_2$ with CO_2 (both natural abundance and ^{13}C-enriched) was performed in C_6D_6 and monitored by ^1H and $^{13}C\{^1H\}$ NMR spectroscopy, thereby demonstrating the generation of a formate species similar to that observed from the WGSR.[26] The peak attributable to the formate moiety in the ^1H NMR spectrum (δ 8.90) couples to the formate carbon ($^1J_{C-H}$ = 189 Hz) when ^{13}C-enriched CO_2 is used. However, unlike the formate species described above the signal corresponding to the formate hydrogen appears as a doublet instead of a quintet. The appearance of this signal is accompanied by a hydride resonance (δ -8.14) that exhibits coupling to four phosphine ligands ($^2J_{P-H}$ = 100, 28). A small degree of coupling to the formate carbon is also present in the ^{13}C-enriched experiment (Figure 3). Thus, the formate species that is generated from the direct reaction of $Ru(PMe_3)_4H_2$ with CO_2 is tentatively assigned as the *cis*-formate hydride complex, *cis*-$Ru(PMe_3)_4[OC(O)H]H$ (Scheme 3).

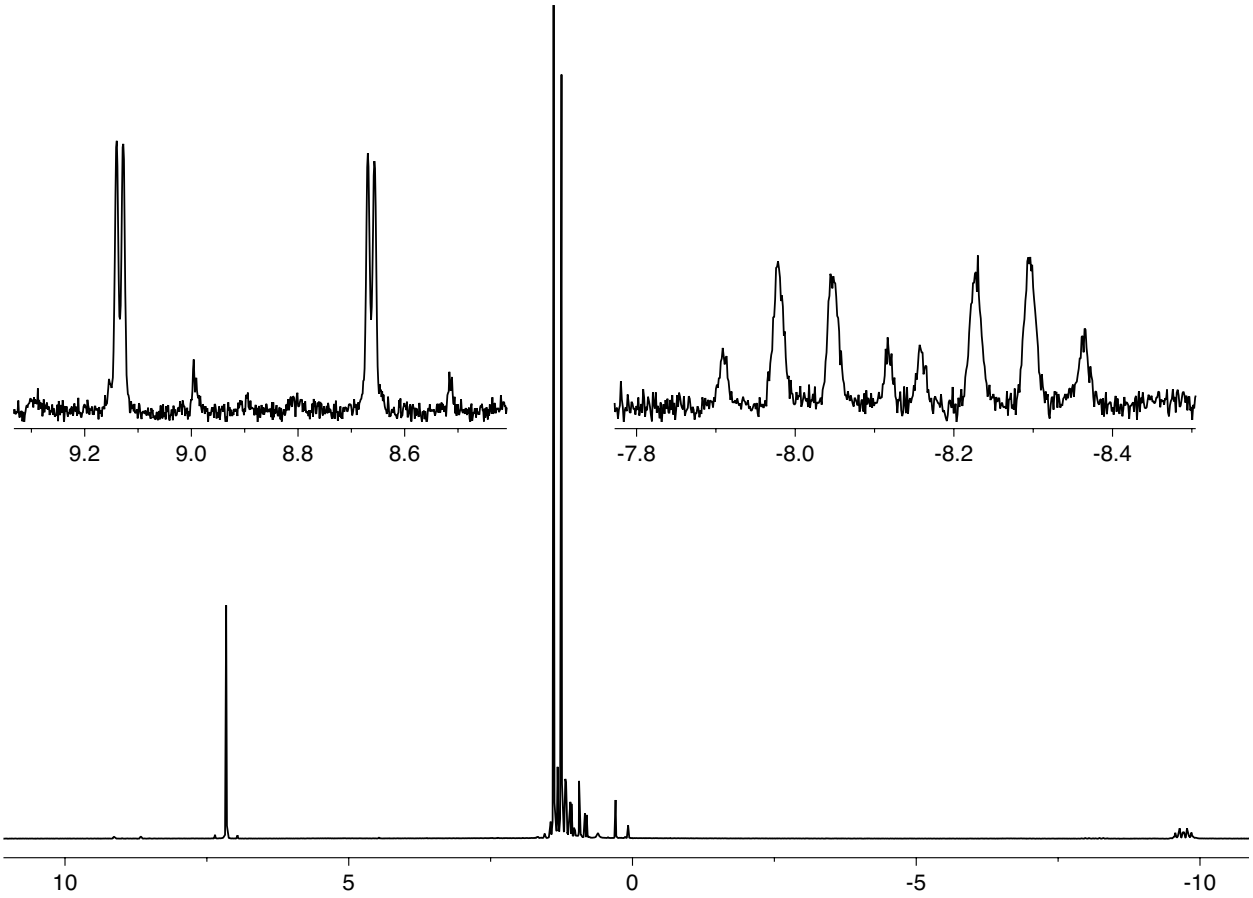

Figure 3. ^{1}H NMR Spectrum of a ^{13}C-enriched Formate Species from the Reaction with CO_2

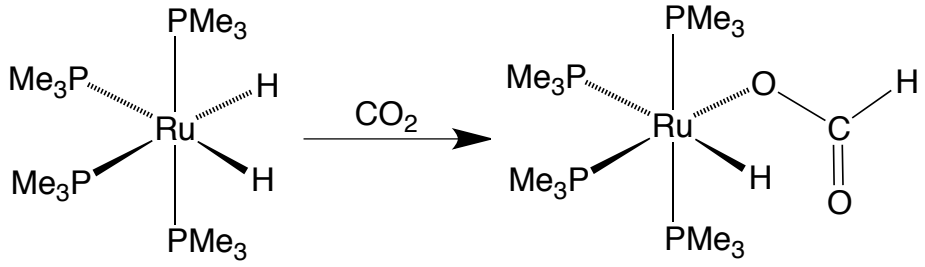

Scheme 3 – Reaction of $Ru(PMe_3)_4H_2$ with CO_2

4.2.4 Reactivity of $Ru(PMe_3)_4H_2$ towards CS_2

The reactivity of $Ru(PMe_3)_4H_2$ with carbon disulfide was also examined. This reaction is facile at room temperature and results in immediate color change of the reaction solution from orange to yellow. The thiocarbonate complex, $Ru(PMe_3)_4(\kappa^2\text{-}S_2\text{-}CS_3)$

(Figure 4), was the only isolated product. While the generation of metal-thiocarbonate species from CS_2 has been reported, these often involve either (*i*) the *in situ* preparation of the CS_3^{2-} anion[27] or (*ii*) addition of CS_2 to a metal sulfide compound.[28,29] The CS_3^{2-} anion is generally prepared by the reaction of CS_2 with a nucleophile in the presence of a base.[27a,30] The transition metal-promoted dimerization of CS_2 has been reported,[31] however, so it is possible that the generation of the thiocarbonate ligand in this system is accompanied by an equivalent of carbon monosulfide, CS, *via* dimerization of CS_2 followed by disproportionation (Scheme 4).[32,33]

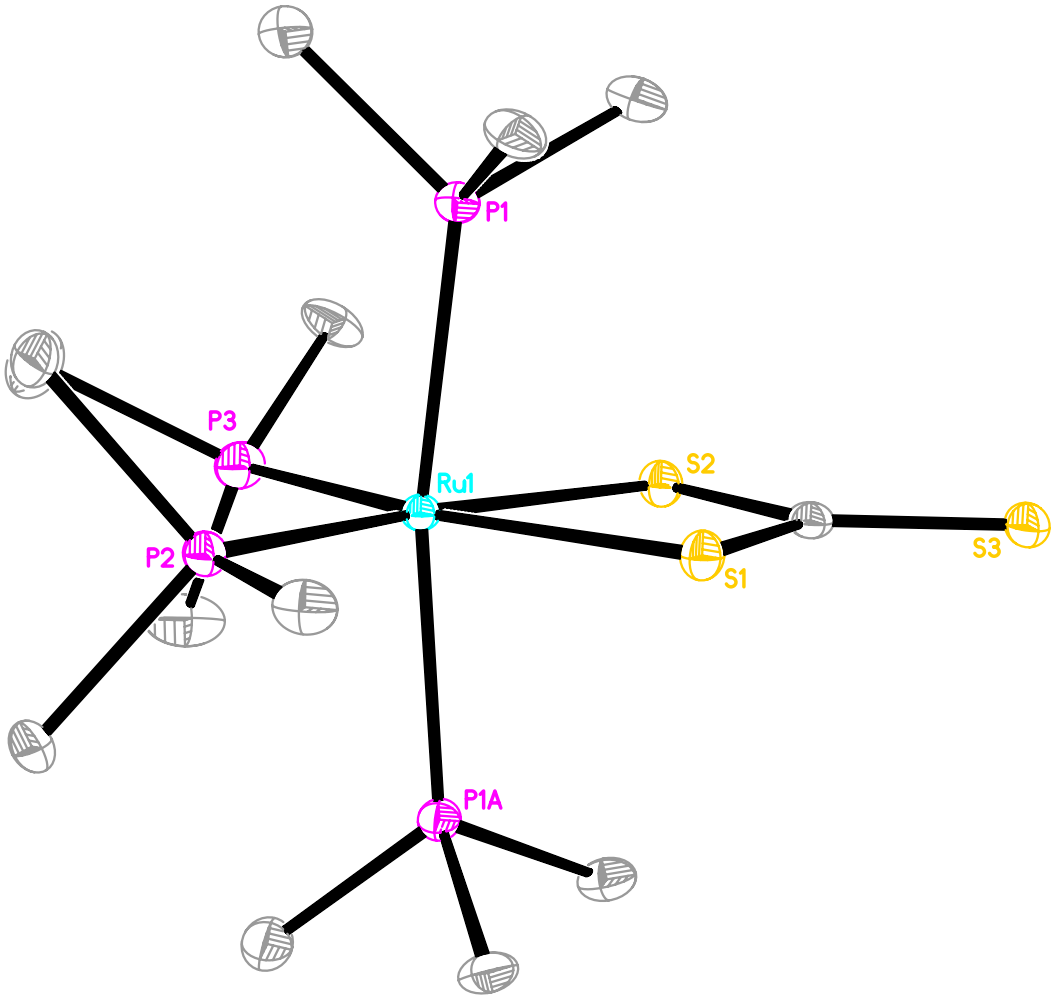

Figure 4. Molecular Structure of $Ru(PMe_3)_4(\kappa^2\text{-}S_2\text{-}CS_3)$

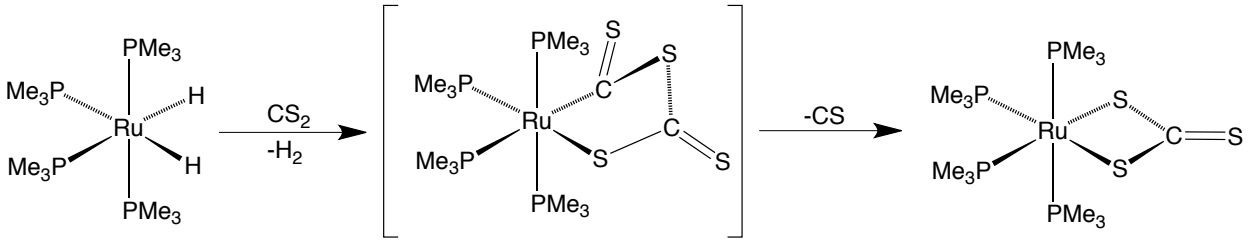

Scheme 4. Reaction of $Ru(PMe_3)_4$ with CS_2

4.2.5 Reactivity of $Ru(PMe_3)_4H_2$ towards H_2O

The reactivity of $Ru(PMe_3)_4H_2$ with water was explored, both as a control for the WGSR and with the goal of preparing a ruthenium hydroxo compound. The isolation of monomeric late transition metal hydroxo compounds is of interest since these species are frequently invoked as intermediates in metal-catalyzed transformations.[34]

The addition of water to $Ru(PMe_3)_4H_2$ in C_6D_6 produces little change in the ^1H NMR spectrum, although a small amount of H_2 is generated, and the formation of a new hydride signal at δ -8.50 is visible. This signal exhibits coupling to four phosphines and may correspond to $Ru(PMe_3)_4H(OH)$.[35] When the reaction of $Ru(PMe_3)_4H_2$ with water was performed in neat H_2O, a mixture of products was formed. The only product that was isolated from this mixture was the bridging hydroxo compound, $[Ru_2(PMe_3)_6(\mu\text{-}OH)_3]Cl$, as determined by X-ray diffraction. The chloride counter-ion presumably comes from an impurity of the precursor to $Ru(PMe_3)_4H_2$, namely $RuCl_3 \bullet xH_2O$. A similar structure with a BF_4^- counterion has also been reported.[25]

4.2.6 Reactivity of $Ru(PMe_3)_4H_2$ towards H_2S

H_2S was also examined with respect to the reactivity of $Ru(PMe_3)_4H_2$. In view of the fact that metal hydrosulfido complexes are invoked as intermediates in, for example, the hydrodesulfurization process[36] and reactions catalyzed by metalloenzymes,[37] the study of metal hydrosulfido complexes is of interest.[38] The reaction of $Ru(PMe_3)_4H_2$ with H_2S proceeds at room temperature in benzene, and crystals of *cis*-$Ru(PMe_3)_4(SH)_2$ (Figure 5) form directly from the reaction solution. Over time, the *cis*-isomer converts to *trans*-

$Ru(PMe_3)_4(SH)_2$ (Scheme 5). The ^1H NMR spectra of these isomers reflect their unique geometries. For example, *cis*-$Ru(PMe_3)_4(SH)_2$ is characterized by two phosphine peaks, a triplet and a doublet, in a 1:1 ratio, whereas the phosphine resonance of *trans*-$Ru(PMe_3)_4(SH)_2$ is one broad singlet. The -SH hydrogen signals appear at δ -2.77 and -4.14 for the *cis*- and *trans*- isomers, respectively (Figure 6).

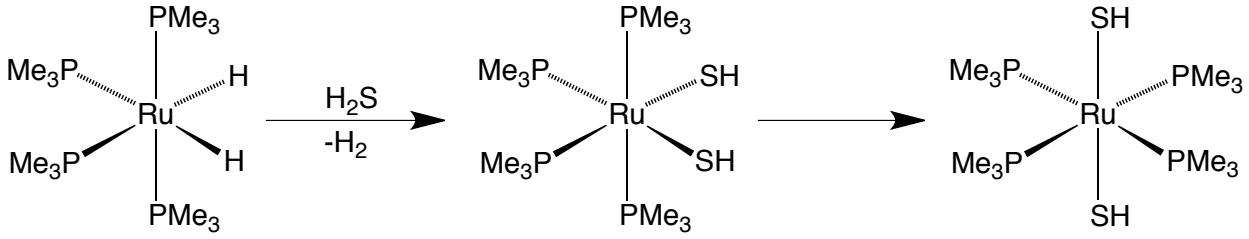

Scheme 5. Reaction of $Ru(PMe_3)_4H_2$ + H_2S

The S-H hydrogens in the crystal structure of *cis*-$Ru(PMe_3)_4(SH)_2$ could be located in the electron density difference map but not freely refined. Support for this configuration comes from the fact that the crystal structure of *cis*-$Ru(PMe_3)_4(SH)_2$ is reproduced well by a density functional theory (DFT) geometry optimization calculation. A geometry optimization of *trans*-$Ru(PMe_3)_4(SH)_2$ was also performed, and a comparison of the energies of the geometry optimized structures indicates that *trans*-$Ru(PMe_3)_4(SH)_2$ is *ca.* 2 kcal mol^{-1} lower in energy than *cis*-$Ru(PMe_3)_4(SH)_2$. Thus, these calculations support the description of *cis*-$Ru(PMe_3)_4(SH)_2$ as the kinetic product and *trans*-$Ru(PMe_3)_4(SH)_2$ as the thermodynamic one. The optimized geometries are shown in Figure 7.

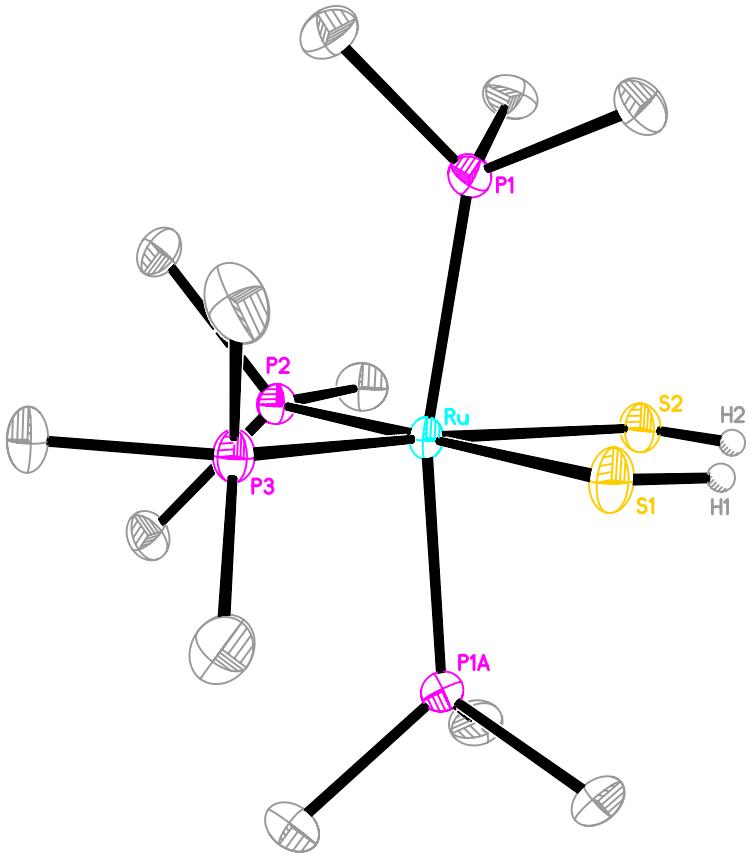

Figure 5. Molecular Structure of $Ru(PMe_3)_4(SH)_2$

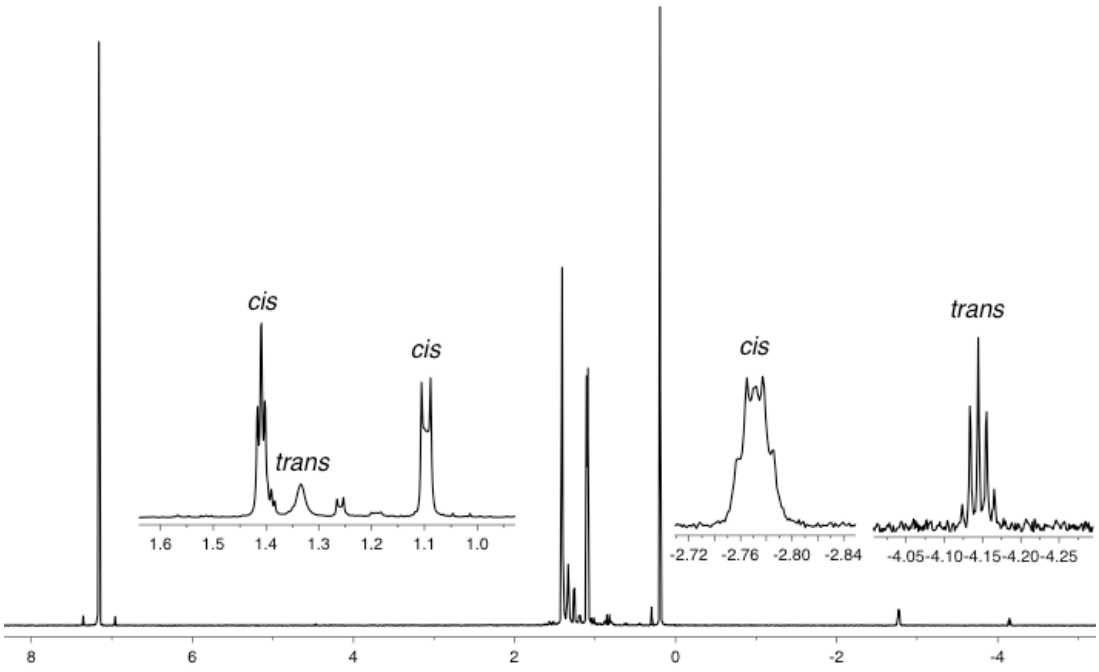

Figure 6. ^1H NMR Spectrum of *cis*- and *trans*-$Ru(PMe_3)_4(SH)_2$

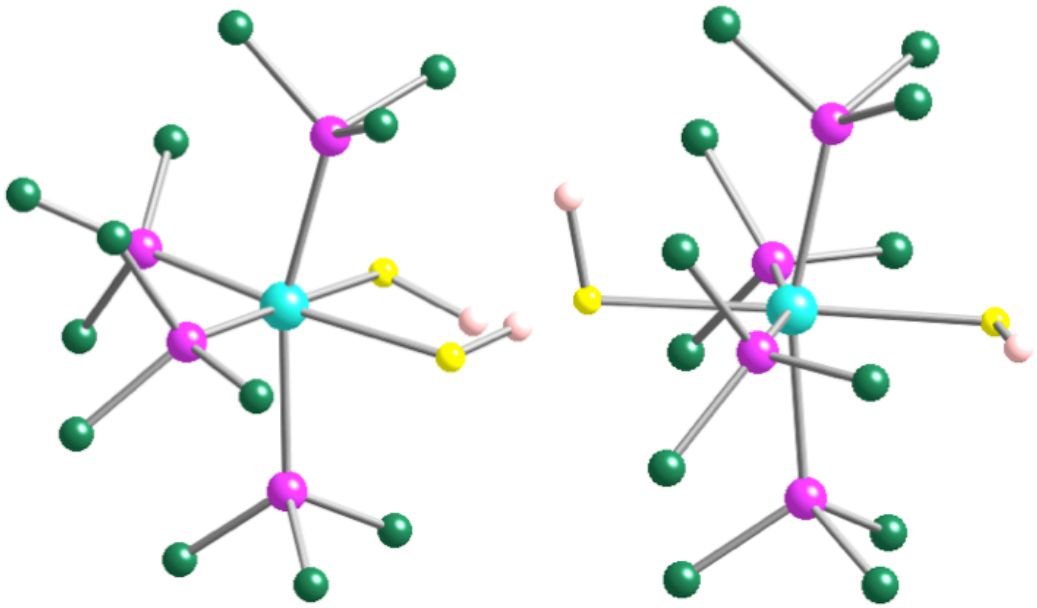

Figure 7. Geometry Optimized Structures of *cis*- and *trans*-Ru(PMe$_3$)$_4$(SH)$_2$

4.3 The Reactivity of Mo(PMe$_3$)$_6$ and W(PMe$_3$)$_4$(η^2-CH$_2$PMe$_2$)H

4.3.1 Background

The reactivity of Mo(PMe$_3$)$_6$ (Chapter 1) and W(PMe$_3$)$_4$(η^2-CH$_2$PMe$_2$)H (Chapter 2) with hydrosilanes has been explored in depth. We were also interested in the reactivity of these complexes towards other substrates, particularly towards oxygen-containing heterocycles relevant to the hydrodeoxygenation industry. The reactivity of Mo(PMe$_3$)$_6$, W(PMe$_3$)$_4$(η^2-CH$_2$PMe$_2$)H, and related molybdenum and tungsten trimethylphosphine complexes in hydrodenitrogenation and hydrodesulfurization processes has been explored in depth by the Parkin group.[39,40] Thus, as an extension of this research, we have examined these complexes as models of hydrodeoxygenation catalysts.

Hydrodeoxygenation currently represents a less critical process than hydrodenitrogenation and hydrodesulfurization, primarily because the combustion of nitrogen- and sulfur-containing compounds produces pollutants, whereas combustion

of oxygen-containing compounds merely produces water as a byproduct.[41] Nonetheless, this process may increase in importance as biomass-derived feeds become more prevalent. For example, the concentration of oxygen in such feeds may be up to 50% by weight, which can result in low quality fuels and catalyst deactivation in refineries.[42] Therefore, we have examined the reactivity of molybdenum and tungsten trimethylphosphine complexes towards hydrodeoxygenation reactions. A significant amount of work towards this end has already been performed by a former Parkin group graduate student, Aaron Sattler;[43,44] some additional contributions are described here.

4.3.2 Reactivity towards Dihydrofurans

Some aspects of the reactivity of $Mo(PMe_3)_6$ and $W(PMe_3)_4(\eta^2\text{-}CH_2PMe_2)H$ with dihydrofurans have been previously determined.[43] For example, it was noted that $W(PMe_3)_4(\eta^2\text{-}CH_2PMe_2)H$ reacts with 2,3-dihydrofuran in the presence of H_2 to form a dihydrofuryl complex, $W(PMe_3)_4(\kappa^1\text{-}C_\alpha\text{-}C_4H_5O)H_3$ (Scheme 6);[43] a yield has now been established for this product. The reactions of $W(PMe_3)_4(\eta^2\text{-}CH_2PMe_2)H$ with 2,3-dihydrofuran or 2,5-dihydrofuran ultimately result in the same final product, $W(PMe_3)_5CO$ (Scheme 7).[43] The reaction of $W(PMe_3)_4(\eta^2\text{-}CH_2PMe_2)H$ with 2,5-dihydrofuran produces 2,3-dihydrofuran, so it is likely that isomerization is responsible for the equivalent reactivities of these substrates. A procedure for synthesizing $W(PMe_3)_5(CO)$, which has been prepared previously in a different manner,[45] from the reaction with 2,5-dihydrofuran has now been ascertained.

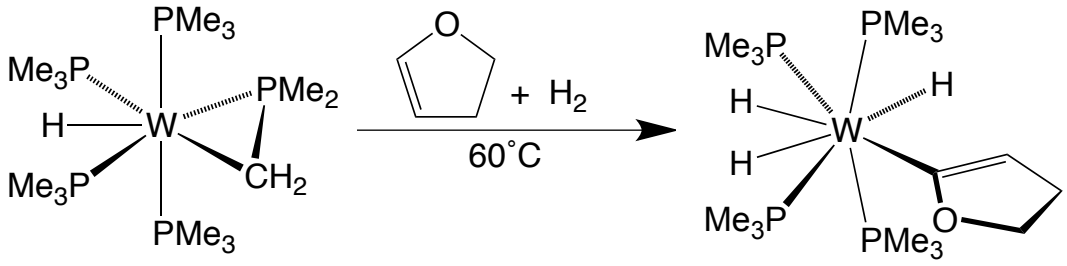

Scheme 6. Reactivity of $W(PMe_3)_4(\eta^2\text{–}CH_2PMe_2)H$ towards 2,3-dihydrofuran and H_2.

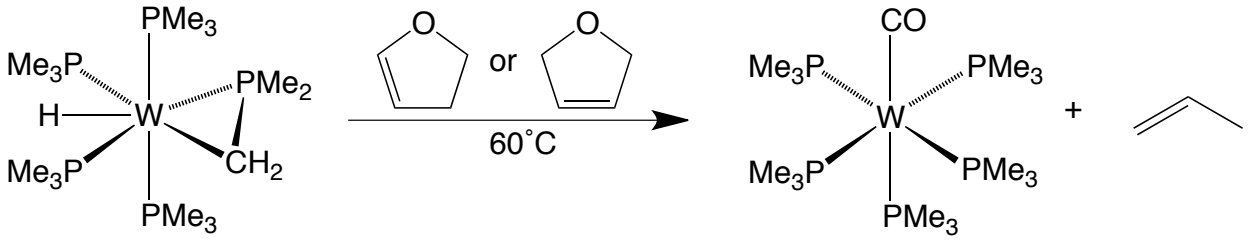

Scheme 7. Reactivity of $W(PMe_3)_4(\eta^2–CH_2PMe_2)H$ towards dihydrofurans.

The reaction of $Mo(PMe_3)_6$ with 2,5-dihydrofuran, on the other hand, produces not only $Mo(PMe_3)_5CO$, but also $Mo(PMe_3)_3(\eta^5–C_4H_5O)H$ (Scheme 8).[43] This complex has been characterized by ^1H and $^{31}P\{^1H\}$ NMR spectroscopy,[43] and now its solid state structure has been obtained (Figure 8). This product may also be generated from the reaction with 2,3-dihydrofuran. Another interesting observation about this system is that treatment of $Mo(PMe_3)_6$ with 2,3-dihydrofuran and H_2 produces a mixture of $Mo(PMe_3)_4H_4$ and tetrahydrofuran (Scheme 9). Since hydrogenation of unsaturated bonds is an important component of the hydrotreating process,[41] the presence of THF in this reaction is noteworthy.

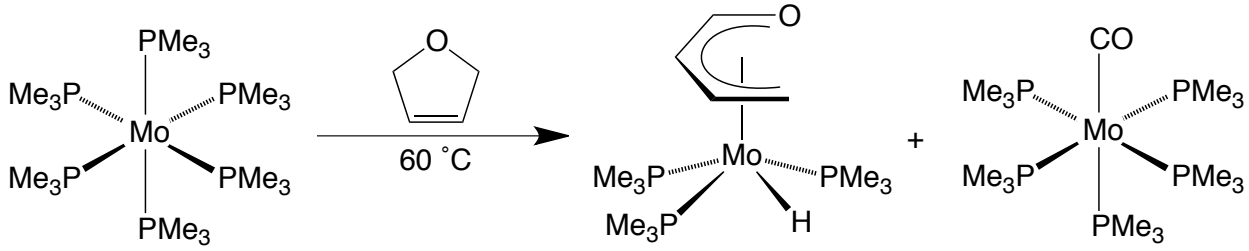

Scheme 8. Reactivity of $Mo(PMe_3)_6$ towards 2,5-Dihydrofuran

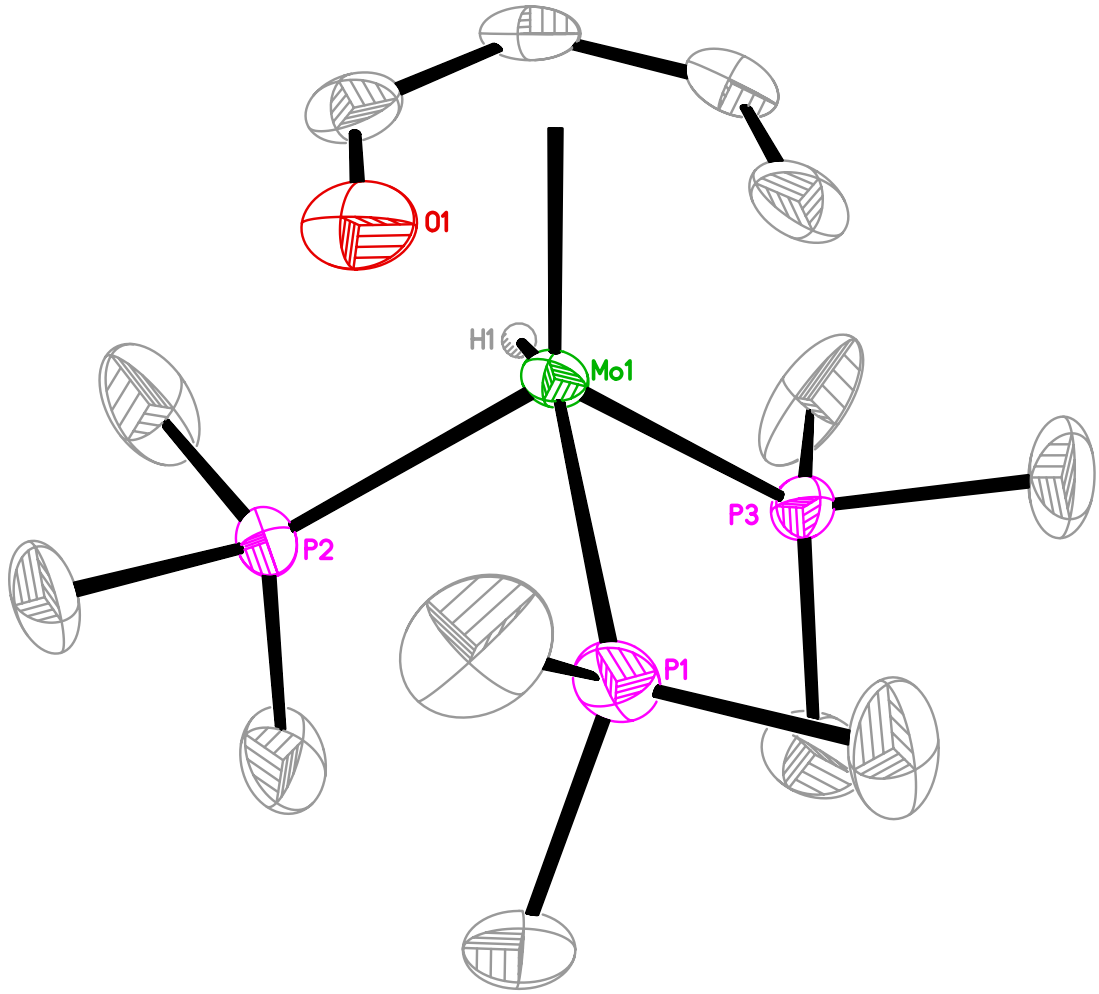

Figure 8. Molecular Structure of $Mo(PMe_3)_3(\eta^5\text{–}C_4H_5O)H$

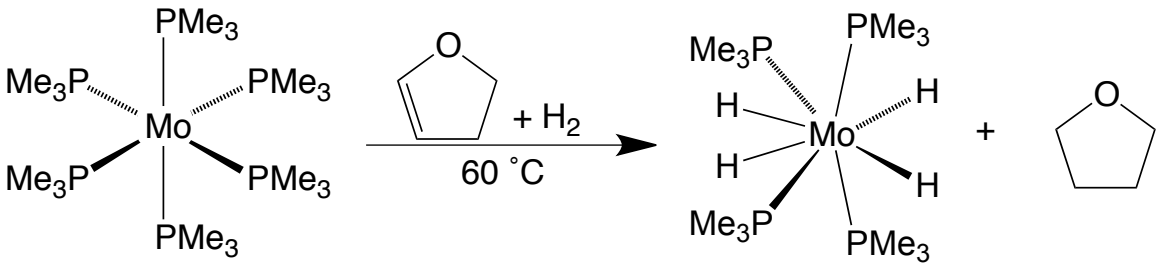

Scheme 9. Reaction of $Mo(PMe_3)_6$ Towards 2,3-Dihydrofuran and H_2

4.3.3 Reactivity towards Benzofuran

The reactivity of $Mo(PMe_3)_6$ and $W(PMe_3)_4(\eta^2\text{-}CH_2PMe_2)H$ with benzofuran has been described, and the products of these reactions have been structurally characterized.[43] The reaction of $W(PMe_3)_4(\eta^2\text{-}CH_2PMe_2)H$ with benzofuran at 60 °C was reported to

proceed with significant decomposition, but crystals of the aryloxide-olefin complex, (κ^1,η^2-$CH_2CHC_6H_4O$)W(PMe_3)$_3$(η^2–CH_2PMe_2), suitable for X-ray diffraction were isolated (Scheme 10).[43] It has now been determined that the reaction proceeds relatively cleanly, albeit slowly, at 40 ˚C. In addition, spectroscopic and analytical data have been obtained for the product.

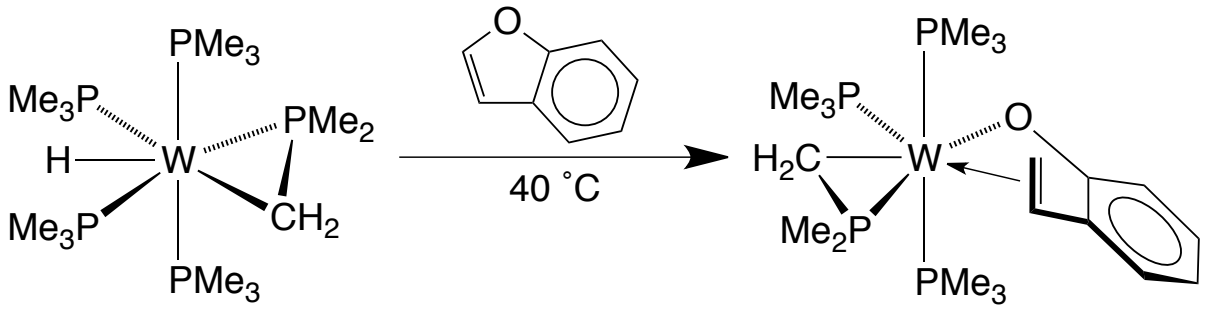

Scheme 10. Reactivity of W(PMe_3)$_4$(η^2-CH_2PMe_2)H towards Benzofuran

Mo(PMe_3)$_6$, in contrast to W(PMe_3)$_4$(η^2-CH_2PMe_2)H, reacts with benzofuran at room temperature (Scheme 11). When two equivalents of benzofuran are added to the molybdenum compound, the major product is (κ^1,η^2-$CH_2CHC_6H_4O$)Mo(κ^1-C_α-$CCHOC_6H_4$)(PMe_3)$_3$, a structure that has two benzofuran-derived ligands. This complex was previously structurally characterized by former Parkin group graduate student Daniela Buccella. Supporting spectroscopic data and another crystal structure of this compound, in which the complex co-crystallizes in a 1:1 ratio with benzofuran, have been obtained (Figure 9). Another complex with a 2:1 benzofuran : molybdenum stoichiometry, namely (κ^1,η^2-$CH_2CHC_6H_4O$)(κ^1,η^2-$HC(PMe_3)CHC_6H_4O$)Mo(PMe_3)$_2$, was also isolated.[43] When Mo(PMe_3)$_6$ is treated with one equivalent of benzofuran, an aryloxy-olefin species, (κ^1,η^2-$CH_2CHC_6H_4O$)Mo(PMe_3)$_3$(η^2–CH_2PMe_2), analogous to the tungsten complex described above, was isolated and structurally characterized.[43] Spectroscopic data for this compound has now been acquired.

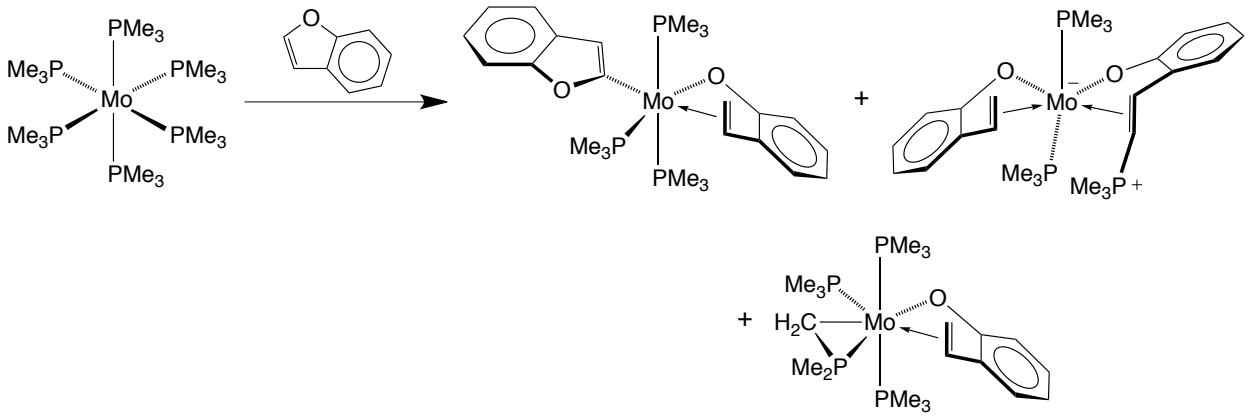

Scheme 11. Reactivity of $Mo(PMe_3)_6$ towards Benzofuran

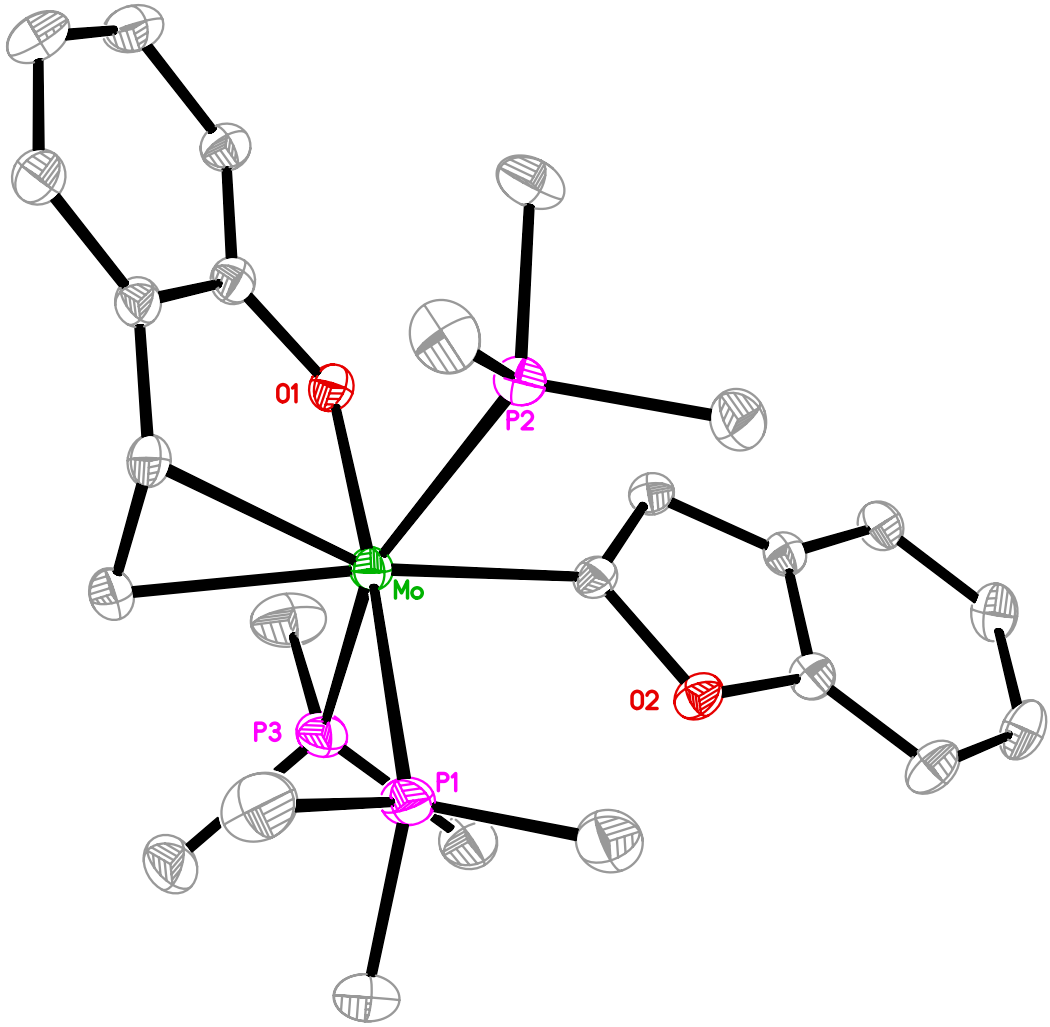

Figure 9. Molecular Structure of $(\kappa^1,\eta^2\text{-}CH_2CHC_6H_4O)Mo(\kappa^1\text{-}C_\alpha\text{-}CCHOC_6H_4)(PMe_3)_3$. Molecule of co-crystallized benzofuran is omitted for clarity.

4.3.4 Reactivity Towards Neopentyl Alcohol

The reactivity of alcohols towards $Mo(PMe_3)_6$ and $W(PMe_3)_4(\eta^2\text{-}CH_2PMe_2)H$ has been examined in the Parkin group, and previously by Parkin and Green.[46,47] With respect to alkyl alcohols, for example, it was demonstrated that both $Mo(PMe_3)_6$[46c] and $W(PMe_3)_4(\eta^2\text{-}CH_2PMe_2)H$[47] form formaldehyde complexes of the type $M(PMe_3)_4H_2(\eta^2\text{-}CH_2O)$ upon treatment with methanol. Similar reactivity was observed between $W(PMe_3)_4(\eta^2\text{-}CH_2PMe_2)H$ and ethanol, which produces an acetaldehyde complex.[43] The formaldehyde and acetaldehyde complexes may be subsequently treated with hydrogen to form the alkoxy-trihydride compounds, $M(PMe_3)_4H_3(OR)$. The reactivity of $Mo(PMe_3)_6$ and $W(PMe_3)_4(\eta^2\text{-}CH_2PMe_2)H$ with aryl alcohols was found to be quite different; for example, $Mo(PMe_3)_6$ effects only O-H bond activation to form molybdenum-aryloxy complexes,[46c] while and $W(PMe_3)_4(\eta^2\text{-}CH_2PMe_2)H$ affords oxametallacycle products derived from O-H and C-H bond cleavage.[46a]

As an extension of this research, we explored the reactivity of $Mo(PMe_3)_6$ and $W(PMe_3)_4(\eta^2\text{-}CH_2PMe_2)H$ towards neopentyl alcohol. This alcohol, like the aryl alcohols, forms unique products with $Mo(PMe_3)_6$ and $W(PMe_3)_4(\eta^2\text{-}CH_2PMe_2)H$ (Schemes 12 and 13). The reaction with $Mo(PMe_3)_6$ produces a 16-electron, paramagnetic complex, namely $Mo(PMe_3)_4(ONp)_2$ (Figure 10). This compound formally results from loss of PMe_3, oxidative addition of two equivalents of alcohol, and elimination of H_2. Similar complexes have been isolated from the reactions of niobium and titanium compounds with aryl alcohols.[48] $W(PMe_3)_4(\eta^2\text{-}CH_2PMe_2)H$, on the other hand, forms the alkoxy-trihydride complex, $W(PMe_3)_4H_3(ONp)$ (Figure 11).

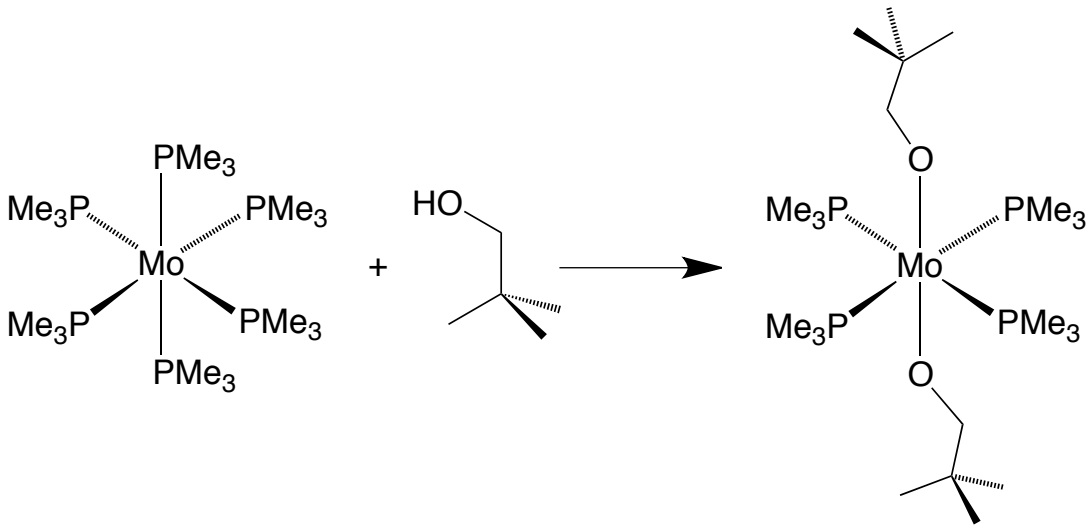

Scheme 12. Reactivity of $Mo(PMe_3)_6$ towards Neopentyl Alcohol

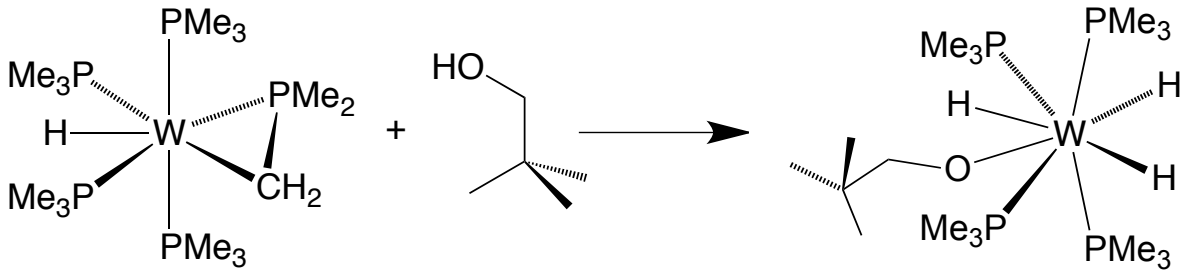

Scheme 13. Reactivity of $W(PMe_3)_4(\eta^2\text{-}CH_2PMe_2)H$ towards Neopentyl Alcohol

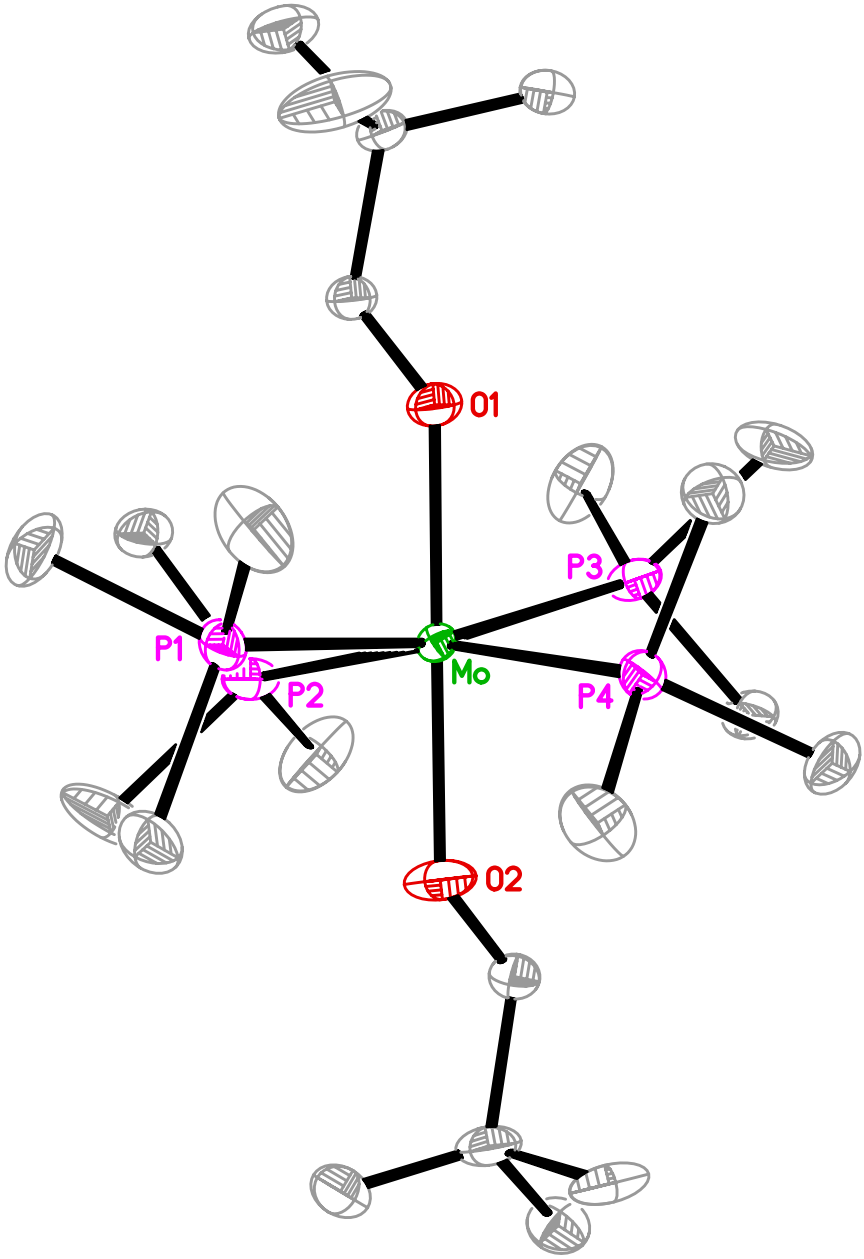

Figure 10. Molecular Structure of $Mo(PMe_3)_4(ONp)_2$

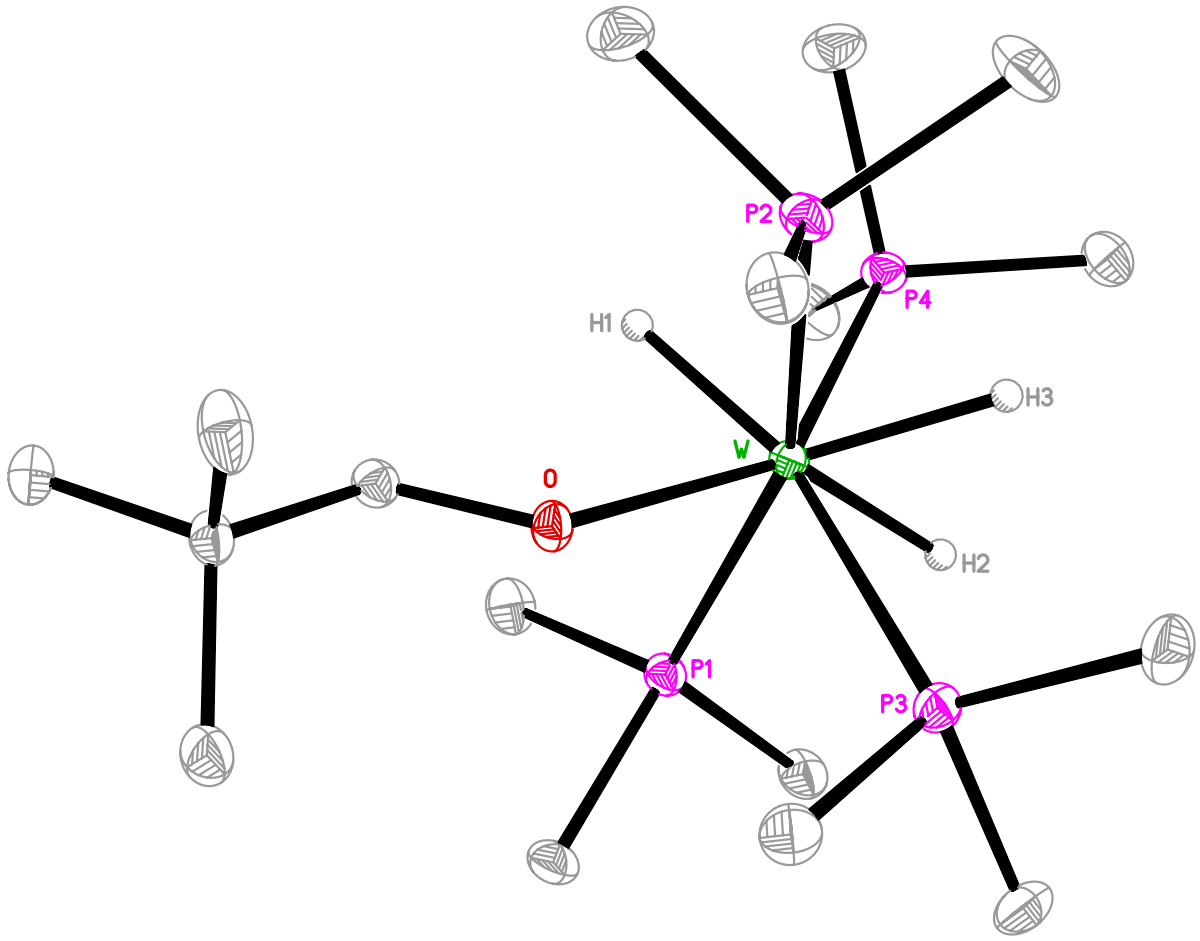

Figure 11. Molecular Structure of $W(PMe_3)_4H_3(ONp)$

4.3.5 Reactivity of $Mo(PMe_3)_4(\eta^2\text{-}CH_2PMe_2)H$ towards PhX (X = F, Cl, Br, I).

The molybdenum congener of $W(PMe_3)_4(\eta^2\text{-}CH_2PMe_2)H$, namely $Mo(PMe_3)_4(\eta^2\text{-}CH_2PMe_2)H$, was prepared, and its reactivity with aryl halides was explored. This is of interest because $W(PMe_3)_4(\eta^2\text{-}CH_2PMe_2)H$ reacts with PhX (X = Br, I) to form cationic alkylidene complexes of the type $[W(PMe_3)_4(\eta^2\text{-}CHPMe_2)H]X$ (X = Br, I).[49] The isolation of these complexes was significant both because of their structurally unique η^2-$CHPMe_2$ alkylidene ligand and because they provided a means to isolate $W(PMe_3)_4(\eta^2\text{-}CHDPMe_2)H$, from which the rate constant for accessing the 16-electron species $[W(PMe_3)_5]$ could be measured.[49] Thus, we sought to determine whether $Mo(PMe_3)_4(\eta^2\text{-}CH_2PMe_2)H$ would exhibit the same reactivity.

Significantly, $Mo(PMe_3)_4(\eta^2\text{-}CH_2PMe_2)H$ does *not* appear to form any analogous alkylidene species in reactions with aryl halides. Treatment of $Mo(PMe_3)_4(\eta^2\text{-}CH_2PMe_2)H$ with PhF resulted in no reaction, while treatment with PhCl produced only $Mo(PMe_3)_4Cl_2$. When treated with PhBr or PhI, however, $Mo(PMe_3)_4(\eta^2\text{-}CH_2PMe_2)H$ formed bright purple crystals, which were suitable for X-ray diffraction in the case of PhI. The resulting complex is a cationic molybdenum alkylidyne species, $[Mo(PMe_3)_4(\equiv CPMe_2Ph)I]I$ (Scheme 14). The assignment of this compound as an akylidyne is supported by the linear geometry around the ($\equiv CPMe_2Ph$) carbon (Mo-C-P = 175.6(7)˚) and the short Mo-C bond distance (1.784(9) Å), which is approximately equal to the average Mo-C triple bond distance reported in the Cambridge Structural Database (1.792 Å). The solid state structure of $[Mo(PMe_3)_4(\equiv CPMe_2Ph)I]I$ is shown in Figure 12. $Mo(PMe_3)_6$ did not react in the same fashion; a gray precipitate was consistently formed, and the only product isolated was $[Me_3PhP]I$.

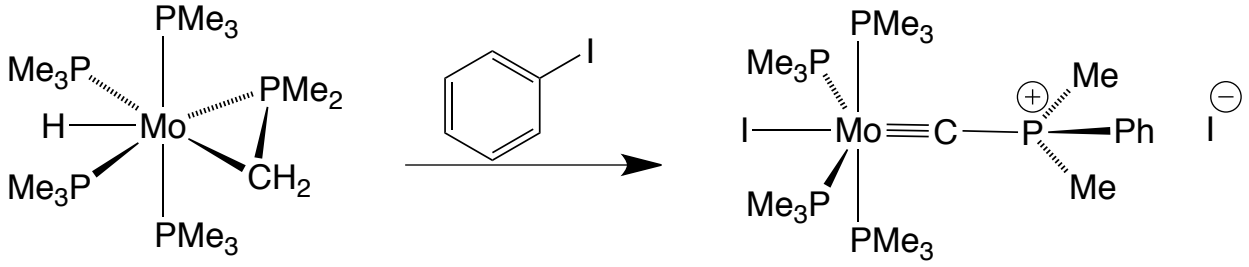

Scheme 14. Reactivity of $Mo(PMe_3)_4(\eta^2\text{-}CH_2PMe_2)H$ towards PhI

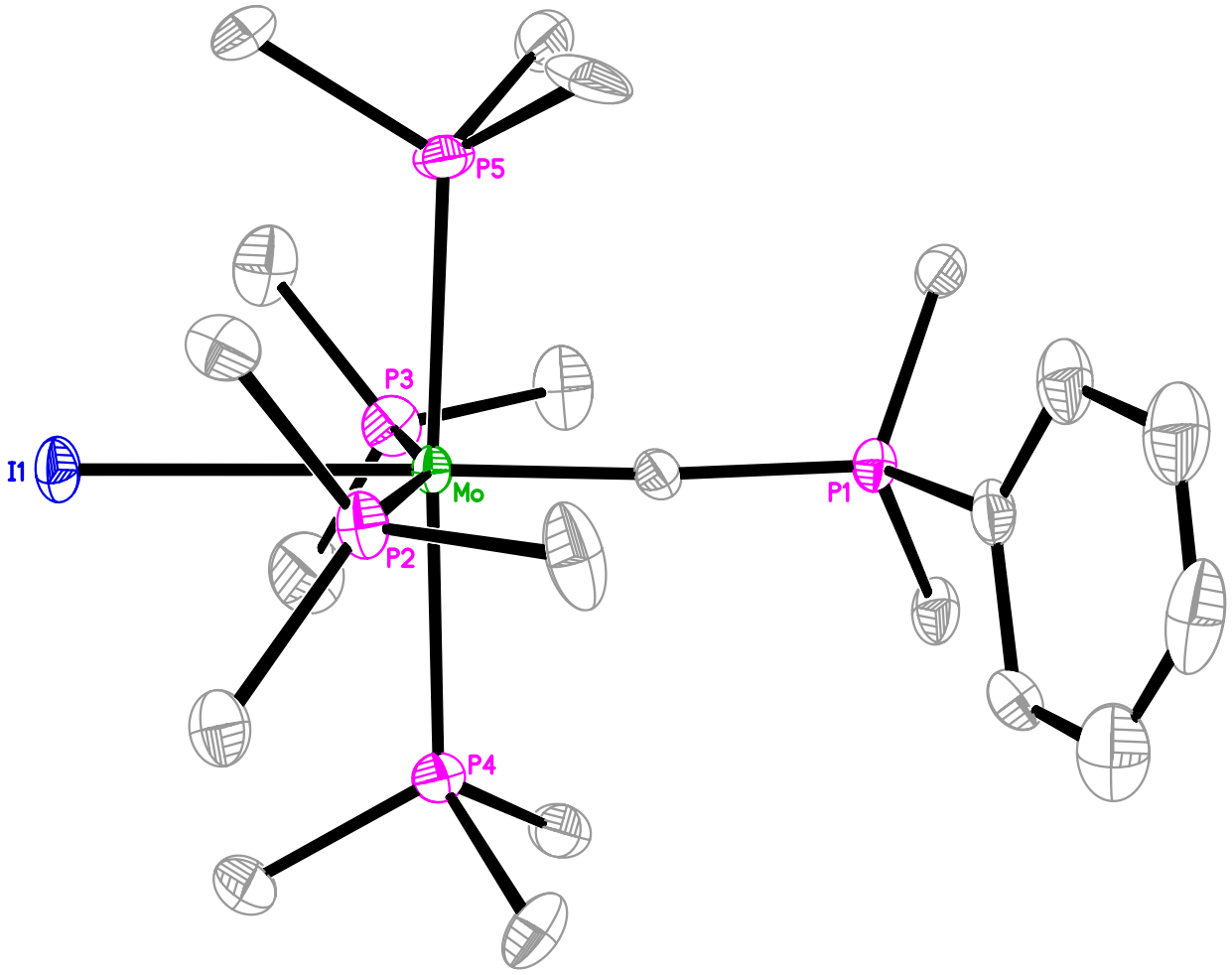

Figure 12. Molecular Structure of [Mo(PMe$_3$)$_4$(≡CPMe$_2$Ph)I]I (anion omitted)

4.3.6 Reactivity with 2-Seleno-1-Methylbenzimidazole

Lastly, the reactivity of W(PMe$_3$)$_4$(η^2-CH$_2$PMe$_2$)H with 2-seleno-1-methylbenimidazole [H(sebenzim^{Me})] was investigated. H(sebenzim^{Me}) was prepared by Joshua Palmer,[50] who is currently a postdoctoral research scientist in the Parkin lab. The reaction of W(PMe$_3$)$_4$(η^2-CH$_2$PMe$_2$)H with one equivalent of H(sebenzim^{Me}) in pentane followed by placement at -15 ˚C affords red crystals of W(PMe$_3$)$_4$(sebenzim^{Me})H, in which the benzimidazole ligand coordinates in a κ^2-fashion *via* the selenium and nitrogen atoms (Figure 13). The same reaction with an excess of H(sebenzim^{Me}) in C$_6$D$_6$ results in an immediate color change of the solution from yellow to a rust-colored red. ^{1}H NMR

spectroscopic analysis indicates that the reaction cleanly affords one product whose ^{1}H NMR spectrum is consistent with $W(PMe_3)_4(sebenzim^{Me})H$.

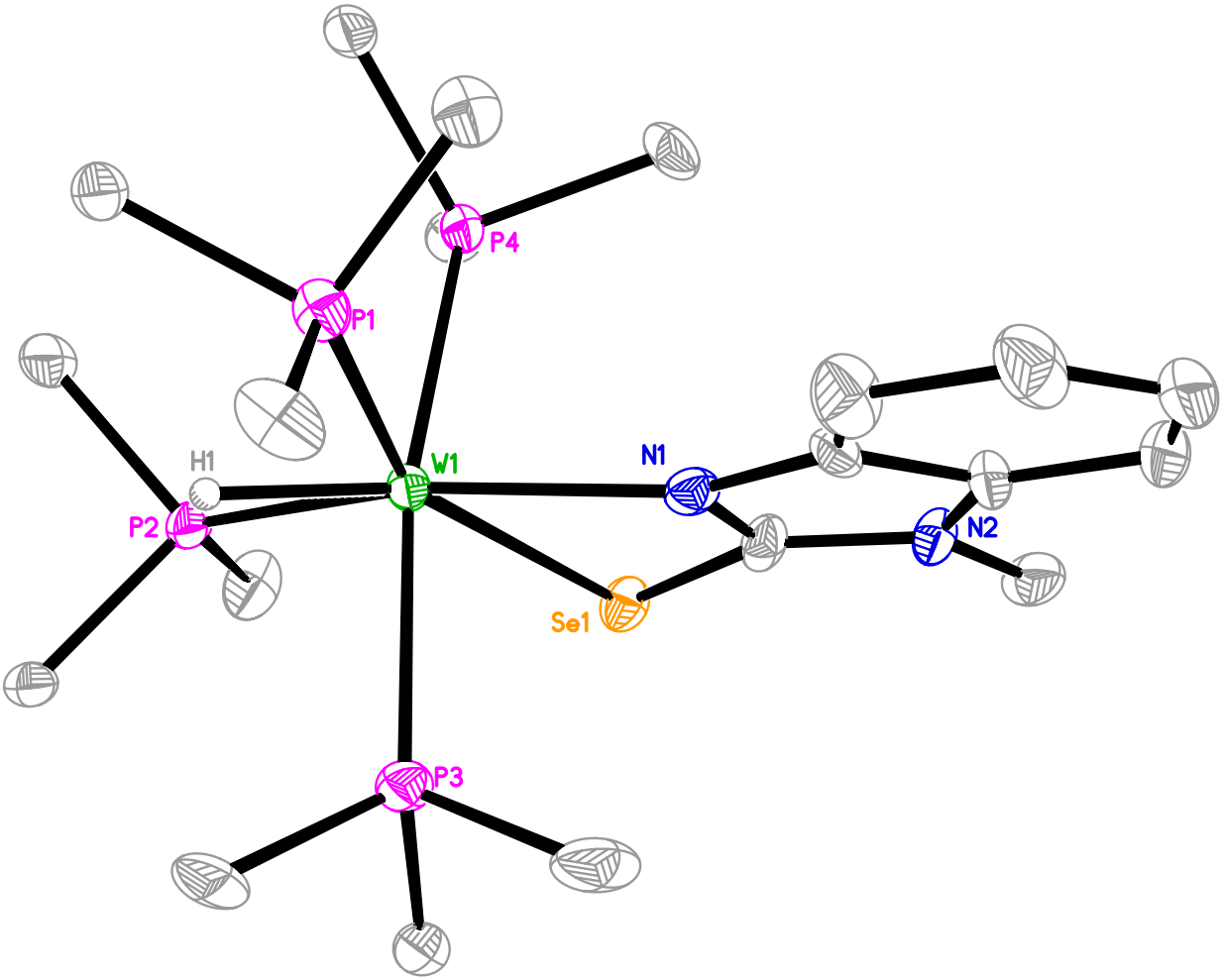

Figure 13. Molecular Structure of $W(PMe_3)_4(sebenzim^{Me})H$

4.4 Reactivity of Vaska's Compound towards SiH_4

4.4.1 Background

Since its initial report in 1961,[9] $IrCl(CO)(PPh_3)_2$, or "Vaska's Compound", has elicited a great degree of interest for its ability to undergo facile oxidative addition with a large number of substrates. For example, Vaska's compound has been shown to undergo oxidative addition of molecules such as H_2,[51] O_2,[52] and HX (X = halogen).[53] In addition, the reactivity of this complex with a number of organohydrosilanes has been

described.[54] Many of these additions are reversible, such that reductive elimination occurs to regenerate $IrCl(CO)(PPh_3)_2$ and the original substrate. Given the fundamental importance of oxidative addition and reductive elimination in many transition metal-catalyzed reactions, the study of Vaska's compound and its reactivity is of significant interest.

Some years after its initial synthesis, the reactivity of Vaska's compound with silane (SiH_4) and other simple hydrosilanes of the type SiH_3X (X = Cl, Br, or I) was described.[55] This seemingly simple analysis was complicated by (*i*) rapid precipitation of the products from solution and (*ii*) complete insolubility of these precipitates. The rapid precipitation precluded analysis of the reaction products by NMR spectroscopy, as did the insolubility of the resulting solid. Furthermore, no crystal suitable for X-ray diffraction was obtained. The geometries of the solid products were therefore tentatively assigned based on IR stretching frequencies as having *trans*- phosphine ligands with the hydride *trans* to the chloride (Scheme 15, **A**). A second geometry in which the hydride is *trans* to the carbonyl group (Scheme 15, **B**) was also discussed but considered to be less consistent with the IR spectra.[55]

Although NMR spectroscopy was not feasible for any silyl species, the authors did find that some of the analogous germyl halides (*i.e.* GeH_3X, where X = Cl, Br, or I) formed complexes that were soluble for a sufficient duration such that analysis by ^1H NMR spectroscopy was possible. The ^1H NMR spectra of these products exhibited resonances corresponding to the GeH hydrogens and IrH hydride that were each characterized by a simple triplet pattern. Thus, these products were assigned a geometry that was also consistent with the IR spectra of the solid products (Scheme 15, **A**). In the case of GeH_3Cl, however, a second set of signals was observed. These resonances were composed of a doublet of triplets (GeH) and a triplet of quartets (IrH), where the extra coupling was attributed to $^3J_{H\text{-}Ge\text{-}Ir\text{-}H}$. The authors concluded that this extra coupling

must arise from a *trans*- configuration of the -H and -GeH_2X groups (Scheme 15, **C**) based on the "general observation that couplings involving protons are usually larger when the coupled atoms are *trans* than when they are *cis*."[55]

Two possibilities for the intractable solid products were addressed: (*i*) either the precipitates possessed the same stereochemistry as the initial soluble products and were produced because the initial solution was supersaturated, or (*ii*) they represented a less soluble isomeric species – for example, one in which the phosphines are *cis*- to each other (Scheme 15, **D**.) The authors favored the latter explanation, although this geometry was not considered to be as consistent with the IR spectra.[55]

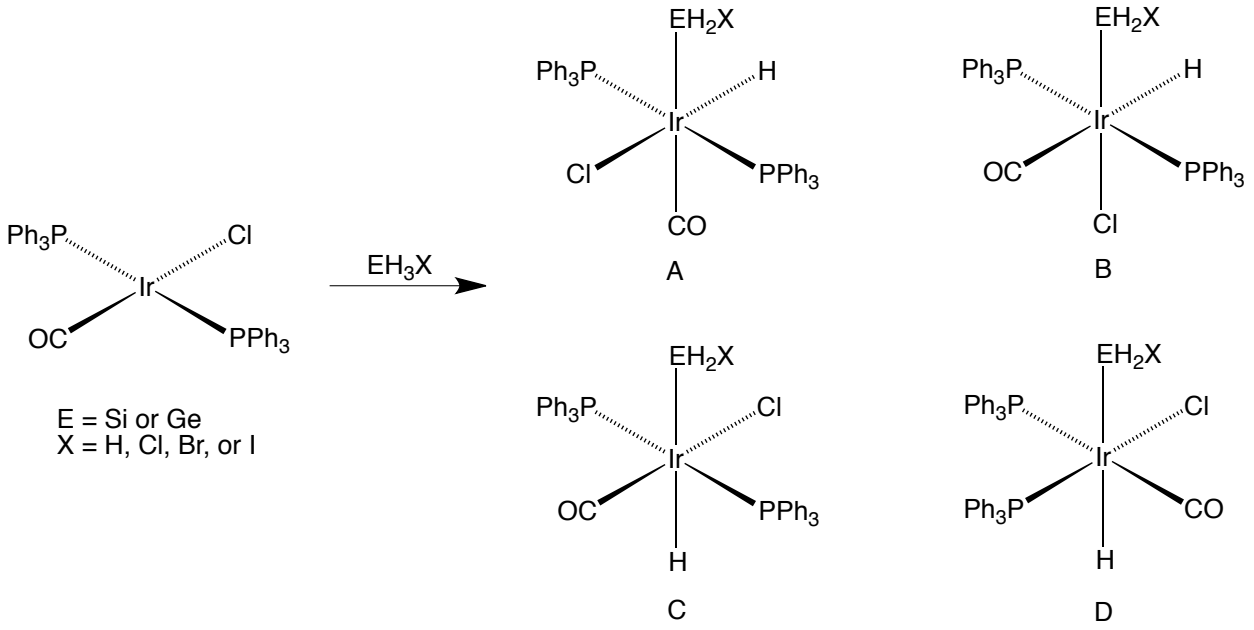

Scheme 15. Suggested Isomers for the Products of $IrCl(CO)(PPh_3)_2$ + EH_3X

In order to better evaluate the nature of the initial adducts (before precipitation) described above, the same group examined the reactivity of hydrosilanes and hydrogermanes with complexes analogous to Vaska's, namely $IrCl(CO)(PEt_3)_2$ and $IrI(CO)(PEt_3)_2$.[56] The authors chose to study these derivatives because transition metal complexes of triethylphosphine are frequently more soluble than their

triphenylphosphine analogues,[57] and indeed, the products of these reactions were sufficiently soluble such that both ^{1}H and ^{31}P NMR spectra were obtained. The reaction of SiH_4 with $IrCl(CO)(PEt_3)_2$, for example, generated a single product whose $^{31}P\{^{1}H\}$ NMR spectrum was characterized by a singlet, and whose -SiH_3 and -IrH resonances in the ^{1}H NMR spectrum appeared as a doublet of triplets and triplet of quartets, respectively. For the same reason as described above, this coupling pattern was attributed to a *trans*-configuration of the silyl and hydride ligands (Scheme 15, **C**). The same reaction using GeH_4 produced two species, each characterized by a single resonance in the $^{31}P\{^{1}H\}$ spectrum. The ^{1}H NMR spectrum of this reaction mixture also indicated the presence of two isomers, one distinguished by signals of the same pattern as the silyl compound, and the other by two triplets. These isomers are assigned as having *trans*- and *cis*- germyl and hydride ligands, respectively. (Scheme 15, **C** and **A**). Significantly, no evidence for isomerization after initial product formation was observed in this system.[56]

In view of the fact that all of the product assignments described above are based on the *assumption* that the coupling between mutually *trans*- ligands will be greater than that between mutually *cis*- ones, it is significant that we have now characterized a silyl-hydride derivative of Vaska's compound by X-ray diffraction and NMR spectroscopy, described herein. We believe that the solid state structure provides strong evidence that the aforementioned assumptions about coupling between *trans*- ligands may be incorrect.

4.4.2 Reaction of $IrCl(CO)(PPh_3)_2$ with SiH_4

When a suspension of $IrCl(CO)(PPh_3)_2$ in C_6D_6 is treated with SiH_4, the yellow solid dissolves and the solution turns immediately from yellow to colorless. It was previously reported that precipitation of a white solid began immediately, before the color of the solution had disappeared;[55] in our hands, however, the product remained in

solution for long enough that a number of NMR spectroscopic experiments were possible.[58]

The ^{1}H NMR spectrum of the product (Figure 14) is in accord with the spectrum of the observed product from the reaction of SiH_4 with $IrCl(CO)(PEt_3)_2$.[56] Specifically, the product is characterized by a silyl resonance at δ 2.79 that appears as a doublet of triplets; this signal also possesses silicon satellites ($^{1}J_{Si\text{-}H}$ = 187). A hydride resonance at δ -6.32 appears as a triplet of quartets. When the hydride signal is irradiated, the silyl resonance becomes a triplet, and irradiation of the silyl resonance causes the hydride signal to appear as a triplet as well. These observations are consistent with a structure in which both the -SiH_3 and -IrH hydrogens couple to equivalent phosphines and to each other. The $^{31}P\{^{1}H\}$ NMR spectrum of this complex possesses a single singlet resonance, which is consistent with the presence of only one isomer in which the phosphine ligands are equivalent and therefore necessarily mutually *trans*.

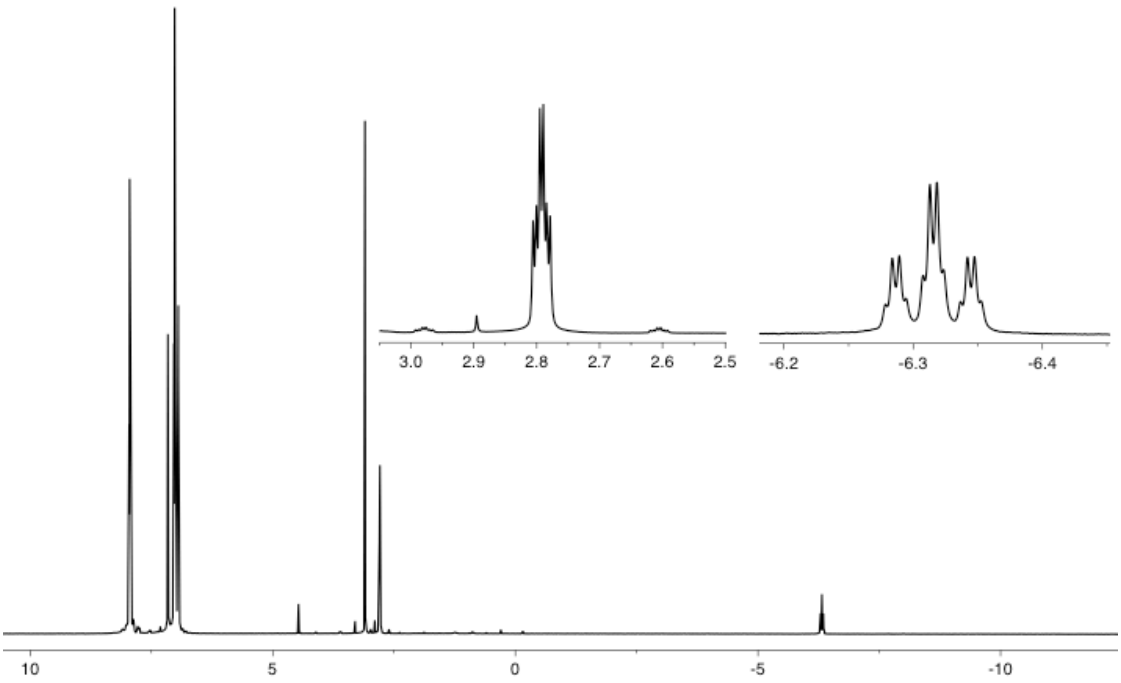

Figure 14. ^{1}H NMR Spectrum of the Product of $IrCl(CO)(PPh_3)_2 + SiH_4$

After these experiments were performed, a precipitate began to form, some of which was crystalline but not suitable for X-ray diffraction. Therefore, the reaction solution was decanted and allowed to slowly evaporate under an argon atmosphere. In this manner, a crystal of *cis*-IrH(SiH_3)(CO)(Cl)(PPh_3)$_2$[59] (H *trans* to CO) suitable for X-ray diffraction was obtained (Figure 15). This complex co-crystallizes with benzene and has no disorder associated with the ligands. The Si-H and Ir-H hydrogens were located and freely refined isotropically.

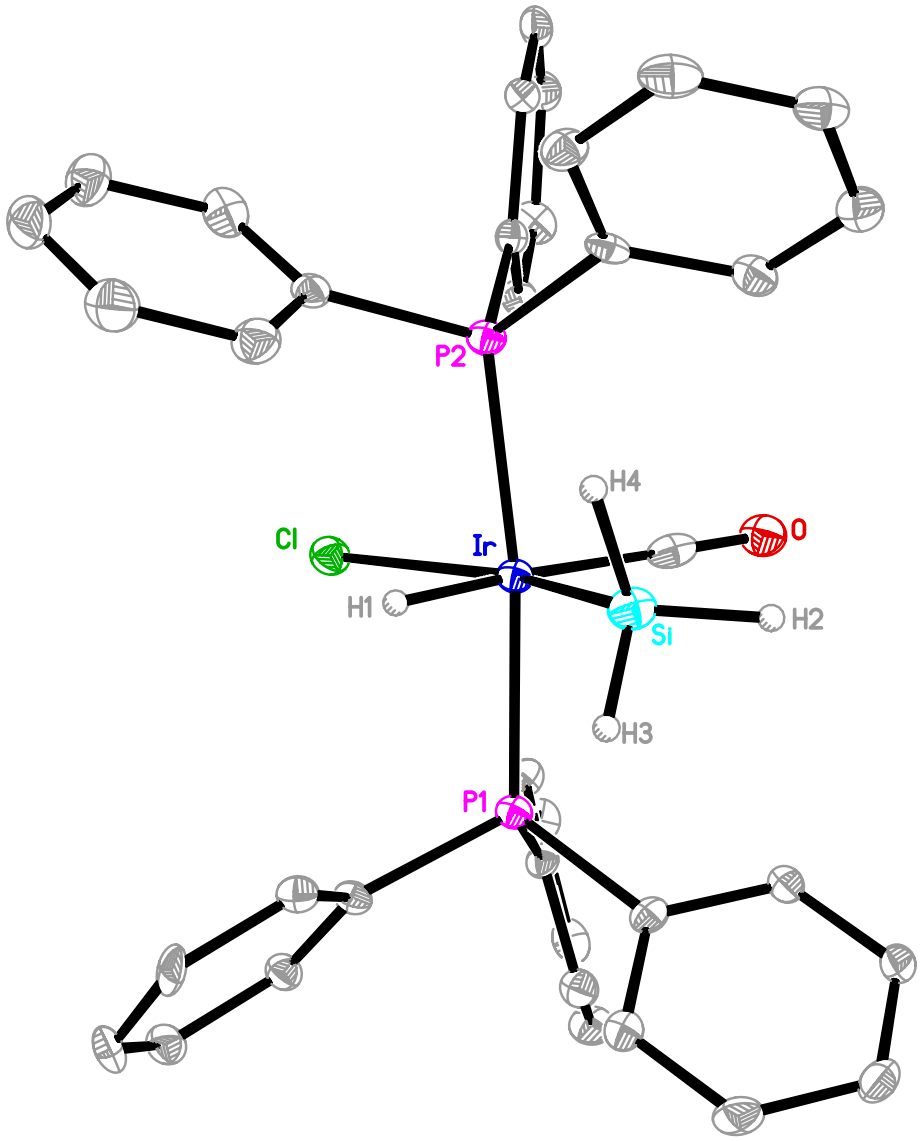

Figure 15. Molecular Structure of *cis*-IrH(SiH_3)(CO)(Cl)(PPh_3)$_2$

The solid state structure of *cis*-$IrH(SiH_3)(CO)(Cl)(PPh_3)_2$ (H *trans* to CO) features a geometry in which the silyl and hydride ligands are mutually *cis*. Furthermore, the hydride is *trans*- to the carbonyl group, while the silyl ligand is *trans*- to the chloride (Scheme 15, **B**). This configuration is in contrast to the structures that were proposed for related products both based on IR and NMR spectroscopy (Scheme 15, **A** and **C**).[55,56] Two possible explanations for this discrepancy are as follows: (*i*) the observed ^1H NMR spectrum and the solid state structure correspond to the same isomer, such that previous assignments are incorrect, or (*ii*) the solution state and solid state structures are different, such that an isomerization process occurs during crystallization.

The former explanation is more plausible for a number of reasons. Firstly, there is no convincing way to account for a *trans*-configuration of the silyl and the hydride groups as a kinetic product resulting from oxidative addition of the Si-H bond at the metal center. Specifically, a concerted oxidative addition is expected to occur in a *cis*-fashion.[60] Mechanisms that are known to cause addition of substrates in a *trans*- fashion – for example, ionic or radical pathways – seem unlikely given the mild reaction conditions, non-polar solvent, and non-polar nature of SiH_4.[55] A *trans*-configuration of the silyl and hydride ligands would therefore likely be the result of some isomerization process after initial *cis*- addition, and there is no evidence for such a process taking place here.

While the formation of a silyl-hydride complex in which these ligands are *trans*- seems unlikely based on kinetic arguments, we were curious to see whether such a product could be favored thermodynamically. We therefore performed DFT geometry optimization calculations on all possible isomers in which the phosphine ligands are *trans* (Scheme 15, **A, B**, and **C**). A comparison of the energies of the geometry optimized structures indicates that *cis*-$IrH(SiH_3)(CO)(Cl)(PPh_3)_2$ (hydride *trans* to CO, **B**), the structure that we have isolated, is in fact the lowest energy isomer (Figure 16). The

other isomer in which the silyl and hydride ligands are *cis*, namely *cis*-$IrH(SiH_3)(CO)(Cl)(PPh_3)_2$ (hydride *trans* to Cl, **A**), is moderately higher in energy, while the isomer in which the hydride and silyl ligands are *trans* (**C**) is substantially higher in energy. This is consistent with previous computational work[60] and suggests that *trans*-$IrH(SiH_3)(CO)(Cl)(PPh_3)_2$ is not favored thermodynamically; thus, these results indicate that a process in which oxidative addition produces a *cis*-adduct followed by isomerization to a *trans*- adduct seems unlikely. Therefore, it seems logical that the initial product observed by ^1H NMR spectroscopy does correspond to *cis*-$IrH(SiH_3)(CO)(Cl)(PPh_3)_2$ (hydride *trans* to CO), and the observed coupling between the silyl and hydride ligands cannot be attributed to a mutually *trans* configuration.

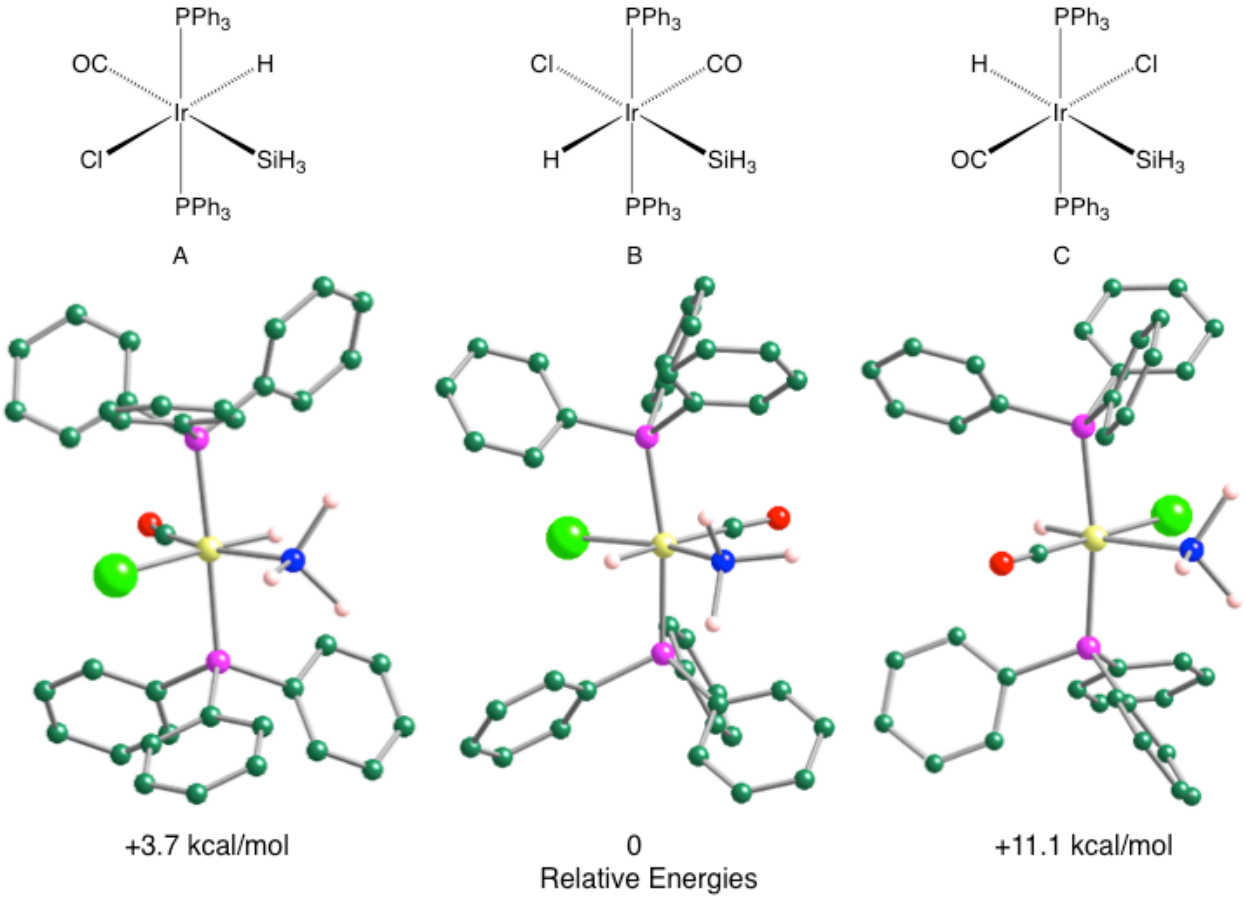

Figure 16. Relative Energies of Geometry Optimized Isomers

4.4.3 Reaction of $IrCl(CO)(PPh_3)_2$ with GeH_4

In addition to the reactivity of silane with Vaska's compound, we investigated the reactivity of germane, GeH_4. As discussed above, the previously reported reaction of $IrCl(CO)(PPh_3)_2$ with GeH_4 resulted in rapid precipitation of a 1:1 adduct that was characterized only by IR spectroscopy.[55] Treatment of the analogous $IrCl(CO)(PEt_3)_2$ complex produced two isomers, which were characterized by ^1H and $^{31}P\{^1H\}$ NMR spectroscopy.[56] In our hands, the reaction of Vaska's compound with GeH_4 gave a colorless solution and, as with silane, the products remained in solution for a sufficient duration that NMR spectroscopic experiments were possible.

The spectra of the products of this reaction are consistent with those observed for $IrCl(CO)(PEt_3)_2$. The ^1H NMR spectrum, for example, contains the two sets of peaks described above (*i.e.* one isomer characterized by a doublet of triplets and a triplet of quartets, the other by two triplets) (Figure 17). Homonuclear decoupling experiments confirm that the extra coupling observed in the first set of peaks is due to $^3J_{H\text{-}Ge\text{-}Ir\text{-}H}$, and heteronuclear decoupling confirms that the observed triplet is in all cases due to coupling to two phosphine ligands.

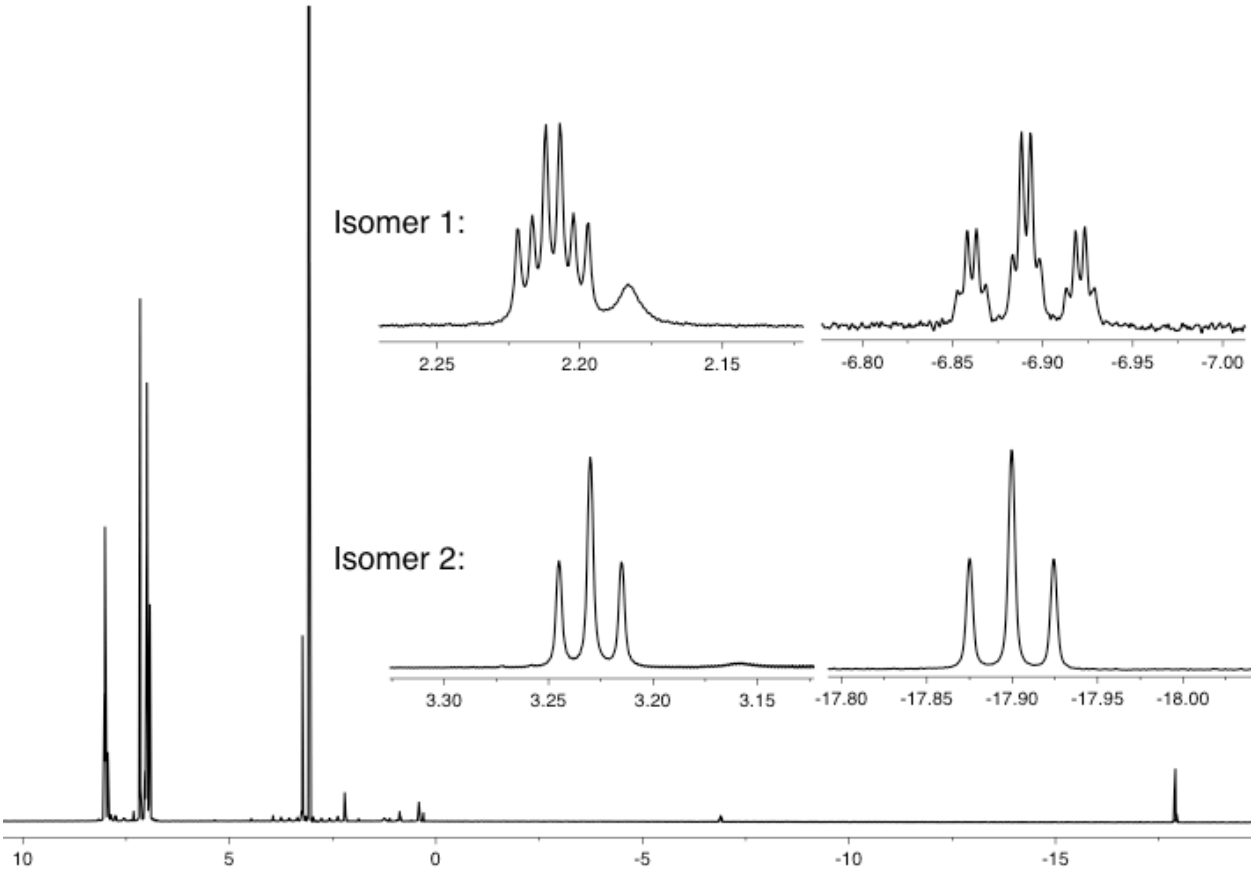

Figure 17. ^{1}H NMR Spectrum of the Products of IrCl(CO)(PPh$_3$)$_2$ + GeH$_4$

As with the silyl adducts, we performed DFT geometry optimization calculations on all of the *trans*-phosphine isomers, namely *cis*-IrH(GeH$_3$)(CO)(Cl)(PPh$_3$)$_2$ (H *trans* to Cl), *cis*-IrH(GeH$_3$)(CO)(Cl)(PPh$_3$)$_2$ (H *trans* to CO), and *trans*-IrH(GeH$_3$)(CO)(Cl)(PPh$_3$)$_2$. Significantly, the geometry optimized energies of these isomers increased in the same order as the analogous silyl complexes, but the differences in energy are smaller. Based on the results with the silyl complex described above, the isomer with the additional coupling is tentatively assigned as *cis*-IrH(GeH$_3$)(CO)(Cl)(PPh$_3$)$_2$ (H *trans* to CO, **B**), and the one without is assigned as *cis*-IrH(GeH$_3$)(CO)(Cl)(PPh$_3$)$_2$ (H *trans* to Cl, **A**). The geometry optimized structures and relative energies of these isomers are shown in Figure 18.

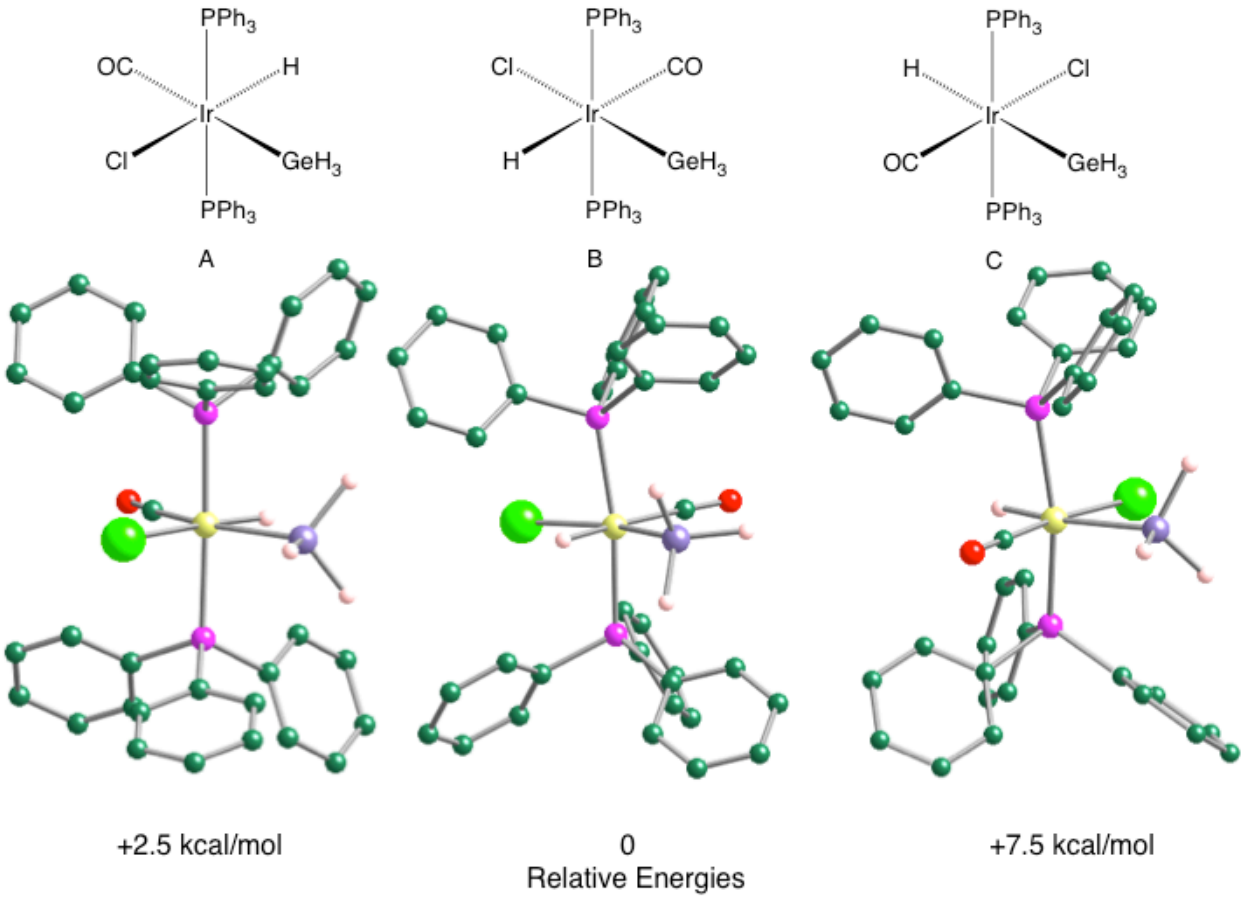

Figure 18. Relative Energies of Geometry Optimized Energies

4.4.4 Further NMR Studies of $IrHCl(CO)(EH_3)(PPh_3)_2$ (E = Si, Ge)

In order to assess further the geometries of the isomers reported herein, we conducted a series of NOE experiments on the adducts of Vaska's compound with SiH_4 and GeH_4. A NOE enhancement between the hydride and silyl or germyl resonances would be expected to correspond to a *cis*- configuration, where the two ligands are in close spatial proximity. The results of these experiments were mixed but generally support the assignment of the isomers described above. For example, in study of the germane complexes, an NOE enhancement was observed for the hydride signal at δ -17.90 but not for the signal at δ -6.89. This could be an indication of respective *cis*- and *trans*-configurations, but more likely it is due to the fact that there is very little of the second isomer present; thus, NMR spectroscopic analysis on this isomer becomes difficult. The

silane complex did exhibit an NOE enhancement between the hydride and silyl signal. The weakness of the observed enhancements is probably due to the fact that the silyl group rotates in solution, averaging the effective NOE that the hydride ligand experiences.[61]

The reactivity of these adducts towards H_2 was also explored. Both $IrHCl(CO)(SiH_3)(PPh_3)_2$ and $IrHCl(CO)(GeH_3)(PPh_3)_2$ react with hydrogen at room temperature to form $IrH_2Cl(CO)(PPh_3)_2$. Perhaps more interesting, however, is that $IrH_2Cl(CO)(PPh_3)_2$ is formed from $IrHCl(CO)(SiH_3)(PPh_3)_2$ and $IrHCl(CO)(GeH_3)(PPh_3)_2$ in the absence of H_2 as well, under analogous conditions (room temperature in benzene). The generation of $IrH_2Cl(CO)(PPh_3)_2$ from a triethoxyhydrosilane compound has been described; the authors proposed that water or oxygen may react with the silyl hydride to form the dihydride complex and silanol or a siloxane.[54c] Although the reactions presented herein were performed under an argon atmosphere in sealed J. Young tubes, it is possible that trace amounts of water or oxygen could be responsible for this transformation (Scheme 16).

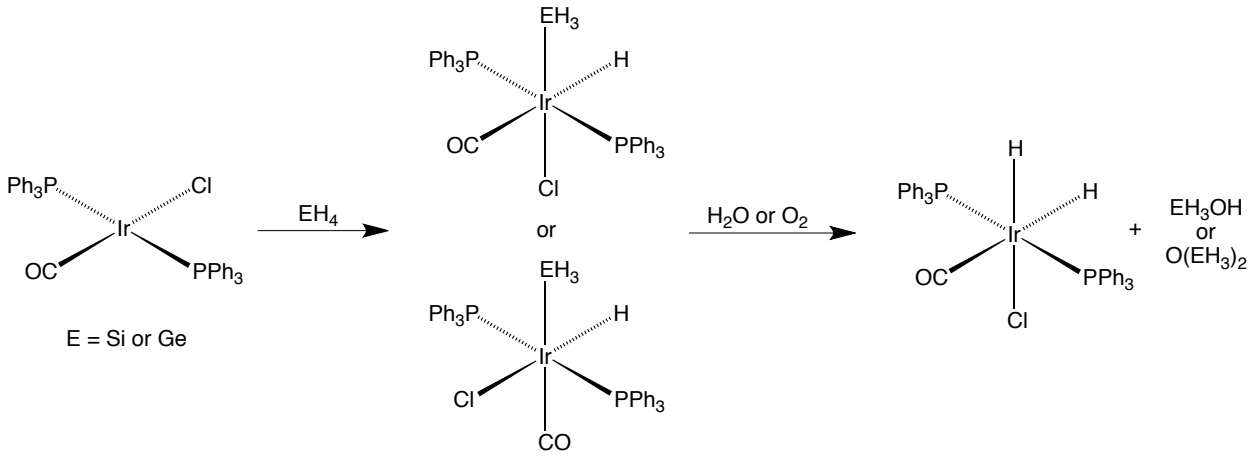

Scheme 16. Reaction of $IrHCl(CO)(EH_3)(PPh_3)_2$ with H_2 (E = Si, Ge)

Another interesting observation is that heating a solution of $IrHCl(CO)(GeH_3)(PPh_3)_2$ with H_2 at 60 ˚C results in the formation of two new hydride peaks of equal intensity at

δ -9.69 and δ -10.96. The chemical shifts of these peaks correspond reasonably closely to those that have been previously reported for $IrH_2(CO)(GeH_3)(PPh_3)_2$ (*i.e.* δ -9.46 and δ -10.81).[62] This product could arise *via* reductive elimination of GeH_3Cl followed by oxidative addition of GeH_4 (Scheme 17).[63] Support for this process is provided by the fact that GeH_4 is evolved when the reaction is left at room temperature, but the signal corresponding to germane disappears when the sample is heated, coinciding with the formation of the new peaks.

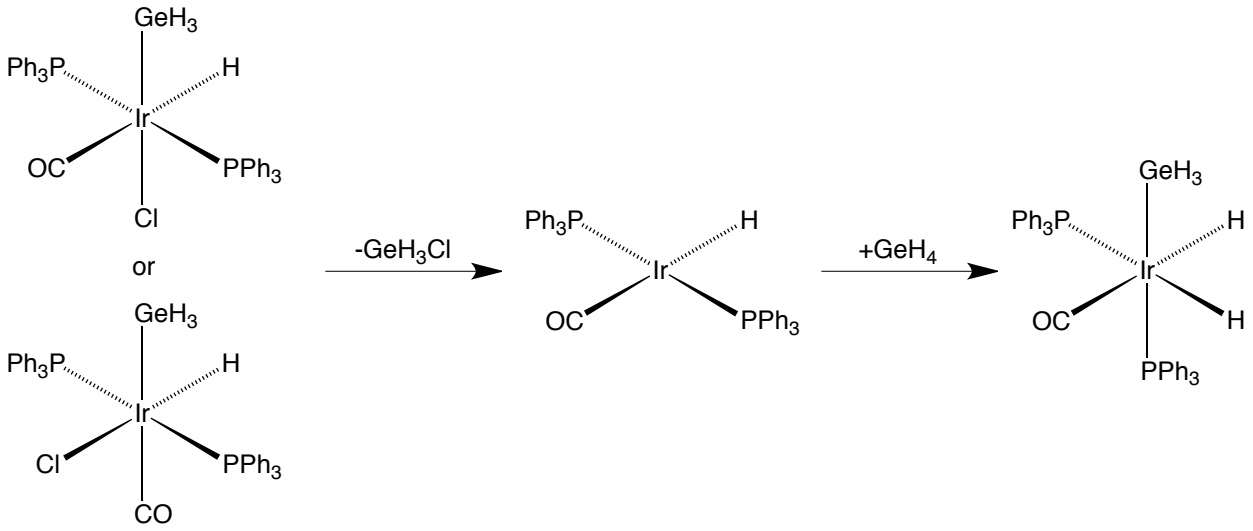

Scheme 17. High Temperature Reaction of $IrHCl(CO)(GeH_3)(PPh_3)_2$ with H_2

Finally, it was also observed that the reaction of $IrHCl(CO)(GeH_3)(PPh_3)_2$ with H_2 produces two new sets of signals whose coupling patterns are virtually identical to those of the initial germane compounds (Figure 19). This is particularly confounding because isomerization would be expected to produce species with very different NMR spectra; displacement of the carbonyl group by free PPh_3 also seems unlikely, since the resulting compound should also be distinct by NMR spectroscopy. One possible explanation may come from the aforementioned hypothesis that germanol or germoxane may be formed. Elimination of GeH_4 followed by oxidative addition of GeH_3OH across the Ge-H bond could, for example, produce species with a very similar

NMR spectrum (Scheme 18). Consistent with this suggestion, the integration of the hydride and the germyl resonances for both new species is 1:2.

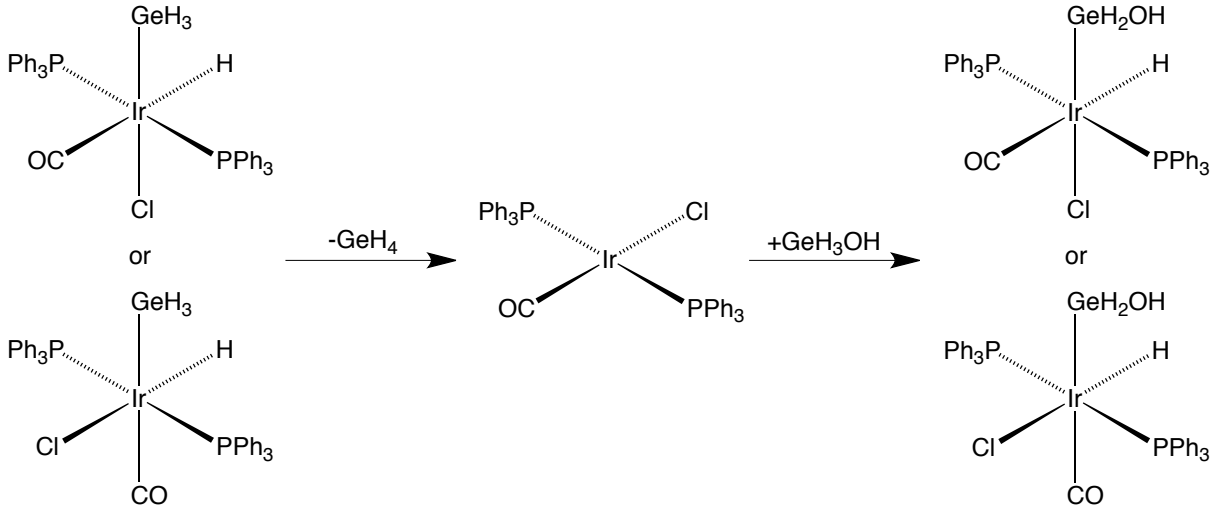

Scheme 18. Possible Formation of New Species *via* $IrHCl(CO)(GeH_3)(PPh_3)_2 + H_2$

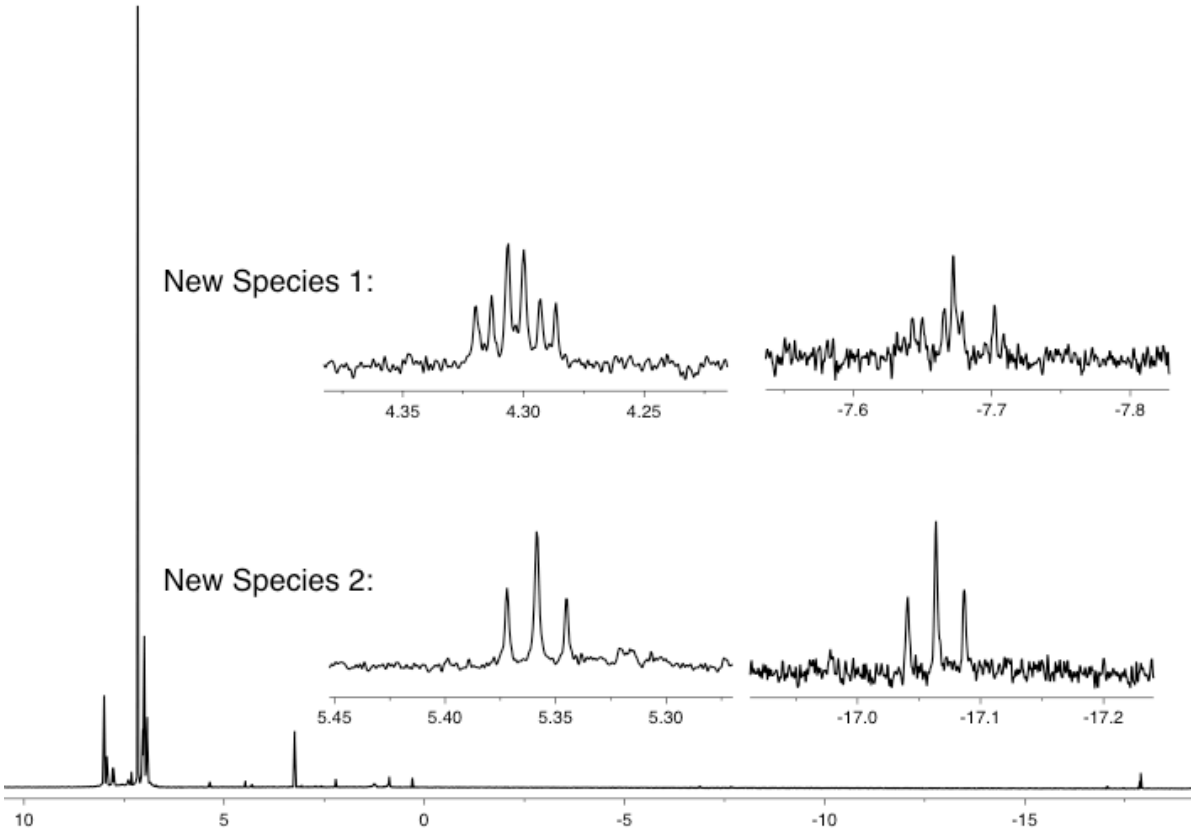

Figure 19. ^1H NMR Spectra of New Species from $IrHCl(CO)(GeH_3)(PPh_3)_2 + H_2$

4.5 Summary and Conclusions

Here we have presented a wide range of transition metal phosphine complexes whose reactivity is exciting and diverse. $Ru(PMe_3)_4H_2$ reacts with a multitude of small molecule substrates to form formate, thiocarbonate, and hydrosulfido complexes. $Mo(PMe_3)_6$ and $W(PMe_3)_4(\eta^2\text{-}CH_2PMe_2)H$ react with oxygen-containing heterocycles to afford products that involve hydrogenation of unsaturated bonds, C-O bond cleavage, and C-H bond cleavage; thus, these complexes serve as interesting models for hydrodeoxygenation and may provide insight into the mechanism of this process. Finally, a reexamination of the reactivity of Vaska's compound with SiH_4 and GeH_4 suggests that the products of these reactions may have been previously misassigned; furthermore, the long-held assumption that mutually *trans*- ligands will have stronger coupling than mutually *cis*-ones appears to be incorrect. In conclusion, these transition metal phosphine complexes effect a number of transformations with substrates related or relevant to industrial processes, and the insights gained by examining the reactivity of these complexes may serve to increase the general understanding of how these processes work.

4.6 Experimental Details

4.6.1 General Considerations

All manipulations were performed using a combination of glovebox, high vacuum, and Schlenk techniques under a nitrogen or argon atmosphere unless otherwise specified.[64] Solvents were purified and degassed by standard procedures. ^1H NMR spectra were measured on Bruker Avance III 400, Bruker Avance III 400 SL, and Bruker Avance III 500 spectrometers. ^1H chemical shifts are reported in ppm relative to $SiMe_4$ ($\delta = 0$) and were referenced internally with respect to the solvent (δ 7.16 for C_6D_5H).[65] ^{13}C NMR spectra are reported in ppm relative to $SiMe_4$ ($\delta = 0$) and were referenced internally with respect to the solvent (δ 128.06 for C_6D_6).[65] ^{31}P chemical shifts are reported in ppm relative to 85% H_3PO_4 ($\delta = 0$) and were referenced using $P(OMe)_3$ ($\delta = 141.0$) as an

external standard.[66] Coupling constants are given in hertz. $Ru(PMe_3)_4H_2$,[67] $Mo(PMe_3)_6$,[8b] $W(PMe_3)_4(\eta^2\text{-}CH_2PMe_2)H$,[68] and $Mo(PMe_3)_4(\eta^2\text{-}CH_2PMe_2)H$[8b] were prepared by the literature methods.

4.6.2 X-ray Structure Determinations

Single crystal X-ray diffraction data were collected on a Bruker Apex II diffractometer, and crystal data, data collection and refinement parameters are summarized in Table 1. The structures were solved using direct methods and standard difference map techniques and were refined by full-matrix least-squares procedures on F^2 with SHELXTL (Version 2008/4).[69]

4.6.3 Computational Details

Calculations were carried out using DFT as implemented in the Jaguar 7.5 [$Ru(PMe_3)_4(SH)_2$] and Jaguar 7.7 [$IrHCl(CO)(EH_3)(PPh_3)_2$] suites of *ab initio* quantum chemistry programs.[70] Geometry optimizations (Table 2) were performed with the B3LYP density functional[71] using the 6-31G** (C, H, S and P) and LACVP** (Ru) basis sets.[72]

4.6.4 Reaction of $Ru(PMe_3)_4H_2$ with CO and H_2O

A solution of $Ru(PMe_3)_4H_2$ (5 mg, 0.01 mmol) in C_6D_6 (0.7 mL) in an NMR tube equipped with a J. Young valve was treated with a drop of H_2O (*ca*. 3 μL), frozen, and degassed to remove the atmosphere of air. The tube was charged with ^{13}C-enriched CO (> 0.25 atm). The solution was heated at 60 ˚C and monitored by ^1H, ^{13}C, and $^{13}C\{^1H\}$ NMR spectroscopy, thereby demonstrating the evolution of H_2 and CO_2 after two hours. After two days at 60 ˚C, the generation of a formate species was observed. Heating at 60˚C for approximately one month resulted in the formation of a number of species, one of which was determined to be $Ru(CO)_3(PMe_3)_2$ by X-ray crystallography. The WGSR using natural abundance CO_2 was performed in the same manner. Data for the formate

species produced in the reaction using ^{13}C-enriched CO is provided here. The phosphine peaks in the ^{13}C NMR spectra were not observed due to insufficient concentration, since they are not ^{13}C-enriched. ^{1}H NMR (C_6D_6): 1.11 [d, $^{2}J_{P-H}$ = 7, 36H of *trans*-Ru(P<u>Me</u>$_3$)$_4$(OC(O)H)X], 8.70 [d, $^{1}J_{C-H}$ = 192, $^{4}J_{P-H}$ = 2, 1H of *trans*-Ru(PMe$_3$)$_4$(OC(O)<u>H</u>)H]. ^{13}C{^{1}H} NMR (C_6D_6): 168.6 [br m, 1C of *trans*-Ru(PMe$_3$)$_4$(O<u>C</u>(O)H)X]. ^{13}C NMR (C_6D_6): 168.6 [d, $^{1}J_{C-H}$ = 192].

4.6.5 Reaction of Ru(PMe$_3$)$_4$H$_2$ with CO

A solution of Ru(PMe$_3$)$_4$H$_2$ (5 mg, 0.01 mmol) in C_6D_6 (0.7 mL) in an NMR tube equipped with a J. Young valve was degassed and charged with CO (1 atm), heated at 60-80 ˚C, and monitored by ^{1}H NMR spectroscopy. A number of ruthenium-hydride species were generated. The peak corresponding to free PMe$_3$ was observed to increase over the course of the reaction, which is consistent with the displacement of phosphine ligands by carbonyl ligands.

4.6.6 Reaction of Ru(PMe$_3$)$_4$H$_2$ with CO$_2$

A solution of Ru(PMe$_3$)$_4$H$_2$ (5 mg, 0.01 mmol) in C_6D_6 (0.7 mL) in an NMR tube equipped with a J. Young valve was degassed and charged with ^{13}C-enriched CO$_2$ (> 0.5 atm) and monitored by ^{1}H and ^{13}C{^{1}H} NMR spectroscopy. A formate species was generated after approximately thirty minutes at room temperature. The reaction with natural abundance CO$_2$ was performed in the same manner using 1 atm CO$_2$. NMR Data for the formate species generated using ^{13}C-enriched CO$_2$ is provided here. ^{1}H NMR (C_6D_6): -8.14 [d quart, $^{2}J_{P-H}$ = 100, $^{2}J_{P-H}$ = 28, 1H of *cis*-Ru(PMe$_3$)$_4$(OC(O)H)<u>H</u>], 0.93 [d, $^{2}J_{P-H}$ = 8, 18H of *cis*-Ru(P<u>Me</u>$_3$)$_4$(OC(O)H)H], 1.18 [d, $^{2}J_{P-H}$ = 6, 18H of *cis*-Ru(P<u>Me</u>$_3$)$_4$(OC(O)H)H], 8.90 [dd, $^{1}J_{C-H}$ = 189, $^{4}J_{P-H}$ = 5, 1H of *cis*-Ru(PMe$_3$)$_4$(OC(O)<u>H</u>)H]. ^{1}H-^{13}C HSQC: 170.8 [1C of *cis*-Ru(PMe$_3$)$_4$(O<u>C</u>(O)H)H].

4.6.7 Structural Characterization of $Ru(PMe_3)_4(\kappa^2\text{-}S_2\text{-}CS_3)$

A solution of $Ru(PMe_3)_4H_2$ (5 mg, 0.01 mmol) in C_6D_6 (0.7 mL) in an NMR tube equipped with a J. Young valve was treated with CS_2. The color of the solution changed immediately from pale orange to yellow. Yellow crystals were deposited directly from the reaction solution, which were confirmed by X-ray diffraction to be $Ru(PMe_3)_4(\kappa^2\text{-}S_2\text{-}CS_3)$.

4.6.8 Reaction of $Ru(PMe_3)_4H_2$ with H_2O

(*i*) A solution of $Ru(PMe_3)_4H_2$ (5 mg, 0.01 mmol) in C_6D_6 (0.7 mL) in an NMR tube equipped with a J. Young valve was treated with a drop of water (*ca*. 3 μL), frozen, and degassed to remove the atmosphere of air. The sample was monitored by ^1H NMR spectroscopy, first at room temperature and then with heating (60-80 ˚C). The only change that was observed to occur by ^1H NMR spectroscopy was the formation of a small hydride peak at δ -8.50 [d quart, $^2J_{P\text{-}H}$ = 106, $^2J_{P\text{-}H}$ = 28], which may correspond to a hydroxide complex of the type $Ru(PMe_3)_4H(OH)$.

(*ii*) A solution of $Ru(PMe_3)_4H_2$ (5 mg, 0.01 mmol) was stirred in water (*ca*. 2 mL) at room temperature for approximately 14 h. The water was removed *in vacuo*, and the contents were redissolved in C_6D_6 and examined by ^1H and $^{31}P\{^1H\}$ NMR spectroscopy, thereby demonstrating the formation of a mixture of products. Orange crystals of $[Ru_2(PMe_3)_6(\mu\text{-}OH)_3]Cl$ suitable for X-ray diffraction were obtained by slow evaporation of the benzene at room temperature under a nitrogen atmosphere.

4.6.9 Reaction of $Ru(PMe_3)_4H_2$ with H_2S

A solution of $Ru(PMe_3)_4H_2$ (5 mg, 0.01 mmol) in C_6D_6 (0.7 mL) in an NMR tube equipped with a J. Young valve was degassed and charged with H_2S (1 atm) and monitored by ^1H NMR spectroscopy at room temperature, thereby demonstrating the conversion to a mixture of *cis*- and *trans*-$Ru(PMe_3)_4(SH)_2$. Colorless crystals of *cis*-$Ru(PMe_3)_4(SH)_2$ were deposited directly from the reaction solution. It was observed by

^{1}H NMR spectroscopy that isolated crystals of *cis*-Ru(PMe_3)$_4$(SH)$_2$ convert to *trans*-Ru(PMe_3)$_4$(SH)$_2$ at room temperature, a process that occurs both in C_6D_6 and CD_3CN. When a mixture of *cis*-Ru(PMe_3)$_4$(SH)$_2$ and *trans*-Ru(PMe_3)$_4$(SH)$_2$ is heated at 60 ˚C in CD_3CN, the -SH resonances disappear, but the phosphine resonances remain unchanged; this may indicate H/D exchange with the –SH protons and the solvent. ^{1}H NMR (C_6D_6) of *cis*-Ru(PMe_3)$_4$(SH)$_2$: -2.78 [dt, $^3J_{P\text{-}H}$ = 5, $^3J_{P\text{-}H}$ = 3, 2H of *cis*-Ru(PMe_3)$_4$(S<u>H</u>)$_2$], 1.10 [d, $^2J_{P\text{-}H}$ = 6, 18 H of *cis*-Ru(P<u>Me</u>$_3$)$_4$(SH)$_2$], 1.41 [vt, "J" = 6, 18H of *cis*-Ru(P<u>Me</u>$_3$)$_4$(SH)$_2$]. ^{1}H NMR (C_6D_6) of *trans*-Ru(PMe_3)$_4$(SH)$_2$: -4.15 [quint, $^3J_{P\text{-}H}$ = 4, 2H of *trans*-Ru(PMe_3)$_4$(S<u>H</u>)$_2$], 1.34 [br s, 36H of *trans*- Ru(P<u>Me</u>$_3$)$_4$(SH)$_2$].

4.6.10 Synthesis of W(PMe_3)$_4$(κ^1-C_α-C_4H_5O)H_3

A solution of W(PMe_3)$_4$(η^2-CH_2PMe_2)H (20 mg, 0.035 mmol) in C_6D_6 (0.7 mL) was treated with 2,3-dihydrofuran (25 mg, 0.36 mmol) and transferred to an NMR tube equipped with a J. Young valve. The solution was heated at 60 ˚C for 6 hours and monitored by ^{1}H NMR spectroscopy, thereby demonstrating its conversion to W(PMe_3)$_4$(κ^1-C_α-C_4H_5O)H_3. The solution was lyophilized, and W(PMe_3)$_4$(κ^1-C_α-C_4H_5O)H_3 was isolated as a light brown powder (12 mg, 62%). The ^{1}H, ^{31}P{^{1}H}, and ^{13}C NMR spectra have been reported by Aaron Sattler.

4.6.11 Synthesis of W(PMe_3)$_5$CO

A solution of W(PMe_3)$_4$(η^2-CH_2PMe_2)H (16 mg, 0.028 mmol) in C_6D_6 (0.7 mL) was treated with 2,5-dihydrofuran (3 mg, 0.043 mmol) and transferred to an NMR tube equipped with a J. Young valve. The solution was heated at 100 ˚C for 2 days, thereby demonstrating conversion to primarily W(PMe_3)$_5$CO. The solution was filtered and lyophilized, thereby affording W(PMe_3)$_5$CO as a light brown powder (7 mg, 49%). ^{1}H NMR (C_6D_6): 1.05 [d, $^2J_{P\text{-}H}$ = 4, 9H of W(P<u>Me</u>$_3$)$_5$CO], 1.45 [br m, 36H of W(P<u>Me</u>$_3$)$_5$CO].

4.6.12 Synthesis of $Mo(PMe_3)_3(\eta^5–C_4H_5O)H$

$Mo(PMe_3)_6$ (15 mg, 0.027 mmol) was treated with a solution of 2,5-dihydrofuran (10 mg, 0.14 mmol) in C_6D_6 (0.7 mL) and transferred to an NMR tube equipped with a J. Young valve. The solution was heated at 60 ˚C for 2h, thereby demonstrating conversion to $Mo(PMe_3)_3(\eta^5–C_4H_5O)H$, $Mo(PMe_3)_5CO$, and 2,3-dihydrofuran. By integration of the ^1H NMR spectrum, the ratio of $Mo(PMe_3)_3(\eta^5–C_4H_5O)H$: $Mo(PMe_3)_5CO$ is approximately 3:2. The sample was lyophilized, thereby affording a red powder (10 mg) that is 60 % $Mo(PMe_3)_3(\eta^5–C_4H_5O)H$ (6 mg, 66 %). Red crystals of $Mo(PMe_3)_3(\eta^5–C_4H_5O)H$ suitable for X-ray diffraction and elemental analysis were obtained from a solution in pentane at -15 ˚C. The ^1H and ^{31}P NMR spectra for this complex were reported by Aaron Sattler. Analysis calcd. for $Mo(PMe_3)_3(\eta^5–C_4H_5O)H$: C, 39.60%; H, 8.44%. Found: C, 38.50%; H, 8.08%.

4.6.13 Reaction of $Mo(PMe_3)_6$ with 2,3-Dihydrofuran and H_2

$Mo(PMe_3)_6$ (15 mg, 0.027 mmol) was treated with a solution of 2,3-dihydrofuran (9 mg, 0.13 mmol) in C_6D_6 (0.7 mL) was degassed and charged with H_2. The solution turned immediately from yellow to golden brown, and ^1H NMR spectroscopy confirmed that the $Mo(PMe_3)_6$ had converted to $Mo(PMe_3)_5H_2$. The solution was heated at 60 ˚C for two hours, thereby demonstrating the formation of tetrahydrofuran and $Mo(PMe_3)_4H_4$.

4.6.14 Synthesis of $(\kappa^1,\eta^2\text{-}CH_2CHC_6H_4O)W(PMe_3)_3(\eta^2–CH_2PMe_2)$

A solution of $W(PMe_3)_4(\eta^2\text{-}CH_2PMe_2)H$ (40 mg, 0.07 mmol) in C_6D_6 (0.7 mL) was treated with benzofuran (20 mg, 0.17 mmol) and transferred to an NMR tube equipped with a J. Young valve. The solution was heated at 40 ˚C and monitored by NMR spectroscopy, thereby demonstrating the formation of primarily $(\kappa^1,\eta^2\text{-}CH_2CHC_6H_4O)W(PMe_3)_3(\eta^2–CH_2PMe_2)$. The solution was lyophilized, redissolved in pentane, and placed at -15 ˚C, thereby depositing yellow-green crystals of $(\kappa^1,\eta^2\text{-}CH_2CHC_6H_4O)W(PMe_3)_3(\eta^2–CH_2PMe_2)$ (2mg, 5%). Analysis Calcd. for $(\kappa^1,\eta^2\text{-}CH_2CHC_6H_4O)W(PMe_3)_3(\eta^2–CH_2PMe_2)$:

C, 39.62%; H, 6.98%. Found: C, 40.39%; H, 6.80%. ^{1}H NMR (C_6D_6): 0.70 [m, 1H of W(η^2-C$\underline{H}_2$PMe$_2$)], 0.90 [signal located by COSY, 1H of W(η^2-C$\underline{H}_2$PMe$_2$)], 0.92 [d, $^2J_{P\text{-}H}$ = 8, 3H of W(η^2-CH$_2$P$\underline{Me}_2$)], 1.00 [d, $^2J_{P\text{-}H}$ = 8, 3H of W(η^2-CH$_2$P$\underline{Me}_2$)], 1.02 [signal located by COSY, 1H of (κ^1,η^2-C$\underline{H}_2$CHC$_6$H$_4$O)], 1.03 [br m, 9H of W(P$\underline{Me}_3$)$_3$], 1.18 [d, $^2J_{P\text{-}H}$ = 7, 9H of W(P$\underline{Me}_3$)$_3$], 1.23 [d, $^2J_{P\text{-}H}$ = 6, 9H of 9H of W(P$\underline{Me}_3$)$_3$], 1.98 [m, 1H of (κ^1,η^2-CH$_2$C$\underline{H}$C$_6$H$_4$O)], 3.83 [m, 1H of (κ^1,η^2-C$\underline{H}_2$CHC$_6$H$_4$O)], 6.59 [d, $^3J_{H\text{-}H}$ = 8, 1H of (κ^1,η^2-CH$_2$CHC$_6\underline{H}_4$O)], 6.71 [dt, $^3J_{H\text{-}H}$ = 7, $^4J_{H\text{-}H}$ = 1, 1H of (κ^1,η^2-CH$_2$CHC$_6\underline{H}_4$O)], 7.05 [dt, $^3J_{H\text{-}H}$ = 8, $^4J_{H\text{-}H}$ = 2, 1H of (κ^1,η^2-CH$_2$CHC$_6\underline{H}_4$O)], 7.37 [dd, $^3J_{H\text{-}H}$ = 7, $^4J_{H\text{-}H}$ = 2, 1H of (κ^1,η^2-CH$_2$CHC$_6\underline{H}_4$O)]. ^{31}P{^{1}H} NMR (C_6D_6) -83.9 [dt, $^2J_{P\text{-}P}$ = 22, $^2J_{P\text{-}P}$ = 5, $^1J_{W\text{-}P}$ = 186, 1P of W(η^2-CH$_2\underline{P}$Me$_2$)], -30.4 [ddd, $^2J_{P\text{-}P}$ = 97, $^2J_{P\text{-}P}$ = 31, $^2J_{P\text{-}P}$ = 5, 1P of W(P$\underline{Me}_3$)$_3$], -28.9 [dt, $^2J_{P\text{-}P}$ = 31, $^2J_{P\text{-}P}$ = 22, 1P of W(P$\underline{Me}_3$)$_3$], -27.0 [dd, $^2J_{P\text{-}P}$ = 97, $^2J_{P\text{-}P}$ = 31, 1P of W(P$\underline{Me}_3$)$_3$].

4.6.15 Synthesis of (κ^1,η^2-CH$_2$CHC$_6$H$_4$O)Mo(κ^1-*C*$_\alpha$-CCHOC$_6$H$_4$)(PMe$_3$)$_3$

Mo(PMe$_3$)$_6$ (20 mg, 0.036 mmol) was treated with a solution of benzofuran (10 mg, 0.08 mmol) in pentane (0.8 mL). The reaction was stirred for 2 days at room temperature, after which point (κ^1,η^2-CH$_2$CHC$_6$H$_4$O)Mo(κ^1-*C*$_\alpha$-CCHOC$_6$H$_4$)(PMe$_3$)$_3$ was obtained as a reddish-brown precipitate (5 mg, 24 %). Orange crystals of (κ^1,η^2-CH$_2$CHC$_6$H$_4$O)Mo(κ^1-*C*$_\alpha$-CCHOC$_6$H$_4$)(PMe$_3$)$_3$ co-crystallized with benzofuran were obtained from a solution in pentane which contained benzofuran at -15 ˚C. ^{1}H NMR (C_6D_6): -40.85 [1H], -33.71 [1H], -10.77 [9H of Mo(P$\underline{Me}_3$)$_3$], -5.71 [9H of Mo(P$\underline{Me}_3$)$_3$], 0.97 [1H], 1.80 [1H], 8.66 [9H of [9H of Mo(P$\underline{Me}_3$)$_3$], 12.49 [1H], 13.17 [1H], 22.31 [1H], 44.60 [1H] (4H not observed).

4.6.16 Synthesis of (κ^1,η^2-CH$_2$CHC$_6$H$_4$O)Mo(PMe$_3$)$_3$(η^2–CH$_2$PMe$_2$)

Mo(PMe$_3$)$_6$(30 mg, 0.054 mmol) was treated with a solution of benzofuran (8 mg, 0.068 mmol) in C_6D_6 (0.7 mL). The solution was transferred to an NMR tube equipped with a J. Young valve and heated at 60 ˚C for 1 day, thereby demonstrating conversion to (κ^1,η^2-CH$_2$CHC$_6$H$_4$O)Mo(PMe$_3$)$_3$(η^2–CH$_2$PMe$_2$). The solution was lyophilized, redissolved in pentane, and placed at -15 ˚C, thereby depositing dark orange crystals of

(κ^1,η^2-$CH_2CHC_6H_4O$)$Mo(PMe_3)_3(\eta^2$–CH_2PMe_2) (1.3 mg, 5%). Analysis calc. for (κ^1,η^2-$CH_2CHC_6H_4O$)$Mo(PMe_3)_3(\eta^2$–CH_2PMe_2): C, 46.34%; H, 8.17 %. Found: C, 45.52%; H, 6.75%. ^{1}H NMR (C_6D_6): 0.26 [m, 1H of Mo(η^2-C$\underline{H}_2$PMe$_2$)], 0.44 [m, 1H of Mo(η^2-C$\underline{H}_2$PMe$_2$)], 0.78 [d, $^2J_{P\text{-}H}$ = 8, 3H of Mo(η^2-CH$_2$P$\underline{Me}_2$)], 0.84 [d, $^2J_{P\text{-}H}$ = 8, 3H of Mo(η^2-CH$_2$P$\underline{Me}_2$)], 0.92 [br d, $^2J_{P\text{-}H}$ = 5, 9H of Mo(P$\underline{Me}_3$)$_3$], 1.10 [br d, $^2J_{P\text{-}H}$ = 4, 9H of Mo(P$\underline{Me}_3$)$_3$], 1.16 [d, $^2J_{P\text{-}H}$ = 7, 9H of Mo(P$\underline{Me}_3$)$_3$], 1.64 [m, 1H of (κ^1,η^2-C$\underline{H}_2$CHC$_6$H$_4$O)], 2.31 [m, 1H of (κ^1,η^2-C$\underline{H}_2$CHC$_6$H$_4$O)], 4.19 [m, 1H of (κ^1,η^2-CH$_2$C$\underline{H}$C$_6$H$_4$O)], 6.60 [d, $^3J_{H\text{-}H}$ = 8, 1H of (κ^1,η^2-CH$_2$CHC$_6\underline{H}_4$O)], 6.68 [t, $^3J_{P\text{-}H}$ = 7, 1H of (κ^1,η^2-CH$_2$CHC$_6\underline{H}_4$O)], 7.07 [dt, $^3J_{P\text{-}H}$ = 8, $^4J_{P\text{-}H}$ = 2, 1H of (κ^1,η^2-CH$_2$CHC$_6\underline{H}_4$O)], 7.34 [dd, $^3J_{H\text{-}H}$ = 7, $^4J_{H\text{-}H}$ = 2, 1H of (κ^1,η^2-CH$_2$CHC$_6\underline{H}_4$O)]. ^{31}P{^{1}H} NMR (C_6D_6) = -47.3 [dt, $^2J_{P\text{-}P}$ = 26, $^2J_{P\text{-}P}$ = 15, 1P of Mo(η^2-CH$_2\underline{P}$Me$_2$)], -7.0 [dt, $^2J_{P\text{-}P}$ = 38, $^2J_{P\text{-}P}$ = 26, 1P of Mo($\underline{P}$Me$_3$)$_3$], 2.4 [ddd, $^2J_{P\text{-}P}$ = 107, $^2J_{P\text{-}P}$ = 38, $^2J_{P\text{-}P}$ = 15, 1P of Mo($\underline{P}$Me$_3$)$_3$], 6.0 [ddd, $^2J_{P\text{-}P}$ = 107, $^2J_{P\text{-}P}$ = 38, $^2J_{P\text{-}P}$ = 15, 1P of Mo($\underline{P}$Me$_3$)$_3$]. ^{1}H-^{13}C HSQC (C_6D_6): 8.12 [1C of Mo(η^2-$\underline{C}$H$_2$PMe$_2$)], 17.7 [1C of Mo(η^2-CH$_2$P$\underline{Me}_2$)], 18.3 [1C of Mo(η^2-CH$_2$P$\underline{Me}_2$)], 18.3 [1C of Mo(P$\underline{Me}_3$)$_3$], 19.6 [1C of Mo(P$\underline{Me}_3$)$_3$], 19.9 [1C of Mo(P$\underline{Me}_3$)$_3$], 45.81 [1C of (κ^1,η^2-$\underline{C}$H$_2$CHC$_6$H$_4$O)], 60.7 [1C of (κ^1,η^2-CH$_2\underline{C}$HC$_6$H$_4$O)], 111.5 [1C of (κ^1,η^2-CH$_2$CH$\underline{C}_6$H$_4$O)], 115.7 [1C of (κ^1,η^2-CH$_2$CH$\underline{C}_6$H$_4$O)], 124.3 [1C of (κ^1,η^2-CH$_2$CH$\underline{C}_6$H$_4$O)], 125.4 [1C of (κ^1,η^2-CH$_2$CH$\underline{C}_6$H$_4$O)].

4.6.17 Structural characterization of $Mo(PMe_3)_4(ONp)_2$

$Mo(PMe_3)_6$ (10 mg, 0.018 mmol) was treated with a solution of neopentyl alcohol (6mg, 0.068 mmol) in C_6D_6 (0.7 mL) and transferred to an NMR tube equipped with a J. Young valve. The solution was heated at 60 ˚C for 2 hours, thereby demonstrating the formation of $Mo(PMe_3)_4(ONp)_2$. The solution was lyophilized, redissolved in pentane, and placed at -15 ˚C, thereby depositing yellow-green crystals of $Mo(PMe_3)_4(ONp)_2$ suitable for X-ray diffraction. ^{1}H NMR (C_6D_6): -2.17 [9H of Mo(OCH$_2$C$\underline{Me}_3$)$_2$], 0.80 [9H of Mo(OCH$_2$C$\underline{Me}_3$)$_2$] 0.93 [36H of Mo(P$\underline{Me}_3$)$_4$], 2.68 [4H of Mo(OC$\underline{H}_2$CMe$_3$)]. Peaks are tentatively assigned.

4.6.18 Structural characterization of $W(PMe_3)_4H_3(ONp)$

$W(PMe_3)_4(\eta^2\text{-}CH_2PMe_2)H$ (13 mg, 0.023 mmol) was treated with a solution of neopentyl alcohol (8 mg, 0.091 mmol) in C_6D_6 (0.7 mL) and transferred to an NMR tube equipped with a J. Young valve. The solution was heated at 80 ˚C for 1.5 days and monitored by NMR spectroscopy, thereby demonstrating the conversion to $W(PMe_3)_4H_3(ONp)$. The solution was lyophilized, redissolved in pentane, and placed at -15 ˚C, thereby depositing crystals of $W(PMe_3)_4H_3(ONp)$ suitable for X-ray diffraction.

4.6.19 Structural characterization of $[Mo(PMe_3)_4(\equiv CPMe_2Ph)I]I$

A solution of $Mo(PMe_3)_4(\eta^2\text{-}CH_2PMe_2)H$ (5 mg, 0.01 mmol) in C_6D_6 (0.7 mL) was treated with PhI (5 mg, 0.02 mmol) and monitored by NMR spectroscopy at room temperature for 3 days. A paramagnetically shifted peak at -8.93 was observed, most likely corresponding to $Mo(PMe_3)_4I_2$. Gray precipitate was observed to form along with purple crystals of $[Mo(PMe_3)_4(\equiv CPMe_2Ph)I]I$ suitable for X-ray diffraction.

4.6.20 Synthesis of $W(PMe_3)_4(sebenzim^{Me})H$

(*i*) A solution of $W(PMe_3)_4(\eta^2\text{-}CH_2PMe_2)H$ (10 mg, 0.018 mmol) in pentane (0.7 mL) was treated with 2-seleno-1-methyl-benzimidazole (4 mg, 0.019 mmol) and stirred for 10 minutes at room temperature. The reaction solution was filtered and placed at -15 ˚C, thereby affording red crystals of $W(PMe_3)_4(sebenzim^{Me})H$ suitable for X-ray diffraction.

(*ii*) A solution of $W(PMe_3)_4(\eta^2\text{-}CH_2PMe_2)H$ (5 mg, 0.009 mmol) in C_6D_6 (0.7 mL) was treated with 2-seleno-1-methyl-benzimidazole (5 mg, 0.024 mmol) and monitored at room temperature by ^1H NMR spectroscopy, thereby indicating the quantitative formation of $W(PMe_3)_4(sebenzim^{Me})H$ within 20 minutes. ^1H NMR (C_6D_6): -7.96 [tt, $^2J_{P\text{-}H}$ = 82, $^2J_{P\text{-}H}$ = 24], 1.31 [br s, 18H of $W(P\underline{Me}_3)_4$], 1.60 [d, $^2J_{P\text{-}H}$ = 6, 9H of $W(P\underline{Me}_3)_4$], 1.80 [d, $^2J_{P\text{-}H}$ = 6, 9H of $W(P\underline{Me}_3)_4$], 3.03 [s, 3H of sebenzim$^{\underline{Me}}$], 6.89[d, partially obscured by free H(sebenzim^{Me}) signal, 1H of $C_6\underline{H}_4$], 6.96 [t, $^3J_{P\text{-}H}$ = 8, 1H of $C_6\underline{H}_4$], 7.12 [t, $^3J_{P\text{-}H}$ = 8, 1H of $C_6\underline{H}_4$], 7.47 [d, $^3J_{P\text{-}H}$ = 8, 1H of $C_6\underline{H}_4$].

4.6.21 Synthesis of *cis*-Ir(SiH_3)(CO)(Cl)(PPh_3)$_2$

A suspension of IrCl(CO)(PPh_3)$_2$ (8 mg, 0.01 mmol) in C_6D_6 (0.7 mL) in an NMR tube equipped with a J. Young valve was degassed and charged with SiH_4. All of the solid was observed to immediately dissolve, and the solution became instantly colorless. A colorless precipitate was observed to form after the course of several hours at room temperature. The solution was decanted from this precipitate, and crystals of *cis*-Ir(SiH_3)(CO)(Cl)(PPh_3)$_2$ suitable for X-ray diffraction were obtained by slow evaporation of the solvent at room temperature. ^{1}H NMR (C_6D_6): -6.32 [t quart, $^2J_{P\text{-}H}$ = 15, $^3J_{H\text{-}Ir\text{-}Si\text{-}H}$ = 3, 1H of Ir<u>H</u>], 2.79 [dt, $^3J_{P\text{-}H}$ = 5, $^3J_{H\text{-}Ir\text{-}Si\text{-}H}$ = 3, $^1J_{Si\text{-}H}$ = 187, 3H of Ir(SiH_3)], 6.95 [t, $^3J_{H\text{-}H}$ = 7, 6H of Ir(PPh_3)$_2$], 7.02 [t, $^3J_{H\text{-}H}$ = 7, 12H of Ir(PPh_3)$_2$], 7.94 [dd, $^3J_{H\text{-}H}$ = 7, $^3J_{P\text{-}H}$ = 7, 12H of Ir(PPh_3)$_2$]. ^{31}P{^{1}H} NMR: 7.9 [s, 2P of Ir(<u>P</u>Ph_3)$_2$].

4.6.22 Synthesis of *cis*-Ir(GeH_3)(CO)(Cl)(PPh_3)$_2$ A solution of IrCl(CO)(PPh_3)$_2$ (3 mg, 0.004 mmol) in C_6D_6 (0.7 mL) in an NMR tube equipped with a J. Young valve was degassed and charged with SiH_4, thereby resulting in an immediate change of the solution from yellow to colorless. The product was examined by ^{1}H and ^{31}P{^{1}H} NMR spectroscopy, thereby demonstrating the formation of two isomeric species assigned as *cis*-Ir(GeH_3)(CO)(Cl)(PPh_3)$_2$ (H *trans* to CO, **B**) and *cis*-Ir(GeH_3)(CO)(Cl)(PPh_3)$_2$ (H *trans* to Cl, **A**). ^{1}H NMR (C_6D_6): -17.9 [t, $^2J_{P\text{-}H}$ = 12, 1H of Ir<u>H</u> (**A**)], -6.89 [t quart, $^2J_{P\text{-}H}$ = 15, $^3J_{H\text{-}Ir\text{-}Ge\text{-}H}$ = 3, 1H of Ir<u>H</u> (**B**)], 2.21 [dt, $^3J_{P\text{-}H}$ = 5, $^3J_{H\text{-}Ir\text{-}Ge\text{-}H}$ = 3, 3H of Ir(Ge<u>H</u>$_3$) (**B**)], 3.23 [t, $^3J_{P\text{-}H}$ = 8, 3H of Ir(Ge<u>H</u>$_3$) (**A**)], 6.93 [m, 6H of Ir(P<u>Ph</u>$_3$)$_2$ (**A** and **B**)], 7.00 [m, 12H of Ir(P<u>Ph</u>$_3$)$_2$ (**A** and **B**)], 7.93 [m, 12H of Ir(P<u>Ph</u>$_3$)$_2$ (**B**)], 8.00 [m, 12H of Ir(P<u>Ph</u>$_3$)$_2$ (**A**)]. ^{31}P{^{1}H} NMR (C_6D_6): -4.60 [s, 1P of Ir(<u>P</u>Ph_3) (**A**)], -4.55 [s, 1P of Ir(<u>P</u>Ph_3) (**A**)], 6.9 [s, 2P of Ir(<u>P</u>Ph_3) (**B**).

4.6.23 Reactions of $IrH(CO)(Cl)(EH_3)(PPh_3)_2$ (E = Si, Ge) with H_2

Suspensions of $IrH(CO)(Cl)(EH_3)(PPh_3)_2$ (5 mg) in C_6D_6 in NMR tubes equipped with J. Young valves were degassed and charged with H_2. Conversion to $IrH_2Cl(CO)(PPh_3)_2$ was observed in both cases, and additional transformations were observed when the samples were heated at 60 ˚C.

4.7 Crystallographic Data

Table 1. Crystal, intensity collection and refinement data

	$Ru(PMe_3)_4(\kappa^2\text{-}S_2\text{-}CS_3)$	**$Ru(PMe_3)_4(SH)_2$**
lattice	Orthorhombic	Orthorhombic
formula	$C_{13}H_{36}P_4RuS_3$	$C_{24}H_{50}P_4RuS_2$
formula weight	513.55	627.71
space group	*Pnma*	*Pnma*
a / Å	18.484(7)	18.035(2)
b / Å	13.515(5)	17.915(2)
c / Å	9.128(3)	9.5219(11)
α / °	90	90
β / °	90	90
γ / °	90	90
V / Å^3	2280.2(14)	3076.5(6)
Z	4	4
temperature (K)	125(2)	170(2)
radiation (λ, Å)	0.71073	0.71073
ρ (calcd.), g cm^{-3}	1.496	1.355
μ (Mo Kα), mm^{-1}	1.236	0.865
θ max, deg.	30.56	30.49
no. of data collected	35085	47507
no. of data	3621	4826
no. of parameters	129	192
R_1 [$I > 2\sigma(I)$]	0.0588	0.0453
wR_2 [$I > 2\sigma(I)$]	0.0932	0.1109
R_1 [all data]	0.1457	0.0760
wR_2 [all data]	0.1187	0.1265
GOF	1.002	1.035

Table 1 cont. Crystal, intensity collection and refinement data

	$Mo(PMe_3)_3(\eta^5–C_4H_5O)H$	$(\kappa^1,\eta^2\text{-}CH_2CHC_6H_4O)Mo(\kappa^1\text{-}C_\alpha\text{-}CCHOC_6H_4)(PMe_3)_3$
lattice	Monoclinic	Monoclinic
formula	$C_{13}H_{33}MoOP_3$	$C_{33}H_{45}MoO_3P_3$
formula weight	394.24	678.54
space group	$P2_1/n$	$P2_1/c$
a / Å	14.4254(9)	17.350(3)
b / Å	17.4887(11)	12.0821(19)
c / Å	16.4131(10)	17.627(3)
α / °	90	90
β / °	109.956(1)	116.734(2)
γ / °	90	90
V / Å^3	3892.1(4)	3300.0(9)
Z	8	4
temperature (K)	150(2)	150(2)
radiation (λ, Å)	0.71073	0.71073
ρ (calcd.), g cm^{-3}	1.346	1.366
μ (Mo Kα), mm^{-1}	0.911	0.574
θ max, deg.	30.65	30.68
no. of data collected	62233	52768
no. of data	11998	10216
no. of parameters	441	451
R_1 [$I > 2\sigma(I)$]	0.0472	0.0449
wR_2 [$I > 2\sigma(I)$]	0.0986	0.0938
R_1 [all data]	0.0977	0.0868
wR_2 [all data]	0.1197	0.1105
GOF	1.022	1.016

Table 1 cont. Crystal, intensity collection and refinement data

	$Mo(PMe_3)_4(ONp)_2$	**$W(PMe_3)_4H_3(ONp)$**
lattice	Triclinic	Orthorhombic
formula	$C_{22}H_{58}MoO_2P_4$	$C_{17}H_{50}OP_4W$
formula weight	574.50	578.30
space group	*P-1*	*Pbca*
a/Å	9.7033(13)	17.214(3)
b/Å	9.8850(13)	17.169(3)
c/Å	17.940(2)	17.834(4)
α/°	100.961(2)	90
β/°	92.671(2)	90
γ/°	110.635(2)	90
V/Å^3	1568.8(3)	5270.8(18)
Z	2	8
temperature (K)	150(2)	150(2)
radiation (λ, Å)	0.71073	0.71073
ρ (calcd.), g cm^{-3}	1.216	1.458
μ (Mo Kα), mm^{-1}	0.637	4.629
θ max, deg.	30.54	32.80
no. of data collected	48109	87902
no. of data	9518	9482
no. of parameters	311	235
R_1 [$I > 2\sigma(I)$]	0.0404	0.0282
wR_2 [$I > 2\sigma(I)$]	0.0918	0.0488
R_1 [all data]	0.0514	0.0610
wR_2 [all data]	0.0970	0.0584
GOF	1.056	1.036

Table 1 cont. Crystal, intensity collection and refinement data

	[Mo(PMe$_3$)$_4$(≡CPMe$_2$Ph)I]I	**IrH(CO)(Cl)(SiH$_3$)(PPh$_3$)$_2$**
lattice	Monoclinic	Orthorhombic
formula	$C_{21}H_{47}I_2MoP_5$	$C_{43}H_{40}ClIrOP_2Si$
formula weight	804.18	890.43
space group	$P2_1/n$	$P2_12_12_1$
a / Å	10.616(3)	11.4205(15)
b / Å	19.920(6)	17.117(2)
c / Å	14.912(5)	19.045(3)
α / °	90	90
β / °	92.606(5)	90
γ / °	90	90
V / Å^3	3150.5(18)	3723.0(9)
Z	4	4
temperature (K)	150(2)	130(2)
radiation (λ, Å)	0.71073	0.71073
ρ (calcd.), g cm^{-3}	1.695	1.589
μ (Mo Kα), mm^{-1}	2.638	3.810
θ max, deg.	29.57	30.684
no. of data collected	55498	59511
no. of data	8748	11440
no. of parameters	263	447
R_1 [$I > 2\sigma(I)$]	0.0746	0.0497
wR_2 [$I > 2\sigma(I)$]	0.1544	0.0869
R_1 [all data]	0.1189	0.0844
wR_2 [all data]	0.1726	0.0989
abs. struct. param.	---	-0.017(9)
GOF	1.029	1.007

Table 1 cont. Crystal, intensity collection and refinement

	$W(PMe_3)_4(sebenzim^{Me})H$
lattice	Monoclinic
formula	$C_{40}H_{88}N_4P_8Se_2W_2$
formula weight	1398.52
space group	$P2_1/c$
a / Å	16.9276(18)
b / Å	9.5318(10)
c / Å	34.520(4)
α / °	90
β / °	90.262(2)
γ / °	90
V / Å^3	5569.7(10)
Z	4
temperature (K)	130(2)
radiation (λ, Å)	0.71073
ρ (calcd.), g cm^{-3}	1.668
μ (Mo Kα), mm^{-1}	5.695
θ max, deg.	30.73
no. of data collected	88925
no. of data	17280
no. of parameters	539
R_1 [$I > 2\sigma(I)$]	0.0731
wR_2 [$I > 2\sigma(I)$]	0.1056
R_1 [all data]	0.1853
wR_2 [all data]	0.1355
GOF	1.000

4.8 Computational Data

Table 2. Cartesian coordinates for geometry optimized structures

cis-$Ru(PMe_3)_4(SH)_2$

-2736.06389287810 Hartrees

Atom	x	y	z
Ru	0.753797458	4.482241379	2.855737029
S	-1.555609177	4.49446538	3.898015758
S	-0.297866665	4.501639391	0.552072491
P	0.449571541	2.04988408	2.544297621
P	2.94621082	4.397983951	1.933169181
P	1.433148904	4.540562739	5.152397229
C	1.133244118	0.754176632	3.700475498
H	0.626824417	0.802662045	4.665497883
H	2.204534545	0.899709213	3.86284407
H	0.97791455	-0.244175802	3.27837701
C	-1.302023361	1.466964695	2.454788569
H	-1.802025326	1.997623073	1.641877375
H	-1.814925494	1.696288675	3.389660621
H	-1.328880878	0.389940652	2.258535367
C	1.069807679	1.334474835	0.942276436
H	0.731563755	0.297710937	0.844958337
H	2.160837667	1.343002655	0.889799201
H	0.66377672	1.927625094	0.120906075
C	4.064163777	3.000893976	2.460578964
H	3.615743686	2.03271561	2.233989677
H	4.229386374	3.049825092	3.54061776
H	5.034765837	3.062621457	1.956825994
C	3.093399228	4.276665542	0.086901084

H	2.577217457	3.386775581	-0.275733566
H	2.608098397	5.142735524	-0.368993352
C	0.376231791	5.57519168	6.279658039
H	0.789137624	5.573624024	7.293998483
H	-0.635130783	5.164075332	6.29803877
H	0.308449244	6.604323001	5.92500614
C	3.111468159	5.18040208	5.654916706
H	-1.573396774	4.75026072	0.911262757
H	-2.3035263	4.160110543	2.82882454
C	4.167269044	5.779107734	2.221863561
H	3.791357832	6.721515255	1.820805178
H	4.35277503	5.909270053	3.289403142
H	5.118077149	5.551922416	1.728419698
H	4.142822348	4.239342522	-0.224770899
C	1.418738139	2.987722195	6.171847318
H	1.643216678	3.216964505	7.219049916
H	0.424935131	2.538053587	6.114342993
H	2.155727054	2.272140543	5.80293023
H	3.244134023	6.208598105	5.311307445
H	3.218781281	5.162651199	6.744598854
H	3.905093989	4.56529214	5.222429249
P	0.6269519	6.899553289	2.620915827
C	1.60583631	8.058104056	3.712008806
H	1.324214497	7.948945429	4.761103689
H	2.675371212	7.852936399	3.620770821
H	1.42785372	9.097732926	3.41695603
C	-1.054799802	7.644402481	2.786123907
H	-1.70732432	7.199653342	2.032206977

H	-1.476543603	7.405972388	3.762881138
H	-1.005312983	8.728606766	2.638105054
C	1.111654754	7.606732701	0.972971547
H	0.914106771	8.683724482	0.954191342
H	2.172057302	7.445710717	0.765312631
H	0.529555317	7.101490505	0.20065545

trans-$Ru(PMe_3)_4(SH)_2$

-2736.06722196854 Hartrees

Atom	x	y	z
Ru	0.553470235	4.259795079	2.944135122
S	0.846857194	1.763376902	3.246542271
S	0.300746184	6.747959408	2.546197539
P	-1.71280226	4.500280897	3.756510857
P	2.756713253	4.66433436	2.0325953
P	1.430095486	4.299012521	5.199293555
C	-1.978704031	5.704543108	5.147373052
H	-1.610786132	6.676705747	4.81164014
H	-1.442361652	5.417951483	6.052234471
H	-3.044882548	5.783055723	5.383798006
C	-2.945052972	5.263706095	2.593739232
H	-3.126946566	4.642568366	1.716587997
H	-2.535407862	6.223508777	2.270172707
H	-3.898552134	5.426767801	3.106871339
C	-2.668353183	3.028332491	4.373899177
H	-3.675073761	3.312655693	4.698341756
H	-2.142418192	2.567740982	5.213893804
H	-2.749869631	2.279708834	3.581889965

C	3.9582413	3.264699536	1.814829385
H	3.52286145	2.504690053	1.161996977
H	4.15402762	2.792638712	2.78037956
H	4.904406945	3.610425542	1.38446284
C	2.837818506	5.489604149	0.369060197
H	2.416146787	4.873621063	-0.424851616
H	2.264690824	6.417265321	0.439704365
C	1.706357438	5.908350851	6.091006342
H	2.111927024	5.744234525	7.095079931
H	0.763830433	6.455193214	6.174787818
H	2.403305676	6.531657643	5.525224915
C	3.058844973	3.449872432	5.482832304
H	0.72710098	7.270967732	3.714479548
H	-0.34361415	1.394310986	3.762992109
C	3.806636724	5.919842632	2.914621509
H	3.246196137	6.857404819	2.9324339
H	4.036955572	5.627407969	3.938883568
H	4.74752432	6.071514219	2.375690582
H	3.877310934	5.720428518	0.113792985
C	0.481324342	3.343727328	6.480893726
H	1.006536176	3.371064445	7.441202418
H	-0.526920234	3.732316645	6.625404794
H	0.415559616	2.309741751	6.134850946
H	3.878212177	3.93853541	4.955321584
H	3.295610082	3.432895553	6.551824167
H	2.960058833	2.426152946	5.113966207
P	-0.250035045	3.573807675	0.769428768
C	-0.788300827	4.84018508	-0.478191527

H	-1.607147632	5.436328046	-0.068942489
H	0.038298154	5.522366908	-0.689756362
H	-1.116200674	4.370711311	-1.412023301
C	-1.68685412	2.394501969	0.744162522
H	-1.390328359	1.508916603	1.310895283
H	-2.583811342	2.817452832	1.19596729
H	-1.919348878	2.103503747	-0.285378731
C	0.884186714	2.506829454	-0.245484993
H	0.371294981	2.168257032	-1.151726311
H	1.79604038	3.026378496	-0.538887374
H	1.150669088	1.642497908	0.367615056

cis-$IrH(SiH_3)(CO)(Cl)(PPh_3)_2$ (**A**)

-3042.89300853456 Hartrees

Atom	x	y	z
C	13.881313	-6.751043349	1.748774101
C	11.55271394	-9.703181827	3.575549246
C	10.44011991	-10.40702412	4.06454381
C	10.37560916	-11.79622437	3.95248779
C	11.41349789	-12.50103448	3.342961321
C	12.51742234	-11.80968403	2.843624176
C	12.58839102	-10.42219166	2.96131749
C	10.70313743	-7.343219768	2.118796919
C	10.77902616	-6.006414328	1.689628666
C	10.06840865	-5.586124761	0.565096742
C	9.284091081	-6.488601516	-0.155199101
C	9.210391603	-7.817428409	0.261161804
C	9.910639376	-8.24354572	1.391474703

C	10.51489098	-7.386459261	5.017663269
C	10.59831159	-8.043664436	6.256824401
C	9.783379723	-7.656832862	7.31954142
C	8.876123537	-6.608680819	7.164930137
C	8.788172985	-5.95041777	5.939664475
C	9.600537749	-6.333417556	4.87315378
C	16.23344305	-4.784081319	5.359834546
C	16.62548482	-5.327353684	6.5949652
C	16.73925395	-4.51485207	7.722779339
C	16.46134804	-3.150348897	7.640196106
C	16.07087342	-2.603872648	6.418321637
C	15.95597794	-3.411056189	5.286934412
C	16.33409569	-4.743994876	2.450430121
C	15.30386989	-3.911807972	1.976658642
C	15.53199068	-3.04787789	0.905468151
C	16.77973711	-3.007814371	0.281249402
C	17.80312544	-3.835575345	0.741471417
C	17.58612574	-4.695306008	1.820168964
C	17.45705566	-7.001225796	3.891338323
C	17.3747361	-8.240916045	3.240929932
C	18.48401939	-9.083782751	3.172850275
C	19.69261664	-8.704337804	3.757593864
C	19.78691014	-7.471219566	4.403787136
C	18.68097496	-6.622719868	4.467313517
Cl	12.79432337	-4.728278544	4.356132843
H	9.623198621	-9.872773274	4.537667514
H	9.511242766	-12.32598959	4.343543366
H	11.3623498	-13.5831419	3.258821899

H	13.33018377	-12.35012487	2.366332904
H	13.45486281	-9.892863888	2.580498376
H	11.38577363	-5.296412429	2.246223069
H	10.13385696	-4.548032752	0.250570007
H	8.738134467	-6.159737389	-1.035155263
H	8.607588617	-8.531202164	-0.293942063
H	9.838856347	-9.281495963	1.697229058
H	11.29539068	-8.861611266	6.396171149
H	9.861734746	-8.177985718	8.269682167
H	8.242293961	-6.307386427	7.994527704
H	8.086492363	-5.131435	5.807997733
H	9.517380503	-5.80611241	3.930867392
H	16.84428178	-6.385160223	6.682051842
H	17.04426618	-4.955373803	8.667994115
H	16.54720472	-2.519498601	8.520500297
H	15.84843048	-1.543338661	6.339849994
H	15.646027	-2.964245806	4.350495945
H	14.32758735	-3.937800786	2.454606035
H	14.72546163	-2.408998946	0.555800832
H	16.95129934	-2.340756609	-0.559033082
H	18.77733449	-3.818468018	0.260260741
H	18.39614933	-5.331435073	2.159519989
H	16.43618439	-8.54839335	2.793208005
H	18.39845467	-10.04152513	2.666964601
H	20.55404202	-9.364637729	3.711855195
H	20.72322115	-7.16497662	4.862161815
H	18.77224345	-5.66649702	4.971720656
H	14.51042212	-8.359132325	3.507668755

Ir	13.85043427	-6.930918225	3.685355543
O	13.99925166	-6.861990691	0.606267944
P	11.63964703	-7.861224578	3.633189593
P	15.99657149	-5.870322095	3.884824147
Si	14.12239459	-7.79003007	5.976460505
H	15.54581713	-8.118048524	6.300119082
H	13.64507948	-6.917404019	7.086852687
H	13.4449316	-9.109394932	6.177522768

cis-$IrH(SiH_3)(CO)(Cl)(PPh_3)_2$ (**B**)

-3042.89895749938 Hartrees

Atom	x	y	z
Ir	3.468649698	-5.486707167	-14.5622031
Cl	1.37626713	-4.561481481	-13.41574103
Si	5.268959474	-5.635922115	-16.14756131
P	4.675677176	-4.025403248	-13.08991008
P	1.941084195	-6.714521768	-15.95039002
O	4.330376649	-8.017393852	-13.02556766
C	3.940800501	-7.060612789	-13.54461621
C	6.493765644	-3.865635578	-13.3786635
C	7.115474822	-2.636774551	-13.63109826
H	6.527526004	-1.725895838	-13.66487491
C	8.495209354	-2.573550619	-13.844285
H	8.961451822	-1.612445943	-14.04329414
C	9.26965754	-3.73128668	-13.80088545
H	10.34175868	-3.679172768	-13.96780327
C	8.657184177	-4.960862375	-13.54485566
H	9.250211187	-5.870438583	-13.51182408

C	7.281214314	-5.029060243	-13.33918419
H	6.818776836	-5.993881397	-13.15046259
C	4.635054876	-4.547834905	-11.3132578
C	3.504732119	-5.191043603	-10.78462161
H	2.641468282	-5.36361924	-11.41868452
C	3.475056088	-5.572851856	-9.442826559
H	2.591692731	-6.069641626	-9.050911095
C	4.564570392	-5.320254095	-8.60892548
H	4.538453241	-5.622837522	-7.565703636
C	5.688635851	-4.674192365	-9.124772496
H	6.543522464	-4.469276398	-8.486044511
C	5.725888696	-4.290231497	-10.46540385
H	6.610923638	-3.794095261	-10.84890939
C	4.052149865	-2.294295383	-13.1001111
C	3.815116605	-1.655127167	-14.32694223
H	3.963302075	-2.19701839	-15.25493683
C	3.369803871	-0.335507767	-14.35946922
H	3.189147184	0.14659186	-15.31632728
C	3.140806435	0.35791916	-13.16920906
H	2.780817322	1.382858001	-13.19583647
C	3.366961555	-0.273295283	-11.94742961
H	3.181896975	0.256160364	-11.01688512
C	3.824558852	-1.591218898	-11.90997327
H	3.990991923	-2.071891701	-10.95224985
C	0.594797304	-5.692363942	-16.67499061
C	0.888097734	-4.414734443	-17.1740037
H	1.890825119	-4.01458357	-17.07266843
C	-0.106416094	-3.649606254	-17.77940087

H	0.134609397	-2.660912135	-18.16016737
C	-1.408137432	-4.143760611	-17.88187608
H	-2.185434957	-3.54156242	-18.34450137
C	-1.708780561	-5.409341429	-17.37986608
H	-2.721236352	-5.797877901	-17.4476654
C	-0.713310866	-6.183470381	-16.782495
H	-0.961322362	-7.165685141	-16.39489859
C	1.072468397	-8.102069313	-15.07895213
C	0.667724015	-7.953789252	-13.74236879
H	0.856215514	-7.017373684	-13.22680259
C	-0.000324772	-8.990784208	-13.08985086
H	-0.306338579	-8.857984487	-12.05562154
C	-0.276119126	-10.18647908	-13.7537856
H	-0.792687221	-10.99280617	-13.24029216
C	0.115205501	-10.33937916	-15.08392742
H	-0.095822415	-11.26434437	-15.6138775
C	0.782855508	-9.306425086	-15.74354858
H	1.080368478	-9.44640319	-16.77683988
C	2.67227459	-7.58574529	-17.40206812
C	3.682927295	-8.534901749	-17.17448794
H	4.019961394	-8.741019035	-16.1624991
C	4.264392816	-9.21737081	-18.23964349
H	5.045248214	-9.94790012	-18.04785206
C	3.851415359	-8.956722936	-19.54854659
H	4.310447291	-9.484291404	-20.38009381
C	2.852755042	-8.013727786	-19.78265517
H	2.526886952	-7.804090017	-20.79784743
C	2.261679567	-7.332779403	-18.71580764

H	1.482696832	-6.603934251	-18.91199562
H	6.134108702	-4.422213155	-16.14579819
H	6.197626699	-6.791538422	-15.9417637
H	4.789383702	-5.751364918	-17.55356504
H	3.264677097	-4.213828009	-15.55439209

trans-$IrH(SiH_3)(CO)(Cl)(PPh_3)_2$ (**C**)

-3042.88125086244 Hartrees

Atom	x	y	z
Ir	3.440216996	-5.335485366	-14.68581955
Si	5.10600221	-5.057836017	-16.52401041
P	4.672132621	-4.001532745	-13.09881264
P	1.976371305	-6.748294225	-15.97337799
O	4.662908235	-7.81071075	-13.49376748
C	4.194464284	-6.852523247	-13.95588562
C	6.515096757	-4.018491817	-13.27927755
C	7.2910756	-2.885241475	-12.99011266
H	6.812442491	-1.959688042	-12.69063772
C	8.682471818	-2.933945547	-13.08847286
H	9.265698709	-2.044281356	-12.86718444
C	9.320808162	-4.113664681	-13.46831016
H	10.40390716	-4.148918256	-13.54771668
C	8.559466925	-5.248010475	-13.75017652
H	9.044176681	-6.172378662	-14.05138088
C	7.169461048	-5.200959694	-13.65937653
H	6.601960341	-6.092710765	-13.89384182
C	4.429000218	-4.6426534	-11.37541194
C	3.137720746	-4.970398109	-10.92916289

H	2.297127118	-4.868595118	-11.60787601
C	2.931022564	-5.434097554	-9.630563755
H	1.923926781	-5.678145856	-9.303217755
C	4.009934939	-5.593570012	-8.758294716
H	3.849587041	-5.967250554	-7.750748075
C	5.295637619	-5.273958227	-9.192765615
H	6.144018366	-5.396818474	-8.524935544
C	5.505254403	-4.795873377	-10.48802146
H	6.512677749	-4.549969329	-10.80495928
C	4.267375392	-2.212169361	-12.99333786
C	4.539612473	-1.393279793	-14.10195661
H	4.945160818	-1.824520929	-15.01056322
C	4.283678034	-0.025581831	-14.0405161
H	4.500335237	0.596947785	-14.90393684
C	3.739003525	0.539751025	-12.88508729
H	3.536137988	1.606304154	-12.84296625
C	3.454757437	-0.271259366	-11.78756286
H	3.031105389	0.158837953	-10.88414294
C	3.719879044	-1.641551751	-11.83732622
H	3.504261228	-2.257356301	-10.97097909
C	0.495539749	-5.948516483	-16.6967431
C	0.654834628	-4.987069893	-17.70852383
H	1.646720172	-4.716127064	-18.05179152
C	-0.461758917	-4.366034525	-18.26358317
H	-0.326912398	-3.624458265	-19.0457159
C	-1.7426709	-4.678049747	-17.80459307
H	-2.610170895	-4.183938821	-18.23376672
C	-1.90535425	-5.619495208	-16.78960296

H	-2.898754768	-5.865170215	-16.42431093
C	-0.792600261	-6.256374027	-16.23894745
H	-0.933023344	-6.991868483	-15.45432197
C	1.291951723	-8.138088735	-14.95497145
C	1.094261099	-7.992020547	-13.5743565
H	1.370295952	-7.060685267	-13.09208647
C	0.553422624	-9.034848632	-12.82106271
H	0.412675127	-8.905749717	-11.75135582
C	0.20396341	-10.23747567	-13.43349509
H	-0.210053659	-11.05125998	-12.84420801
C	0.39400781	-10.39266731	-14.80722536
H	0.126471662	-11.32679471	-15.29357927
C	0.932563645	-9.352892796	-15.56338099
H	1.078365231	-9.492415853	-16.62928539
C	2.750980473	-7.679805864	-17.37428214
C	3.947119343	-8.377201363	-17.137118
H	4.428736192	-8.325363846	-16.16680204
C	4.532422292	-9.146558437	-18.14035377
H	5.458069614	-9.677034026	-17.93557984
C	3.938881863	-9.229248039	-19.40154877
H	4.399015656	-9.824481249	-20.18518724
C	2.752495994	-8.540106801	-19.64711961
H	2.280034701	-8.596575566	-20.62406475
C	2.157974504	-7.774381993	-18.64114651
H	1.230135934	-7.253518019	-18.84910727
H	5.842114882	-3.758629065	-16.43903124
H	6.192730273	-6.090439229	-16.62408777
H	4.463251019	-5.06267521	-17.8730179

Cl	2.473120157	-3.294455	-15.69523773
H	2.167977997	-5.202973056	-13.63775742

cis-$IrH(GeH_3)(CO)(Cl)(PPh_3)_2$ (**A**)

-2757.16363485541 Hartrees

Atom	x	y	z
C	13.87633678	-6.755731878	1.784261953
C	11.54096368	-9.704178592	3.591718288
C	10.41329821	-10.4009467	4.054509883
C	10.34339511	-11.78947922	3.938030116
C	11.39104245	-12.49925698	3.351007908
C	12.51112341	-11.81433353	2.879632411
C	12.58720936	-10.42774335	3.001529363
C	10.74061331	-7.355110086	2.093117349
C	10.811019	-6.014158201	1.675541575
C	10.14728721	-5.60223029	0.520672679
C	9.418511546	-6.518253581	-0.239262653
C	9.349633057	-7.850093799	0.165951951
C	10.00194049	-8.268003366	1.32720395
C	10.47751463	-7.367930548	4.991077608
C	10.5359291	-8.010640502	6.238603584
C	9.696436738	-7.614127278	7.278182225
C	8.790206309	-6.570457308	7.091306036
C	8.727191444	-5.926507592	5.85700843
C	9.563771573	-6.319689958	4.813057302
C	16.25941345	-4.786242591	5.345285671
C	16.68244096	-5.339760575	6.565235993
C	16.8366463	-4.533598787	7.691936795

C	16.56757469	-3.166997221	7.620966668
C	16.14496153	-2.610420957	6.414971595
C	15.99043099	-3.411355805	5.284330747
C	16.29497078	-4.72922858	2.441105684
C	15.25617991	-3.892949377	1.99497233
C	15.46593903	-3.017327996	0.930146568
C	16.70327347	-2.970599675	0.2870175
C	17.73522065	-3.80204386	0.719008124
C	17.53641064	-4.673724651	1.790871901
C	17.45020051	-6.989028451	3.839904458
C	17.3583631	-8.219841063	3.174757843
C	18.47140346	-9.052347507	3.064600725
C	19.69136962	-8.66996508	3.622110734
C	19.79543335	-7.446184581	4.283750584
C	18.68552856	-6.607846899	4.388901602
Cl	12.78638502	-4.737011885	4.392846162
H	9.588705283	-9.86161711	4.508230985
H	9.466678187	-12.31492188	4.306621893
H	11.33469417	-13.58070769	3.262035241
H	13.33159372	-12.35878632	2.420450022
H	13.46479216	-9.902360567	2.641439703
H	11.38123778	-5.296824362	2.260892929
H	10.20708048	-4.561959843	0.212225285
H	8.910642665	-6.195892986	-1.144310892
H	8.788956592	-8.571570731	-0.422242747
H	9.93706235	-9.308416959	1.625855406
H	11.23111285	-8.826009497	6.402135071
H	9.754846894	-8.124091627	8.235684859

H	8.137720327	-6.261193462	7.90325204
H	8.02659874	-5.110951453	5.700418514
H	9.499485724	-5.804125791	3.862881718
H	16.89654855	-6.399588212	6.640131834
H	17.16609744	-4.979350173	8.626341228
H	16.68567481	-2.540404835	8.500768065
H	15.92978465	-1.547578222	6.348717237
H	15.65804219	-2.958701484	4.358518589
H	14.28887298	-3.9241949	2.490216213
H	14.65457212	-2.373870281	0.600714461
H	16.86086106	-2.293165669	-0.548013852
H	18.70094337	-3.777649094	0.221271139
H	18.3521549	-5.312818727	2.109701867
H	16.41084811	-8.527258749	2.746676158
H	18.38118026	-10.00312369	2.546645797
H	20.55685422	-9.321987852	3.542225396
H	20.74226463	-7.139515066	4.719730955
H	18.78300298	-5.657037902	4.902129869
H	14.5080289	-8.35717487	3.53607359
Ir	13.84460027	-6.931743402	3.701230725
O	13.99014137	-6.842418341	0.638596352
P	11.63218406	-7.862231003	3.63740387
P	15.98781561	-5.864593864	3.873950113
Ge	14.12617522	-7.814457087	6.095905098
H	15.59955611	-8.181122822	6.419809252
H	13.65859636	-6.890005384	7.242792894
H	13.39734378	-9.16737313	6.319742685

cis-$IrH(GeH_3)(CO)(Cl)(PPh_3)_2$ (**B**)

-2757.16766360078 Hartrees

Atom	x	y	z
Ir	3.438865097	-5.404754644	-14.60400795
Cl	1.373575048	-4.471275635	-13.46803205
Ge	5.324120216	-5.575695351	-16.25044639
P	4.659251527	-3.976955731	-13.10958805
P	1.897961006	-6.652948809	-15.96614113
O	4.300062169	-7.941121357	-13.07967812
C	3.910739595	-6.98264378	-13.59621721
C	6.481384587	-3.844713172	-13.38199921
C	7.125538603	-2.623956689	-13.61504731
H	6.55233998	-1.703559289	-13.64876612
C	8.509533682	-2.581106556	-13.80643042
H	8.994122228	-1.625994751	-13.98977087
C	9.264894202	-3.75140571	-13.76043589
H	10.3404846	-3.714949656	-13.90853465
C	8.629008096	-4.973626754	-13.5258305
H	9.20667182	-5.893096144	-13.49090242
C	7.249167394	-5.021393529	-13.34231774
H	6.768992221	-5.980221431	-13.16774023
C	4.595094736	-4.532590959	-11.3394598
C	3.444754944	-5.156448354	-10.83043529
H	2.581137194	-5.293450585	-11.47240069
C	3.397202302	-5.571488415	-9.498982208
H	2.49836187	-6.053935162	-9.124528045
C	4.489000276	-5.372064216	-8.653728393
H	4.44961406	-5.701973913	-7.619109805

C	5.632621304	-4.744432393	-9.14827515
H	6.490195789	-4.580606847	-8.501183505
C	5.687217238	-4.327054034	-10.47872471
H	6.588464168	-3.846946595	-10.84362561
C	4.071103244	-2.230854275	-13.08822859
C	3.814692393	-1.573366137	-14.30087587
H	3.918854774	-2.110970647	-15.23737877
C	3.407485935	-0.240571233	-14.30835783
H	3.212332492	0.254727918	-15.25555477
C	3.237677318	0.450523899	-13.10687109
H	2.909339569	1.486182327	-13.11383285
C	3.482426565	-0.199942467	-11.89789056
H	3.344243944	0.325847272	-10.95709224
C	3.900911288	-1.53159331	-11.88575898
H	4.084106192	-2.024826756	-10.93735332
C	0.507854226	-5.691437504	-16.7044579
C	0.627618267	-4.313666543	-16.92416268
H	1.520154355	-3.796690617	-16.59226426
C	-0.406041961	-3.606678552	-17.53949321
H	-0.3006821	-2.537184081	-17.69885408
C	-1.572715461	-4.262156269	-17.93298418
H	-2.378605741	-3.707857892	-18.40617253
C	-1.704429527	-5.633090296	-17.70444126
H	-2.613218309	-6.151780538	-17.9975595
C	-0.672615795	-6.344716389	-17.0935566
H	-0.792326519	-7.408823814	-16.91617928
C	1.053684557	-8.02856665	-15.0469766
C	0.627374657	-7.827418061	-13.72388307

H	0.794174537	-6.866704226	-13.24724469
C	-0.026376094	-8.846478526	-13.03116486
H	-0.347749434	-8.671971618	-12.00787442
C	-0.267747537	-10.07874006	-13.63996875
H	-0.772870919	-10.87115411	-13.09447301
C	0.144222856	-10.28421226	-14.95624069
H	-0.038298688	-11.23772175	-15.44480676
C	0.798112729	-9.268703602	-15.65631598
H	1.113400453	-9.452709536	-16.67736074
C	2.635852865	-7.552152637	-17.39785297
C	3.62394766	-8.519460958	-17.14573919
H	3.931598047	-8.732450737	-16.12576825
C	4.218430287	-9.214051876	-18.19575308
H	4.978805198	-9.960521279	-17.98368764
C	3.844116024	-8.945783889	-19.51472119
H	4.312578816	-9.483575488	-20.33438184
C	2.872216465	-7.981873196	-19.77391763
H	2.579224014	-7.763929748	-20.79730535
C	2.266643464	-7.289489565	-18.72232564
H	1.508470828	-6.544549422	-18.93873344
H	6.224810443	-4.321298847	-16.23017553
H	6.270510767	-6.78372783	-16.01827803
H	4.823508304	-5.696256426	-17.70494121
H	3.252000839	-4.130532295	-15.5990631

trans-$IrH(GeH_3)(CO)(Cl)(PPh_3)_2$ (**C**)

-2757.15574610697 Hartrees

Atom	x	y	z

Ir	3.590149022	-5.472312591	-14.70753932
Ge	5.733146457	-5.93410635	-16.096918
P	4.645583896	-3.947037447	-13.16677761
P	1.994759852	-6.751820594	-15.95918543
O	4.305071876	-7.763787349	-12.89684089
C	4.013744952	-6.884518775	-13.59567782
C	6.482879309	-4.058941745	-12.99395144
C	7.322089279	-2.938333543	-13.0406805
H	6.907242446	-1.951450534	-13.21113152
C	8.701123158	-3.080428771	-12.86856476
H	9.338648915	-2.201764085	-12.91501651
C	9.256500316	-4.336932351	-12.63766074
H	10.3295534	-4.445069998	-12.50576476
C	8.426183083	-5.457980678	-12.5794284
H	8.847662092	-6.443390889	-12.40198702
C	7.052423408	-5.321819305	-12.75947782
H	6.428421099	-6.207901537	-12.71620012
C	4.099365405	-4.249691627	-11.41824324
C	2.808669243	-4.721475927	-11.13530626
H	2.128682458	-4.933625059	-11.95330229
C	2.397136641	-4.923024007	-9.816920219
H	1.393683099	-5.290906758	-9.620237239
C	3.267510819	-4.662083009	-8.75855237
H	2.949150062	-4.828146562	-7.733115527
C	4.552724524	-4.189986705	-9.028371165
H	5.241212943	-3.983946383	-8.213370372
C	4.965776357	-3.982815737	-10.34443465
H	5.96978688	-3.618150618	-10.53269617

C	4.303068091	-2.165393517	-13.45242354
C	4.775374805	-1.552206549	-14.62525465
H	5.322780801	-2.130439314	-15.36041253
C	4.53171198	-0.199180911	-14.85512319
H	4.904057763	0.262021343	-15.76533805
C	3.802318521	0.553818584	-13.93314243
H	3.609591397	1.606770571	-14.11912986
C	3.318294364	-0.05347419	-12.7746295
H	2.748168246	0.523513412	-12.0516
C	3.568654241	-1.405029395	-12.53152266
H	3.192509185	-1.861935745	-11.62245772
C	0.318882243	-5.985734943	-16.14641368
C	0.068745332	-4.641763812	-15.84366881
H	0.885921149	-4.000401667	-15.5363854
C	-1.224107373	-4.124881303	-15.96171345
H	-1.401093399	-3.079214565	-15.72514806
C	-2.277645906	-4.936394714	-16.38001248
H	-3.281733792	-4.529980574	-16.4664136
C	-2.035009968	-6.277855382	-16.68442124
H	-2.848335373	-6.922631412	-17.00638375
C	-0.748240455	-6.799472915	-16.56730284
H	-0.579443633	-7.848273394	-16.79282717
C	1.525380487	-8.306845058	-15.06461276
C	1.089180938	-8.18075002	-13.73460697
H	1.081106811	-7.202912604	-13.2619914
C	0.663512704	-9.295118923	-13.01691921
H	0.330638084	-9.177503634	-11.98930382
C	0.668118008	-10.55786352	-13.61275269

H	0.340400728	-11.42838215	-13.05114377
C	1.093654976	-10.69354617	-14.93208255
H	1.096336183	-11.6708893	-15.4071722
C	1.515027378	-9.576291303	-15.65761639
H	1.828890837	-9.702490276	-16.68753688
C	2.447478952	-7.301856223	-17.65253228
C	3.508709305	-8.207016083	-17.82146437
H	4.057159553	-8.572718556	-16.95797243
C	3.871298441	-8.643296114	-19.09424827
H	4.6889765	-9.349757348	-19.20566419
C	3.198919518	-8.161626925	-20.21940999
H	3.486770411	-8.496430698	-21.2119747
C	2.16596314	-7.238600803	-20.0617409
H	1.646999462	-6.846137339	-20.93183854
C	1.787995842	-6.811397993	-18.78742848
H	0.981485617	-6.09463591	-18.68095475
H	6.731569828	-4.753417299	-15.99261353
H	6.573954491	-7.186642842	-15.6910301
H	5.456118922	-6.116239219	-17.60417377
Cl	3.256773948	-3.730380997	-16.43315535
H	2.219033326	-4.92533132	-13.98009294

4.9 References and Notes

(**1**) Young, J. F.; Osborn, J. A.; Jardine, F. H.; Wilkinson, G. *J. Chem. Soc., Chem. Commun.* **1965**, 131-132.

(**2**) Slaugh, L. H.; Mullineaux, R. D. *J. Organomet. Chem.* **1968**, *13*, 469-477.
(**2**) Slaugh, L. H.; Mullineaux, R. D. *J. Organomet. Chem.* **1968**, *13*, 469-477.
(**3**) Drent, E.; Arnoldy, P.; Budzelaar, P. H. M. *J. Organomet. Chem.* **1994**, *475*, 57-63.
(**3**) Drent, E.; Arnoldy, P.; Budzelaar, P. H. M. *J. Organomet. Chem.* **1994**, *475*, 57-63.

(**4**) Brisdon, A. K.; Herbert, C. J. *Coord. Chem. Rev.* **2013**, *257*, 880-901.

(**5**) Tolman, C. A. *Chem. Rev.* **1977**, *77*, 313-348.

(**6**) Cornils, B.; Herrmann, W. A. *J. Catal.* **2003**, *216*, 23-31.

(**7**) Noyori, R. *Adv. Synth. Catal.* **2003**, *345*, 25-32.

(**8**) (a) Sattler, A.; Parkin, G. *Nature* **2010**, *463*, 523-526.
(b) Murphy, V. J.; Parkin, G. *J. Am. Chem. Soc.* **1995**, *117*, 3522-3528.
(c) Zhu, G.; Parkin, G. *Inorg. Chem.* **2005**, *44*, 9637-9639.
(d) Sattler, A.; Parkin, G. *J. Am. Chem. Soc.* **2011**, *133*, 3748-3751.
(e) Zuzek, A. A.; Parkin, G. *J. Am. Chem. Soc.* **2014**, *136*, 8177-8180.

(**9**) Vaska, L.; DiLuzio, J. W. *J. Am. Chem. Soc.* **1961**, *83*, 2784-2785.

(**10**) Trnka, T. M.; Grubbs, R. H. *Acc. Chem. Res.* **2001**, *34*, 18-29.

(**11**) Zhao, J.; Hartwig, J. F. *Organometallics* **2005**, *24* 2441-2446.

(**12**) (a) Blum, Y.; Czarkie, D.; Rahamim, Y.; Shvo, Y. *Organometallics* **1985**, *4*, 1459.
(b) Shvo, Y.; Czarkie, D.; Rahamim, Y.; Chodosh, D. F. *J. Am. Chem. Soc.* **1986**, *108*, 7400-7402.

(**13**) Jessop, P. G.; Ikariya, T.; Noyori, R. *Nature* **1994**, *368*, 231-233.

(**14**) Cheng, C.-H.; Hendriksen, D. E.; Eisenberg, R. *J. Am. Chem. Soc.* **1977**, *99*, 2791-2792.

(**15**) (a) Shelef, M.; Gandhi, H. S. *Ind. Eng. Chem., Prod. Proc. Dev.* **1974**, *13*, 80-84.
(b) Querido, R.; Short, W. L. *Ind. Eng. Chem., Prod. Proc. Dev.* **1973**, *12*, 10-18.

(**16**) Thomas, C. L. *Catalytic Processes and Proven Catalysts*. Academic Press, New York 1970.

(**17**) The thermodynamics of this reaction are as follows: $CO(g) + H_2O(g) \leftrightarrows H_2(g) + CO_2(g)$: ΔG°_{298} = -6.82 kcal, ΔH°_{298} = -9.84 kcal, ΔS°_{298} = -10.1 cal/deg; $CO(g) + H_2O(l) \leftrightarrows H_2(g) + CO_2(g)$: ΔG°_{298} = -4.76 kcal, ΔH°_{298} = +0.68 kcal, ΔS°_{298} = +18.3

cal/deg. See: King Jr., A. D.; King, R. B.; Yang, D. B. *J. Am. Chem. Soc.* **1980**, *102*, 1028-1032.

(**18**) For example, K_P is 228 at 200 ˚C but only 11.8 at 400 ˚C. See: Jacobs, G.; Davis, B. H. *Catalysis* **2007**, *20*, 122-285.

(**19**) Laine, R. M.; Rinker, R. G.; Ford, P. C. *J. Am. Chem. Soc.* **1977**, *99*, 252-253.

(**20**) Kang, H.; Maudlin, C. H.; Cole, T.; Slegeir, W.; Cann, K.; Pettit, R. *J. Am. Chem. Soc.* **1977**, *99*, 8323-8325.

(**21**) (a) Ungermann, C.; Landis, V.; Moya, S. A.; Cohen, H.; Walker, H.; Pearson, R. G.; Rinker, R. G.; Ford, P. C. *J. Am. Chem. Soc.* **1979**, *101*, 5922-5929.
(b) Bricker, J. C.; Nagel, C. C.; Bhattacharyya, A. A.; Shore, S. G. *J. Am. Chem. Soc.* **1985**, *107*, 377-384.
(c) Gross, D. C.; Ford, P. C. *J. Am. Chem. Soc.* **1985**, *107*, 585-593.

(**22**) (a) Ishida, H.; Tanaka, K.; Morimoto, M.; Tanaka, T. *Organometallics* **1986**, *5*, 724-730.
(b) Haukka, M.; Kiviaho, J.; Ahlgrén, M.; Pakkanen, T. A. *Organometallics* **1995**, *14*, 825-833.

(**23**) Yoshida, T.; Ueda, Y.; Otsuka, S. *J. Am. Chem. Soc.* **1978**, *100*, 3941-3942.

(**24**) The hydrogenation of CO_2 is thermodynamically uphill, with ΔG° $CO_2(g) + H_2(g) \leftrightarrows HCOOH$ = 33 kJ/mol. Thus, it is not surprising that formic acid is not generated under these conditions, but the addition of a base and the use of high pressures may shift the equilibrium to towards the product. See reference 13.

(**25**) Jones, R. A.; Wilkinson, G.; Galas, A. M. R.; Hursthouse, M. B.; Abdul Malik, K. M. *J. Chem. Soc., Dalton Trans.* **1980**, 1771-1778.

(**26**) Two formate species actually appear, where the minor product is characterized by a signal slightly upfield of the one described here. The peaks are not well resolved enough in the ^{13}C-enriched CO_2 experiment to conclusively say by what kind of splitting pattern they are characterized. In the experiment using natural abundance CO_2, however, an analogous quartet peak is observed, suggesting that the formate couples to three phosphine ligands. A structure in which one phosphine has been replaced by a CO ligand, generated *via* reduction of CO_2, may be responsible. The chemical shifts of these peaks do not match those of the formate complex produced *via* the WGSR, although it is possible that the chemical shifts of these species are dependent on concentration.

(**27**) (a) Fackler, J. P.; Coucouvanis, D. *J. Am. Chem. Soc.* **1966**, *88*, 3913-3920.
(b) Aucott, S. A.; Slawin, A. M. Z.; Woollins, J. D. *Polyhedron* **2000**, *19*, 499-502.

(**28**) Coucouvanis, D. *Adv. Inorg. Chem.* **1998**, *45*, 1-73.

(**29**) (a) Simmonet-Jégat, C.; Cadusseau, E.; Dessapt, R.; Sécheresse, F. *Inorg. Chem.* **1999**, *38*, 2335-2339.
(b) Coucouvanis, D.; Draganjac, M. E.; Koo, S. M.; Toupadakis, A.; Hadjikyriacou, A. I. *Inorg. Chem.* **1992**, *31*, 1186-1196.

(**30**) Deskin, W. A. *J. Am. Chem. Soc.* **1958**, *80*, 5680-5682.

(**31**) (a) Werner, H.; Kolb, O.; Feser, R.; Schubert, U. *J. Organomet. Chem.* **1980**, *191*, 283-293.
(b) Cowie, M.; Dwight, S. K. *J. Organomet. Chem.* **1981**, *214*, 233-252.

(**32**) Ibers, J. A.; *Chem. Soc. Rev.* **1982**, *11*, 57-73.

(**33**) Thewissen, D. H. M. W. *J. Organomet. Chem.* **1980**, *188*, 211-221.

(**34**) Bergman, R. G. *Polyhedron* **1995**, *14*, 3227-3237.

(**35**) Although the chemical shift of the hydride resonance observed here in benzene (δ -8.50) does not match that reported for the hydride signal of $Ru(PMe_3)_4H(OH)$ in benzene (δ -8.31), the phosphorous coupling in both species is identical (*i.e.* $^2J_{P-H}$ = 28, 28, 105). Thus, it is possible that $Ru(PMe_3)_4H(OH)$ is the product here, but that its chemical shift may vary. See: Burn, M. J.; Fickes, M. G.; Hartwig, J. F.; Hollander, F. J.; Bergman, R. G. *J. Am. Chem. Soc.* **1993**, *115*, 5875-5876.

(**36**) Sánchez-Delgado, R. A. *J. Mol. Cat.* **1994**, *86*, 287-307.

(**37**) Hille, R. *Chem. Rev.* **1996**, *96*, 2757-2816.

(**38**) Kuwata, S.; Hidai, M. *Coord. Chem. Rev.* **2001**, *213*, 211-305.

(**39**) (a) Zhu, G.; Tanksi, J. M.; Churchill, D. G.; Janak, K. E.; Parkin, G. *J. Am. Chem. Soc.* **2002**, *124*, 13658-13659.
(b) Zhu, G.; Pang, K.; Parkin, G. *Inorg. Chim. Acta* **2008**, *361*, 3221-3229.
(c) Sattler, A.; Zhu, G.; Parkin, G. *J. Am. Chem. Soc.* **2009**, *131* 7828-7838.

(**40**) (a) Janak, K. E.; Tanski, J. M.; Churchill, D. G.; Parkin, G. *J. Am. Chem. Soc.* **2002**, *124*, 4182-4183.
(b) Buccella, D.; Janak, K. E.; Parkin, G. *J. Am. Chem. Soc.* **2008**, *130*, 16187-16189.
(c) Sattler, A.; Parkin, G. *J. Am. Chem. Soc.* **2011**, *133*, 3748-3751.
(d) Sattler, A.; Janak, K. E.; Parkin, G. *Inorg. Chim. Acta* **2011**, *369*, 197-202.

(**41**) Sanchez-Delgado, R. A. *Organometallic Modeling of the Hydrodesulfurization and Hydrodenitrogenation Reactions*, Kluwer Academic Publishers, Boston, 2002.

(**42**) Furimsky, E. *Appl. Catal., A* **2000**, 147-190.

(**43**) Sattler, A. Ph. D. Thesis, Columbia University, New York, NY, 2012 (Chapter 5).

(**44**) Among other things, the reactivity of furan has been studied in detail. The reactions of furan with $Mo(PMe_3)_6$ and $W(PMe_3)_4(\eta^2\text{–}CH_2PMe_2)H$ were shown to result in facile C-O bond cleavage. See reference 43.

(**45**) Allen, D. L.; Green, M. L. H.; Bandy, J. A. *J. Chem. Soc., Dalton Trans.* **1990**, 541-549.

(**46**) (a) Rabinovich, D.; Zelman, R.; Parkin, G. *J. Am. Chem. Soc.* **1992**, *114*, 4611-4621
(b) Hascall, T.; Murphy, V. J.; Parkin, G. *Organometallics* **1996**, *15*, 3910-3912.
(c) Hascall, T.; Murphy, V. J; Janak, K. E.; Parkin, G. *J. Organomet. Chem.* **2002**, *652*, 37-49.

(**47**) Green, M. L. H.; Parkin, G.; Moynihan, K. J.; Prout, K. *J. Chem. Soc., Chem. Commun.* **1984**, 1540.

(**48**) See, for example: (a) Coffindaffer, T. W.; Steffy, B. D.; Rothwell, I. P.; Folting, K.; Huffman, J. C.; Streib, W. E. *J. Am. Chem. Soc.* **1989**, *111*, 4742-4749.
(b) Morris, R. J.; Girolami, G. S. *Inorg. Chem.* **1990**, *29*, 4167-4169.

(**49**) Sattler, A.; Parkin, G. *Chem. Commun.* **2011**, *47*, 12828-12830.

(**50**) Palmer, J. H.; Parkin, G. *Polyhedron* **2013**, *52*, 658-668.

(**51**) DiLuzio, J. W.; Vaska, L. *J. Am. Chem. Soc.* **1962**, *84*, 679-680.

(**52**) Vaska, L. *Science* **1963**, *140*, 809-810.

(**53**) Vaska, L. *J. Am. Chem. Soc.* **1966**, *88*, 5325-5327.

(**54**) (a) Chalk, A. J.; Harrod, J. F. *J. Am. Chem. Soc.* **1965**, *87*, 16-21.
(b) Chalk, A. J.; *J. Chem. Soc., Chem. Commun.* **1969**, 1207-1208.
(c) Nishihara, Y.; Takemura, M.; Osakada, K. *Inorg. Chim. Acta* **2009**, *362*, 2009-2956.

(**55**) Ebsworth, E. A. V.; Leitch, D. M. *J. Chem. Soc., Dalton Trans.* **1973**, 1287-1292.

(**56**) Ebsworth, E. A. V.; Fraser, T. E. *J. Chem. Soc., Dalton Trans.* **1979**, 1960-1964.

(**57**) Chatt, J.; Shaw, B. L.; Field, A. E. *J. Chem. Soc.* **1964**, 3466-3475.

(**58**) This critical difference in reactivity may be due to the more dilute conditions used here. For example, Ebsworth and Leitch used 0.1 mmol of Vaska's compound in 1 mL benzene, whereas we used 0.006 mmol of the Ir complex in 0.7 mL benzene. A slightly greater excess of silane may also be partly responsible – we used approximately 3 equivalents, based on the ^1H NMR spectrum of the reaction solution, whereas Ebsworth and Leitch used a 2:1 or 1:1 ratio.

(**59**) Throughout this discussion, *trans*-IrH(EH_3)(Cl)(CO)(PPh_3)$_2$ refers to the isomer (Scheme 15, **C**) in which the hydride and germyl or silyl ligands are *trans*; the phosphine ligands are mutually *trans*, as are the carbonyl and chloride group. *cis*-IrH(EH_3)(Cl)(CO)(PPh_3)$_2$ refer to the isomers (Scheme 15, **A** and **B**) in which the hydride and silyl or germyl ligands are *cis*. The two are then distinguished by specifying the ligand *trans* to the hydride; phosphine ligands are mutually *trans* in all cases unless otherwise specified.

(**60**) Sakaki, S.; Ujino, Y.; Sugimoto, M. *Bull. Chem. Soc. Jpn.* **1996**, *69*, 3047-3057.

(**61**) Neuhaus, D.; Williamson, M. P. *The Nuclear Overhauser Effect in Structural and Conformational Analysis*, 2nd ed. WILEY-VCH, New York, 2000.

(**62**) Ebsworth, E. A. V.; Fraser, T. E.; Henderson, S. G.; Leitch, D. M.; Rankin, D. W. H. *J. Chem. Soc., Dalton Trans.* **1981**m 1010-1018.

(**63**) Elimination of Et_3SiCl from the corresponding silyl hydride adduct has been reported. See references 54a and b.

(**64**) (a) McNally, J. P.; Leong, V. S.; Cooper, N. J. in *Experimental Organometallic Chemistry*; Wayda, A. L.; Darensbourg, M. Y., Eds.; American Chemical Society: Washington, DC, 1987; Chapter 2, pp 6-23.
(b) Burger, B.J.; Bercaw, J. E. in *Experimental Organometallic Chemistry*; Wayda, A. L.; Darensbourg, M. Y., Eds.; American Chemical Society: Washington, DC, 1987; Chapter 4, pp 79-98.
(c) Shriver, D. F.; Drezdzon, M. A.; *The Manipulation of Air-Sensitive Compounds*, 2nd Edition; Wiley-Interscience: New York, 1986.

(**65**) (a) Gottlieb, H. E.; Kotlyar, V.; Nudelman, A. *J. Org. Chem.* **1997**, *62*, 7512-7515.
(b) Fulmer, G. R.; Miller, A. J. M.; Sherden, N. H.; Gottlieb, H. E.; Nudelman, A.; Stoltz, B. M.; Bercaw, J. E.; Goldberg, K. I. *Organometallics* **2010**, *29*, 2176-2179.

(**66**) "Nuclear Magnetic Resonance Spectroscopy" Nelson, J. H. Prentice Hall, New Jersey (2003), p 79.

(**67**) Gusev, D. G.; Hübener, R.; Burger, P.; Orama, O.; Berke, H. *J. Am. Chem. Soc.* **1997**, *119*, 3716-3731.

(**68**) Green, M. L. H.; Parkin, G.; Chen, M.; Prout, K. *J. Chem. Soc., Dalton Trans.* **1986**, 2227–2236.

(**69**) (a) Sheldrick, G. M. SHELXTL, An Integrated System for Solving, Refining and Displaying Crystal Structures from Diffraction Data; University of Göttingen, Göttingen, Federal Republic of Germany, 1981.
(b) Sheldrick, G. M. *Acta Cryst.* **2008**, *A64*, 112-122.

(**70**) (a) Jaguar 7.5, Schrödinger, LLC, New York, NY 2008.
(b) Jaguar 7.7. Schrödinger LLC, New York, NY 2010.

(**71**) (a) Becke, A. D. *J. Chem. Phys.* **1993**, *98*, 5648-5652.
(b) Becke, A. D. *Phys. Rev. A* **1988**, *38*, 3098-3100.
(c) Lee, C. T.; Yang, W. T.; Parr, R. G. *Phys. Rev. B* **1988**, *37*, 785-789.
(d) Vosko, S. H.; Wilk, L.; Nusair, M. *Can. J. Phys.* **1980**, *58*, 1200-1211.
(e) Slater, J. C. *Quantum Theory of Molecules and Solids, Vol. 4: The Self-Consistent Field for Molecules and Solids*; McGraw-Hill: New York, 1974.

(**72**) (a) Hay, P. J.; Wadt, W. R. *J. Chem. Phys.* **1985**, *82*, 270-283.
(b) Wadt, W. R.; Hay, P. J. *J. Chem. Phys.* **1985**, *82*, 284-298.
(c) Hay, P. J.; Wadt, W. R. *J. Chem. Phys.* **1985**, *82*, 299-310.

CHAPTER 5

Determination of the Molecular Structure of $W(PMe_3)_3H_6$ in Solution and in the Solid State – NMR Spectroscopic Studies to Confirm a Classical Hydride Structure

Table of Contents

Reproduced in part from: Sattler, A.; Zuzek, A. A.; Parkin, G. Accepted to *Inorganica Chimica Acta*, **2014**.

5.1 Introduction

Transition metal polyhydride compounds have had an immense impact on the development of coordination chemistry. These complexes exhibit great diversity in their structures, spectroscopic properties, and reactivities, which all contribute to the significance of these complexes.[1] For example, the structures of polyhydride compounds[2] may be either classical or nonclassical (*i.e.* dihydrogen complexes)[3,4,5] and are often fluxional on the NMR timescale in solution.[6] These compounds may also exhibit quantum mechanical exchange coupling, which is manifested by very large coupling constants in their ^{1}H NMR spectra.[7] The reactivity of polyhydride compounds is significant because metal hydride species play important roles in a number of catalytic transformations, as described in Chapter 4; among these are reactions such as hydrogenation,[8] hydroformylation,[8,9] and hydrosilation.[8,10] While there are many different types of transition metal polyhydride compounds, structures of the type $M(PR_3)_xH_y$, where PR_3 is a tertiary phosphine ligand, have received particular attention.[1] As an extension of our work on tungsten trimethylphosphine derivatives, we have explored the nature of $W(PMe_3)_3H_6$ in solution and in the solid state.

5.2 Molecular Structure of $W(PMe_3)_3H_6$

Tungsten forms three classes of polyhydride compounds of the type $M(PR_3)_xH_y$. Specifically, derivatives of the type $W(PR_3)_5H_2$,[11] $W(PR_3)_4H_4$,[11,12] and $W(PR_3)_3H_6$[13,14] have all been reported. The first example of the last type of complex is $W(PMe_2Ph)_3H_6$, which was prepared by Moss and Shaw *via* the treatment of $W(PMe_2Ph)_2Cl_4$ with $NaBH_4$ in methanol.[13a] The trimethylphosphine derivative was subsequently generated *via* the reaction of $W(PMe_3)_3Cl_4$ with $LiAlH_4$.[13f] This complex was identified as being fluxional in solution, such that the six hydrides are equivalent, as are the phosphine ligands. Although crystals suitable for X-ray diffraction were not obtained, two idealized geometries were considered for the static structure: (*i*) a tricapped trigonal prism with D_{3h} symmetry, in which the hydride ligands form a trigonal prism and the PMe_3 ligands

cap the rectangular faces[15] and (*ii*) a trigonal prism with C_{2v} symmetry, in which two of the PMe_3 ligands adopt eclipsed positions on the triangular faces and one PMe_3 ligand caps a rectangular face.[13c,d] These idealized geometries are depicted in Figure 1.[16]

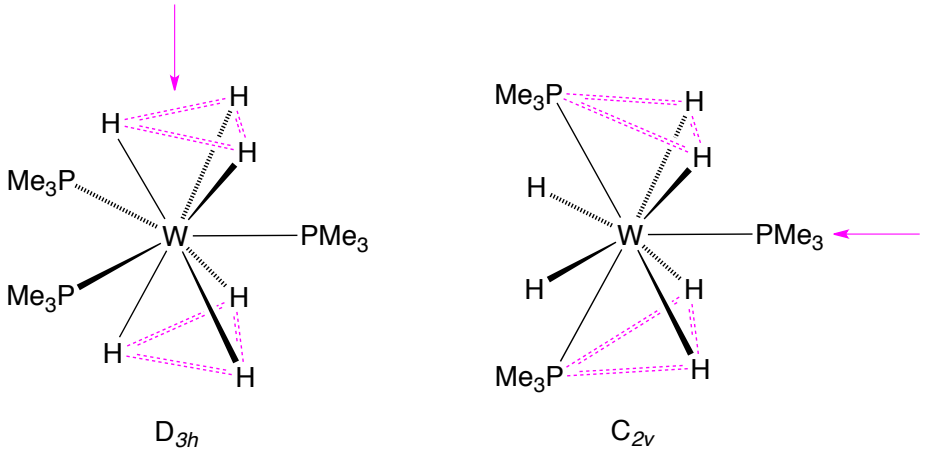

Figure 1. Structures proposed[13f] for $W(PMe_3)_3H_6$ – dashed lines indicate the trigonal prism motif and pink arrows show the symmetry axis

It is noteworthy, therefore, that the low temperature (-123 ˚C) molecular structure of $W(PMe_3)_3H_6$ has been determined by X-ray diffraction. This structure was obtained by Aaron Sattler, a former Parkin group graduate student.[17] Significantly, all six hydrides were located and freely refined isotropically, thereby demonstrating that the molecule has the approximate C_{2v} structure shown in Figure 1 (right). Specifically, there is one PMe_3 ligand on each triangular face and one that caps a rectangular face.

The lack of D_{3h} symmetry is made clear by the fact that there is no C_3 axis; for example, the P-W-P angles deviate substantially from 120˚, ranging from 102.49(3)˚ to 128.57(2)˚. The W-P distances vary from 2.4156(8) Å to 2.4706(6) Å,[18] which further indicates that the structure does not possess a D_{3h}-symmetry. Instead, these structural parameters are consistent with a C_{2v}-symmetric structure, as demonstrated in Figure 2.[17]

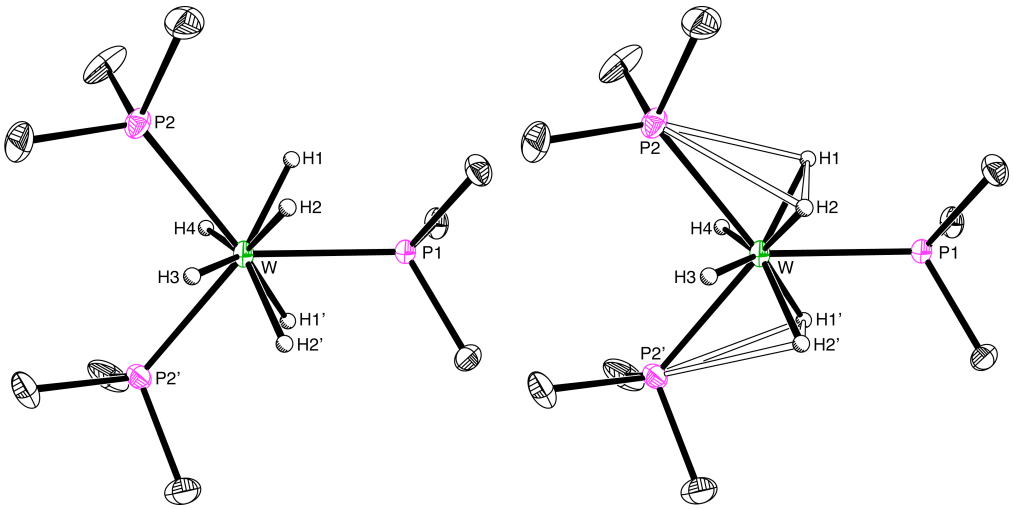

Figure 2. Molecular Structure of $W(PMe_3)_3H_6$ (left) with the trigonal prismatic geometry specified with hollow lines (right)[17]

A density functional theory geometry optimization calculation on $W(PMe_3)_3H_6$ was also performed by Aaron Sattler.[17] The molecular structure is reproduced well by this calculation; for example, the calculations predict P-W-P angles that range from 101.4° to 129.8° and non-equivalent W-P bond lengths.[17,19]

Further support for the C_{2v} symmetry of $W(PMe_3)_3H_6$ comes from solid state ^{13}C and ^{31}P NMR spectroscopic studies, which indicate the presence of two different types of PMe_3 ligands.[20] Furthermore, a related complex, namely $W(PPhPr^i_2)_3H_6$,[13c,d] possesses a C_{2v} symmetric structure similar to that of $W(PMe_3)_3H_6$. Given that $W(PMe_3)_3H_6$ and $W(PPhPr^i_2)_3H_6$ possess similar structures despite having ligands with very different steric demands, it is likely that the C_{2v} arrangement will be common for other $W(PR_3)_3H_6$ derivatives.

In addition to the overall geometry of the $W(PMe_3)_3H_6$ molecule, the question of whether the compound should be classified as a classical or nonclassical hydride complex is also of interest. The distinction between these two types of complexes is based on the distances between the hydride ligands, H•••H. Distances of ≤ 1.0 Å are

considered to be indicative of a "true" dihydrogen complex, while distances of > 1.6 Å are considered to signify a dihydride complex.[3c] However, a range of distances have been observed in these systems. Both the X-ray and geometry optimized structures are consistent with a classical hydride formulation because the shortest H•••H distance is greater than 1.6 Å in both cases; specifically, the shortest distance in the experimental structure is 1.647 Å, and that in the calculated structure is 1.914 Å.

5.3 T_1 Relaxation Studies

After the structure of $W(PMe_3)_3H_6$ in the solid state was established, we were interested in determining whether this compound exists as a classical hydride in solution as well. One means of distinguishing between classical and nonclassical hydride complexes in solution is the T_1 method, in which the relaxation time of the hydride ligands is measured. Specifically, the T_1 method, where T_1 is the spin lattice relaxation time, is based on the fact that that dipole-dipole relaxation is a major contributor to the total spin-lattice relaxation rate (R) for short distances (r) between protons. The relaxation rate will be faster at short H•••H distances, since $R \propto 1/r^6$. Because the relaxation rate and relaxation time are inversely related, $T_1 \propto r^6$, such that the value of T_1 helps to differentiate between classical and nonclassical hydrides.[21,22,23,24,25] One complication of this method, however, is that T_1 is temperature dependent. Specifically, dipole-dipole relaxation is dependent on the correlation time (τ_c) of a molecule, which is directly proportional to temperature and generally unknown.[24,26,27,28] This issue is resolved by the fact that the correlation time has a precise value of $0.62/\omega$, where ω is the Larmor frequency, at the temperature at which T_1 has its minimum value (*i.e.* $T_{1(min)}$). Thus, if the value of $T_{1(min)}$ is determined, the value of r may be extracted.[21a,22] For example, in a system with only two hydrogen atoms that undergo relaxation *via* the dipole-dipole mechanism, the distance between the two hydrogen atoms (in Å) is related to $T_{1(min)}$ by the expression $r = 5.815[T_{1(min)}/\nu]^{1/6}$, where ν is the spectrometer frequency in MHz.[24]

Therefore, we have determined the value of $T_{1(min)}$ for the hydride ligands of $W(PMe_3)_3H_6$ at 400 and 500 MHz by examining the temperature dependence of the T_1 relaxation time (Table 2 and Figure 3). At 500 MHz, the minimum value of T_1 occurs at *ca*. 210 K and has a value of 380 ms, whereas at 400 MHz the minimum value is 310 ms at *ca*. 195 K. This is in accord with the fact that $T_{1(min)}$ is directly proportional to field strength.[21,22] Furthermore, these values support the description of $W(PMe_3)_3H_6$ as a classical hydride; specifically, classical hydride compounds are generally considered to possess $T_{1(min)}$ values > 200 ms at 500 MHz, whereas nonclassical hydrides are generally distinguished by values < 80 ms.[21b]

Table 2. T_1 relaxation times for the hydride ligands of $W(PMe_3)_3H_6$ as a function of temperature

Temperature/K	T_1 (400 MHz)/ms	T_1 (500 MHz)/ms
300	2370	2070
270	1300	1170
250	950	730
240	800	580
230	570	460
220	440	390
210	360	380
205	340	420
200	310	500
195	310	560
190	320	650
185	340	

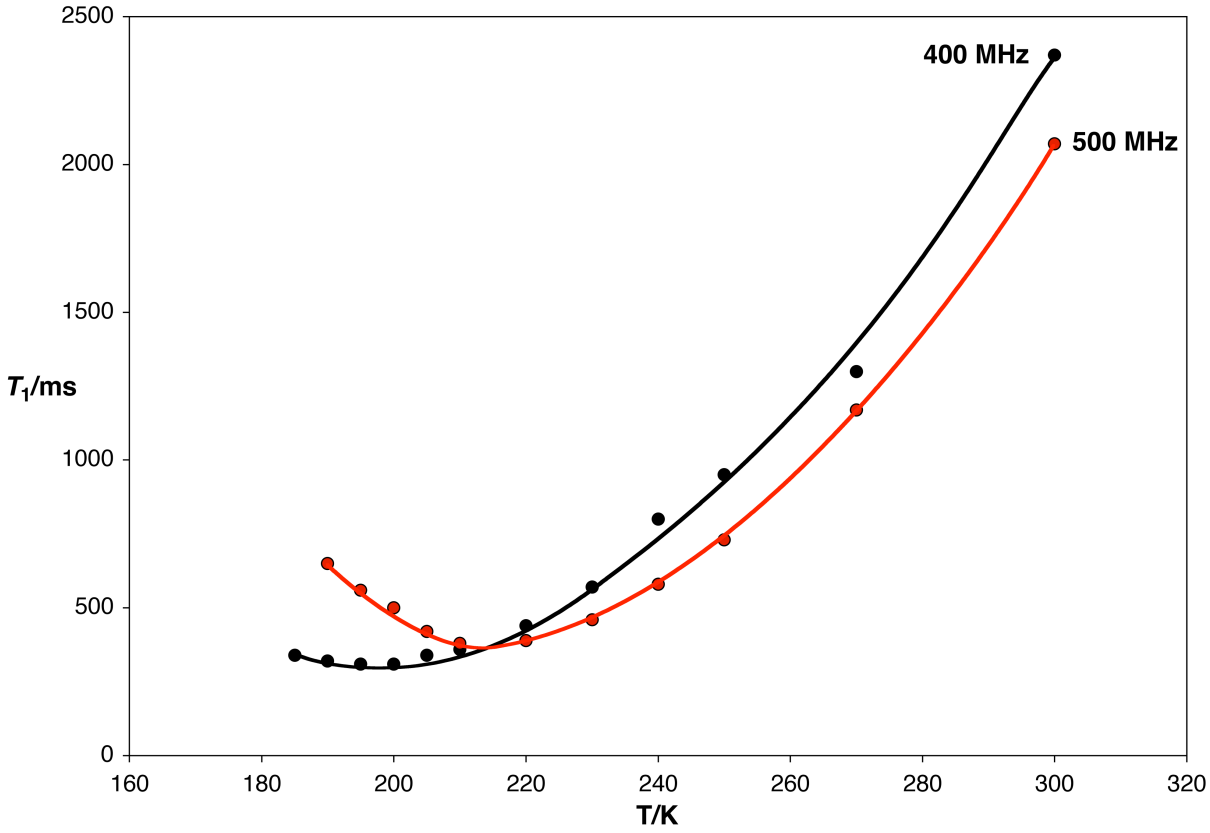

Figure 3. Observed temperature dependence of T_1 for the hydride ligands of $W(PMe_3)_3H_6$

It is important to note, however, that dipole-dipole relaxation is not dependent solely on the interactions between hydride ligands. Specifically, the T_1 relaxation time of a proton in a polyhydride is dependent both on the interaction of that proton with other hydrides and on its interaction with all other magnetically active nuclei.[21,22,29] Thus, the relaxation rate of the hydride ligands of $W(PMe_3)_3H_6$ is a sum of components due to (*i*) interactions between the hydride ligands (R_{HWH}), *(ii)* interactions between the hydride ligands and the hydrogen atoms of the methyl groups (R_{HMe}), and *(iii)* interactions between the hydride ligands and the phosphorus nuclei (R_{HP}).[22] These components were calculated by Gerard Parkin and Aaron Sattler for the geometry optimized structure, verifying that the dominant contribution to the relaxation rate comes from the interactions between the hydride ligands (R_{HWH} = 2.89 s^{-1}). Nonetheless, relaxation due

to the interaction of the hydrides with the methyl groups is significant (R_{HMe} = 0.97 s^{-1}). The interaction of the hydrides with the phosphorus nuclei, on the other hand, represents a negligible contribution to the overall relaxation rate (R_{HP} = 0.08 s^{-1}).[30,31] The total relaxation rate for the hydride ligands is the sum of these contributions and is therefore calculated to be 3.94 s^{-1} at 500 mHz, corresponding to a $T_{1(min)}$ value of 253 ms. Although this value is considerably smaller than the experimentally determined value of $T_{1(min)}$ at this frequency (380 ms), it also supports the assignment of $W(PMe_3)_3H_6$ as a classical hydride. The difference in the calculated and experimental values of $T_{1(min)}$ suggests that the average H•••H distance in the geometry optimized structure is less than that in the actual solution state structure.[32] Nonetheless, the dependence of $T_{1(min)}$ on r^6 means that only small changes in structure may effect differences of this magnitude. $T_{1(min)}$ data for related tungsten compounds are compiled in Table 3,[13g,33,34] from which it is evident that the neutral compounds are all classical, while the cationic complexes are nonclassical.

Table 3. $T_{1(min)}$ values for some tungsten phosphine hydride compounds at 11.7 T (*i.e.* 500 MHz). Values have been scaled from the original frequencies as indicated[22]

Compound	$T_{1(min)}$/ms	Reference
$W(PMe_3)_3H_6$	380	this work
$W(PPh_3)_3H_6$	245[a]	34
$W[PhP(CH_2CH_2PPh_2)_2]H_6$	206, 252[b,c]	33
$\{W[PhP(CH_2CH_2PPh_2)_2](\eta^2\text{-}H_2)_xH_{7-2x}\}^+$	42[d]	33
$\{W[PhP(C_6H_4\text{-}o\text{-}PPh_2)_2](\eta^2\text{-}H_2)_xH_{7-2x}\}^+$	64[e]	33

(a) converted from a value of 147 ms at 300 MHz.

(b) converted from values of 103 ms and 126 ms at 250 MHz.

(c) chemically inequivalent hydride ligands.

(d) converted from a value of 21 ms at 250 MHz.

(e) converted from a value of 32 ms at 250 MHz.

5.4 Generation of $W(PMe_3)_3H_{6-x}D_x$

In addition to the T_1 method, another means to investigate the nature of a polyhydride compound in solution is to examine deuterium isotope effects in partially deuterated isotopologues. For example, the observation of a substantial J_{H-D} coupling constant (>15 Hz) is generally interpreted to be indicative of a dihydrogen tautomer.[23,35,36] A substantial secondary deuterium isotope shift[37] of a hydride signal in the ^1H NMR spectrum is also suggestive of a dihydrogen species. Therefore, we generated a series of isotopologues of $W(PMe_3)_3H_6$, namely $W(PMe_3)_3H_{6-x}D_x$, with the goal of obtaining more evidence for the nature of this complex in solution. The isotopologues were formed by hydrogen/deuterium exchange with either deuterobenzene or deuterotoluene.

This reaction was monitored by ^1H and ^2H NMR spectroscopy, thereby demonstrating deuterium incorporation into both the hydride ligands and the PMe_3 groups. However, it was observed that incorporation into the hydride ligands occurred much more readily than that into the phosphine ligands. For example, after heating for 8 days at 40 ˚C, the ratio of deuterium incorporation into the hydride and PMe_3 groups is approximately 10:1. Isotope exchange reactions of this type are well known and have been reported for a number of complexes.[38] Some early examples are provided by $Re(PR_3)_2H_7$,[39] $Ta(Me_2PCH_2CH_2PMe_2)_2H_5$,[40] $Ir(PR_3)_2H_5$,[41] $M(PR_3)_4H_4$ (M = Mo, W),[42] and Cp_2MH_3 (M = Nb, Ta).[41b,43] By analogy with these examples, the mechanism for deuterium incorporation to form $W(PMe_3)_3H_{6-x}D_x$ may involve (*i*) reductive elimination of H_2, (*ii*) oxidative addition of Ar-D, (*iii*) reductive elimination of Ar–H, and (*iv*) oxidative addition of H_2.[44] Deuterium incorporation into the PMe_3 groups presumably involves an additional cyclometallation sequence involving oxidative addition of a C-H bond.[45,46] For this reason, there is less deuterium incorporation into the PMe_3 groups than into the hydrides.

The nature of the oxidative addition of the C-H bond (*i.e.* which bond is cleaved) is highly dependent on the system. Reactions involving toluene typically exhibit a preference for cleavage of the phenyl rather than the methyl C–H bonds. The *ortho*/*meta*/*para* selectivity may vary; however, cleavage of the *ortho* bond is rarely observed. For example, photolysis of Cp_2WH_2 in toluene gives $Cp_2W(C_4H_4Me)H$ as a 0.1:1 ratio of *meta* and *para* isomers.[47,48] Photolysis of $[Tp^{Me_2}]Rh(CNNp)(\eta^2\text{–}PhNCNNp)$ in toluene, on the other hand, gives $[Tp^{Me_2}]Rh(CNNp)(C_6H_4Me)H$ as a kinetic 1.33:1 ratio of *meta* and *para* isomers, which converts to the statistical 2:1 ratio after heating.[49,50] Based on the site selectivity for cleaving the C-H bonds of toluene in other systems,[51] it is evident that there can be a kinetic preference for cleaving either the *meta* or *para* C-H bonds. Therefore, we examined the extent of ^1H incorporation into the phenyl sites of deuterotoluene[52] by integration of the ^1H NMR spectra and have found that incorporation into the *meta* and *para* sites is statistical throughout the process (Figure 4).

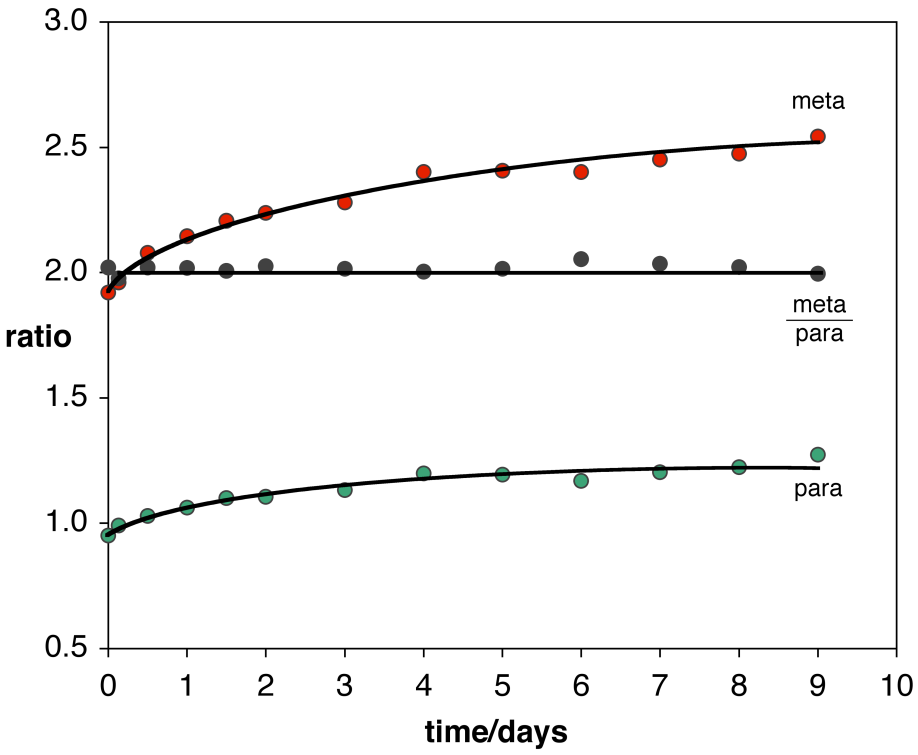

Figure 4. ^1H incorporation into the *meta* and *para* sites of deuterotoluene relative to the *ortho* site upon treatment with $W(PMe_3)_3H_6$ at 40 °C

5.5 Deuterium Isotope Effects

Each resulting isotopologue of $W(PMe_3)_3H_{6-x}D_x$ that contains at least one hydrogen on the tungsten center may be observed by ^1H and $^1H\{^{31}P\}$ NMR spectroscopy. The signals are progressively shifted upfield by 13 ppb upon increasing deuterium incorporation, as shown in Figure 5.

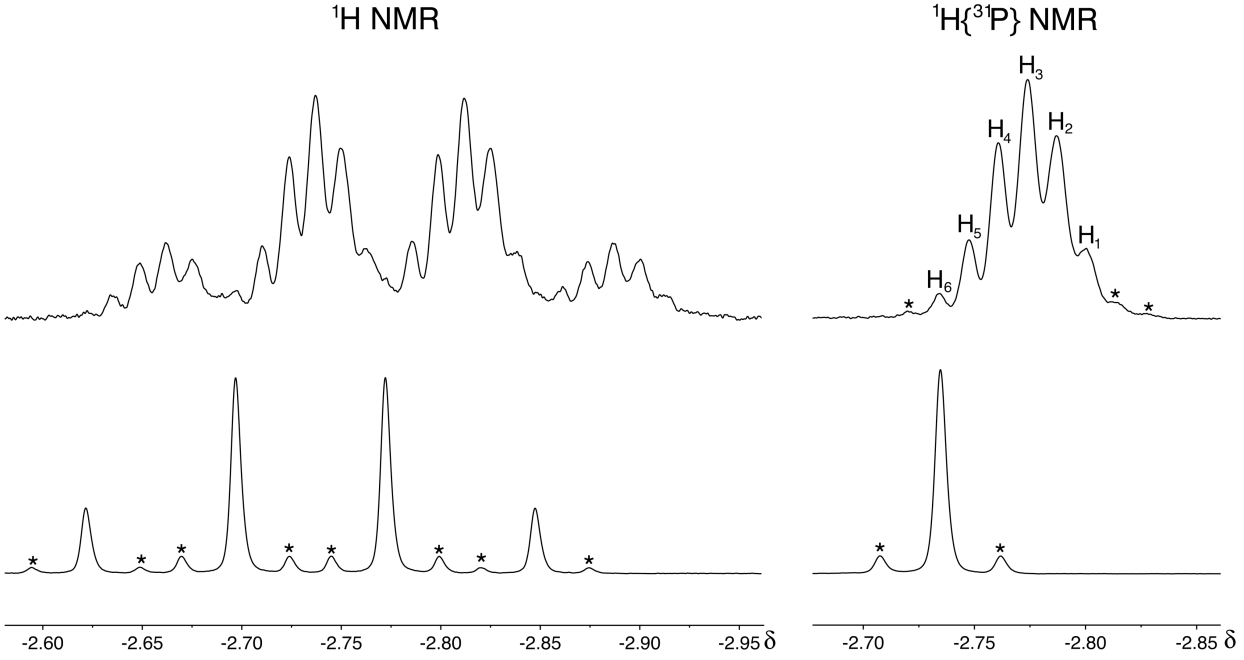

Figure 5. NMR Spectra of $W(PMe_3)_3H_{6-x}D_x$ (top) and $W(PMe_3)_3H_6$ (bottom). The $^1H\{^{31}P\}$ NMR spectrum of $W(PMe_3)_3H_{6-x}D_x$ (top right) is labeled according to the number of hydrogen atoms in the hydride site. Tungsten satellites are marked by *

The isotopic perturbation of the chemical shift of a polyhydride compound is due to both (*i*) an intrinsic isotope effect and (*ii*) a manifestation of the relative classical/nonclassical site preferences of deuterium and hydrogen. With respect to intrinsic isotope effects, two-bond $^2\Delta^1H(D)$ isotope shifts are typically upfield;[37] for example, the isotopologues of methane, $CH_{4-x}D_x$, exhibit upfield ^1H NMR shifts of *ca*. 15 ppb per deuterium.[53,54,55] On the other hand, isotope effects resulting from the relative classical/nonclassical site preferences of deuterium and hydrogen can be either upfield

or downfield. The observed shift will depend on both *(i)* whether the classical or nonclassical site is more upfield and *(ii)* whether deuterium prefers to reside in the classical or nonclassical site.

Transition metal polyhydride compounds have been reported to exhibit both upfield and downfield $^2\Delta^1$H(D) secondary isotope shifts.[56] For example, upfield isotope shifts have been noted for $Re(PCy_3)_2H_7$,[57] $Re(PPh_3)_2H_7$,[58] $[Me_2Si(C_5Me_4)_2]Mo(\eta^2\text{–}H_2)H]^+$,[59] $[Me_2C(C_5H_4)_2]Mo(\eta^2\text{–}H_2)H]^+$,[60] and Cp_2NbH_3.[61] Downfield shifts have been observed for $Os(PTol_3)_3H_4$,[22] $[\{P(CH_2CH_2PPh_2)_3\}Os(H)(\eta^2\text{-}H_2)]^+$,[62] and $[Tp]Ir(PMe_3)(\eta^2\text{-}H_2)H]^+$.[63]

As noted above, two-bond intrinsic isotope shifts are typically upfield. Therefore, downfield shifts are generally associated with nonclassical hydride compounds. For example, $^2\Delta^1$H(D) for the H_2D isotopologue of $\{[Tp]Ir(PMe_3)(\eta^2\text{-}H_2)H\}^+$ is -228 ppb at 215 K and -149 ppb at 281 K;[63] both the downfield nature of the shift and its temperature dependence have been explained by suggesting that the deuterium resides preferentially in a classical site whose shift is upfield of the nonclassical site. Upfield shifts may also be indicative of a nonclassical structure if their values are anomalously large. As an illustration, deuterium incorporation into $[Me_2Si(C_5Me_4)_2]Mo(\eta^2\text{–}H_2)H]^+$ results in upfield shifts with incremental values of 50 ppb and 90 ppb. These shifts are considerably larger than those for typical hydride compounds; furthermore, they are significantly different from each other.[59,64] Both the magnitude of these shifts and their variation indicate that the upfield isotope shifts for this complex are a consequence of the relative site preferences of hydrogen and deuterium, rather than being intrinsic. In contrast, the constant (13 ppb per deuterium) upfield shifts for the $W(PMe_3)_3H_{6-x}D_x$ isotopologues are consistent with an intrinsic isotope effect and a classical hydride description for the compound. In accord with this suggestion, none of the signals exhibit an observable $J_{H\text{-}D}$ coupling.

5.6 Summary and Conclusions

In conclusion, the structure of $W(PMe_3)_3H_6$ has been studied extensively in the solid state and in solution. X-ray diffraction has elucidated both the overall geometry of this molecule and the positions of the hydride ligands, whose H•••H distances demonstrate that this compound is best described as a classical hydride in the solid state.[17] The classical hydride formulation is confirmed for the molecule in solution through a series of NMR spectroscopic experiments. Specifically, measurements of the T_1 values of the hydride ligands as a function of temperature have enabled the determination of $T_{1(min)}$, and the experimental value of 380 ms at 500 MHz suggests that this molecule is best described as a classical hydride in solution. Facile hydrogen/deuterium exchange of $W(PMe_3)_3H_6$ occurs in either deuterotoluene or deuterobenzene, thereby generating the series of isotopologues, $W(PMe_3)_3H_{6-x}D_x$. These species exhibit a constant upfield isotope shift of 13 ppb, which is consistent with an intrinsic two-bond isotope effect. Together, these data indicate that $W(PMe_3)_3H_6$ exists as a classical hydride compound in the solid state and in solution.

5.7 Experimental Section

5.7.1 General Considerations

All manipulations were performed using a combination of glovebox, high vacuum, and Schlenk techniques under an argon atmosphere unless otherwise specified.[65] Solvents were purified and degassed by using standard procedures. ^1H NMR spectra were measured on Bruker Avance III 500 and Avance III 400SL spectrometers. ^1H chemical shifts are reported in ppm relative to $SiMe_4$ ($\delta = 0$) and were referenced internally with respect to the protio solvent impurity (δ 2.08 for C_7D_7H).[66] $W(PMe_3)_3H_6$ was prepared by photolysis of $W(PMe_3)_4H_4$ with H_2.[14,17]

5.7.2 T_1 Measurements

T_1 measurements were performed by using the standard 180–τ–90 inversion recovery method. Each T_1 experiment used 13 mixing times ranging from 1 ms to 15 s, depending upon the value of T_1. For each mixing time, the spectrum was composed of four scans with a delay time of > $5T_1$. The T_1 value was measured for each component of the hydride quartet and averaged to give the values listed in Table 2. Calculations to estimate the $T_{1(min)}$ value of $W(PMe_3)_3H_6$ were performed on the geometry optimized structure of $W(PMe_3)_3H_6$ using a previously described method.[22]

5.7.3 Generation of $W(PMe_3)_3H_{6-x}D_x$ Isotopologues

A solution of $W(PMe_3)_3H_6$ (3 mg, 0.007 mmol) in C_7D_8 (0.7 mL) was heated at 40 ˚C and was monitored by ^1H and $^1H\{^{31}P\}$ NMR spectroscopy, thereby demonstrating the sequential formation of $W(PMe_3)_3H_{6-x}D_x$ isotopologues over a period of several days. Deuterium incorporation into the PMe_3 groups was also demonstrated by ^2H NMR spectroscopy, albeit at a slower rate than into the hydride sites. Isotope exchange was also observed by using C_6D_6 as the solvent.

5.8 References and Notes

(**1**) (a) *Recent Advances in Hydride Chemistry*, Peruzzini, M.; Poli, R. (Eds.), Elsevier, Amsterdam, 2001.
(b) McGrady, G. S.; Guilera, G. *Chem. Soc. Rev.* **2003**, *32*, 383-392.
(c) Hlatky, G. G.; Crabtree, R. H. *Coord. Chem. Rev.* **1985**, *65*, 1-48.(d) McCue, J. P. *Coord. Chem. Rev.* **1973**, *10*, 265-333.
(e) Kaesz, H. D.; Saillant, R. B. *Chem. Rev.* **1972**, *72*, 231-281.

(**2**) (a) Bau, R.; Drabnis, M. H. *Inorg. Chim. Acta* **1997**, *259*, 27-50.
(b) Teller, R. G.; Bau, R. *Struct. Bond.* **1981**, *44*, 1-82.

(**3**) (a) Kubas, G. J. *Metal Dihydrogen and σ-Bond Complexes: Structure, Theory, and Reactivity*, Kluwer Academic/Plenum Publishers, New York, 2001.
(b) Kubas, G. J. *J. Organomet. Chem.* **2001**, *635*, 37-68.
(c) Kubas, G. J. *Proc. Natl. Acad. Sci. U. S. A.* **2007**, *104*, 6901-6907.
(d) Kubas, G. J. *Chem. Rev.* **2007**, *107*, 4152-4205.
(e) Kubas, G. J. *J. Organomet. Chem.* **2009**, *694*, 2648-2653.
(f) Gordon, J. C.; Kubas, G. J. *Organometallics* **2010**, *29*, 4682-4701.

(**4**) Maseras, F.; Lledós, A.; Clot, E.; Eisenstein, O. *Chem. Rev.* **2000**, *100*, 601-636.

(**5**) Green, J. C.; Green, M. L. H.; Parkin, G. *Chem. Comm.* **2012**, *48*, 11481-11503.

(**6**) Gusev, D. G.; Berke, H. *Chem. Ber.* **1996**, *129*, 1143-1155.

(**7**) (a) Sabo-Etienne, S.; Chaudret, B. *Chem. Rev.* **1998**, *98*, 2077-2091.
(b) Heinekey, D. M. *J. Label. Compd. Radiopharm.* **2007**, *50*, 1063-1071.
(c) Lledós, A.; Lluch, J. M.; Maseras, F.; Moreno, M. in *Recent Advances in Hydride Chemistry*, Peruzzini, M.; Poli, R. (Eds.), Elsevier, Amsterdam, 2001, Chapter 15, pp 419-461.

(**8**) Hartwig, J. F. *Organotransition Metal Chemistry – From Bonding to Catalysis*, University Science Books, Mill Valley, California (2010).

(**9**) Breit, B. *Top. Curr. Chem.* **2007**, *279*, 139–172.

(**10**) (a) Troegel, D.; Stohrer, J. *Coord. Chem. Rev.* **2011**, *255*, 1440-1459.
(b) Roy, A. K. *Adv. Organomet. Chem.* **2008**, *55*, 1-59.
(c) Kim, B.-H.; Woo, H.-G. *Adv. Organomet. Chem.* **2005**, *52*, 143-174.

(**11**) The only example of this class of compound is $W(PMe_3)_5H_2$. See:
(a) Chiu, K. W.; Jones, R. A.; Wilkinson, G.; Galas, A. M. R.; Hursthouse, M. B.; Malik, K. M. A. *J. Chem. Soc., Dalton Trans.* **1981**, 1204-1211.
(b) Green, M. L. H.; Parkin, G.; Mingqin, C.; Prout, K. *J. Chem. Soc., Chem. Commun.* **1984**, 1400-1402.
(c) Green, M. L. H.; Parkin, G.; Chen, M.; Prout, K. *J. Chem. Soc., Dalton Trans.* **1986**, 2227-2236.

(**12**) (a) Pennella, F. *Chem. Commun.* **1971**, 158.
(b) Bell, B.; Chatt, J.; Leigh, G. J.; Ito, T. *J. Chem. Soc., Chem. Commun.* **1972**, 34-35.
(c) Meakin, P.; Guggenberger, L. J.; Peet, W. G.; Muetterties, E. L.; Jesson, J. P. *J. Am. Chem. Soc.* **1973**, *95*, 1467-1474.
(d) Crabtree, R. H.; Hlatky, G. G. *Inorg. Chem.* **1982**, *21*, 1273-1275.
(e) Dai, Q. X.; Seino, H.; Mizobe, Y. *Eur. J. Inorg. Chem.* **2011**, 141-149.
(f) Lobkovskii, E. B.; Borisov, A. P.; Makhaev, V. D.; Semenenko, K. N. *J. Struct. Chem.* **1980**, *21*, 100-104.
(g) Lobkovskii, É. B.; Makhaev, V. D.; Borisov, A. P.; Semenenko, K. N. *J. Struct. Chem.* **1979**, *20*, 812-813.

(**13**) (a) Moss, J. R.; Shaw, B. L. *Chem. Commun.* **1968**, 632-633.
(b) Moss, J. R.; Shaw, B. L. *J. Chem. Soc., Dalton Trans.* **1972**, 1910-1911.
(c) Gregson, D.; Howard, J. A. K.; Nicholls, J. N.; Spencer, J. L.; Turner, D. G. *J. Chem. Soc., Chem. Commun.* **1980**, 572-573.
(d) Gregson, D.; Mason, S. A.; Howard, J. A. K.; Spencer, J. L.; Turner, D. G. *Inorg. Chem.* **1984,** *23*, 4103-4107.
(e) Crabtree, R. H.; Hlatky, G. G. *J. Organomet. Chem.* **1982,** *238*, C21-C23.
(f) Lyons, D.; Wilkinson, G. *J. Chem. Soc., Dalton Trans.* **1985**, 587-590.
(g) Lee, M.-Y.; Nam, S.-S.; Kang, S.-O.; Kim, Y. *Bull. Kor. Chem. Soc.* **1995**, *16*, 1237-1239.
(h) Bell, B.; Chatt, J.; Leigh, G. J. *J. Chem. Soc., Dalton Trans.* **1972**, 2492-2496.

(**14**) Parkin, G. *Rev. Inorg. Chem.* **1985**, *7*, 251-297.

(**15**) Bau, R.; Carroll, W. E.; Hart, D. W.; Teller, R. G.; Koetzle, T. F. *Adv. Chem. Ser.* **1977**, *167*, 73-92.

(**16**) The symmetry labels of D_{3h} and C_{2v} do not consider the position of the methyl groups in the trimethylphosphine ligands and refer only to the coordination environment around tungsten.

(**17**) Sattler, A. Ph. D. Thesis, Columbia University, New York, NY, 2012 (Chapter 4).

(**18**) For comparison, the average W-PMe_3 bond length reported in the Cambridge Structural Database (Version 5.35) is 2.49 Å.

(**19**) The W-H distances in the geometry optimized structure (W-H_{av} = 1.74 Å) are longer than those in the structure as determined by X-ray diffraction (W-H_{av} = 1.58 Å.) This is to be expected since the distances determined by X-ray diffraction refer to the distances between positions of electron density maxima and not those between nuclei; the electron density maxima and nuclear positions do not necessarily coincide for hydrogen atoms in a molecule, hence the discrepancy. See, for example:
(a) Coppens, P. *Angew. Chem. Int. Edit. Engl.* **1977**, *16*, 32-40.
(b) Cotton, F. A.; Luck, R. L. *Inorg. Chem.* **1989**, *28*, 3210-3213.

(**20**) Heyes, S. J.; Green, M. L. H.; Dobson, C. M. *Inorg. Chem.* **1991**, *30*, 1930-1937.

(**21**) (a) Hamilton, D. G.; Crabtree, R. H. *J. Am. Chem. Soc.* **1988**, *110*, 4126-4133.
(b) Crabtree, R. H. *Angew. Chem. Int. Ed.* **1993**, *32*, 789-805.
(c) Crabtree, R. H.; Lavin, M. *J. Chem. Soc. Chem. Commun.* **1985**, 1661-1662.
(d) Luo, X.-L.; Crabtree, R. H. *Inorg. Chem.* **1990**, *29*, 2788-2791.

(**22**) Desrosiers, P. J.; Cai, L.; Lin, Z.; Richards, R.; Halpern, J. *J. Am. Chem. Soc.* **1991**, *113*, 4173-4184.

(**23**) Morris, R. H. *Coord. Chem. Rev.* **2008**, *252*, 2381-2394.

(**24**) Bakhmutov, V. I.; Vorontsov, E. V. *Rev. Inorg. Chem.* **1998**, *18*, 183-221.

(**25**) Bayse, C. A.; Luck, R. L.; Schelter, E. J. *Inorg. Chem.* **2001**, *40*, 3463-3467.

(**26**) Abragam, A. *The Principles of Nuclear Magnetism*, Oxford University Press, Oxford, 1961.

(**27**) Ghosh, P.; Desrosiers, P. J.; Parkin, G. *J. Am. Chem. Soc.* **1998**, *120*, 10416-10422.

(**28**) Bertini, I.; Luchinat, C.; Parigi, G. *Current Methods of Inorganic Chemistry, Vol. 2., Solution NMR of Paramagnetic Molecules: Applications to Metallobiomolecules and Models.* Elsevier, 2001.

(**29**) These interactions all result in a decreased value of T_1. Rotation of a dihydrogen ligand, on the other hand, serves to increase T_1. See reference 23.

(**30**) This value is calculated *via* the expression $R_{HP} = 0.027n\ s^{-1}$, where n is the number of phosphorus nuclei. See reference 22.

(**31**) The relaxation of the hydrides due to interaction with ^{183}W is negligible, such that the hydrides bonded to this nucleus, which are represented by the tungsten satellites, have similar T_1 values as the hydrides that are attached to non-magnetically active tungsten nuclei.

(**32**) Alternatively, the hydrogen atoms of the PMe_3 ligands may be closer to the hydrides in the calculated structure than in the actural structure.

(**33**) Michos, D.; Luo, X.; Faller, J. W.; Crabtree, R. H. *Inorg. Chem.* **1993**, *32*, 1370-1375.

(**34**) Lee, M. Y.; Nam, S. S.; Kang, S. O.; Kim, Y. *Bull. Korean Chem. Soc.* **1995**, *16*, 1237-1239.

(**35**) Heinekey, D. M. *J. Label Compd. Radiopharm.* **2007**, *50*, 1063-1071.

(**36**) Heinekey, D. M.; Oldham, W. J., Jr. *Chem. Rev.* **1993**, *93*, 913-926.

(**37**) (a) Hansen, P. E. *Ann. Rep. NMR Spectrosc.* **1983**, *15*, 105-234.
(b) Hansen, P. E. *Prog. NMR Spectrosc.* **1988**, *20*, 207-255.
(c) de Dios, A. C.; Jameson, C. J. *Ann. Rep. NMR. Spectrosc.* **1994**, *29*, 1-69.

(d) Jankowski, S. *Ann. Rep. NMR Spectrosc.* **2009**, *68*, 149-191.
(e) Gombler, W. *J. Am. Chem. Soc.* **1982**, *104*, 6616-6620.

(**38**) Lockley, W. J. S.; Heys, J. R. *J. Label Compd. Radiopharm* **2010**, *53*, 635–644.

(**39**) Chatt, J.; Coffey, R. S. *J. Chem. Soc. (A)* **1969**, 1963-1972.

(**40**) Tebbe, F. N. *J. Am. Chem. Soc.* **1973**, *95*, 5823-5824.

(**41**) (a) Klabunde, U.; Parshall, G. W. *J. Am. Chem. Soc.* **1972**, *94*, 9081-9087.
(b) Cameron, C. J.; Felkin, H.; Fillebeen-Khan, T.; Forrow, N. J.; Guittet, E. *J. Chem. Soc. Chem. Commun.* **1986**, 801-802.

(**42**) (a) Pivovarov, A. P.; Ioffe, L. M.; Gak, Y. V.; Makhaev, V. D.; Borisov, A. P.; Borod'ko, Y. G. *Bull. Acad. Sci. USSR Div. Chem. Sci.* **1987**, *36*, 928-930.
(b) Pivovarov, A. P.; Ioffe, L. M.; Gak, Y. V.; Borod'ko, Y. G. *Bull. Acad. Sci. USSR Div. Chem. Sci.* **1984**, *33*, 700-702.

(**43**) (a) Barefield, E. K.; Parshall, G. W.; Tebbe, F. N. *J. Am. Chem. Soc.* **1970**, *92*, 5234-5235.
(b) Tebbe, F. N.; Parshall, G. W. *J. Am. Chem. Soc.* **1971**, *93*, 3793-3795.

(**44**) In accord with this mechanism, HD is formed catalytically *via* H/D exchange between H_2 and deuterotoluene in the presence of $W(PMe_3)_3H_6$.

(**45**) There is precedent for the cyclometallation of PMe_3 ligands in tungsten chemistry. See, for example:
(a) Rabinovich, D.; Parkin, G. *J. Am. Chem. Soc.* **1990**, *112*, 5381-5383.
(b) Rabinovich, D.; Zelman, R.; Parkin, G. *J. Am. Chem. Soc.* **1992**, *114*, 4611-4621.

(**46**) Although the reactions of $W(PMe_3)_xH_y$ compounds are generally interpreted by invoking oxidative addition and reductive elimination, metathesis pathways could be considered. See: Perutz, R. N.; Sabo-Etienne, S. *Angew. Chem. Int. Edit.* **2007**, *46*, 2578-2592.

(**47**) Berry, M.; Elmitt, K.; Green, M. L. H. *J. Chem. Soc., Dalton Trans.* **1979**, 1950-1958.

(**48**) Cleavage of the methyl C-H bond is also observed in this system, thereby generating $Cp_2W(C_4H_4Me)(CH_2Ph)$.

(**49**) Jones, W. D.; Hessell, E. T. *J. Am. Chem. Soc.* **1993**, *115*, 554-562.

(**50**) As with reference 47, a significant amount of methyl C-H cleavage is observed.

(**51**) See, for example:
(a) Butschke, B.; Schwarz, H. *Organometallics* **2011**, *30*, 1588-1598.
(b) Burger, P.; Bergman, R. G. *J. Am. Chem. Soc.* **1993**, *115*, 10462-10463.
(c) Brainard, R. L.; Nutt, W. R.; Lee, T. R.; Whitesides, G. M. *Organometallics* **1988**, *7*, 2379-2386.

(d) Liang, L.-C.; Chien, P.-S.; Huang, Y.-L. *J. Am. Chem. Soc.* **2006**, *128*, 15562-15563.
(e) Johansson, L.; Ryan, O. B.; Rømming, C.; Tilset, M. *J. Am. Chem. Soc.* **2001**, *123*, 6579-6590.
(e) Zhao, S.-B.; Song, D.; Jia, W.-L.; Wang, S. *Organometallics* **2005**, *24*, 3290-3296.
(f) Norris, C. M.; Reinartz, S.; White, P. S.; Templeton, J. L. *Organometallics* **2002**, *21*, 5649-5656.
(g) Reinartz, S.; White, P. S.; Brookhart, M.; Templeton, J. L. *Organometallics* **2001**, *20*, 1709-1712.
(h) Jones, W. D.; Feher, F. J. *J. Am. Chem. Soc.* **1984**, *106*, 1650-1663.

(**52**) For the assignment of the ^{1}H NMR spectrum of toluene, see: Schaefer, T.; Hutton, H. M. *Org. Mag. Res.* **1979**, *12*, 645-646.

(**53**) Stahl, S. S.; Labinger, J. A.; Bercaw, J. E. *J. Am. Chem. Soc.* **1996**, *118*, 5961-5976.

(**54**) Looney, A.; Parkin, G. *Polyhedron* **1990**, *9*, 265-276.

(**55**) A previous report lists increments of 19, 8, and 18 ppb, in contrast to the 15 ppb reported above. See: Bernheim, R. A.; Lavery, B. J. *J. Chem. Phys.* **1965**, *42*, 1464.

(**56**) In the $^{n}\Delta X(Y)$ notation, the value of the observed isotope shift corresponds to the chemical shift of X in the molecule with the lighter isotope of Y minus the chemical shift of X in the molecule with the heavier isotope of Y, such that an upfield shift for the heavier isotope is characterized by a positive value of $^{n}\Delta X(Y)$. In this system, for example, the hydride signal of $W(PMe_3)_3H_6$ appears at δ -2.734, while the signal for $W(PMe_3)_3H_5D$ appears at δ -2.747. Thus, $^{2}\Delta^{1}H(D)$ = [(-2.734) - (-2.747)] = 0.013 ppm = 13 ppb.

(**57**) Luo, X.-L.; Crabtree, R. H. *J. Am. Chem. Soc.* **1990**, *112*, 4813-4821.

(**58**) Wazio, J. A.; Jimenez, V.; Soparawalla, S.; John, S.; Moehring, G. A. *Inorg. Chim. Acta* **2009**, *362*, 159-165.

(**59**) Janak, K. E.; Shin, J. H.; Parkin, G. *J. Am. Chem. Soc.* **2004**, *126*, 13054-13070.

(**60**) Pons, V.; Conway, S. L. J.; Green, M. L. H.; Green, J. C.; Herbert, B. J.; Heinekey, D. M. *Inorg. Chem.* **2004**, *43*, 3475-3483.

(**61**) Bakhmutov, V. I.; Vorontsov, E. V.; Nikonov, G. I.; Lemenovskii, D. A. *Inorg. Chem.* **1998**, *37*, 279-282.

(**62**) Bianchini, C.; Linn, K.; Masi, D.; Peruzzini, M.; Polo, A.; Vacca, A.; Zanobini, F. *Inorg. Chem.* **1993**, *32*, 2366-2376.

(**63**) (a) Heinekey, D. M.; Oldham, W. J. *J. Am. Chem. Soc.* **1994**, *116*, 3137-3138.
(b) Oldham, W. J.; Hinkle, A. S.; Heinekey, D. M. *J. Am. Chem. Soc.* **1997**, *119*, 11028-11036.

(**64**) $[H_2C(C_5H_4)_2]Mo(\eta^2–H_2)H]^+$ exhibits similar behavior upon isotopic substitution. See reference 60.

(**65**) (a) McNally, J. P.; Leong, V. S.; Cooper, N. J. in *Experimental Organometallic Chemistry*, Wayda, A. L.; Darensbourg, M. Y., Eds.; American Chemical Society: Washington, DC, 1987; Chapter 2, pp 6-23.
(b) Burger, B.J.; Bercaw, J. E. in *Experimental Organometallic Chemistry*; Wayda, A. L.; Darensbourg, M. Y., Eds.; American Chemical Society: Washington, DC, 1987; Chapter 4, pp 79-98.
(c) Shriver, D. F.; Drezdzon, M. A.; *The Manipulation of Air-Sensitive Compounds*, 2nd Edition; Wiley-Interscience: New York, 1986.

(**66**) Gottlieb, H. E.; Kotlyar, V.; Nudelman, A. *J. Org. Chem.* **1997**, *62*, 7512-7515.